

Dissertation zur Erlangung des Doktorgrades  
der Fakultät für Chemie und Pharmazie  
der Ludwig-Maximilians-Universität München



**Analysis of the isoprenoid part of sterol biosynthesis in fungal and  
mammalian matrices**

Maximilian Leonhard Liebl

aus

München

2025



## **Erklärung**

Diese Dissertation wurde im Sinne von § 7 der Promotionsordnung vom 28. November 2011 von Herrn Prof. Dr. Franz Bracher betreut.

## **Eidesstattliche Versicherung**

Diese Dissertation wurde eigenständig und ohne unerlaubte Hilfe erarbeitet.

München, den 20.03.2025

---

Maximilian Liebl

Dissertation eingereicht am 20.03.2025

1. Gutachter: Prof. Dr. Franz Bracher

2. Gutachter: Prof. Dr. Oliver Scherf-Clavel

Mündliche Prüfung am 06.05.2025



# Danksagung

Mein Dank gilt an erster Stelle meinem Doktorvater Prof. Dr. Franz Bracher für die stets wohlwollende und großzügige Unterstützung meiner Projekte.

Des Weiteren danke ich Prof. Dr. Oliver Scherf-Clavel für die freundliche Übernahme des Koreferats. Ihm und allen Mitgliedern der Prüfungskommission gilt mein Dank für ihre Zeit und Unterstützung.

Ganz besonders danke ich Dr. Christoph Müller, der mich in allen meinen Projekten stets unterstützte und mir immer mit Rat und Tat zur Seite stand. Danke dir, dass du mir so viel beigebracht hast und auch neben der Arbeit immer ein offenes Ohr für mich hattest.

Ich möchte mich auch bei all meinen Kooperationspartnern bedanken, insbesondere Assoz.-Prof. Fabio Gsaller von der medizinischen Universität Innsbruck, Prof. Johannes Wagener vom Trinity College Dublin und Dr. Jan Klein von der Friedrich-Schiller-Universität Jena, mit denen ich an verschiedenen Projekten arbeiten durfte.

Bei meinen Kolleginnen und Kollegen aus dem Arbeitskreis Bracher bedanke ich mich für die gemeinsame Zeit. Vielen Dank an Anna, Marco, Sandra und allem voran der gesamten Kaffee-Gang (Christoph, Lars, Ludwig, Michelle, Sonja und Sebastian). Die Pausen vom Laboralltag mit euch waren stets eine Bereicherung, egal ob sie durch fachliche Diskussionen oder die neusten BILD-Schlagzeilen geprägt waren. Danke auch an Ina und Irene, deren Labortür mir immer offen stand, falls ich mal aus dem zweiten Stock fliehen wollte.

Für die angenehme Arbeitsatmosphäre im Laboralltag danke ich meinen Laborkolleginnen und -kollegen Anna, Sonja, Lorenz, Michelle und Christoph. Für ihre große Begeisterung und Eigeninitiative, die die beiden während ihrer Projekte bei mir als Bachelorand/ HiWi an den Tag gelegt haben, bedanke ich mich bei Ludwig Huber und Florian Olander. Viel Erfolg euch beiden in eurer weiteren wissenschaftlichen Karriere!

Georg Höfner und Julian Marschner danke ich für die wertvollen Diskussionen, sei es über Analytik, Datenverarbeitung oder die neuesten alpinen Klettertrends.

Für die langjährige Unterstützung und das stets makellose Äußere meiner Arbeiten bedanke ich mich bei Paulo.

Vielen Dank an meine Freunde und meine Familie, die immer für mich da waren und mich durch die Höhen und Tiefen meiner Promotionszeit begleitet haben. Ihr habt mich unterstützt, wenn es nicht lief und mit mir angestoßen, wenn es etwas zu feiern gab. Danke euch!

Ganz besonders möchte ich mich bei Julia bedanken, die während der gesamten Zeit immer für mich da war und mir den Rücken gestärkt hat.

Mein größter Dank gilt meinen Eltern und meinem Bruder Florian. Durch euren Rückhalt, euer Vertrauen und eure Unterstützung habt ihr mir die Chance gegeben diesen Weg zu gehen. Dafür bin ich euch unendlich dankbar.



# Table of Contents

<b>1. Introduction</b> .....	<b>1</b>
<b>1.1 Sterol Biosynthesis</b> .....	<b>1</b>
1.1.1 The Mevalonate Pathway .....	2
1.1.2 The Isoprenoid Pathway .....	3
1.1.3 The Post-Squalene Pathway .....	5
<b>1.2 Physiological Role of Isoprenoids as Molecules Involved in Posttranslational Modifications</b> .....	<b>7</b>
1.2.1 tRNA Modification .....	8
1.2.2 Prenylation of Ras Proteins .....	8
1.2.3 Ubiquinone Biosynthesis .....	9
1.2.4 Heme A Biosynthesis.....	10
1.2.5 Formation of Dolichols.....	10
1.2.6 Fungal Carotenoid Biosynthesis.....	11
1.2.7 Fungal Quorum Sensing .....	11
<b>1.3 Regulation of Cholesterol Biosynthesis</b> .....	<b>12</b>
<b>1.4 Endogenous Control of Cholesterol Biosynthesis</b> .....	<b>13</b>
<b>1.5 Inhibitors of the Mevalonate Pathway</b> .....	<b>14</b>
<b>1.6 Defects in Cholesterol Biosynthesis</b> .....	<b>14</b>
<b>1.7 Inhibitors of Ergosterol Biosynthesis</b> .....	<b>15</b>
<b>2. Objective</b> .....	<b>17</b>
<b>3. Azole Resistance in <i>Aspergillus fumigatus</i></b> .....	<b>19</b>
<b>3.1 Summary</b> .....	<b>19</b>
<b>3.2 Personal Contribution</b> .....	<b>20</b>
<b>3.3 Article</b> .....	<b>21</b>
<b>3.4 Supporting Information</b> .....	<b>32</b>
<b>4. Quantifying Isoprenoids in the Ergosterol Biosynthesis by Gas Chromatography–Mass Spectrometry</b> .....	<b>36</b>
<b>4.1 Summary</b> .....	<b>36</b>
<b>4.2 Personal Contribution</b> .....	<b>37</b>
<b>4.3 Article</b> .....	<b>39</b>

4.4	<i>Supporting Information</i> .....	60
5.	<b>Targeting the Isoprenoid Pathway in Cholesterol Biosynthesis: An Approach to Identify Isoprenoid Biosynthesis Inhibitors</b> .....	72
5.1	<i>Summary</i> .....	72
5.2	<i>Personal Contribution</i> .....	73
5.3	<i>Article</i> .....	74
5.4	<i>Supporting Information</i> .....	90
5.5	<i>Is there an antifungal activity of mammalian isoprenoid biosynthesis inhibitors?</i> .....	92
6.	<b>Is Dehydroepiandrosterone Excretion a Defense Mechanism of Plants Affecting Ergosterol Biosynthesis of <i>Alternaria brassicicola</i>?</b> .....	94
6.1	<i>Summary</i> .....	94
6.2	<i>Personal contribution</i> .....	95
6.3	<i>Article</i> .....	96
6.4	<i>Supporting Information</i> .....	114
7.	<b>Summary</b> .....	129
8.	<b>Abbreviations</b> .....	131
9.	<b>Literature</b> .....	133

# 1. Introduction

*“Cholesterol is the most highly decorated small molecule in biology.”*[1]

*Nobel lecture December 1985; Michael S. Brown and Joseph L. Goldstein*

While mammalian cells produce cholesterol, the main fungal sterol is ergosterol. Plants are even capable to produce several main sterols including campesterol, sitosterol and stigmasterol. Since the focus of this work is on mammalian and fungal sterol biosynthesis, details on plant sterol biosynthesis will not be included in this work.

Sterols are essential due to their role in membrane fluidity, flexibility, rigidity, and stability [2,3]. For this reason, the individual sterol biosynthesis is of pivotal importance in all eucaryotic organisms [3]. Since cholesterol was first extracted from gallstones in the late 18<sup>th</sup> century, it was in the center of scientific interests. In total thirteen Nobel Prizes have been awarded in relation to cholesterol [1]. The efforts in understanding, regulating, and influencing sterol biosynthesis have been enormous for almost 250 years now, and are still ongoing. Even though, the main enzymatic steps of sterol biosynthesis including their differences and similarities across the kingdoms have been widely investigated, mechanistic details of the highly specific enzymatic reactions are in several cases still not fully understood [4].

## 1.1 Sterol Biosynthesis

The most important mechanistic insights into sterol biosynthesis can be attributed to the work of Konrad Bloch and Feodor Lynen who shared the 1964 Nobel Prize in Physiology or Medicine for their research in the field of mechanisms and regulation of cholesterol and fatty acid metabolism [1]. The Bloch pathway – named after its explorer – is next to the later explored Kandutsch-Russell pathway one of two possible distal cholesterol biosynthesis pathways that are connected *via* a sterol C24-reductase leading to the final product cholesterol (see Chapter 1.1.3).

While in distal sterol biosynthesis the formation of different sterol intermediates is described, that are needed to form biosynthesis products like cholesterol and ergosterol, the earlier steps which lead to the sterol precursor squalene, are described in the pre-squalene pathway. The pre-squalene pathway itself can be further subdivided into two minor sections, the mevalonate pathway (see Chapter 1.1.1), in which isopentenyl pyrophosphate is formed from citric acid, and the isoprenoid pathway (see Chapter 1.1.2), in which squalene is synthesized (**Figure 1**) [5].

## Introduction

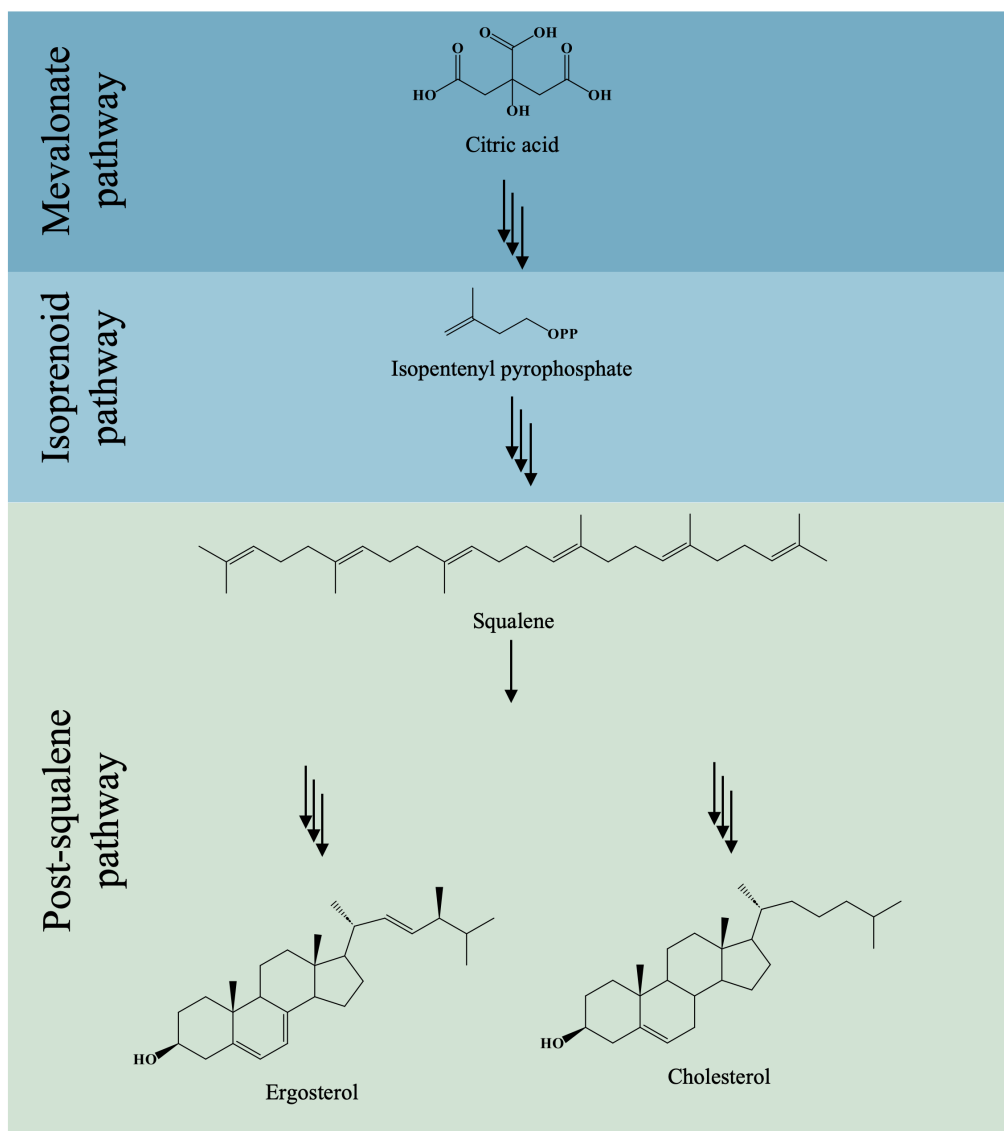


**Figure 1:** Schematic overview of the subpathways of sterol biosynthesis and their most important intermediates. Different colors contain different biosynthesis pathways. PP: pyrophosphate

### 1.1.1 The Mevalonate Pathway

Eukaryotic sterol biosynthesis begins with the mevalonate pathway (**Figure 2**). In a first of seven steps, the C2 building block acetyl-coenzyme A (acetyl-CoA) is formed from citrate, the physiological form of citric acid, which originates from the citric acid cycle. The reaction is catalyzed by adenosine triphosphate (ATP) citrate lyase (**a**) [6]. In the following enzymatic steps, two molecules of acetyl-CoA are combined in a Claisen-type condensation reaction catalyzed by the thiolase acetoacetyl-CoA synthase (**b**). In the next enzymatic step, another unit of acetyl-CoA is added to form 3-hydroxy-3-methylglutaryl (HMG)-CoA. This physiologically irreversible reaction is carried out by the enzyme HMG-CoA synthase (**c**) [7,8]. The rate-determining step in sterol biosynthesis is the enzyme-catalyzed reduction of the thioester group in HMG-CoA by HMG-CoA reductase (**d**), which produces mevalonate using two equivalents of nicotinamide adenine dinucleotide phosphate (NADP). The reactions from acetyl-CoA to HMG-CoA take place in the cytosol [8], whereas the enzymes catalyzing the following reactions up to farnesyl pyrophosphate are more commonly found in peroxisomes [8,9]. The subsequent step in the enzymatic cascade is a phosphorylation reaction catalyzed by mevalonate kinase (**e**) using one

## Introduction

equivalent of ATP to produce mevalonate-5-phosphate. This first phosphorylation reaction is regulated by a specific feedback mechanism in which the activity of the enzyme (mevalonate kinase, **e**) is influenced by the concentrations of farnesyl pyrophosphate (FPP) and geranyl pyrophosphate (GPP) [7]. FPP and GPP are intermediates of the upstream isoprenoid pathway (see Chapter 1.1.2). A second phosphorylation is catalyzed by phosphomevalonate kinase (**f**) using another equivalent of ATP [7]. The resulting intermediate, mevalonate-5-pyrophosphate, is further decarboxylated in an ATP-dependent reaction by the enzyme diphosphomevalonate decarboxylase (**g**). The product of decarboxylation and dehydration is isopentenyl pyrophosphate (IPP), the first isoprenoid in the enzymatic cascade [7].

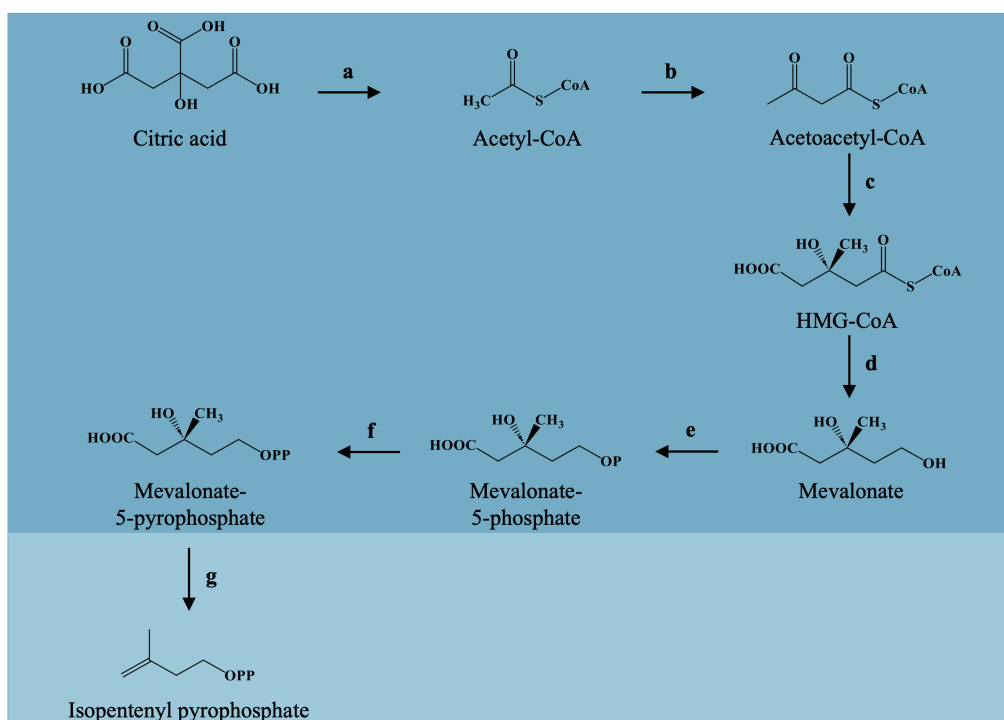


**Figure 2:** In deep blue: the mevalonate pathway, showing the separate intermediates, starting from citric acid to mevalonate-5-pyrophosphate. In light blue: isopentenyl pyrophosphate, the product of the mevalonate pathway which is also the educt of the isoprenoid pathway. Enzymes: ATP citrate synthase (**a**); acetoacetyl-CoA thiolase (**b**); HMG-CoA synthase (**c**); HMG-CoA reductase (**d**); mevalonate kinase (**e**); phosphomevalonate kinase (**f**); mevalonate pyrophosphate decarboxylase (**g**). P: phosphate; PP: pyrophosphate.

### 1.1.2 The Isoprenoid Pathway

IPP and its isomer dimethylallyl pyrophosphate (DMAPP) are the educts of the isoprenoid pathway (**Figure 3**), interconverted by isopentenyl pyrophosphate isomerase (**h**) [7]. Prior to the formation of higher isoprenoids, the isomerization of IPP to DMAPP is necessary, due to the insufficient reactivity of IPP to be ionized and initiate the first condensation reaction, catalyzed by farnesyl pyrophosphate synthase (**i**) [4]. In the initial head-to-tail condensation reaction, one pyrophosphate group is eliminated from the farnesyl pyrophosphate synthase (**i**) bound DMAPP to create a carbocation intermediate. IPP adds to the intermediate, thereby a new carbocation is created, which is transformed to the monoterpene geranyl pyrophosphate (GPP) by the elimination of one proton [8]. In the same manner, a second condensation reaction is catalyzed by farnesyl pyrophosphate synthase (**i**), where another equivalent of IPP is combined with a GPP carbocation to form the sesquiterpene farnesyl pyrophosphate (FPP) [5,8].

## Introduction

At the stage of FPP, there is a branch point of isoprenoid biosynthesis. With a third IPP building block, geranylgeranyl pyrophosphate synthase (**j**) catalyzes the third condensation reaction of the enzymatic cascade to form the diterpene geranylgeranyl pyrophosphate (GGPP) [8]. GGPP is neither an intermediate of mammalian nor fungal sterol biosynthesis. However, GGPP next to FPP, is involved in multiple posttranslational modification reactions and biological regulation mechanisms outside sterol biosynthesis (for details see Chapter 1.2) [10]. Heme A and dolichols are modified with FPP, while GGPP is required for the biosynthesis of ubiquinone and carotenoids [2,11-15].

Squalene, the product of the isoprenoid pathway is formed in a head-to-head condensation reaction from two equivalents FPP. The two-step mechanism suggests that the loss of one pyrophosphate group leads to the addition of the remaining allylic carbocation to the alkene end of the other FPP, which is accompanied by the loss of one proton, to form a “pre-squalene pyrophosphate” (PSPP) intermediate. In a second step, the PSPP loses the pyrophosphate moiety to create a cyclopropylcarbinyl carbocation, which, after ring opening, gets reduced by NADP to squalene [4,8]. The catalyzing enzyme, squalene synthase (**k**), is located in the endoplasmic reticulum (ER) [9]. Squalene is the product of the pre-squalene pathway as well as the educt of the biosynthesis of mammalian cholesterol and fungal ergosterol [4,16].

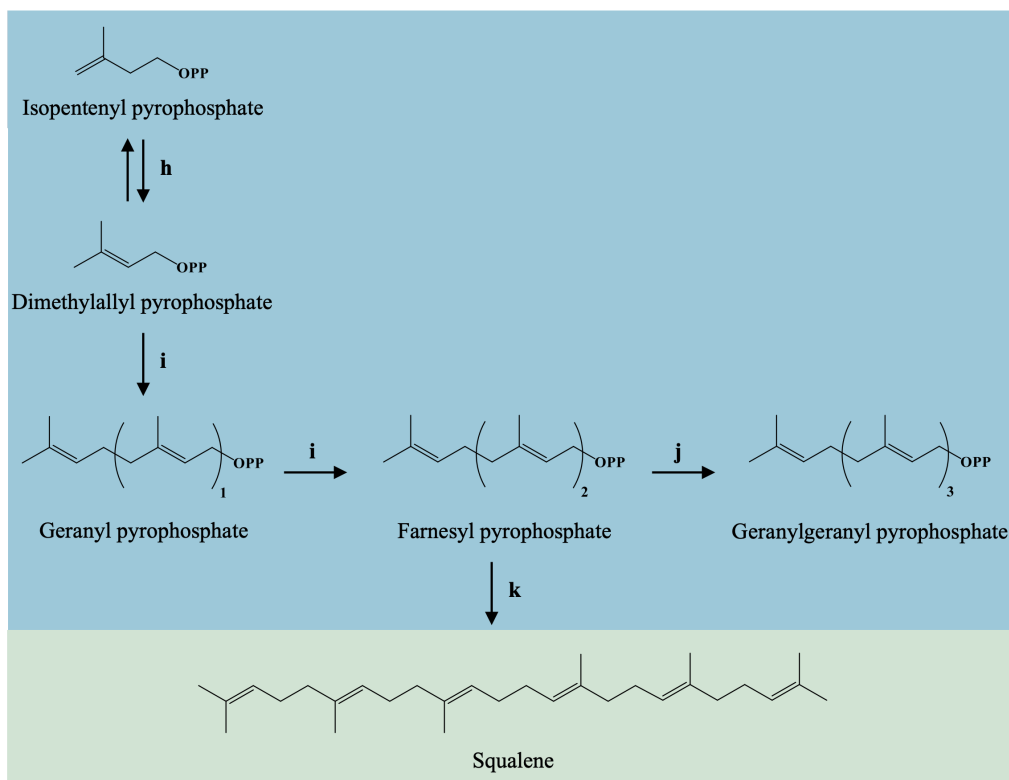


**Figure 3:** In light blue: the isoprenoid pathway starting with isopentenyl pyrophosphate. In green: squalene, the educt of the post-squalene pathway. Enzymes: isopentenyl pyrophosphate isomerase (**h**); farnesyl pyrophosphate synthase (**i**); geranylgeranyl pyrophosphate synthase (**j**); squalene synthase (**k**). PP: pyrophosphate.

## Introduction

### 1.1.3 The Post-Squalene Pathway

The formation of lanosterol, the first sterol, remains identical in all eukaryotic cells, whereas the further post-squalene pathway is catalyzed by organism specific enzymes (**Figure 4**). In the initial step of the post-squalene pathway, squalene is epoxidated to (*S*)-2,3-oxidosqualene. The reaction is catalyzed by squalene monooxygenase (**l**) and followed by the formation of lanosterol, which is catalyzed by one single enzyme (for details see [17]), 2,3-oxidosqualene cyclase (**m**).

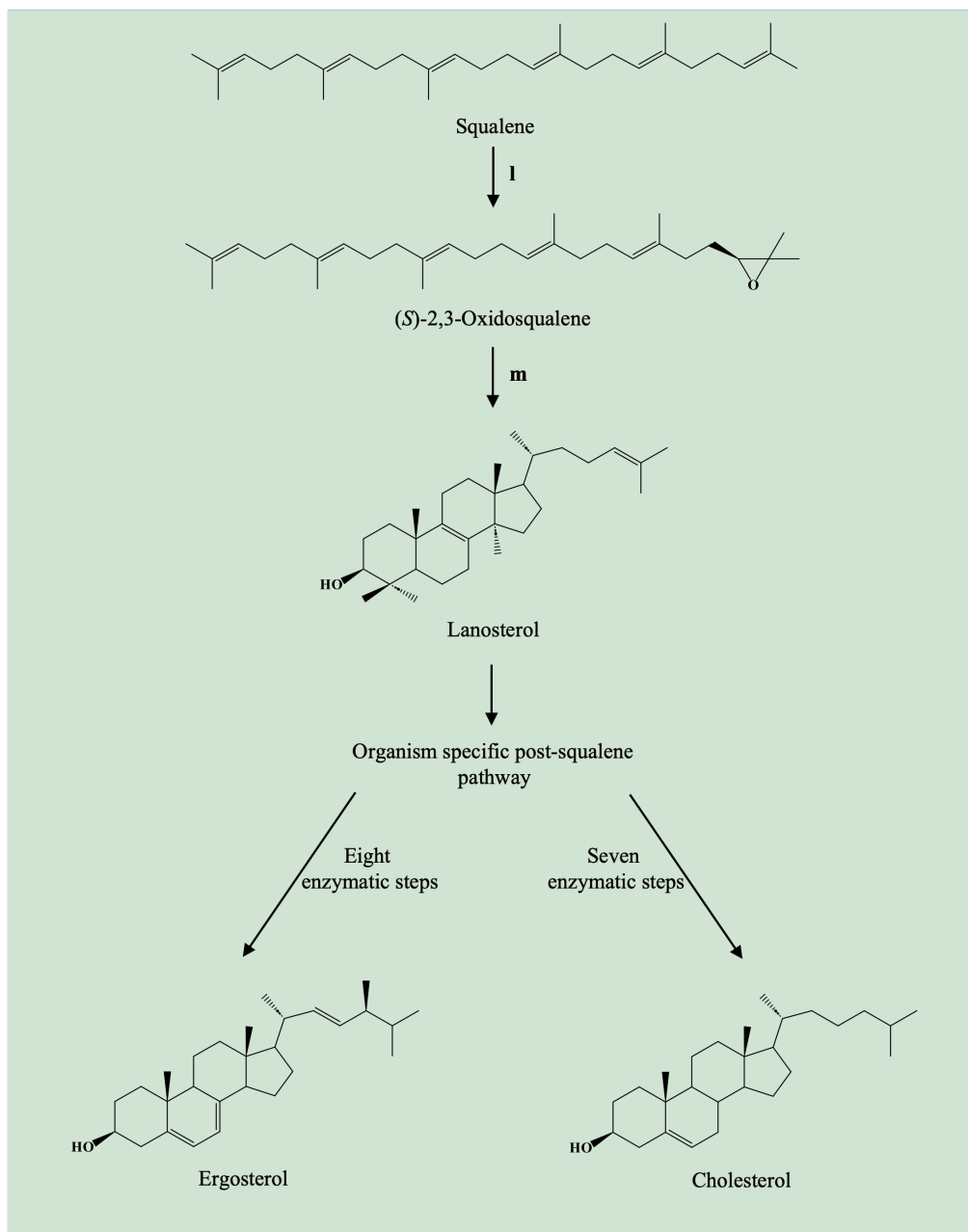


**Figure 4:** Schematic overview of the post-squalene pathway starting with the formation of lanosterol from squalene *via* (*S*)-2,3-oxidosqualene. From lanosterol, different intermediates lead to organism specific sterols. Enzymes: squalene monooxygenase (**l**); 2,3-oxidosqualene cyclase (**m**).

Cholesterol biosynthesis can be performed *via* the Kandutsch-Russell pathway or the Bloch pathway (**Figure 5**), which are interconnected by the enzyme C24-dehydrocholesterol reductase (DHCR24 = sterol C24-reductase, **n**). From lanosterol seven enzymatic steps are required to form the final product cholesterol [4,18].

## Introduction

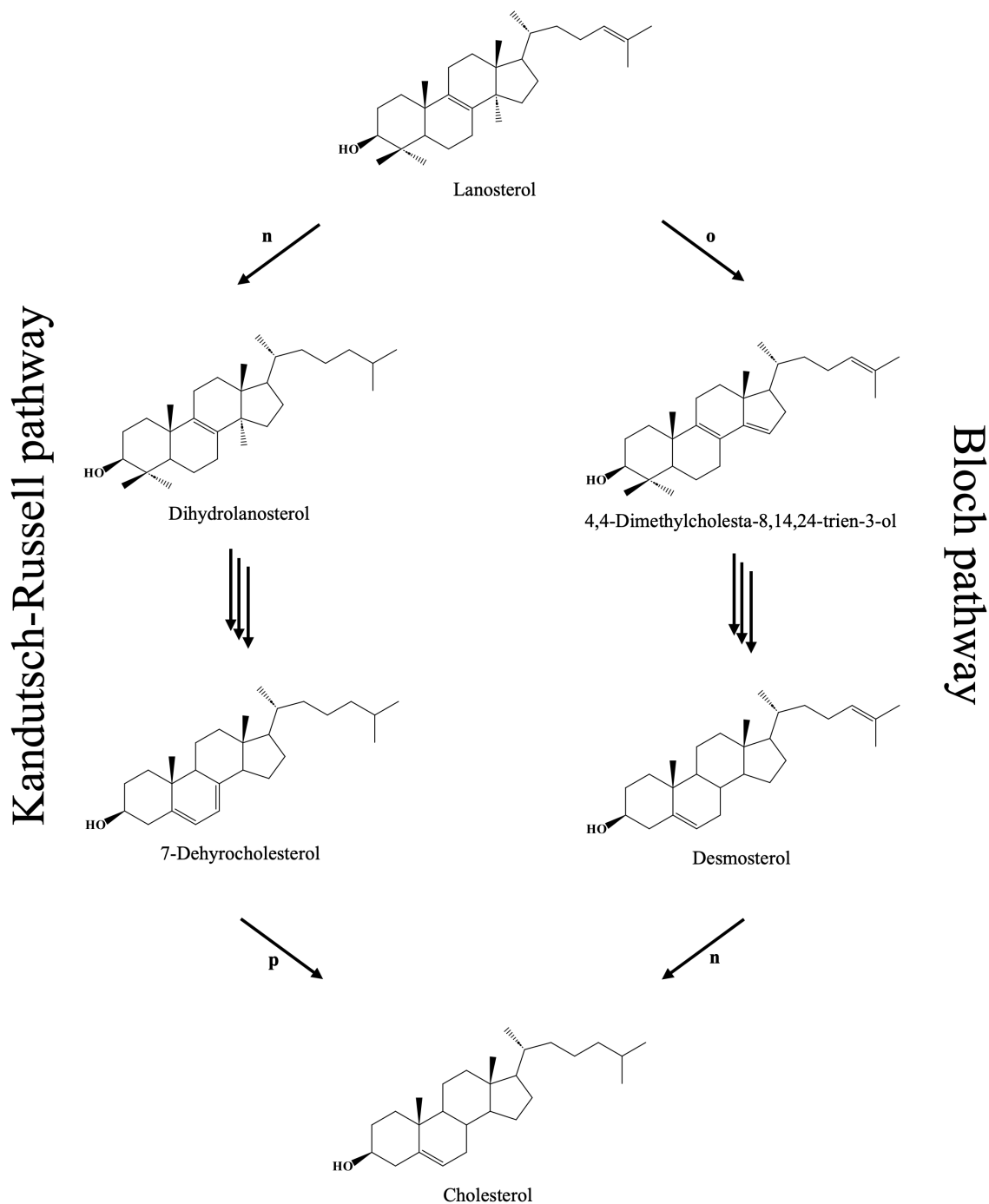


**Figure 5:** Distal cholesterol biosynthesis *via* Bloch or Kandutsch-Russell pathway. Enzymes: C24-dehydrocholesterol reductase (DHCR24 = sterol C24-reductase) (**n**), sterol C14-demethylase (**o**), sterol C7-reductase (**p**).

In ergosterol biosynthesis lanosterol is also a branching point. Depending on the fungal species, the ergosterol biosynthesis intermediate fecosterol can be formed *via* two pathways, starting with C24-methylation (enzyme: sterol C24-methyltransferase, **n**<sup>\*</sup>) or C14-demethylation (enzyme: sterol C14-demethylase, **o**<sup>\*</sup>) of lanosterol (see Chapter 6.3 Article Figure 12B, **Figure 6**). Yeasts, *e.g.*, *Saccharomyces cerevisiae* and *Candida albicans* usually start distal ergosterol biosynthesis *via* formation of 4,4-dimethylcholesta-8,14,24-trien-3-ol from lanosterol (*via* enzyme **o**<sup>\*</sup>). Molds *e.g.*, *Aspergillus fumigatus* as well as the necrotic pathogenic fungus *Alternaria brassicicola* (see Chapter 6) prefer ergosterol biosynthesis after C24 methylation (*via* enzyme **n**<sup>\*</sup>) of lanosterol to

## Introduction

eburicol [19-21]. Independent of the preferred pathway, from lanosterol at least eight enzymatic steps are required to form the final product ergosterol [22].

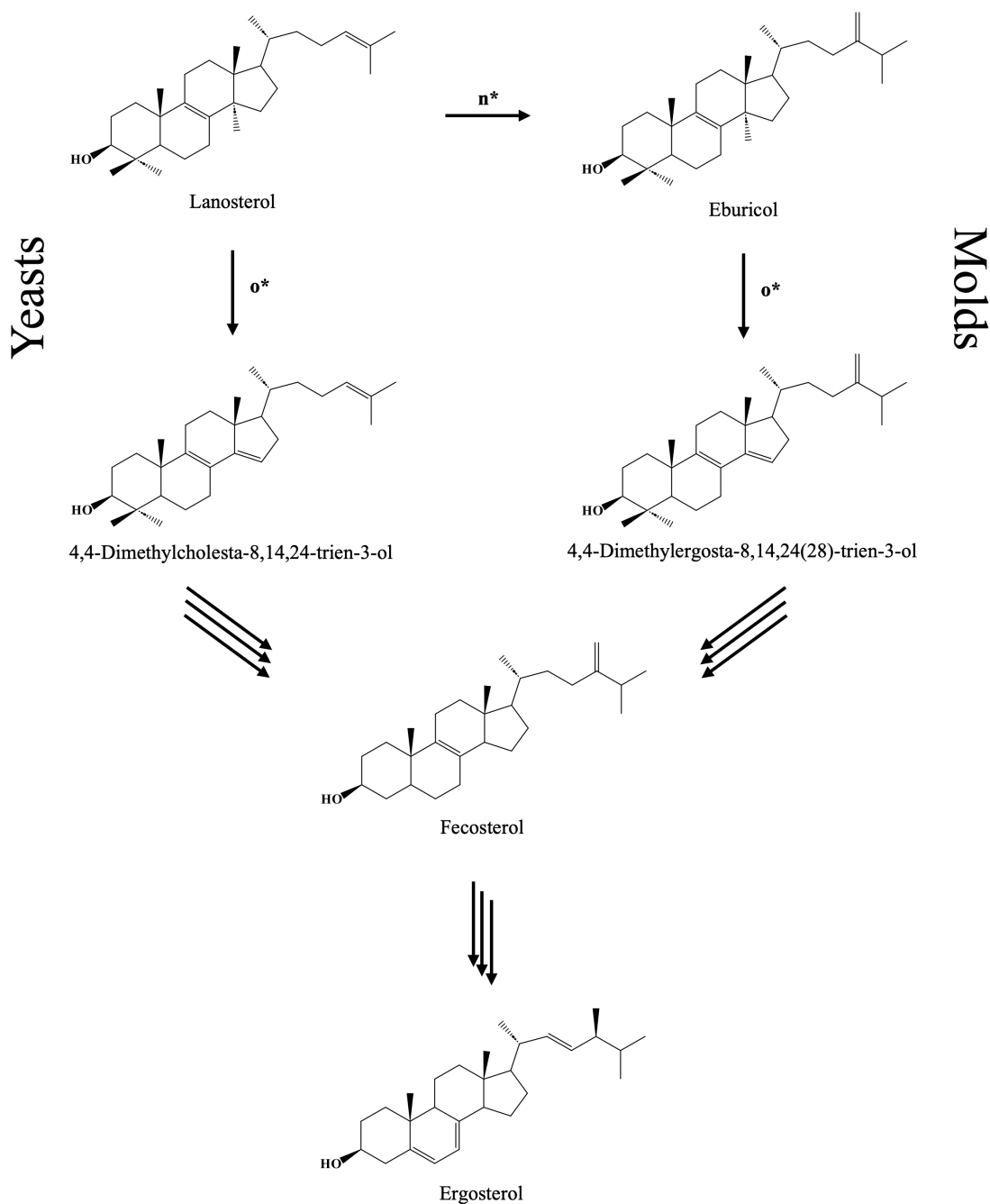


**Figure 6:** Distal ergosterol biosynthesis *via* two organism specific pathways molds and yeasts use to form fecosterol. Enzymes: sterol C24-methyltransferase ( $n^*$ ), sterol C14-demethylase ( $o^*$ ).

### 1.2 Physiological Role of Isoprenoids as Molecules Involved in Posttranslational Modifications

The physiological role of isoprenoids is diverse, as they are part of multiple biosynthesis pathways besides sterol biosynthesis (**Figure 7**). They are essential for posttranslational modification reactions, including the prenylation of proteins (see Chapter 1.2.2), formation of ubiquinones (see Chapter 1.2.3) and dolichols (see Chapter 1.2.5), as well as heme A biosynthesis (see Chapter 1.2.4). Isopentenyl pyrophosphate is additionally used in the

## Introduction

modification of specific tRNA (see Chapter 1.2.1). In fungal cells, isoprenoids can also be part of carotenoid biosynthesis (1.2.6) next to their role as quorum sensing molecules (1.2.7).

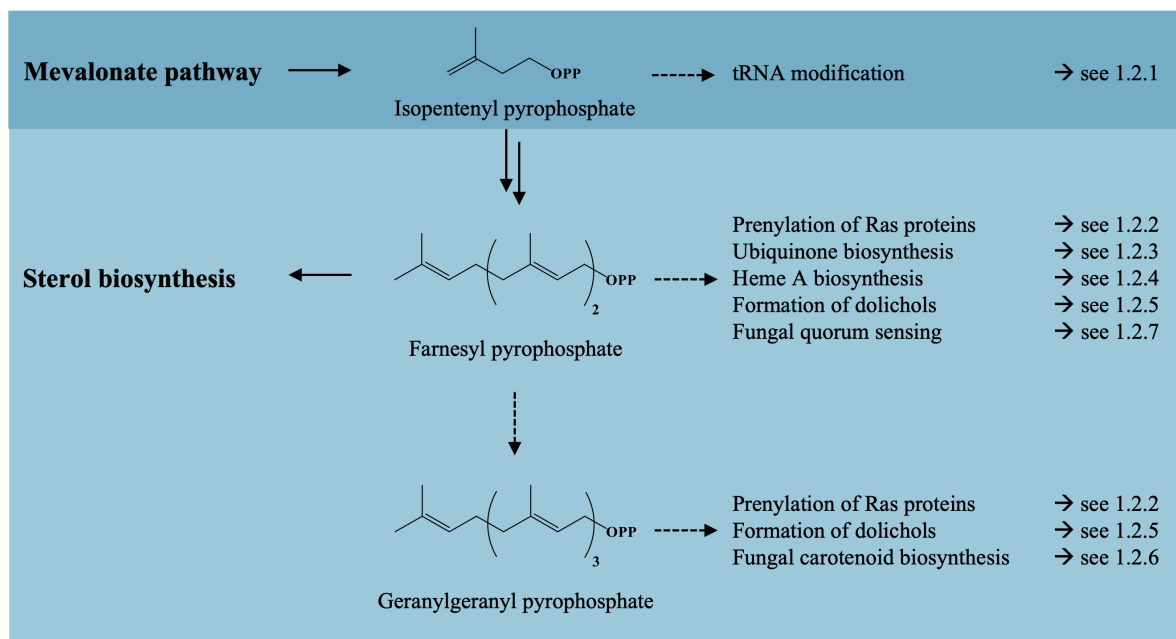


**Figure 7:** Overview of the diverse roles, isoprenoid pyrophosphates take in mammalian and fungal cells. Solid arrows: preferred pathways, dotted arrows: side pathways, PP: pyrophosphate.

### 1.2.1 tRNA Modification

Isoprenylation of tRNA is a rare modification in eukaryotes and bacteria, whose function is not fully understood, but is linked to quality of translation, and suppression of non-sense mutations [23]. tRNA isopentenyl transferase binds base A37 of the anticodon stem loop and catalyzes the interaction of adenine with DMAPP in a nucleophilic  $S_N2$  reaction with pyrophosphate as leaving group (**Figure 8**) [23].

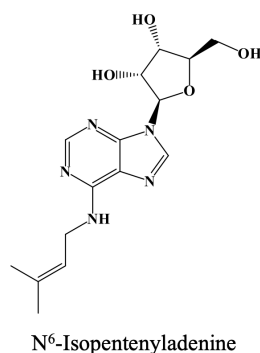


**Figure 8:** Structure of prenylated adenine: N<sup>6</sup>-isopentenyladenine.

### 1.2.2 Prenylation of Ras Proteins

Counting more than 150 human analogues, the Ras (“Rat sarcoma virus”) guanosine triphosphatases (GTPases) are the best-known group of small G-proteins, binding and hydrolyzing guanosine triphosphate (GTP) [24]. Even though GTPases show high affinity towards GTP and guanosine diphosphate (GDP), the proteins have a low intrinsic hydrolysis activity [25]. Therefore, guanine-nucleotide-exchange factors (GEFs) and GTPase-activating proteins (GAPs) are mandatory to form an active GTP/inactive GDP bound form [24,25]. The Ras

## Introduction

superfamily can be divided into five smaller groups: Ras, Rho, Rab, Ran and Arf. While the Ran group does not undergo posttranslational modification reactions and the members of the Arf group are modified with the fatty acid myristate, a majority of the remaining groups undergo posttranslational modification reactions by prenylation [24].

Protein prenylation is a posttranslational modification reaction, in which farnesyl and/or geranylgeranyl moieties get linked to the C-terminal cysteine to enable a better membrane association or subcellular localization of a protein. The enzymes catalyzing these reactions are called farnesyl transferases (FTs) or geranylgeranyl transferases (GGTs), respectively [10]. In which way a G-protein is prenylated depends on the C-terminal amino acid sequence. Typically, proteins from the Ras and Rho family share a CAAX recognition motif (C = cysteine, A = aliphatic amino acid, X = variable amino acid), which can be recognized by FT and GGT1 (**Figure 9**). While FT prefers X to be methionine, serine, glutamine or cysteine, GGT1 prefers X to be leucine or isoleucine [10,24,25]. Proteins from the Rab family are usually prenylated by GGT2 [24].

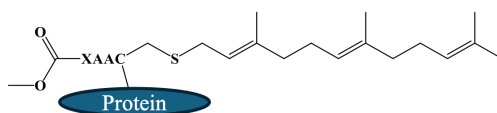


**Figure 9:** General structure of prenylated (farnesylated) G-proteins, including the CAAX recognition motif (C = cysteine, A = aliphatic amino acid, X = variable amino acid).

Ras proteins are important signaling nodes affecting diverse cytoplasmatic effectors and thereby influence the cytoplasmatic signaling networks. Gene expression, cell proliferation, differentiation and survival are influenced by them [24]. The interest in FT inhibitors arose, when in cancer research the *ras* gene was attributed to oncogenic activities and prenylation steps were identified to activate their malignant effects [10].

The Rho GTPases have been implicated in multiple diverse roles including the modulation of gene expression and cell cycle progression *via* signaling networks. Further the small G-proteins are necessary for cell-cell/cell-matrix interactions, as well as endo- and exocytosis processes. Due to their multi-dimensional roles, different GEFs and GAPs are needed to regulate the diverse functions so their multiple downstream effectors can be utilized [24].

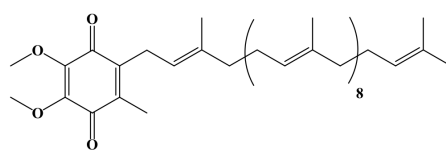
Rab proteins are the biggest group in the Ras superfamily. In their function they mainly regulate the intracellular transport of vesicles between donor and acceptor compartments as well as proteins between cellular organelles [24].

### 1.2.3 Ubiquinone Biosynthesis

Ubiquinone, also known as coenzyme Q (CoQ) is an important lipophilic membrane stabilizer and antioxidant biosynthesized endogenously in the mitochondria of eukaryotic cells which prevents the oxidation of proteins, lipids and DNA (**Figure 10**) [14]. In mitochondria it further influences the membrane transition pore, protein uncoupling, fatty acid oxidation, uridine biosynthesis and oxidative phosphorylation which finally leads to the production of ATP [13,14]. Ubiquinones consist of a redox active quinone head group and a hydrophobic polyisoprenoid tail that get attached to each other by the prenyltransferase COQ2 (human)/ Coq2p (fungal). While the quinone head group originates from amino acid tyrosine, the isoprenoid tail arises in the isoprenoid biosynthesis pathway (see Chapter 1.1.2). Both structure motives are generated outside the mitochondria before they are brought into them by so far unknown mechanisms. The prenyltransferases, decaprenyl-diphosphate synthase

## Introduction

subunit (PDSS) 1 and PDSS2 (human)/ Coq1p (fungal) catalyze the head-to-tail chain polymerization of IPP units on FPP [14]. Chain length mainly depends on the organism. While human PDSS1/2 predominantly catalyzes the formation of chains with ten isoprenoid units, the *S. cerevisiae* enzyme, Coq1p, prefers six isoprenoid units [13].



Ubiquinone

**Figure 10:** Structure of ubiquinone (coenzyme Q) as it can be found in human cells.

### 1.2.4 Heme A Biosynthesis

In the group of Heme proteins, the probably most important member is Heme B. Besides its role as a component of hemoglobin, Heme B additionally serves as the educt for the formation of Heme A, which is an important prosthetic group in the cytochrome A-containing respiratory oxidases [26]. Besides a formyl group instead of a methyl group on position C8 of the porphyrin complex, Heme A also contains a hydroxyethylfarnesyl chain, which is in place of the vinyl group on C2 (**Figure 11**). The formation of Heme A is catalyzed by two enzymes. In a first reaction, heme O synthase catalyzes the modification of the educt, Heme B, in position C2. Heme O synthase therefore uses FPP as a co-substrate to form the stable intermediate Heme O. The subsequent reaction providing Heme A, is catalyzed by Heme A synthase and requires molecular oxygen [26].

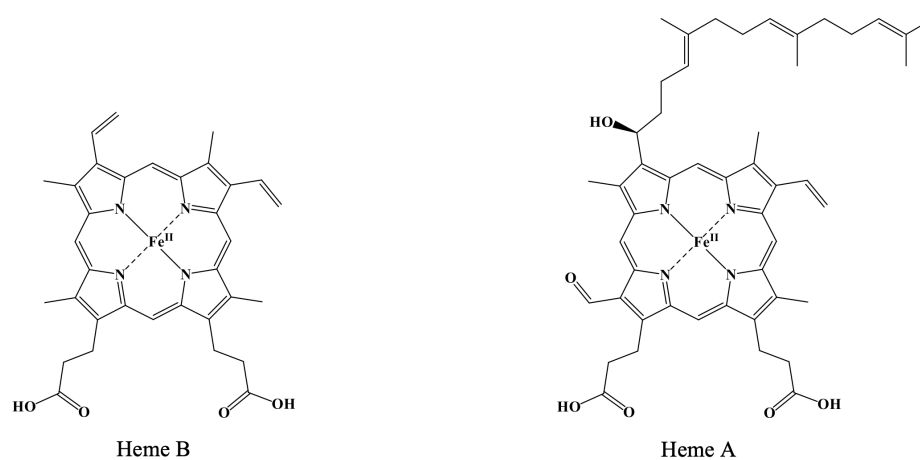


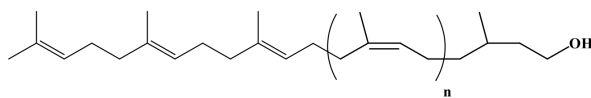
**Figure 11:** Structure of the two porphyrin complexes heme B and heme A.

### 1.2.5 Formation of Dolichols

While fungal dolichols range from 14-17 isoprenoid units, mammalian dolichols range from 18-21 isoprenoid units (**Figure 12**). The main functions of dolichols are *O*-/ and *N*-glycosylations of proteins, as well as the biosynthesis of glycosylphosphatidylinositol anchors in the endoplasmic reticulum [12,27]. Formation of dolichols starts with FPP or GGPP, to which IPP units are added subsequently until the specific chain length is reached. The elongation of the polyprenyl pyrophosphate (PolyP-PP) is considered to be fully catalyzed by *cis*-isoprenyl transferase in yeasts and humans [27]. For further dolichol biosynthesis, PolyP-PP undergoes enzymatic modifications, whose respective enzymes are not fully described [27]. Starting with the dephosphorylation of

## Introduction

PolyP-PP to the single phosphorylated intermediate (PolyP-P) in a second dephosphorylation the free polyprenol is generated. The alpha-isoprene of the polyprenol intermediate is subsequently reduced by an NADPH consuming reductase to form the alpha saturated dolichol. In a final step, dolichol kinase phosphorylates dolichol to dolichol phosphate, which functions as the lipid anchor in the ER membrane [12,27].

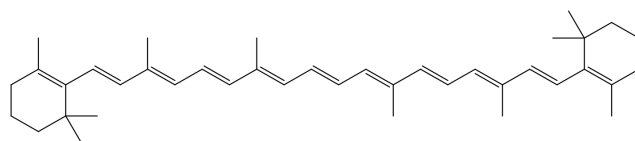


Dolichol

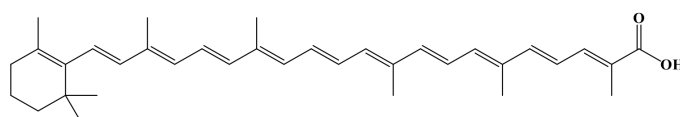
**Figure 12:** General structure of dolichols. While  $n$  is between 11-14 in fungal cells, in mammalian cells  $n$  ranges from 15-18.

### 1.2.6 Fungal Carotenoid Biosynthesis

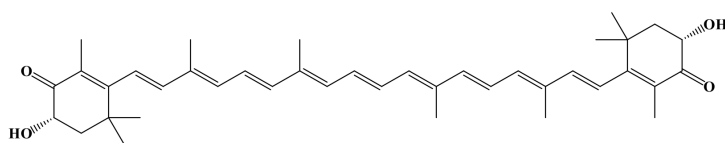
Carotenoids are a class of terpenoids, that are widespread in nature but not produced in animal cells. In plants they have important functions in metabolic and physiological processes including photosynthesis [28]. Even though they are not essential in fungal survival, several fungi can produce carotenoids. In their function as antioxidants, they help to inactivate oxygen radicals that occur due to light and UV radiation. Therefore, the carotenoid biosynthesis is photo-regulated in several fungi. Fungal carotenoid biosynthesis starts using two units GGPP, that condensate to phytoene. Phytoene is desaturated to lycopene from which on diverse carotenoids, *e.g.*,  $\beta$ -carotenes, neurosporaxanthins and astaxanthins are formed (**Figure 13**) [28,29].



$\beta$ -Carotene



Neurosporaxanthin



Astaxanthin

**Figure 13:** Structure of the fungal carotenoids,  $\beta$ -carotene, neurosporaxanthin and astaxanthin.

### 1.2.7 Fungal Quorum Sensing

Quorum sensing (QS) describes the ability of a growing microorganism to exchange signals with the extracellular chemical and physical environment [30]. The mechanism is used to sense the presence of other species and communicate with them [31]. QS was exclusively described for prokaryotes until in 2001 Hornby *et al.* [30] identified farnesol as a quorum sensing molecule (QSM) in the dimorphic fungus *Candida albicans*. Dimorphism is the ability of a fungus to either appear as a budding yeast or germ-tube forming mycelia. In *C.*

## Introduction

*albicans* farnesol influences the yeast-to-mycelium conversion [30,32]. Whether there is a high concentration of farnesol *C. albicans* appears as a yeast, without the formation of new germ tubes. Increased concentrations of farnesol usually occur in growing fungi, but the same effect could be observed when farnesol was added during experimental conditions [30]. Next to the morphological appearance, QSMs can influence biofilm formation, virulence, antimicrobial resistance, and mycotoxin production [31-33]. In addition, fungi use QS to determine the cell density of their own population [31,33].

First hints for a correlation between increased virulence and high farnesol levels were figured out by Navarathna *et al.* [34], who investigated the pathogenicity of *C. albicans* pre-treated with subinhibitory (“still... some cell growth” [34]) concentrations of the post-squalene pathway inhibitor fluconazole in a mouse model. Mice administered pre-treated *C. albicans* showed an up to four times higher mortality rate than the control group, infected with untreated pathogens. Extracellular farnesol concentrations were twelve times higher, intracellular levels were six times higher in the fluconazole group than the levels of the control group [34].

Further evidence for decreased lethality in combination with low farnesol concentrations was found in a second *Candida* mouse model by Tashiro *et al.* [35]. In their experiment they evaluated the effects of pravastatin on *Candida* infections. Therefore, statin concentrations were increased above the typical range used for the treatment of hyperlipidemia, to target the fungal HMG-CoA reductase. A positive correlation between decreased farnesol concentrations and an increased survival rate of the mice was concluded [35].

Leonhardt *et al.* [36] additionally investigated the effects of the fungal QSM on the cells of human immune response that are known to be important for fungal clearance. On the one hand, farnesol induced the activation of monocytes and neutrophils and thereby enhanced inflammation. On the other hand, the activated monocytes were interfered in their differentiation to immature dendritic cells by the QSM. Consequently, the immature dendritic cells were only capable to give dysfunctional response and lacked in T-cell activation and excretion of Th1 [36].

In combination with antimycotics, *e.g.*, fluconazole and micafungin, synergistic effects of farnesol have been observed in the treatment of several *Candida* infections. Even fluconazole resistance reversion could be achieved for *C. albicans* strains, when they were additionally exposed to farnesol [33]. An explanation for the synergism could be an increased level of reactive oxygen species, as well as the influence of the amphiphilic farnesol on membrane integrity, fluidity and permeability [33].

### 1.3 Regulation of Cholesterol Biosynthesis

Cholesterol homeostasis is a highly regulated process, which is affected at several levels. In the human body a small portion of this important biomolecule is resorbed from nutrients while up to 80% (800 mg) are synthesized *via* endogenous cholesterol biosynthesis every day [5,37]. The endogenous biosynthesis itself is regulated by feedback mechanisms, with HMG-CoA reductase as the rate determining enzyme (see Chapter 1.4).

However, cholesterol biosynthesis can also be influenced exogenously, by mevalonate pathway inhibitors, that are useful in the treatment of hypercholesterolemia. HMG-CoA reductase (**Figure 2**, enzyme **e**) inhibitors and ATP citrate lyase (**Figure 2**, enzyme **a**) inhibitors are the only two approved classes of cholesterol biosynthesis lowering drugs (see Chapter 1.5). However, a lack of isoprenoids, which is accompanied by insufficient prenylation reactions (see Chapter 1.2) can induce severe side effects [38].

Strategies to develop inhibitors targeting enzymes of the post-squalene pathway and thereby avoiding a loss of isoprenoids failed so far. Triparanol, which was launched on the market in 1960 as a sterol C24-reductase

## Introduction

inhibitor, was later identified to be a multienzyme inhibitor [39] and already withdrawn two years after it was launched. The reasons were numerous side effects including vomiting, nausea, hair loss and compromised vision. In few cases triparanol was also suspected to reduce the number of white blood cells [40]. Late cholesterol biosynthesis as potential target additionally seems inappropriate, when considering various inherited genetic defects that disrupt endogenous cholesterol biosynthesis and are often associated with significant symptoms and increased mortality (see Chapter 1.6).

Interestingly no approved cholesterol lowering drug is on the market that targets the isoprenoid pathway, even though the pathway contains potential target enzymes [38] and no inherited disorders are described that affect its enzymes. Therefore, development of an isoprenoid pathway inhibitor could be a promising objective for a new class of cholesterol lowering drugs (see Chapter 2).

In antifungal treatment, however, the enzymes of the post-squalene pathway are a prominent target for azoles (sterol C14-demethylase, **Figure 6**, enzyme **o\***), morpholines (sterol C14-reductase and sterol C8-isomerase) and allylamines (squalene epoxidase, **Figure 4**, enzyme **I**) (see Chapter 1.7). Also, in the field of antimycotics, no drugs are on the market targeting the isoprenoid pathway even though it contains putative target enzymes (see Chapter 4) [41] for potential new classes of inhibitors (see Chapter 2).

### 1.4 Endogenous Control of Cholesterol Biosynthesis

The rate limiting step of mammalian cholesterol biosynthesis is catalyzed by the enzyme HMG-CoA reductase (HMGR), which is regulated by multivalent feedback mechanisms in its activity. Next to a sterol dependent transcription control, mRNA translation can be influenced, as well as the rate of reductase degradation and phosphorylation [42,43].

Transcriptional regulation of the *HMGR* gene is mediated by sterol regulatory element binding proteins (SREBPs). SREBPs are associated with a SREBP-cleavage-activating protein (SCAP) in the endoplasmic reticulum (ER) membrane. In the case of high sterol concentrations, the SREBP2-SCAP agglomerate interacts with an insulin-induced gene (INSIG) protein, which blocks the binding site of coat protein II (COPII) and causes the complex to retain in the ER membrane. Whereas when ER cholesterol is depleted, the SREBP2-SCAP complex is transferred to the Golgi apparatus *via* COPII vesicles, while INSIG proteins get ubiquitinated and degraded in proteasomes. At the Golgi apparatus the proteolytic activation of SREBP is proposed by two membrane specific proteases, site 1 protease (S1P) and site 2 protease (S2P). The processed SREBP is then transferred to the nucleus where it activates the transcription of specific sterol regulatory genes including *HMGR* and *INSIG1*. Besides the direct *INSIG* regulated feedback mechanism, further regulatory mechanisms exist, that hinder SREBP2 from exiting the ER membrane [5,8,42].

On the level of HMGR mRNA translation, a poorly described isoprenoids-including mechanism is responsible for the translational regulation of the enzyme [44].

Degradation of the ER membrane bound HMGR is induced by ubiquitylation *via* INSIG and elevated sterol levels. At high concentrations of oxysterols *e.g.*, 25/27-hydroxycholesterol and methylated sterols such as lanosterol, they interact with the HMGR's sensitive binding sites, followed by an INSIG induced ubiquitylation and proteasomal degradation of HMGR. Geranylgeraniol can accelerate this mechanism by facilitating the transfer of a specific prenyltransferase (UBIAD1) to the Golgi apparatus, which would otherwise disturb the INSIG-HMGR interaction [5,42].

## Introduction

A further regulating mechanism influencing the activity of HMGR is the phosphorylation state of a specific serine (in humans: Ser872) of the enzyme's catalytic domain. HMGR can be phosphorylated by adenosine monophosphate activated protein kinase (AMPK), which blocks the enzyme, when intracellular adenosine triphosphate (ATP) levels are low [42,43].

### 1.5 *Inhibitors of the Mevalonate Pathway*

Next to autoregulatory mechanisms influencing endogenous sterol levels, sterol biosynthesis enzymes are an important target for the treatment of several diseases including cardiovascular diseases (CVDs) and mycoses (see Chapter 1.7). According to the World Health Organization (WHO), CVDs are the leading cause of global mortality, accounting for approximately 17.9 million deaths, or 32% of all global deaths annually (2019) [45]. Atherosclerotic CVD (ACVD), in particular, has been strongly correlated with increased low-density lipoprotein (LDL) levels. LDLs are the predominant transport form of cholesterol, with approximately 50% of the sterol as their main component. The development of atherosclerotic plaques is initiated by the gradual accumulation of LDL particles in the blood, leading to their deposition on the surfaces of epithelial cells. Concurrently, the oxidation of LDLs in the bloodstream stimulates inflammatory responses, which in turn promote the proliferation of foam cells, further contributing to the development of atherosclerotic plaques [5].

As a first line treatment for hypercholesterolemia, statins are used to prevent ACVD. Therefore, atorvastatin was the best-selling drug worldwide in 2006 [4]. However, side effects including muscle weakness, cramps, several myopathies, and life-threatening rhabdomyolyses, prevent 7-29% of all statin-treated patients from receiving the guideline's required doses [38,46]. One explanation to the numerous side effects is the loss of isoprenoids that were needed for secondary prenylation reactions (see Chapter 1.2) [38].

Besides statins, bempedoic acid was approved by the Food and Drug Administration (FDA) and the European Medicines Agency (EMA) in 2020 for the treatment of hypercholesterolemia in statin intolerant patients. Bempedoic acid is a liver specific, first in class prodrug which inhibits ATP citrate lyase, the enzyme providing acetyl-CoA for sterol biosynthesis [46,47]. Due to the specific activation of bempedoic acid in liver tissue, side effects that affect skeletal muscle may be reduced [46]. Nevertheless, side effects induced by a lack of prenylation remain.

### 1.6 *Defects in Cholesterol Biosynthesis*

A potential answer to the lack of cholesterol lowering drugs targeting the post-squalene pathway are six inherited disorders, that have been linked to specific enzymatic defects in cholesterol biosynthesis. Two further disorders, mevalonic aciduria (MAA) and a syndrome called hyperimmunoglobulinemia D and periodic fever syndrome (HIDS) affect the same gene encoding the enzyme mevalonate kinase (MVK, **Figure 2**, enzyme **e**), an enzyme of the mevalonate pathway [43]. MAA and HIDS occur due to defects of the MVK gene and are therefore often summarized as mevalonate kinase deficiency because the clinical symptoms are overlapping. The autoinflammatory disease is characterized by skin rash, abdominal pain, recurrent episodes of fever and other inflammatory symptoms [48]. Cells of patients with HIDS have a MVK enzyme activity up to 10% compared to control values, whereas MAA patients have no detectable activity [43]. As a consequence, biosynthesis of essential isoprenoids is lacking, which hinders an appropriate prenylation of several molecules, e.g., the small G-proteins of the Ras superfamily. There is evidence that inflammatory hyperresponsiveness, especially the hypersecretion of IL-1 $\beta$  may be affected by the lack of prenylation, rather than the accumulation of mevalonic acid [49].

## Introduction

The remaining genetic disorders exclusively affect enzymes of the post-squalene pathway in cholesterol biosynthesis, while there is no inherited disorder described that affects the enzymes of the isoprenoid pathway. In **Table 1** an overview of the relevant genetic disorders and thereby affected enzymes is listed. In contrast to the remaining defects, the gene encoding sterol C14-demethylase is not directly affected in the Antley-Bixler syndrome. In fact, the decreased activity of sterol C14-demethylase is a secondary effect, due to mutations in the *POR* gene encoding cytochrome P450 (CYP450) oxidoreductase, a mandatory electron donor of sterol C14-demethylase [50]. Sufficient electron supply is essential for CYP450 activity and inhibiting its electron supply was identified as a promising, novel strategy in antifungal therapy (see Chapter 3).

Affected enzyme	Associated inherited disorder
Mevalonate kinase	Mevalonic aciduria
Mevalonate kinase	Hyperimmunoglobulinemia D and periodic fever syndrome
Sterol C7-reductase	Smith-Lemli-Opitz syndrome
Sterol C24-reductase	Desmosterolosis
Sterol C5-desaturase	Lathosterolosis
Sterol C14-reductase	Greenberg skeletal dysplasia /HEM skeletal dysplasia
Sterol C8-isomerase	Conradi-Hünemann-Happle syndrome, CHILD syndrome
Sterol C4-demethylase complex	CHILD syndrome
(Sterol C14-demethylase	Antley-Bixler syndrome)

**Table 1:** Genetic disorders affecting cholesterol biosynthesis. In brackets: cholesterol biosynthesis associated inherited disorder. CHILD: Congenital hemidysplasia with ichthyosiform erythroderma and limb defects; HEM: Hydrops ectopic calcification-moth-eaten.

### 1.7 Inhibitors of Ergosterol Biosynthesis

Inhibiting sterol biosynthesis is not only an effective way to prevent CVDs (see Chapter 1.5) but also a valuable tool to treat fungal infections. Fungal germs are often underestimated but cause up to 3.8 million deaths per year (2019-21) of which 2.5 million were directly attributed to fungal infections [51]. The most dangerous of them are invasive mycoses that are in some cases not immediately recognized as fungal infections which can make them life threatening. Inhibitors of ergosterol biosynthesis, antimycotics, can be classified according to their molecular or enzymatic target. While polyenes interact with ergosterol itself (lower affinity to cholesterol [52]) imidazoles/triazoles, morpholines and allylamines affect enzymes of the post-squalene pathway.

For polyenes there are two postulated mechanisms of action. According to the first model (ion channel model), polyenes like amphotericin B (AmB) lead to an accumulation of reactive oxygen species in the cytoplasm after forming 1:1 adducts with ergosterol. Those aggregates form small channels that increase fungal membrane permeability [52-54]. The second model suggests the formation of large, extracellular AmB aggregates that extract ergosterol from fungal bilayer membranes and thereby kill the fungal cell (sponge model) [54].

Imidazoles (*e.g.*, clotrimazole, ketoconazole)/triazoles (*e.g.*, fluconazole, posaconazole) are inhibitors of the enzyme sterol C14-demethylase. Their mechanism of action is based on the direct interaction of one nitrogen in the imidazole/triazole ring with the heme iron of the enzyme. As a result of that interaction, oxygen can no longer be activated, which is the necessary step for sterol C14-demethylase activity [55,56]. A possible mechanism

## Introduction

of fungal azole resistance is in relation to the electron supply of sterol C14-demethylase (see Chapter 3) which was already identified to be crucial for the mammalian enzyme (see Chapter 1.6, Antley-Bixler syndrome).

Morpholines (*e.g.*, amorolfine) are capable to inhibit two ergosterol biosynthesis enzymes, sterol C14-reductase and sterol C8-isomerase, in a synergistic way. The mechanism of action is based on the protonated form of morpholines at physiological pH, imitating two reactive carbenium ion intermediates in the conversions catalyzed by these enzymes [57].

Inhibitors of the allylamine class target the enzyme squalene epoxidase, which is followed by an accumulation of toxic squalene and reduced ergosterol levels [57].

The effects of inhibitors affecting the isoprenoid biosynthesis pathway will explicitly be highlighted in Chapter 5.

## 2. Objective

The increasing number of invasive fungal infections caused the WHO to rise the “WHO fungal priority pathogens list to guide research, development and public health action”[58] in 2022. The document classified *Aspergillus fumigatus* among others as one of the most critical fungal germs. Fungal infections threaten human health and account up to 3.8 million deaths per year (2019-21) [51]. By the analysis of the distal sterol patterns of *A. fumigatus* strains that were provided by the group of Assoc.-Prof. Fabio Gsaller of Medical University of Innsbruck, we revealed that specific mutations in the cytochrome P450 gene affect azole resistance (see Chapter 3). As this is only one of multiple adaptations and resistance mechanisms fungal germs develop, the urge to identify new targets for antifungal therapy is high. The latest antimycotics in development are using innovative modes of action *e.g.*, Gwt1 (Glycosylphosphatidylinositol-anchored wall protein transfer 1) inhibitors (fosmanogepix, phase III) and dihydroorotate dehydrogenase inhibitors (olorofim, phase III) [59]. Fosmanogepix (FSX) targets a fungal specific inositol acyltransferase which is necessary for glycosylphosphatidylinositol (GPI) biosynthesis and thereby hinders GPI-anchored mannoprotein from expression on fungal cell surfaces [59,60]. Olorofim (OLF) inhibits fungal pyrimidine biosynthesis by hindering the formation of orotate from dihydroorotate [59].

As further potential targets we identified ergosterol biosynthesis and its early enzymes of the isoprenoid pathway to be essential for fungal survival (see Chapter 4) [41]. Therefore, the primary objective of this work was the development of a gas chromatography-mass spectrometry (GC-MS) based analytical approach which can be used to analyze isoprenoids and isoprenoid pyrophosphates from different matrices such as cells and growth media (see Chapter 4). The assay should be an extension to the already established approaches of Müller *et al.* to analyze ergosterol [22] and cholesterol [18] biosynthesis intermediates in the post-squalene pathway.

First steps to analyze the isoprenoid pathway were already done by Dr. Florian Vetter in the Bracher group in 2018, who developed an assay to identify inhibitors in the pre-squalene pathway of cholesterol biosynthesis [61]. The work of Dr. Vetter was the basis of my Master’s thesis project in which the approach should have been adapted to analyze fungal matrices [62]. However, the original assay described by Dr. Vetter [61] was lacking in precision and robustness. One of the main issues was an insufficient derivatization of isoprenoids with benzoyl chloride (esterification). Derivatization is essential due to the large variability in isoprenoid molecule size (C<sub>5</sub>-C<sub>20</sub>). On the one hand retention of small analytes like prenol and isoprenol (C<sub>5</sub> isomers) must be sufficient to separate the isomers, on the other hand geranylgeraniol (C<sub>20</sub> isoprenoid) should still be detectable within the same run. Therefore, silylation with a bulky silylation reagent like *tert*-butyldiphenylchlorosilane (*t*BDPSCI) was established as part of my Master’s thesis project to guarantee complete derivatization and sufficient retention [62].

Subsequently, further weaknesses of the original method [61] were revealed, including contaminations, an insufficient extraction resulting in low recovery, as well as ineffective conditions for enzymatic deconjugation of pyrophosphates. Deconjugation of pyrophosphates from isoprenoids was a crucial step in sample preparation. While isoprenoids are easily evaporable in a GC-MS setup, their corresponding pyrophosphates remain unvaporizable under GC-MS conditions. In addition, uncharged isoprenoids can be extracted from aqueous milieus like cell pellets or growth media with organic solvents more easily than the at physiological pH charged pyrophosphates.

## Objective

Within the scope of my Master's thesis project, these weaknesses were systematically identified and investigated. Nevertheless, the optimization of all critical steps was beyond the scope of that thesis [62]. Consequently, in my ongoing PhD project the approach was fully optimized and finally validated in line with the 2011 European Medicines Agency (EMA) "Guideline on bioanalytical method validation" [63] (see Chapter 4).

The final approach was applied to *A. fumigatus* mutant strains with specific modifications in isoprenoid pathway genes, provided by Prof. Johannes Wagener from Trinity College Dublin in cooperation with Assoc.-Prof. Fabio Gsaller. Next to establishing a novel analytical approach, one of the main findings was the identification of fungal squalene synthase gene *erg9*, encoding for the respective enzyme, to be essential which therefore could be a novel target in future antifungal drug development.

To avoid negative side effects, selectivity of experimental compounds or promising drug candidates is a pivotal aim in drug development. By expanding the analytical approach from the fungal pre-squalene pathway to the mammalian pre-squalene pathway, the selectivity of experimental drugs targeting the pre-squalene pathway of cholesterol biosynthesis could be investigated and sufficient inhibition of a specific fungal/mammalian target could be identified more easily. As, in addition, the isoprenoid section of sterol biosynthesis is not the primary target of established cholesterol biosynthesis inhibitors, even though several enzymes of it were suggested to be potentially druggable [38], a further aim of my work was to adapt the new approach to mammalian matrices (see Chapter 5).

Our findings from fungal strains (see Chapter 4) also rose the interest in investigating isoprenoid patterns, showing the distribution of isoprenoids and their respective pyrophosphates between cellular and extracellular matrices. By testing literature described inhibitors of fungal and mammalian sterol biosynthesis on human leukemia 60 (HL60) cells, structure-activity relationships were investigated and made the developed assay even more widely applicable.

Due to the wide scope of our assays to analyze isoprenoids and sterols in mammalian and fungal cells, we were interested to test our approaches on the fungal strain *Alternaria brassicicola* which showed reduced growth in presence of the plant sterol dehydroepiandrosterone (DHEA) in a previously not investigated way (see Chapter 6). As a proof of concept, whether DHEA affected the isoprenoid or post-squalene pathway of ergosterol biosynthesis, the group of Dr. Jan Klein from Friedrich Schiller University Jena provided us with samples of DHEA treated *A. brassicicola* which were analyzed with our approaches according to Liebl *et al.* (see Chapter 4) and Müller *et al.* [22] (see Chapter 6).

### 3. Azole Resistance in *Aspergillus fumigatus*

A. Kühbacher, P. Merschak, H. Haas, **M. Liebl**, C. Müller, F. Gsaller; The cytochrome P450 reductase CprA is a rate-limiting factor for Cyp51A-mediated azole resistance in *Aspergillus fumigatus*. *Antimicrobial Agents and Chemotherapy*. 2023; 67(11). Impact factor: 4.1 (2/2025)

#### 3.1 Summary

The cytochrome P450 (CYP450) enzyme sterol C14-demethylase (called CYP51 in *Aspergillus fumigatus*) has a pivotal role in ergosterol biosynthesis and is therefore a prominent target addressed by the class of azole antifungals. The catalyzed reaction is a three-step oxidation which requires molecular oxygen and NADPH in every step to transform the C14-methyl group into a formic acid leaving group. The formal demethylation is accompanied by the introduction of a C14, C15 double bond [64]. Electron support, necessary for these redox reactions is covered by additional cytochrome P450 reductases.

Azole antifungals target the heme iron in the active site of CYP51 and thereby prevent the oxidation of the natural substrates [16]. Inhibition of this enzyme in *A. fumigatus* is followed by an accumulation of C14-methylated ergosterol biosynthesis intermediates, e.g., eburicol and lanosterol. However, the toxic 14-methylergosta-8,24-diene-3,6-diol, which has fungicidal effects is not formed in quantities in *A. fumigatus* under azole treatment [20]. Therefore, the accumulation of C14-methylated sterols in combination with ergosterol depletion has only a fungistatic effect in *A. fumigatus*, which gives the microorganisms time to adapt and develop resistance mechanisms [56]. The most frequent resistance mechanisms include amino acid substitutions that change the constitution of the active binding site, overexpression of efflux pumps, and overexpression of target enzymes like CYP51 itself [16,65].

In this work our focus was on the investigation of cytochrome P450 reductases, *cprA*, *cprB* and cytochrome b<sub>5</sub>-reductase (*CybE*), that deliver the essential electrons for CYP51 function [66]. As the level of *cyp51* transcription does not fully correlate with fungal azole resistance, it was considered that sufficient electron supply is a complementary factor elevating antimicrobial resistance in CYP51 overexpressing strains. By generating several inducible *A. fumigatus* mutant strains, in which *cprA*, *cprB* or *CybE* could be separately activated, the effect of each electron supporter was characterized. Increased azole resistance could be observed through elevated minimal inhibitory concentrations (MIC). In addition, changes in the sterol pattern could be observed when different mutant strains and growth conditions were compared to their respective control groups. Decreased eburicol and elevated ergosterol levels were indicators for the observed azole resistance and increased MICs. For clinically relevant isolates carrying mutations e.g., tandem repeats (TRs) in the *cyp51* promotor, that induce CYP51 overexpression, azole resistance could be increased by additionally overexpressing *cprA*, which was identified as the pivotal rate-limiting factor. Until now, the synergistic role of *cprA* overexpression on antimicrobial resistance was not investigated in clinically isolates. Therefore, a screening of clinically relevant isolates for mutations affecting CYP51 electron supporters could bring insight, whether these mutations also occur naturally.

### 3.2 Personal Contribution

#### Overview:

Conceptualization:	F.G.
Methodology:	A.K., P.M., <b>M.L.</b> , C.M., F.G.
Data curation:	A.K., P.M., H.H., <b>M.L.</b> , C.M., F.G.
Formal analysis:	A.K., P.M., H.H., <b>M.L.</b> , C.M., F.G.
Writing – original draft:	F.G.
Writing – review and editing:	A.K., H.H., <b>M.L.</b> , C.M., F.G.

#### Note:

My contribution to this work was the sterol profiling according to Müller *et al.* [22], including sample preparation, the analysis of the data, formal analysis and data curation. From the created data Figure 3 and Table S3 were designed by me. Further, the draft for the “sterol measurements” section in the “Materials and methods” section was prepared by me.

Dr. Christoph Müller was involved in this work as he and Assoc.-Prof. Gsaller conceptualized the required sterol measurements in which Dr. Müller supervised me.

The creation of the different inducible fungal strains, creation of further figures, data analysis as well as the experimental processing were done by Alexander Kühbacher.

Prof. Hubertus Haas was also involved in data curation and analysis.

All mentioned co-authors contributed to this work in editing and reviewing of the manuscript.

Petra Merschak was involved in this work by MIC testing and preparing the lyophilized samples that were used for sterol profiling.

## 3.3 Article

Antimicrobial Agents  
and Chemotherapy

Mycology | Full-Length Text

## The cytochrome P450 reductase CprA is a rate-limiting factor for Cyp51A-mediated azole resistance in *Aspergillus fumigatus*

Alexander Kühbacher,<sup>1</sup> Petra Merschak,<sup>1</sup> Hubertus Haas,<sup>1</sup> Maximilian Lieb,<sup>2</sup> Christoph Müller,<sup>2</sup> Fabio Gsaller<sup>1</sup>**AUTHOR AFFILIATIONS** See affiliation list on p. 8.

**ABSTRACT** Azole antifungals remain the “gold standard” therapy for invasive aspergillosis. The world-wide emergence of isolates resistant to this drug class, however, developed into a steadily increasing threat to human health over the past years. In *Aspergillus fumigatus*, major mechanisms of resistance involve increased expression of *cyp51A* encoding one of two isoenzymes targeted by azoles. Yet, the level of resistance caused by *cyp51A* upregulation, driven by either clinically relevant tandem repeat mutations within its promoter or the use of high expressing heterologous promoters, is limited. Cytochrome P450 enzymes such as Cyp51A rely on redox partners that provide electrons for their activity. *A. fumigatus* harbors several genes encoding putative candidate proteins including two paralogous cytochrome P450 reductases, CprA and CprB, and the cytochrome *b<sub>5</sub>* CybE. In this work, we investigated the contribution of each *cprA*, *cprB*, and *cybE* overexpression to *cyp51A*-mediated resistance to different medical and agricultural azoles. Using the bidirectional promoter *Pxy1P*, we conditionally expressed these genes in combination with *cyp51A*, revealing *cprA* as the main limiting factor. Similar to this approach, we overexpressed *cprA* in an azole-resistant background strain carrying a *cyp51A* allele with TR34 in its promoter, which led to a further increase in its resistance. Employing sterol measurements, we demonstrate an enhanced eburicol turnover during upregulation of either *cprA* or *cyp51A*, which was even more pronounced during their simultaneous overexpression. In summary, our work suggests that mutations leading to increased Cyp51A activity through increased electron supply could be key factors that elevate azole resistance.

**KEYWORDS** *Aspergillus fumigatus*, azole resistance, *cyp51A*, sterol C14-demethylase, cytochrome P450 reductase

Members of the azole antifungal drug class constitute the preferred option for first-line treatment of invasive aspergillosis (1, 2), an often deadly infection that is mainly caused by the ubiquitous fungal mold pathogen *Aspergillus fumigatus* (3). Four years ago, the Centers for Disease Control and Prevention in the United States put azole-resistant *A. fumigatus* on the watch list for antimicrobial resistance threats, and only recently, this pathogenic mold was listed within the critical group of the World Health Organization’s fungal priority pathogens list (4, 5). The world-wide occurrence and increase in azole-resistant isolates progressively develop into a threat to current medical therapeutic strategies (6, 7). Clinical resistance is mainly connected to mutations of the azole drug target encoding gene *cyp51A* or its promoter. However, a large proportion is attributed to non-*cyp51A*-based resistance mechanisms such as those arising from mutations of genes encoding 3-hydroxy-3-methyl-glutaryl-coenzyme A reductase Hmg1, components of the CCAAT-binding complex, efflux pumps as well as so far uncharacterized mutations (8–10).

Inhibition of Cyp51 by azoles leads to the accumulation of toxic C14-methylated sterols and concomitant reduced ergosterol production (11). TR34/L98H and TR46/

**Editor** Andreas H. Groll, University Children’s Hospital, Münster, Münster, Germany

Address correspondence to Fabio Gsaller, Fabio.Gsaller@i-med.ac.at.

The authors declare no conflict of interest.

See the funding table on p. 9.

**Received** 12 July 2023

**Accepted** 12 August 2023

**Published** 10 October 2023

Copyright © 2023 Kühbacher et al. This is an open-access article distributed under the terms of the [Creative Commons Attribution 4.0 International license](https://creativecommons.org/licenses/by/4.0/).

Y121F/289A (12–15), two of the most common mechanisms of azole resistance found in clinical isolates across the world (9), diminish growth-hampering, antifungal effects by azoles at least, in part, by overexpressing *cyp51A*. TR34 and TR46 (14, 15) as well as the less common TR53 and TR120 (16, 17) illustrate tandem repeats (TRs) in the *cyp51A* promoter that contain duplications of binding sites for its transcriptional activators SrbA and AtrR (18–22). *In vitro* studies using recombinant strains demonstrated that increased expression of *cyp51A* caused by TR34, TR46 or high-expressing constitutive promoters, is limited to approximately 2- to 4-fold (12, 13, 15, 23). In this regard, it has to be mentioned that cytochrome P450 enzymes such as sterol C14-demethylase Cyp51A require two electrons for their catalytic activity that are provided by redox partners such as the NADPH cytochrome P450 reductase (CPR) and/or cytochrome *b*<sub>5</sub>, which is part of the cytochrome *b*<sub>5</sub> reductase (CB5R) system (24, 25) (Fig. 1). Through the NADPH-connected electron transport chain, it was originally proposed that P450 enzymes receive the electrons that are critical for their enzymatic activity *via* two single electron steps from NADPH cytochrome P450 reductase. Cytochrome *b*<sub>5</sub> was also suggested to provide electrons, however, only the second in this cycle (26). Later, work on Cyp51-based azole sensitivity in yeast revealed cytochrome P450 reductase as the main, but not only factor providing the two electrons for Cyp51 activity (27) as overexpression of the cytochrome *b*<sub>5</sub> encoding gene *CYB5* could increase ketoconazole resistance in a CPR-deficient background (28). This led to the hypothesis that both necessary electrons

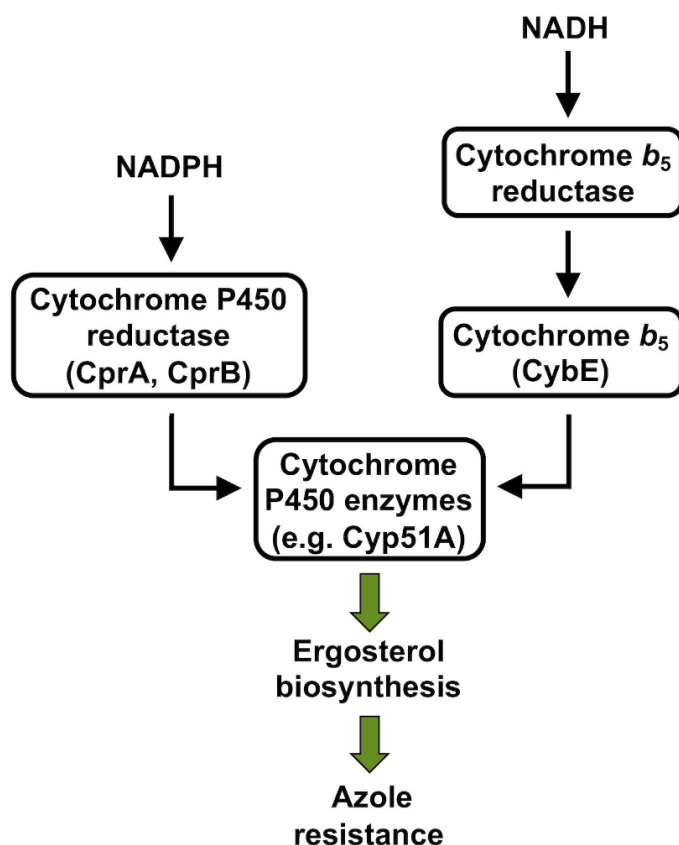


**FIG 1** Proposed electron transfer path from NADPH and NADH by cytochrome P450 reductase and cytochrome *b*<sub>5</sub> to cytochrome P450 enzymes in *A. fumigatus*. Black arrows illustrate the delivery of electrons. Green arrows indicate the consequent positive impact on ergosterol biosynthesis and azole resistance.

for Cyp51 activity can be delivered by the CB5R system, which was confirmed soon after (25). Based on the necessity of sufficient electron supply for P450 enzymatic activity, it is somewhat not surprising that the increase in *cyp51A* transcript or protein content does not fully correlate with the level of resistance. The *A. fumigatus* genome encodes two putative CPRs, CprA (AFUB\_077020) and CprB (AFUB\_023960), as well as the cytochrome *b*<sub>5</sub> CybE (AFUB\_021740) which together with NADH cytochrome *b*<sub>5</sub> reductase constitutes the CB5R system in this fungus (29).

In this work, we studied the consequences of overexpression of each component *cprA*, *cprB*, and *cybE* during simultaneous upregulation of *cyp51A* on *A. fumigatus* resistance to triazole-based sterol C14-demethylase inhibitors (further called azoles) of medical (voriconazole, VRZ; itraconazole, ITZ; isavuconazole, ISZ) and agricultural (tebuconazole, TBZ; epoxiconazole, EPZ) importance (1, 30, 31). For the conditional expression mutant displaying the highest degree of azole resistance, sterol measurements were carried out to monitor the impact of its increased activity on the turnover of eburicol, substrate of Cyp51A, as well as ergosterol. We further conditionally expressed the candidate in a recipient strain carrying a *cyp51A* allele with TR34 in its promoter, to assess the consequences of increased activity of the Cyp51A redox partner during TR-driven upregulation of *cyp51A*.

## RESULTS

### Combined overexpression of *cyp51A* and *cprA* leads to high levels of azole resistance

Similar to the clinically relevant tandem repeat mutations found in TR34/L98H and TR46/Y121F/T289A (12, 13, 15), it has been demonstrated that overexpression of *cyp51A* increases resistance to azoles, however, only to a certain extent (23). Based on previous work that focused on CPR and cytochrome *b*<sub>5</sub> (25, 27–29, 32, 33), we speculated that a shortage of Cyp51A redox partners could be rate-limiting in this scenario. To test this hypothesis, we overexpressed *cyp51A* (strain *cyp51A<sup>PxyIP</sup>*) together with *cprA* (strain *cprAcyp51A<sup>biPxyIP</sup>*) and *cprB* (strain *cprBcyp51A<sup>biPxyIP</sup>*) as well as *cybE* (strain *cybEcyp51A<sup>biPxyIP</sup>*), utilizing the bidirectional, xylose-inducible promoter *PxyIP* (34, 35). Susceptibilities of strains (Fig. 2) to different azoles were monitored during non-inducing (–xylose) and inducing (+xylose) conditions (Table 1). In comparison to wild type (wt), overexpression of *cyp51A* on its own raised minimum inhibitory concentration (MIC) levels 2- to 4-fold to VRZ, ITZ, ISZ, TBZ, and EPZ. While increased expression of *cprB* and *cybE* together with *cyp51A* elevated resistance only marginally in comparison with *cyp51A<sup>PxyIP</sup>* only, concomitant upregulation of *cyp51A* and *cprA* led to a ≥8-fold increase in resistance to all compounds tested. To assess the influence of increased *cprA* expression on its own, we generated the strain *cprA<sup>PxyIP</sup>* carrying a *PxyIP*-driven *cprA* copy. Upregulation of *cprA* elevated MICs similar to that observed for induction of *cyp51A* only.

TABLE 1 MIC values of strains carrying tunable gene variants of *cyp51A* as well as its potential redox partners<sup>a</sup>

	VRZ MIC (μg/mL)		ITZ MIC (μg/mL)		ISZ MIC (μg/mL)		TBZ MIC (μg/mL)		EPZ MIC (μg/mL)	
	–xyl	+ xyl								
A1160P+ (wt)	0.25	0.25	0.5	0.5	0.5	0.5	1	1	4	4
<i>cyp51A<sup>PxyIP</sup></i>	0.25	0.5–1	0.5	1	0.5	1	1	4	4	16
<i>cprAcyp51A<sup>biPxyIP</sup></i>	0.25	2–4	0.5	>16	0.5	4	1	16	4	>16
<i>cprBcyp51A<sup>biPxyIP</sup></i>	0.25	1	0.5	1	0.5	1	1	4	4	16
<i>cybEcyp51A<sup>biPxyIP</sup></i>	0.25	1	0.5	1	0.5	1	1	4	4	16
<i>cprA<sup>PxyIP</sup></i>	0.25	0.5–1	0.5	1	0.5	1	1	4	4	16

<sup>a</sup>Voriconazole (VRZ), itraconazole (ITZ), isavuconazole (ISZ), tebuconazole (TBZ), and epoxiconazole (EPZ) susceptibilities of strains were analyzed following the broth microdilution method according to EUCAST (37). Strains were grown in the presence (+xyl) and absence (–xyl) of 1% xylose.

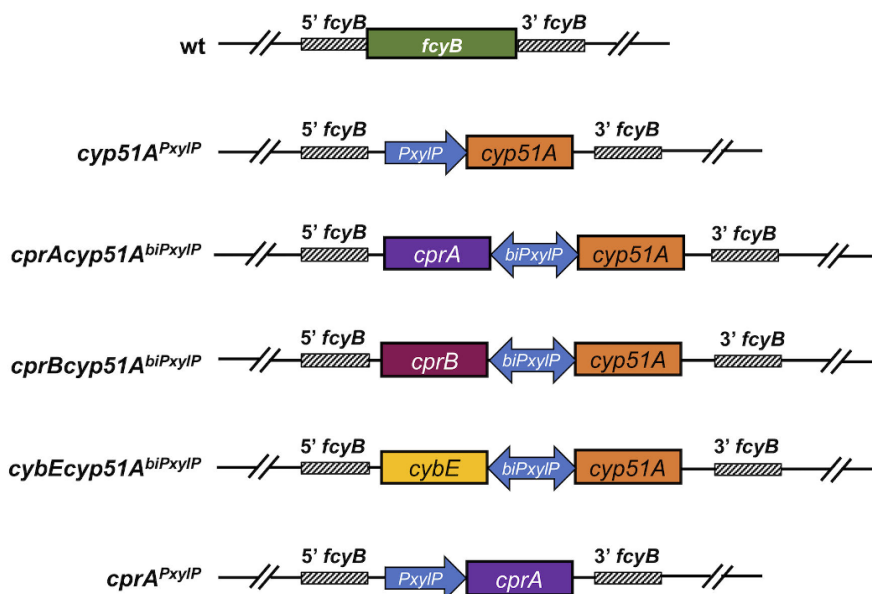


**FIG 2** Scheme of strains carrying tunable gene variants of *cyp51A* and its potential redox partners. Constructs comprising gene cassettes with *P*<sub>XylP</sub>-driven *cyp51A* (*cyp51A*<sup>*P*<sub>XylP</sub></sup>) and *cprA* (*cprA*<sup>*P*<sub>XylP</sub></sup>) as well as *cyp51A* in combination with *cprA* (*cprAcyp51A*<sup>*biP*<sub>XylP</sub></sup>), *cprB* (*cprBcyp51A*<sup>*biP*<sub>XylP</sub></sup>), and *cybE* (*cybEcyp51A*<sup>*biP*<sub>XylP</sub></sup>) under bidirectional (*biP*<sub>XylP</sub>) control of *P*<sub>XylP</sub> (35) were site-directed integrated at the counterselectable marker locus *fcyB* (36).

### Overexpression of *cprA* leads to increased eburicol turnover and elevates ergosterol levels during voriconazole treatment

The high level of resistance of the strain carrying *cprAcyp51A*<sup>*biP*<sub>XylP</sub></sup> suggests that this strain harbors significantly increased Cyp51A activity during *P*<sub>XylP</sub>-inducing conditions. To monitor the corresponding effects on sterol C14-demethylation and ergosterol biosynthesis, we analyzed the impact of individual and combined overexpression of *cyp51A* and *cprA* on the sterol pattern with focus on the turnover of the Cyp51A substrate eburicol and the final product ergosterol, in the presence and absence of VRZ which is employed as a first-line treatment against invasive aspergillosis (1). Under non-inducing conditions, eburicol and ergosterol levels in wt were 0.6% and 92.4% relative to the total sterol content, respectively (Fig. 3, for details, see Table S3). VRZ exposure led to an increase of eburicol to 17.1% and reduction of ergosterol to 76.5%. Similar levels of eburicol (17.1%–17.6%) and ergosterol (76.0%–76.5%) were detected in the tunable mutant strains without induction. In agreement with their potential contribution to Cyp51A-mediated sterol C14-demethylation, induction of either *cprA* or *cyp51A* decreased the eburicol content (*cprA*<sup>*P*<sub>XylP</sub></sup>: 10.4%; *cyp51A*<sup>*P*<sub>XylP</sub></sup>: 5.8%) and increased ergosterol levels (*cprA*<sup>*P*<sub>XylP</sub></sup>: 82.7%; *cyp51A*<sup>*P*<sub>XylP</sub></sup>: 86.8%). This effect was most pronounced in *cprAcyp51A*<sup>*biP*<sub>XylP</sub></sup>. During simultaneous overexpression of both genes, eburicol levels were reduced to 3.2% and ergosterol levels were increased to 89.2%.

### Overexpression of *cprA* in strains carrying *cyp51A*<sup>TR34</sup> alleles potentiates resistance to azoles

Similar to *P*<sub>XylP</sub>-induced upregulation of *cyp51A*, TR34 leads to elevated *cyp51A* expression and as a result increased azole resistance (13, 15). Our data suggest that additional mutations that elevate CprA activity could further elevate azole resistance in clinical isolates that carry TRs causing increased *cyp51A* expression. To test this idea, a mutant

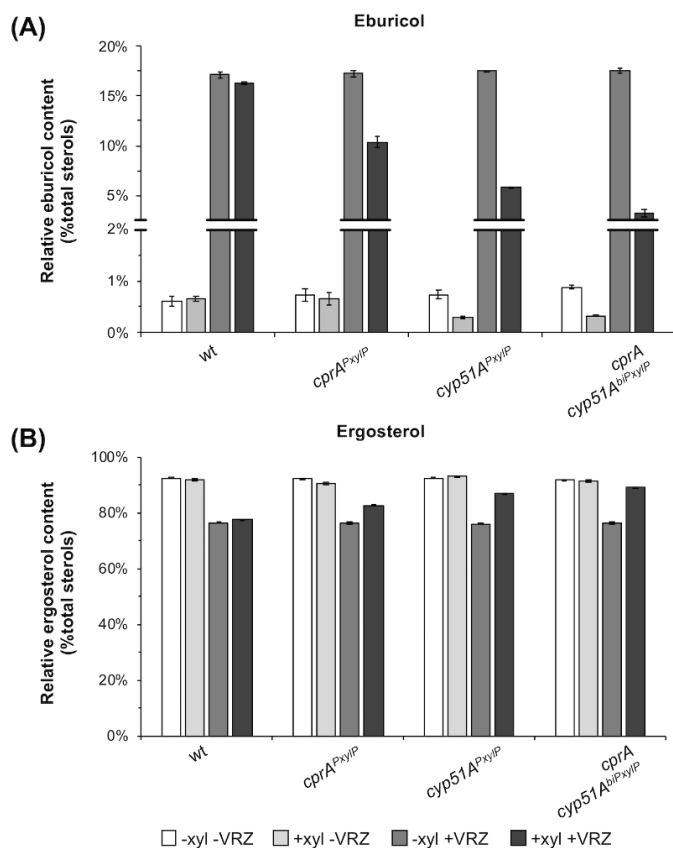


**FIG 3** Relative amounts of (A) eburicol and (B) ergosterol in conditional expression strains in the presence (+VRZ) and absence of voriconazole (–VRZ). Strains were grown in liquid AMM during inducing (+xyl) and non-inducing (–xyl) conditions. Error bars indicate the standard deviation of the respective samples.

carrying a *cyp51A* allele with the TR34 mutation in its promoter (*cyp51A*<sup>TR34</sup>) was generated and subsequently equipped with the tunable *cprA* expression cassette (*cyp51A*<sup>TR34</sup>*cprA*<sup>PxyIP</sup>, Fig. 4). The strain *cyp51A*<sup>TR34/L98H</sup> harboring the combined *cyp51A* mutation TR34/L98H, resembling one of the most common alleles conferring clinical pan-azole resistance, served as high azole resistance control. As a further reference, strain *cyp51A*<sup>WT</sup> (21) carrying a non-mutated *cyp51A* allele was employed which displayed wt-like azole susceptibilities (Table 2). Depending on the compound tested, *cyp51A*<sup>TR34</sup> and *cyp51A*<sup>TR34/L98H</sup> showed an increase in the MICs of 2- to ≥4-fold and 8- to ≥32-fold,

**TABLE 2** MIC values of strains with the clinically relevant mutation TR34 and/or the xylose inducible *cprA*<sup>a</sup>

	VRZ MIC (µg/mL)		ITZ MIC (µg/mL)		ISZ MIC (µg/mL)		TBZ MIC (µg/mL)		EPZ MIC (µg/mL)	
	–xyl	+xyl								
<i>cyp51A</i> <sup>WT</sup>	0.25	0.25	0.5	0.5	0.5	0.5	1	1	4–8	4–8
<i>cyp51A</i> <sup>TR34</sup>	1	1	1–2	1–2	2	1–2	4	4	>16	>16
<i>cyp51A</i> <sup>WT</sup> <i>cprA</i> <sup>PxyIP</sup>	0.25	1	0.5	1	0.5	1	1	4	4	16
<i>cyp51A</i> <sup>TR34</sup> <i>cprA</i> <sup>PxyIP</sup>	1	4	1–2	>16	2	4	4	16	>16	>16
<i>cyp51A</i> <sup>TR34/L98H</sup>	2–4	2–4	>16	>16	4–8	4	16	16	>16	>16

<sup>a</sup>Voriconazole (VRZ), itraconazole (ITZ), isavuconazole (ISZ), tebuconazole (TBZ), and epoxiconazole (EPZ) susceptibilities of strains were analyzed following the broth microdilution method according to EUCAST (37). Strains were grown in the presence (+xyl) and absence (–xyl) of 1% xylose.

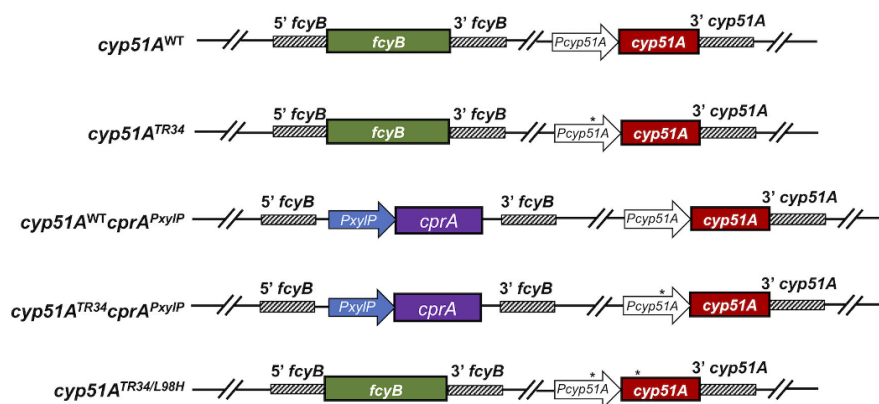


**FIG 4** Strains carrying the clinically relevant mutation TR34 and/or the xylose inducible *cprA*. wt and resistance-conferring *cyp51A* alleles were inserted at the *cyp51A* locus in a *cyp51A* deletion background. The inducible *cprA* construct was integrated in *cyp51A*<sup>WT</sup> (non-mutated reference allele) and *cyp51A*<sup>TR34</sup> at the *fcyB* locus (36). \* denotes TR34 and/or the L98H mutation in the promoter and coding sequence of *cyp51A*, respectively.

respectively. Similar to *cyp51A*<sup>TR34</sup>, overexpression of *cprA* on its own (*cyp51A*<sup>WT</sup>*cprA*<sup>PxyIP</sup>) increased resistance 2- to 4-fold. In combination with the TR34-allele (*cyp51A*<sup>TR34</sup>*cprA*<sup>PxyIP</sup>), induction of *cprA* elevated MIC levels of the different azoles 8- to  $\geq 32$ -fold, resembling a similar level of resistance than that observed for *cyp51A*<sup>TR34/L98H</sup>.

## DISCUSSION

Members of the sterol C14-demethylase Cyp51 family are highly conserved among eukaryotes and one of the best-studied cytochrome P450 enzymes in fungi (38, 39). Cyp51 enzymes in pathogenic fungi are of particular interest for antifungal therapy, as one of the most used antifungal drug classes in clinical treatment, the azoles, target this enzyme (40). The future clinical use of azoles has been challenged over the past years by a dramatic rise in resistance (6, 7). Hence, increasing our knowledge on mechanisms that confer resistance is crucial for the adaptation and optimization of current therapeutic approaches. As stated above, upregulation of *cyp51A* is a key characteristic of TR34/L98H and TR46/Y121F/T289A that contributes to pan-azole resistance (12, 13, 15). In this work, we aimed to elucidate the main redox partner of Cyp51A that might limit azole resistance in *A. fumigatus*. The candidates investigated included CprA and CprB as well as CybE (29, 41). We overexpressed the respective genes together with *cyp51A* using the bidirectional promoter *PxyIP* (35) and unveiled CprA as the major factor contributing to Cyp51A-driven azole resistance. Upregulation of *cprA* on its own already led to a moderate increase in resistance to the different azoles tested (2- to 4-fold), which suggests that at least during azole treatment, CprA activity is limiting for Cyp51A activity. The combined overexpression of *cprA* and *cyp51A* elevated MIC levels for all medical azole compounds above the clinical breakpoints suggested by EUCAST (42).

With regard to the distinctive role of CprA in this context, it has to be mentioned that *A. fumigatus* is predicted to express 77 cytochrome P450 enzymes and each CprA, CprB, and CybE might have different specificities for the individual P450 enzymes (29, 41, 43) that have yet to be characterized. Despite the fact that co-overexpression of *cybE* and *cyp51A* did not have a major impact on azole resistance when compared to overexpression of *cyp51A* only (Table 1), previous work demonstrated that the absence of CybE leads to an accumulation of eburicol, a decrease in ergosterol and, in line, increased VRZ susceptibility (29). Moreover, its loss led to a compensatory upregulation of *cyp51A* and *cprA* gene expression (29). Therefore, CybE might not be a rate-limiting factor to elevate azole resistance during *cyp51A* overexpression, but the reduced eburicol turnover in a

*cybE* null mutant clearly suggests a crucial role of this component to maintain wt-like sterol C14-demethylation.

The present study suggests that increased activity of the Cyp51A redox partner CprA can further elevate azole resistance during *cyp51A* overexpression. Thus, mutations elevating its activity, e.g., *cprA* promoter mutations or those affecting transcription factors that lead to upregulation of the gene, could cause an unfavorable increase azole resistance during treatment, particularly in strains with preceding mutations that lead to *cyp51A* upregulation such as the abovementioned TRs. In this regard, it is interesting to note that a previously identified clinically resistant isolate carrying TR53, did not contain mutations within the *cyp51A* coding sequence (16). Its level of resistance could not be explained by the TR mutation on its own but rather resulted from extracistronic alterations such as modification of *cprA*. Testing a similar scenario, we overexpressed *cprA* in the strain containing TR34 in the *cyp51A* promoter, which raised resistance to different azoles 4- to  $\geq 8$ -fold (compare strain *cyp51A*<sup>TR34</sup> with *cyp51A*<sup>TR34</sup>*cprA*<sup>PxyIP</sup>, Table 2).

Collectively, as already indicated in previous work (27, 44–46) and further corroborated by this work, we anticipate that inhibitors of CPRs could serve as promising synergistic compounds to counteract azole resistance or to decrease the azole concentrations required for treatment.

## MATERIALS AND METHODS

### Determination of the minimum inhibitory concentration

MIC analyses were performed according to the EUCAST broth microdilution method (37). To induce *PxyIP*-driven expression of genes, 1% xylose was supplemented to the medium. Azole compounds used in this study were VRZ, ITZ, ISZ, EPZ, and TBZ (Sigma-Aldrich Corp., St. Louis, MI, USA).

### Generation of plasmids and fungal transformation

Oligonucleotides, strains, and plasmids used in this work are displayed in Tables S1 and S2; Fig. S1, respectively. Generally, to assemble DNA fragments with the plasmid backbones, the NEBuilder HiFi DNA assembly Master Mix (New England Biolabs, Ipswich, MA, USA) was used. Plasmids containing inducible expression cassettes of *cyp51A* only as well as its combination with *cprA*, *cprB*, and *cybE* were constructed as follows. First, the plasmid p $\Delta$ fcyB\_*cyp51A*<sup>PxyIP</sup> was generated carrying *cyp51A* under control of *PxyIP*. Prior to assembly, the *PxyIP*-*cyp51A* expression cassette was amplified from p $\Delta$ fcyA\_*cyp51A*<sup>PxyIP</sup> (47) using primers pX-cass-FW/RV, the backbone allowing integration of the linearized plasmid at the counterselectable marker locus *fcyB* from plasmid pfcyB using primers BBdel-FW/RV (36). To generate bidirectional expression constructs, a backbone was generated by amplifying the plasmid p $\Delta$ fcyB\_*cyp51A*<sup>PxyIP</sup> with primers bixylP-BB-FW/RV. *cprA*, *cprB*, and *cybE* coding sequences including 500–800 bp 3' non-translated region were amplified from genomic DNA employing primers cprAbixylP-FW/RV, cprBbixylP-FW/RV, and cybEbixylP-FW/RV, respectively. Subsequently, the backbone and each component were assembled giving rise to p $\Delta$ fcyB\_*cprA**cyp51A*<sup>bipxyIP</sup>, p $\Delta$ fcyB\_*cprB**cyp51A*<sup>bipxyIP</sup>, and p $\Delta$ fcyB\_*cybE**cyp51A*<sup>bipxyIP</sup>. For single overexpression of *cprA*, the coding sequence was amplified from genomic DNA using cprAxyIP-FW/RV. The fragment was then assembled with a backbone amplified from p $\Delta$ fcyB\_*cyp51A*<sup>PxyIP</sup> using primers pX-FW.2/RV.2 yielding plasmid p $\Delta$ fcyB\_*cprA*<sup>PxyIP</sup>. The plasmid pcyp51A<sup>TR34</sup>, comprising TR34 within the *cyp51A* promoter, was created with the plasmid pcyp51A<sup>WT</sup> (21) using a DNA duplex. Therefore, 50  $\mu$ M of each primer 34mer-FW/RV was mixed and annealed by denaturation at 95 °C for 3 min and gradually cooling to room temperature. Subsequently, the duplex was phosphorylated with T4 Polynucleotide kinase (New England Biolabs, Ipswich, MA, USA). Next, the pcyp51A<sup>WT</sup> plasmid was linearized with *cyp51A*-TR-BB-FW/RV and ligated with the phosphorylated primer-duplex using T4 DNA ligase (New England Biolabs, Ipswich, MA, USA). The L98H point mutation was

introduced into *pcyp51A*<sup>TR34</sup> with primers *cyp51A*-L98H-FW/RV giving rise to *pcyp51A*<sup>TR34/L98H</sup>.

With the exception of *pcyp51A*<sup>TR34</sup> and *pcyp51A*<sup>TR34/L98H</sup>, plasmids were *NotI*-linearized and transformed into A1160P+ (48), here referred to as wt, resulting in site-directed integration at the marker locus *fcyB* (47). *pcyp51A*<sup>TR34</sup> and *pcyp51A*<sup>TR34/L98H</sup> were *KpnI*-linearized and transformed into  $\Delta$ *cyp51A*, which led to site-specific integration at the *cyp51A* deletion locus as described recently for *pcyp51A*<sup>WT</sup> (21). The resulting strains were designated *cyp51A*<sup>TR34</sup> and *cyp51A*<sup>TR34/L98H</sup>. *cyp51A*<sup>TR34</sup> and its reference strain *cyp51A*<sup>WT</sup> were further transformed with *p* $\Delta$ *fcyB\_cprA*<sup>PxyIP</sup> giving rise to *cyp51A*<sup>TR34</sup>*cprA*<sup>PxyIP</sup> and *cyp51A*<sup>WT</sup>*cprA*<sup>PxyIP</sup>.

Fungal transformation of plasmids targeting the *fcyB* and *cyp51A* loci was carried out as previously described (21, 36). Correct integrations of constructs were validated by Southern blot analysis.

### Sterol measurements

Sterol analysis of wt, *cyp51A*<sup>PxyIP</sup>, *cprA*<sup>PxyIP</sup>, and *cprA**cyp51A*<sup>bipxyIP</sup> was performed in triplicates in AMM (49) containing 1% glucose and 20 mM ammonium tartrate as carbon and nitrogen source, respectively. The xylanase promoter was induced with 1% xylose, and VRZ was used in a final concentration of 0.02  $\mu$ g/mL. Cultures were inoculated with  $1 \times 10^6$  spores/mL and incubated at 37 °C for 20 h at 200 rpm. Mycelia were harvested by filtration, shock-frozen, and lyophilized. Subsequently, freeze-dried mycelia were pulverized.

Sterol extraction was performed according to Müller *et al.* (50) using 6 mg freeze-dried mycelia. As described by Müller *et al.* (51), sterols were analyzed as their corresponding trimethylsilyl (TMS) ethers using GC-MS. The individual sterol TMS ethers were identified by their relative retention times (RRT) as well as their specific mass spectra. In total, 12 sterols were detected (for details, see Table S3), and the base peak of each sterol TMS ether was taken as a quantifier ion for calculating the peak areas: cholestane (internal standard, IS) *m/z* 217, RRT 1.00; ergosta-5,8,22-trien-3 $\beta$ -ol (lichesterol) *m/z* 363, RRT 1.29; ergosta-5,7,22-trien-3 $\beta$ -ol (ergosterol) *m/z* 363, RRT 1.32; ergosta-7,22-dien-3 $\beta$ -ol (5-dihydroergosterol) *m/z* 343, RRT 1.34; ergosta-5,7,22,24(28)-tetraen-3 $\beta$ -ol *m/z* 466, RRT 1.35; ergosta-7,22,24(28)-trien-3 $\beta$ -ol *m/z* 343, RRT 1.37; ergosta-5,7,24(28)-trien-3 $\beta$ -ol (5-dehydroepisterol) *m/z* 363, RRT 1.38; ergosta-5,7-dien-3 $\beta$ -ol *m/z* 365, RRT 1.40; ergosta-7,24(28)-dien-3 $\beta$ -ol (episterol) *m/z* 343, RRT 1.40; 4,4,14-trimethylcholesta-8,24(28)-dien-3 $\beta$ -ol (lanosterol) *m/z* 343, RRT 1.43; 4-methylergosta-8,24(28)-dien-3 $\beta$ -ol (4-methylfecosterol) *m/z* 379, RRT 1.45; 4,4-dimethylergosta-8,24(28)-dien-3 $\beta$ -ol (eburicol) *m/z* 407, RRT 1.49; 4,4-dimethylergosta-8,24(28)-dien-3 $\beta$ -ol *m/z* 408, RRT 1.51.

For quantification, an external calibration with ergosterol TMS ether was used. The relative sterol levels were determined by plotting the amount of each sterol against the total amount of sterols found in one sample (52).

### ACKNOWLEDGMENTS

This project has received funding from the Austrian Science Fund (FWF) (grant P35951 to F.G.)

### AUTHOR AFFILIATIONS

<sup>1</sup>Institute of Molecular Biology, Biocenter, Medical University of Innsbruck, Innsbruck, Austria

<sup>2</sup>Department of Pharmacy, Center for Drug Research, Ludwig-Maximilians Universität München, Munich, Germany

AUTHOR ORCID*s*Hubertus Haas  <http://orcid.org/0000-0003-2472-9878>Fabio Gsaller  <http://orcid.org/0000-0002-9257-8648>

## FUNDING

Funder	Grant(s)	Author(s)
Austrian Science Fund (FWF)	P35951	Fabio Gsaller

## AUTHOR CONTRIBUTIONS

Alexander Kühbacher, Data curation, Formal analysis, Investigation, Methodology, Validation, Visualization, Writing – review and editing | Petra Merschak, Data curation, Formal analysis, Methodology | Hubertus Haas, Formal analysis, Investigation, Writing – review and editing | Maximilian Liebl, Data curation, Formal analysis, Methodology, Validation, Writing – review and editing | Christoph Müller, Data curation, Formal analysis, Methodology, Validation, Writing – review and editing | Fabio Gsaller, Conceptualization, Funding acquisition, Investigation, Project administration, Resources, Supervision, Writing – original draft, Writing – review and editing

## ADDITIONAL FILES

The following material is available [online](#).

## Supplemental Material

Tables S1 to S3 & Fig. S1 (AAC00918-23-s0001.pdf). The file contains all supplemental Tables and Figures mentioned in the manuscript.

## REFERENCES

- Ullmann AJ, Aguado JM, Arikan-Akdagli S, Denning DW, Groll AH, Lagrou K, Lass-Flörl C, Lewis RE, Munoz P, Verweij PE, Warris A, Ader F, Akova M, Arendrup MC, Barnes RA, Beigelman-Aubry C, Blot S, Bouza E, Brüggemann RJM, Buchheidt D, Cadranel J, Castagnola E, Chakrabarti A, Cuenca-Estrella M, Dimopoulos G, Fortun J, Gangneux J-P, Garbino J, Heinz WJ, Herbrecht R, Heussel CP, Kibbler CC, Klimko N, Kullberg BJ, Lange C, Lehnbecher T, Löffler J, Lortholary O, Maertens J, Marchetti O, Meis JF, Pagano L, Ribaud P, Richardson M, Roilides E, Ruhnke M, Sanguinetti M, Sheppard DC, Sinkó J, Skiada A, Vehreschild MJGT, Viscoli C, Cornely OA. 2018. Diagnosis and management of *Aspergillus* diseases: executive summary of the 2017 ESCMID-ECMM-ERS guideline. *Clin Microbiol Infect* 24 Suppl 1:e1–e38. <https://doi.org/10.1016/j.cmi.2018.01.002>
- Patterson TF, Thompson GR, Denning DW, Fishman JA, Hadley S, Herbrecht R, Kontoyiannis DP, Marr KA, Morrison VA, Nguyen MH, Segal BH, Steinbach WJ, Stevens DA, Walsh TJ, Wingard JR, Young J-A, Bennett JE. 2016. Practice guidelines for the diagnosis and management of Aspergillosis: 2016 update by the infectious diseases society of America. *Clin Infect Dis* 63:433–442. <https://doi.org/10.1093/cid/ciw444>
- Earle K, Valero C, Conn DP, Vere G, Cook PC, Bromley MJ, Bowyer P, Gago S. 2023. Pathogenicity and virulence of *Aspergillus fumigatus*. *Virulence* 14:2172264. <https://doi.org/10.1080/21505594.2023.2172264>
- World Health Organization. 2022. Fungal priority pathogens list to guide research, development and public health action. Available from: <https://www.who.int/publications/i/item/9789240060241>
- Centers for Disease Control and Prevention. 2018. Antibiotic resistance threats in the United States. Available from: <https://www.cdc.gov/drugresistance/biggest-threats.html>
- Verweij PE, Lucas JA, Arendrup MC, Bowyer P, Brinkmann AJF, Denning DW, Dyer PS, Fisher MC, Geenen PL, Gisi U, Hermann D, Hoogendijk A, Kiers E, Lagrou K, Melchers WJG, Rhodes J, Rietveld AG, Schoustra SE, Stenzel K, Zwaan BJ, Fraaije BA. 2020. The one health problem of azole resistance in *Aspergillus fumigatus*: current insights and future research agenda. *Fung Biol Rev* 34:202–214. <https://doi.org/10.1016/j.fbr.2020.10.003>
- Meis JF, Chowdhary A, Rhodes JL, Fisher MC, Verweij PE. 2016. Clinical implications of globally emerging azole resistance in *Aspergillus fumigatus*. *Philos Trans R Soc Lond B Biol Sci* 371:20150460. <https://doi.org/10.1098/rstb.2015.0460>
- Nywening AV, Rybak JM, Rogers PD, Fortwendel JR. 2020. Mechanisms of triazole resistance in *Aspergillus fumigatus*. *Environ Microbiol* 22:4934–4952. <https://doi.org/10.1111/1462-2920.15274>
- Garcia-Rubio R, Cuenca-Estrella M, Mellado E. 2017. Triazole resistance in *Aspergillus* species: an emerging problem. *Drugs* 77:599–613. <https://doi.org/10.1007/s40265-017-0714-4>
- Hortschansky P, Misslinger M, Morl J, Gsaller F, Bromley MJ, Brakhage AA, Groll M, Haas H, Huber EM. 2020. Structural basis of HapE(P88L)-linked antifungal triazole resistance in *Aspergillus fumigatus*. *Life Sci Alliance* 3. <https://doi.org/10.26508/lsa.202000729>
- Dhingra S, Cramer RA. 2017. Regulation of sterol biosynthesis in the human fungal pathogen *Aspergillus fumigatus*: opportunities for therapeutic development. *Front Microbiol* 8:92. <https://doi.org/10.3389/fmicb.2017.00092>
- Snelders E, Camps SMT, Karawajczyk A, Rijs AJMM, Zoll J, Verweij PE, Melchers WJG. 2015. Genotype-phenotype complexity of the TR46/Y121F/T289A *cyp51A* azole resistance mechanism in *Aspergillus fumigatus*. *Fungal Genet Biol* 82:129–135. <https://doi.org/10.1016/j.fgb.2015.06.001>
- Snelders E, Karawajczyk A, Verhoeven RJA, Venselaar H, Schaftenaar G, Verweij PE, Melchers WJG. 2011. The structure-function relationship of the *Aspergillus fumigatus cyp51A* L98H conversion by site-directed mutagenesis: the mechanism of L98H azole resistance. *Fungal Genet Biol* 48:1062–1070. <https://doi.org/10.1016/j.fgb.2011.08.002>
- van der Linden JWM, Camps SMT, Kampinga GA, Arends JPA, Debets-Ossenkopp YJ, Haas PJA, Rijnders BJA, Kuijper EJ, van Tiel FH, Varga J, Karawajczyk A, Zoll J, Melchers WJG, Verweij PE. 2013. Aspergillosis due

- to voriconazole highly resistant *Aspergillus fumigatus* and recovery of genetically related resistant isolates from domiciles. *Clin Infect Dis* 57:513–520. <https://doi.org/10.1093/cid/cit320>
15. Mellado E, Garcia-Effron G, Alcázar-Fuoli L, Melchers WJG, Verweij PE, Cuenca-Estrella M, Rodríguez-Tudela JL. 2007. A new *Aspergillus fumigatus* resistance mechanism conferring *in vitro* cross-resistance to azole antifungals involves a combination of *cyp51A* alterations. *Antimicrob Agents Chemother* 51:1897–1904. <https://doi.org/10.1128/AAC.01092-06>
  16. Hodiament CJ, Dolman KM, Ten Berge IJM, Melchers WJG, Verweij PE, Pajkrt D. 2009. Multiple-azole-resistant *Aspergillus fumigatus* osteomyelitis in a patient with chronic granulomatous disease successfully treated with long-term oral posaconazole and surgery. *Med Mycol* 47:217–220. <https://doi.org/10.1080/13693780802545600>
  17. Hare RK, Gertsen JB, Astvad KMT, Degn KB, Løkke A, Stegger M, Andersen PS, Kristensen L, Arendrup MC. 2019. *In vivo* selection of a unique tandem repeat mediated azole resistance mechanism (TR120) in *Aspergillus fumigatus cyp51A*, Denmark. *Emerg Infect Dis* 25:577–580. <https://doi.org/10.3201/eid2503.180297>
  18. Gsaller F, Hortschansky P, Furukawa T, Carr PD, Rash B, Capilla J, Müller C, Bracher F, Bowyer P, Haas H, Brakhage AA, Bromley MJ. 2016. Sterol biosynthesis and azole tolerance is governed by the opposing actions of SrbA and the CCAAT binding complex. *PLoS Pathog*. 12:e1006106. <https://doi.org/10.1371/journal.ppat.1006106>
  19. Hagiwara D, Miura D, Shimizu K, Paul S, Ohba A, Gonoï T, Watanabe A, Kamei K, Shintani T, Moye-Rowley WS, Kawamoto S, Gomi K. 2017. A novel Zn2-Cys6 transcription factor AtrR plays a key role in an azole resistance mechanism of *Aspergillus fumigatus* by co-regulating *cyp51A* and *cdr1B* expressions. *PLoS Pathog* 13:e1006096. <https://doi.org/10.1371/journal.ppat.1006096>
  20. Paul S, Stannes M, Thomas GH, Liu H, Hagiwara D, Gomi K, Filler SG, Moye-Rowley WS. 2019. AtrR is an essential determinant of azole resistance in *Aspergillus fumigatus*. *mBio* 10:e02563-18. <https://doi.org/10.1128/mBio.02563-18>
  21. Kühbacher A, Peiffer M, Hortschansky P, Merschak P, Bromley MJ, Haas H, Brakhage AA, Gsaller F. 2022. Azole resistance-associated regulatory motifs within the promoter of *cyp51A* in *Aspergillus fumigatus*. *Microbiol Spectr* 10:e0120922. <https://doi.org/10.1128/spectrum.01209-22>
  22. Paul S, Verweij PE, Melchers WJG, Moye-Rowley WS, Goldman GH. 2022. Differential functions of individual transcription factor binding sites in the tandem repeats found in clinically relevant *cyp51A* promoters in *Aspergillus fumigatus*. *mBio* 13:e0070222. <https://doi.org/10.1128/mbio.00702-22>
  23. Rybak JM, Ge WB, Wiederhold NP, Parker JE, Kelly SL, Rogers PD, Fortwendel JR. 2019. Mutations in *hmg1*, challenging the paradigm of clinical triazole resistance in *Aspergillus fumigatus*. *mBio* 10:e00437-19. <https://doi.org/10.1128/mBio.00437-19>
  24. van den Brink HM, van Gorcom RF, van den Hondel CA, Punt PJ. 1998. Cytochrome P450 enzyme systems in fungi. *Fungal Genet Biol* 23:1–17. <https://doi.org/10.1006/fgbi.1997.1021>
  25. Lamb DC, Kelly DE, Manning NJ, Kaderbhai MA, Kelly SL. 1999. Biodiversity of the P450 catalytic cycle: yeast cytochrome *b5*/NADH cytochrome *b5* reductase complex efficiently drives the entire sterol 14-demethylation (CYP51) reaction. *FEBS Lett* 462:283–288. [https://doi.org/10.1016/s0014-5793\(99\)01548-3](https://doi.org/10.1016/s0014-5793(99)01548-3)
  26. Black SD, Coon MJ. 1987. P-450 cytochromes: structure and function. *Adv Enzymol Relat Areas Mol Biol* 60:35–87. <https://doi.org/10.1002/9780470123065.ch2>
  27. Sutter TR, Loper JC. 1989. Disruption of the *Saccharomyces cerevisiae* gene for NADPH-cytochrome P450 reductase causes increased sensitivity to ketoconazole. *Biochem Biophys Res Commun* 160:1257–1266. [https://doi.org/10.1016/s0006-291x\(89\)80139-1](https://doi.org/10.1016/s0006-291x(89)80139-1)
  28. Truan G, Epinat JC, Rougeulle C, Cullin C, Pompon D. 1994. Cloning and characterization of a yeast cytochrome *b5*-encoding gene which suppresses ketoconazole hypersensitivity in a NADPH-P-450 reductase-deficient strain. *Gene* 142:123–127. [https://doi.org/10.1016/0378-1119\(94\)90366-2](https://doi.org/10.1016/0378-1119(94)90366-2)
  29. Misslinger M, Gsaller F, Hortschansky P, Müller C, Bracher F, Bromley MJ, Haas H. 2017. The cytochrome *b5* CybE is regulated by iron availability and is crucial for azole resistance in *A. fumigatus*. *Metallomics* 9:1655–1665. <https://doi.org/10.1039/c7mt00110j>
  30. Jørgensen LN, Heick TM. 2021. Azole use in agriculture, Horticulture, and wood preservation - is it indispensable? *Front Cell Infect Microbiol* 11:730297. <https://doi.org/10.3389/fcimb.2021.730297>
  31. Schoustra SE, Debets AJM, Rijs AJMM, Zhang J, Snelders E, Leendertse PC, Melchers WJG, Rietveld AG, Zwaan BJ, Verweij PE. 2019. Environmental hotspots for azole resistance selection of *Aspergillus fumigatus*, the Netherlands. *Emerg Infect Dis* 25:1347–1353. <https://doi.org/10.3201/eid2507.181625>
  32. van den Brink HJ, van Nistelrooy HJ, de Waard MA, van den Hondel CA, van Gorcom RF. 1996. Increased resistance to 14 $\alpha$ -demethylase inhibitors (DMIs) in *Aspergillus niger* by coexpression of the *Penicillium italicum* eburicol 14  $\alpha$ -demethylase (*cyp51*) and the *A. niger* cytochrome P450 reductase (*cprA*) genes. *J Biotechnol* 49:13–18. [https://doi.org/10.1016/0168-1656\(96\)01403-4](https://doi.org/10.1016/0168-1656(96)01403-4)
  33. Keniya MV, Ruma YN, Tyndall JDA, Monk BC. 2018. Heterologous expression of full-length lanosterol 14 $\alpha$ -demethylases of prominent fungal pathogens *Candida albicans* and *Candida glabrata* provides tools for antifungal discovery. *Antimicrob Agents Chemother* 62:e01131-18. <https://doi.org/10.1128/AAC.01131-18>
  34. Zadra I, Abt B, Parson W, Haas H. 2000. *xylP* promoter-based expression system and its use for antisense downregulation of the *Penicillium chrysogenum* nitrogen regulator NRE. *Appl Environ Microbiol* 66:4810–4816. <https://doi.org/10.1128/AEM.66.11.4810-4816.2000>
  35. Yap A, Glarher I, Misslinger M, Haas H. 2022. Characterization and engineering of the xylose-inducible *xylP* promoter for use in mold fungal species. *Metab Eng Commun* 15:e00214. <https://doi.org/10.1016/j.mec.2022.e00214>
  36. Birštonas L, Dallemulle A, López-Berges MS, Jacobsen ID, Offterdinger M, Abt B, Straßburger M, Bauer I, Schmidt O, Sarg B, Lindner H, Haas H, Gsaller F. 2020. Multiplex genetic engineering exploiting pyrimidine salvage pathway-based endogenous counterselectable markers. *mBio* 11:e00230-20. <https://doi.org/10.1128/mBio.00230-20>
  37. Guinea J, Meletiadis J, Arikani-Akdagli S, Muehlethaler K, Kahlmeter G, Arendrup MC, Eucast A. 2022. EUCAST definitive document EDef 9.4: method for the determination of broth dilution minimum inhibitory concentrations of antifungal agents for conidia forming moulds EDef 9.4. EUCAST-AFST.
  38. van den Brink H (J) M, van Gorcom RFM, van den Hondel CAMJJ, Punt PJ. 1998. Cytochrome P450 enzyme systems in fungi. *Fungal Genet Biol* 23:1–17. <https://doi.org/10.1006/fgbi.1997.1021>
  39. Geisler K, Hughes RK, Sainsbury F, Lomonosoff GP, Rejzek M, Fairhurst S, Olsen CE, Motawia MS, Melton RE, Hemmings AM, Bak S, Osbourn A. 2013. Biochemical analysis of a multifunctional cytochrome P450 (*cyp51*) enzyme required for synthesis of antimicrobial triterpenes in plants. *Proc Natl Acad Sci U S A* 110:E3360–7. <https://doi.org/10.1073/pnas.1309157110>
  40. Teixeira MM, Carvalho DT, Sousa E, Pinto E. 2022. New antifungal agents with azole moieties. *Pharmaceuticals* 15:1427. <https://doi.org/10.3390/ph15111427>
  41. Kelly DE, Krasevec N, Mullins J, Nelson DR. 2009. The CYPome (cytochrome P450 complement) of *Aspergillus nidulans*. *Fungal Genet Biol* 46 Suppl 1:S53–61. <https://doi.org/10.1016/j.fgb.2008.08.010>
  42. Guinea J. 2020. Updated EUCAST clinical breakpoints against *Aspergillus*, implications for the clinical microbiology laboratory. *J Fungi (Basel)* 6:343. <https://doi.org/10.3390/jof6040343>
  43. Park J, Lee S, Choi J, Ahn K, Park B, Park J, Kang S, Lee YH. 2008. Fungal cytochrome P450 database. *BMC Genomics* 9:402. <https://doi.org/10.1186/1471-2164-9-402>
  44. He D, Feng Z, Gao S, Wei Y, Han S, Wang L. 2021. Contribution of NADPH-cytochrome P450 reductase to azole resistance in *Fusarium oxysporum*. *Front Microbiol* 12:709942. <https://doi.org/10.3389/fmicb.2021.709942>
  45. Zhang X, Fang Y, Jaiseng W, Hu L, Lu Y, Ma Y, Furuyashiki T. 2015. Characterization of tamoxifen as an antifungal agent using the yeast *Schizosaccharomyces pombe* model organism. *Kobe J Med Sci* 61:E54–63.
  46. Liu Q, Guo X, Jiang G, Wu G, Miao H, Liu K, Chen S, Sakamoto N, Kuno T, Yao F, Fang Y. 2020. NADPH-cytochrome P450 reductase Ccr1 is a target of tamoxifen and participates in its antifungal activity via regulating cell wall integrity in fission yeast. *Antimicrob Agents Chemother* 64. <https://doi.org/10.1128/AAC.00079-20>

# Azole Resistance in *Aspergillus fumigatus*

Full-Length Text

Antimicrobial Agents and Chemotherapy

47. Baldin C, Kühbacher A, Merschak P, Wagener J, Gsaller F. 2022. Modular inducible multigene expression system for filamentous fungi. *Microbiol Spectr* 10:e0367022. <https://doi.org/10.1128/spectrum.03670-22>
48. Fraczek MG, Bromley M, Buied A, Moore CB, Rajendran R, Rautemaa R, Ramage G, Denning DW, Bowyer P. 2013. The *cdr1B* efflux transporter is associated with non-*cyp51A*-mediated itraconazole resistance in *Aspergillus fumigatus*. *J Antimicrob Chemother* 68:1486–1496. <https://doi.org/10.1093/jac/dkt075>
49. Pontecorvo G, Roper JA, Hemmons LM, Macdonald KD, Bufton AWJ. 1953. The genetics of *Aspergillus nidulans*. *Advanc Genet Incorporat Mol Genet Med* 5:141–238. [https://doi.org/10.1016/S0065-2660\(08\)60408-3](https://doi.org/10.1016/S0065-2660(08)60408-3)
50. Müller C, Staudacher V, Krauss J, Giera M, Bracher F. 2013. A convenient cellular assay for the identification of the molecular target of ergosterol biosynthesis inhibitors and quantification of their effects on total ergosterol biosynthesis. *Steroids* 78:483–493. <https://doi.org/10.1016/j.steroids.2013.02.006>
51. Müller C, Binder U, Bracher F, Giera M. 2017. Antifungal drug testing by combining minimal inhibitory concentration testing with target identification by gas chromatography-mass spectrometry. *Nat Protoc* 12:947–963. <https://doi.org/10.1038/nprot.2017.005>
52. Müller C, Neugebauer T, Zill P, Lass-Flörl C, Bracher F, Binder U. 2018. Sterol composition of clinically relevant mucorales and changes resulting from posaconazole treatment. *Molecules* 23:1218. <https://doi.org/10.3390/molecules23051218>

## 3.4 Supporting Information

## Supplemental Information

Table S1. Oligonucleotides used in this study.

Primer	Sequence 5' → 3'
pX-cass-FW	AATCATGGTCATAGCTGTTTCTGATGCGAGCAACAGTATGC
pX-cass-RV	GAGCGGATAACAATTTACATGAGGGTTGAGTACGAGATTGG
BBdel-FW	TGTGAAATTGTTATCCGCTCACAA
BBdel-RV	AAACAGCTATGACCATGATTACGC
bixylP-BB-FW	TGTCGTCAAGATTGTAGTGTGTGA
bixylP-BB-RV	AAACAGCTATGACCATGATTACGC
pX-FW.2	CCATGGCAGCAGTGATTTCA
pX-RV.2	GGTTGGTTCTTCGAGTCGATG
cprAbixylP-FW	ACACTACAATCTTGACGACAATGGCGCAACTTGACACG
cprAbixylP-RV	AATCATGGTCATAGCTGTTTCCGACTCGTTGTCTCCAGG
cprBbixylP-FW	ACACTACAATCTTGACGACAATGTCGCTTTTCTCTCAATGGAG
cprBbixylP-RV	AATCATGGTCATAGCTGTTTAAACGCCTTTGAGACAAACGC
cybEbixylP-FW	ACACTACAATCTTGACGACAATGTCGCTCCAAGGAATTC
cybEbixylP-RV	AATCATGGTCATAGCTGTTTCCGCAACGACTACCGAGTTA
cprAxyIP-FW	ATCGACTCGAAGAACCAACCATGGCGCAACTTGACACG
cprAxyIP-RV	TGAAATCACTGCTGCCATGGTCACGACCAGACATCCTCCT
cyp51A-TR-BB-FW	GAATCACGCGGTCCGGAT
cyp51A-TR-BB-RV	TAGACAACTCTGAAGTGGTGCTG
34mer-FW	GAATCACGCGGTCCGGATGTGTGCTGAGCCGAAT
34mer-RV	ATTCCGGCTCAGCACACATCCGGACCGGTGATTC
cyp51A-L98H-FW	CAAGGATGTCAATGCGGAAGAGG
cyp51A-L98H-RV	CTTCCGCATTGACATCCTTGTGCTTGCCGTTGAGAATAAACTCG

## Azole Resistance in *Aspergillus fumigatus*

Table S2. Strains used in this study.

Strain	Genotype	Reference
A1160P+ (wt)		(1)
<i>cyp51A</i> <sup>P<sub>xylP</sub></sup>	$\Delta fcyB::P_{xylP}$ - <i>cyp51A</i>	This study
<i>cprA</i> <sup>P<sub>xylP</sub></sup>	$\Delta fcyB::P_{xylP}$ - <i>cprA</i>	This study
<i>cybE</i> <i>cyp51A</i> <sup>biP<sub>xylP</sub></sup>	$\Delta fcyB::cybE$ - <i>P<sub>xylP</sub></i> - <i>cyp51A</i>	This study
<i>cprA</i> <i>cyp51A</i> <sup>biP<sub>xylP</sub></sup>	$\Delta fcyB::cprA$ - <i>P<sub>xylP</sub></i> - <i>cyp51A</i>	This study
<i>cprB</i> <i>cyp51A</i> <sup>biP<sub>xylP</sub></sup>	$\Delta fcyB::cprB$ - <i>P<sub>xylP</sub></i> - <i>cyp51A</i>	This study
<i>cyp51A</i> <sup>WT</sup>	$\Delta cyp51A::ble$ , <i>P<sub>cyp51A</sub></i> - <i>cyp51A</i> , <i>hph</i>	(2)
<i>cyp51A</i> <sup>TR34</sup>	$\Delta cyp51A::ble$ , <i>P<sub>cyp51A</sub></i> <sup>TR34</sup> - <i>cyp51A</i> , <i>hph</i>	This study
<i>cyp51A</i> <sup>TR34/L98H</sup>	$\Delta cyp51A::ble$ , <i>P<sub>cyp51A</sub></i> <sup>TR34</sup> - <i>cyp51A</i> <sup>L98H</sup> , <i>hph</i>	This study
<i>cyp51A</i> <sup>WT</sup> <i>cprA</i> <sup>P<sub>xylP</sub></sup>	$\Delta cyp51A::ble$ , <i>P<sub>cyp51A</sub></i> - <i>cyp51A</i> , <i>hph</i> , $\Delta fcyB::P_{xylP}$ - <i>cprA</i>	This study
<i>cyp51A</i> <sup>TR34</sup> <i>cprA</i> <sup>P<sub>xylP</sub></sup>	$\Delta cyp51A::ble$ , <i>P<sub>cyp51A</sub></i> <sup>TR34</sup> - <i>cyp51A</i> , <i>hph</i> , $\Delta fcyB::P_{xylP}$ - <i>cprA</i>	This study

### References

1. Fraczek MG, Bromley M, Buied A, Moore CB, Rajendran R, Rautemaa R, Ramage G, Denning DW, Bowyer P. 2013. The *cdr1B* efflux transporter is associated with non-*cyp51a*-mediated itraconazole resistance in *Aspergillus fumigatus*. *Journal of Antimicrobial Chemotherapy* 68:1486-1496.
2. Kuhbacher A, Peiffer M, Hortschansky P, Merschak P, Bromley MJ, Haas H, Brakhage AA, Gsaller F. 2022. Azole Resistance-Associated Regulatory Motifs within the Promoter of *cyp51A* in *Aspergillus fumigatus*. *Microbiol Spectr* 10:e0120922.

## Azole Resistance in *Aspergillus fumigatus*

Table S3. Sterol composition in wt, *cprA<sup>PxyIP</sup>*, *cyp51A<sup>PxyIP</sup>* and *cprAcyp51A<sup>biPxyIP</sup>* grown in liquid cultures during inducing (+xyl) and non-inducing (-xyl) conditions in the presence (+VRZ) and absence (-VRZ) of voriconazole. **1**, lichesterol; **2**, ergosterol; **3**, 5-dihydroergosterol; **4**, ergosta-5,7,22,24(28)-tetraen-3 $\beta$ -ol; **5**, ergosta-7,22,24(28)-trien-3 $\beta$ -ol; **6**, 5-dehydroepisterol; **7**, ergosta-5,7-dien-3 $\beta$ -ol; **8**, episterol; **9**, lanosterol; **10**, 4-methylfecosterol; **11**, eburicol; **12**, 4,4-dimethylergosta-8,24(28)-dien-3 $\beta$ -ol.

		1	2	3	4	5	6	7	8	9	10	11	12
<b>-xyl/-VRZ</b>	<b>wt</b>	0.5%	92.4%	1.0%	0.3%	1.1%	0.2%	0.2%	1.5%	1.1%	0.4%	0.6%	0.7%
	<i>cprA<sup>PxyIP</sup></i>	0.5%	92.1%	0.9%	0.3%	1.2%	0.2%	0.2%	1.6%	1.0%	0.4%	0.7%	0.8%
	<i>cyp51A<sup>PxyIP</sup></i>	0.6%	92.5%	1.0%	0.3%	1.1%	0.2%	0.2%	1.5%	0.7%	0.4%	0.7%	0.8%
	<i>cprAcyp51A<sup>biPxyIP</sup></i>	0.6%	91.7%	1.0%	0.4%	1.4%	0.2%	0.2%	1.6%	0.8%	0.5%	0.9%	0.9%
<b>+xyl/-VRZ</b>	<b>wt</b>	0.6%	91.9%	0.9%	0.4%	1.1%	0.3%	0.2%	1.5%	1.5%	0.4%	0.7%	0.7%
	<i>cprA<sup>PxyIP</sup></i>	0.8%	90.6%	0.9%	0.4%	1.3%	0.6%	1.1%	1.7%	1.0%	0.4%	0.7%	0.7%
	<i>cyp51A<sup>PxyIP</sup></i>	0.6%	93.0%	0.9%	0.4%	1.0%	0.3%	0.2%	1.6%	0.7%	0.4%	0.3%	0.7%
	<i>cprAcyp51A<sup>biPxyIP</sup></i>	0.8%	91.3%	0.9%	0.4%	1.4%	0.7%	0.6%	1.9%	0.8%	0.3%	0.3%	0.6%
<b>-xyl/+VRZ</b>	<b>wt</b>	0.5%	76.5%	0.5%	0.3%	0.6%	0.1%	0.1%	0.8%	3.1%	0.1%	17.1%	0.2%
	<i>cprA<sup>PxyIP</sup></i>	0.6%	76.3%	0.5%	0.3%	0.6%	0.1%	0.2%	0.8%	3.1%	0.1%	17.3%	0.2%
	<i>cyp51A<sup>PxyIP</sup></i>	0.6%	76.0%	0.5%	0.4%	0.6%	0.1%	0.2%	0.8%	3.1%	0.1%	17.5%	0.2%
	<i>cprAcyp51A<sup>biPxyIP</sup></i>	0.6%	76.2%	0.5%	0.4%	0.5%	0.1%	0.1%	0.7%	3.1%	0.1%	17.6%	0.2%
<b>+xyl/+VRZ</b>	<b>wt</b>	0.5%	77.6%	0.4%	0.4%	0.4%	0.1%	0.1%	0.7%	3.2%	0.1%	16.3%	0.1%
	<i>cprA<sup>PxyIP</sup></i>	0.8%	82.7%	0.7%	0.4%	0.9%	0.4%	0.6%	1.1%	1.5%	0.2%	10.4%	0.4%
	<i>cyp51A<sup>PxyIP</sup></i>	0.7%	86.8%	0.8%	0.4%	1.3%	0.2%	0.2%	1.5%	1.4%	0.3%	5.8%	0.7%
	<i>cprAcyp51A<sup>biPxyIP</sup></i>	0.7%	89.2%	0.9%	0.4%	1.2%	0.3%	0.4%	1.4%	1.2%	0.3%	3.2%	0.7%

## Azole Resistance in *Aspergillus fumigatus*

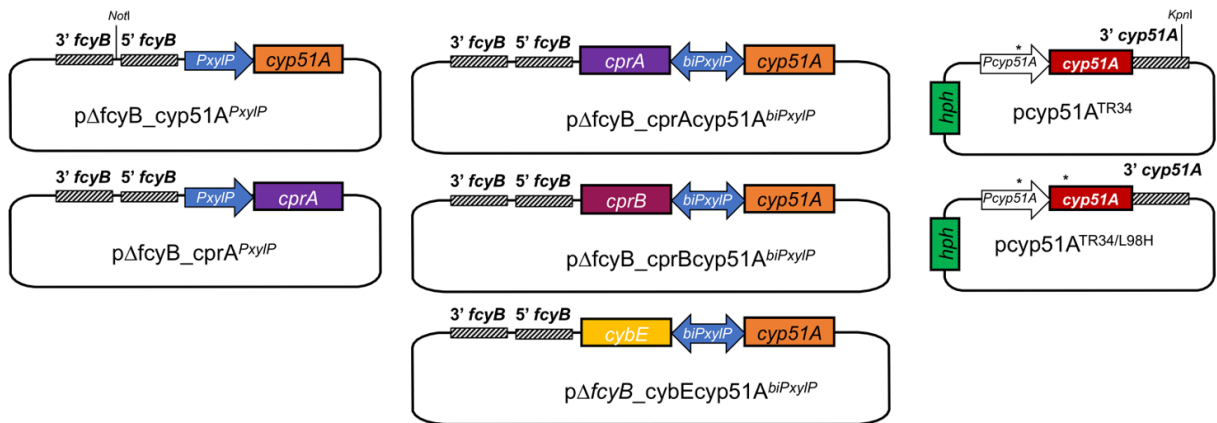


Fig S1. **Scheme of plasmids used in this study.** \* denotes TR34 and/or the L98H mutation in the promoter and coding sequence of *cyp51A*, respectively.

## 4. Quantifying Isoprenoids in the Ergosterol Biosynthesis by Gas Chromatography–Mass Spectrometry

M. Liebl, L. Huber, H. Elsaman, P. Merschak, J. Wagener, F. Gsaller, C. Müller; Quantifying Isoprenoids in the Ergosterol Biosynthesis by Gas Chromatography–Mass Spectrometry. *Journal of Fungi*. 2023; 9, 768. Impact factor: 4.2 (2/2025)

### 4.1 Summary

The pressure to launch new antimycotic drugs on the market is high, due to permanently evolving and fast adapting fungal microorganisms, that continuously develop resistance mechanisms (see Chapter 3). According to a 2024 review [51], invasive fungal infections threaten more than 6.5 million people per year and cause up to 3.8 million deaths annually.

The development of new antifungals is a challenging task. Nevertheless, continuous approaches are made to increase the number of antifungal tools. Next to the very recent approval of inhibitors using already established targets and mechanisms, *e.g.*, the azoles opelconazole (triazole for application *via* inhalation) and oteseconazole (tetrazole targeting sterol C14-demethylase) or rezafungin (echinocandine targeting cell wall biosynthesis), the identification of novel targets can bring decisive advantage in antifungal therapy [59,67]. The latest innovations are fosmanogepix (FSX) and olorofim (OLF), two drug candidates, using novel mechanisms of action. FSX (phase III) is the first inhibitor of Gwt1 (Glycosylphosphatidylinositol-anchored wall protein transfer 1) which is essential for GPI-anchor biosynthesis, while OLF (in clinical development, phase III) affects pyrimidine biosynthesis in fungal cells by inhibiting the fungal dihydroorotate dehydrogenase [59,65,67].

In this work we introduced an analytical approach that could be used to identify and quantify isoprenoid pathway intermediates after final adaptations (see Chapter 2). Those included the optimization of the extraction solvent, which was a final mixture of *n*-hexane/acetone/acetonitrile (12/2/1, *v/v/v*), as well as the optimization of the crucial enzymatic pyrophosphate deconjugation step using alkaline phosphatase from bovine intestinal mucosa (40 min at 37 °C; 1 M aqueous diethanolamine buffer pH 8.6 containing 0.5 mM magnesium chloride hexahydrate). This represents the first described gas chromatography (GC) based approach to analyze the whole isoprenoid section of ergosterol biosynthesis. Following a detailed validation, we tested our assay on *A. fumigatus* mutant strains that contained doxycycline inducible isoprenoid pathway genes for either *erg9* (squalene synthase) or *erg1* (squalene epoxidase). While the role of *erg1* is known to be crucial, and allylamines (*e.g.*, terbinafine) are potent inhibitors of fungal squalene epoxidase, the effects of *erg9* downregulation were not yet investigated in that detail. By specifically regulating *erg1/erg9*, the respective enzymes can only be formed up to a limited degree. If there are no further genes encoding for analogous enzymes, the biological pathway accumulates a specific intermediate. In the case of essential genes, the fungus can be limited in growth and even total survival without the formation of its enzyme. By comparing mutant strains with equally treated wildtype strains, differences in growth and overall survival were observed (**Figure 14**).

## Quantifying Isoprenoids in the Ergosterol Biosynthesis by GC-MS

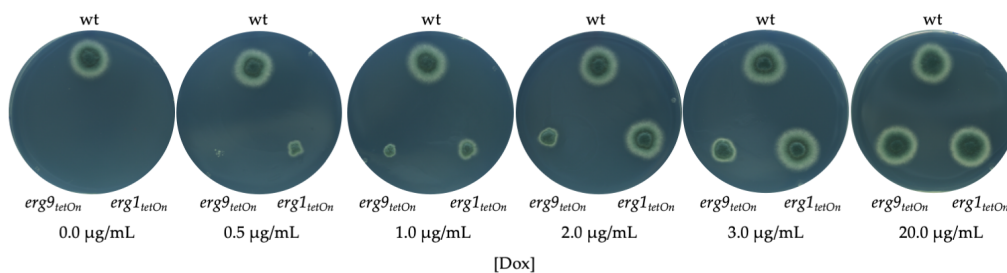


**Figure 14:** Comparison of doxycycline (Dox) inducible (*tetOn*) *A. fumigatus* mutant strains containing mutations in *erg9/1* with wildtype (wt) strains after 48 h incubation at 37°C (more information can be found in Chapter 4.4).

Subsequent isoprenoid pathway analysis confirmed an accumulation of the expected isoprenoids, as well as the role of squalene synthase (Erg9) as an essential enzyme. So far there are no antimycotics described that target fungal squalene synthase, therefore the development of this new class of antifungals could be an interesting approach (see Chapter 5.5).

### 4.2 Personal Contribution

#### Overview:

Conceptualization:	M.L., J.W., F.G., C.M.
Methodology:	M.L., H.E., P.M., C.M.
Data curation:	M.L., L.H., J.W., F.G., C.M.
Formal analysis:	M.L., L.H., P.M., F.G.
Writing – original draft:	M.L., C.M.
Writing – review and editing:	M.L., J.W., F.G., C.M.

#### Note:

My contribution to this work was the improvement and implementation of the final analytical methodology which was in part developed during my Master's thesis project (see Chapter 2). Also, conceptualization and experimental design were part of my contribution. The subsequent performance of the experiments, as well as the analysis of the data, formal analysis and data curation were done by me. Finally, I was involved in visualization of the experimental results, writing the original draft as well as reviewing and editing this article.

Validation of the assay, including data analysis and formal analysis of the validation data were carried out by Ludwig Huber as a part of his Bachelor's thesis (Pharmaceutical Sciences) which was supervised by me.

Hesham Elsaman and Prof. Johannes Wagener contributed to the project as they produced the fungal strains and described them in the "Materials and methods" section of the manuscript. Further Figure S1 was provided by them. In addition, Prof. Wagener was included in conceptualization, reviewing, and editing the manuscript.

Petra Merschak supported this publication by preparing the fungal samples, including different growth conditions, terbinafine treatment and lyophilization of the samples.

Assoc.-Prof. Fabio Gsaller was included in the conceptualization of this work. He further took part in reviewing and editing of the manuscript.

## Quantifying Isoprenoids in the Ergosterol Biosynthesis by GC-MS

Dr. Christoph Müller contributed to the planning of the experimental design and in the whole investigation. He was involved in the development of the article structure, writing of the original draft as well as reviewing and editing.

The project was supervised by Prof. Wagener, Assoc.-Prof. Gsaller and Dr. Müller, who were also providing the required resources.

## 4.3 Article



## Article

# Quantifying Isoprenoids in the Ergosterol Biosynthesis by Gas Chromatography–Mass Spectrometry

Maximilian Liebl <sup>1</sup>, Ludwig Huber <sup>1</sup>, Hesham Elsaman <sup>2</sup>, Petra Merschak <sup>3</sup>, Johannes Wagener <sup>2,4</sup> ,  
Fabio Gsaller <sup>3</sup> and Christoph Müller <sup>1,\*</sup>

<sup>1</sup> Department of Pharmacy, Center for Drug Research, Ludwig-Maximilians University, 81377 Munich, Germany; maximilian.liebl@cup.uni-muenchen.de (M.L.); lu.huber@campus.lmu.de (L.H.)

<sup>2</sup> Institute for Hygiene and Microbiology, Julius-Maximilians-University Wuerzburg, 97080 Wuerzburg, Germany; hesham.elsaman@uni-wuerzburg.de (H.E.); wagenerj@tcd.ie (J.W.)

<sup>3</sup> Institute of Molecular Biology, Biocenter, Medical University of Innsbruck, 6020 Innsbruck, Austria; petra.merschak@i-med.ac.at (P.M.); fabio.gsaller@i-med.ac.at (F.G.)

<sup>4</sup> Department of Clinical Microbiology, School of Medicine, Trinity College Dublin, The University of Dublin, D08 RX0X Dublin, Ireland

\* Correspondence: christoph.mueller@cup.uni-muenchen.de

**Abstract:** The ergosterol pathway is a promising target for the development of new antifungals since its enzymes are essential for fungal cell growth. Appropriate screening assays are therefore needed that allow the identification of potential inhibitors. We developed a whole-cell screening method, which can be used to identify compounds interacting with the enzymes of isoprenoid biosynthesis, an important part of the ergosterol biosynthesis pathway. The method was validated according to the EMEA guideline on bioanalytical method validation. *Aspergillus fumigatus* hyphae and *Saccharomyces cerevisiae* cells were lysed mechanically in an aqueous buffer optimized for the enzymatic deconjugation of isoprenoid pyrophosphates. The residual alcohols were extracted, silylated and analyzed by GC-MS. The obtained isoprenoid pattern provides an indication of the inhibited enzyme, due to the accumulation of specific substrates. By analyzing terbinafine-treated *A. fumigatus* and mutant strains containing tunable gene copies of *erg9* or *erg1*, respectively, the method was verified. Downregulation of *erg9* resulted in a high accumulation of intracellular farnesol as well as elevated levels of geranylgeraniol and isoprenol. The decreased expression of *erg1* as well as terbinafine treatment led to an increased squalene content. Additional analysis of growth medium revealed high farnesyl pyrophosphate levels extruded during *erg9* downregulation.

**Keywords:** *Aspergillus fumigatus*; *erg1*; *erg9*; ergosterol biosynthesis; farnesol; GC-MS; isoprenoids; terbinafine



**Citation:** Liebl, M.; Huber, L.; Elsaman, H.; Merschak, P.; Wagener, J.; Gsaller, F.; Müller, C. Quantifying Isoprenoids in the Ergosterol Biosynthesis by Gas Chromatography–Mass Spectrometry. *J. Fungi* **2023**, *9*, 768. <https://doi.org/10.3390/jof9070768>

Academic Editor: Scott D. Briggs

Received: 30 May 2023  
Revised: 14 July 2023  
Accepted: 19 July 2023  
Published: 20 July 2023



**Copyright:** © 2023 by the authors. Licensee MDPI, Basel, Switzerland. This article is an open access article distributed under the terms and conditions of the Creative Commons Attribution (CC BY) license (<https://creativecommons.org/licenses/by/4.0/>).

## 1. Introduction

Fungal infections threaten the health of more than one billion people worldwide. While most of them are inconvenient topical or vulvovaginal mycoses, some can be life-threatening invasive infections that lead to approximately 1.7 million deaths per year [1–3]. As a consequence of those often underrecognized emerging fungal threats that are accompanied by an increasing antimycotic resistance, the World Health Organization (WHO) recently published the first fungal priority pathogens list (October 2022) [4]. The document classifies pathogens in three priorities (critical, high and medium) by multi-criteria decision analysis, considering *Aspergillus fumigatus*, *Candida albicans*, *Candida auris* and *Cryptococcus neoformans* as the most critical threats [3,4]. An accelerator increasing the number of invasive mycoses such as mucormycosis, aspergillosis and candidiasis was the global coronavirus disease 2019 (COVID-19) [5–7]. Patients suffering from severe acute respiratory syndrome coronavirus type 2 (SARS-CoV-2) have a significantly lower number of T-cells; in addition, the first-line treatment of severe COVID-19 pneumonia with corticosteroids impairs the immune system [6,8]. In an aggressive disease course, SARS-CoV-2

may even damage lung tissue and cause alveolar-intestinal lesions, leading to a higher susceptibility for pulmonary infections [8].

Considering those current hazards caused by fungal germs, potent antifungal therapies are mandatory. The first time a targeted antifungal therapy became available was in the 1950s with the introduction of the polyene amphotericin B (AMB), a broad-spectrum antifungal agent that is still the first-line treatment of invasive mycoses [1]. Besides polyenes that can interact with ergosterol directly, several clinically relevant classes of ergosterol biosynthesis inhibitors including imidazoles/triazoles (e.g., clotrimazole/fluconazole), morpholines (e.g., amorolfine) and allylamines (e.g., terbinafine) were launched on the market. The efficacy of those sterol biosynthesis inhibitors is based on the pivotal role of ergosterol for fungal membrane flexibility, rigidity and permeability. Even though the efficacy of imidazoles/triazoles is indisputable, all known ergosterol biosynthesis inhibitors exclusively inhibit enzymes of the post-squalene pathway [9], whereas the pre-squalene part was disregarded until now.

Isoprenoids with the formula  $(C_5H_8)_n$  are formed from acetyl-coenzyme A (acetyl-CoA) in the mevalonate pathway, the first part of the pre-squalene pathway. From here on, isoprenoids are involved in the synthesis of numerous bioactive compounds. Besides the biosynthesis of sterols, they take part in the formation of dolichols, ubiquinone, as well as the post-translational modifications of proteins by prenylation reactions (Figure 1) [10,11].

Dimethylallyl pyrophosphate (DMAPP) and isopentenyl pyrophosphate (IPP) are the substrates for the biosynthesis of terpenes. Both molecules are hemiterpenes ( $C_5H_8$ ) that can be interconnected by the enzyme isopentenyl pyrophosphate isomerase (Idi1) [11–13]. In a head-to-tail condensation, each equivalent DMAPP and IPP result in the monoterpene ( $C_{10}H_{16}$ ) geranyl pyrophosphate (GPP) [12,14]. Therefore, the reaction is catalyzed by the enzyme farnesyl pyrophosphate synthase (Erg20), which also catalyzes the following reaction from GPP to farnesyl pyrophosphate (FPP) using a second unit of IPP [14]. With the sesquiterpene ( $C_{15}H_{24}$ ) FPP, the reaction cascade reaches a branching point, where FPP can be directly converted to farnesol by farnesyl pyrophosphatase (FPPase), or used in other biosynthesis reactions outside sterol biosynthesis, e.g., biosynthesis of carotenoids, sesquiterpenoids and *N*-glycans [15–18]. The diterpene ( $C_{20}H_{32}$ ) geranylgeranyl pyrophosphate (GGPP) is synthesized from FPP and IPP in an addition-elimination-condensation catalyzed by geranylgeranyl pyrophosphate synthase (Bts1) [16]. GGPP is not a precursor of ergosterol but is also used for the biosynthesis of further bioactive molecules, e.g., G-proteins, ubiquinone and carotenoids [19,20]. The major part of FPP is used for the synthesis of the triterpene ( $C_{30}H_{50}$ ) squalene (SQ), which is the final product of the isoprenoid pathway [11,15,16,21]. Squalene is synthesized by squalene synthase (Erg9) starting from two units of FPP. In contrast to the post-squalene/lanosterol pathway, which contains specific intermediates depending on the organism, the isoprenoid pathway intermediates are identical in fungi, mammals and plants [21]. Also, in several bacteria, e.g., *Escherichia coli* or *Staphylococcus aureus*, isoprenoids can be detected [22,23].

For the development of novel antifungals, the isoprenoid part of the pre-squalene pathway could be a promising target since its enzymes play an essential role in fungal cell growth [13,15,24–27]. Those findings were confirmed by studying the impact of conditional downregulation of *erg9* and *erg1* on the growth of *A. fumigatus* (Supplementary Material Figure S1). In the literature, evidence can be found that also a deletion of *erg20* results in a lack of FPP and is lethal to fungal cells, due to the necessity of FPP as a metabolic intermediate. In addition, an accumulation of monoterpenes can be toxic for microorganisms [26,27]. The essential role of *IDI1* in *S. cerevisiae* was highlighted by Mayer et al. [13].

Even though the precursors of ergosterol and involved enzymes are well known, their qualitative and quantitative measurement remains difficult due to their widely varying physicochemical properties. Molecules of the post-squalene pathway are lipophilic because of their sterol backbone with one or two hydroxyl groups, which makes them accessible for analysis by gas chromatography (GC) [9,28,29]. In contrast, the compounds of the pre-squalene pathway consist of phosphorylated isoprenoids that are negatively charged under

physiological conditions. The phosphorylated isoprenoids are better accessible for the analysis by liquid chromatography (LC) due to their water solubility. To make isoprenoids vaporable and available for a GC analysis, the isoprenoids must be dephosphorylated. Besides acidic or basic hydrolysis, enzymatic deconjugation is a convenient way to generate isoprenoids [30–33]. Nevertheless, only few approaches exist where the intermediates of the pre-squalene pathway are analyzed. An overview of methods described in the literature for the analysis of intermediates of the pre-squalene pathway is given in Table 1. The first assays describing the analysis of intermediates of the pre-squalene pathway were using radioactive labeled precursors such as [5-<sup>3</sup>H]mevalonolactone [34], [1-<sup>14</sup>C]isopentenyl diphosphate or [1-<sup>3</sup>H]farnesyl diphosphate [35].

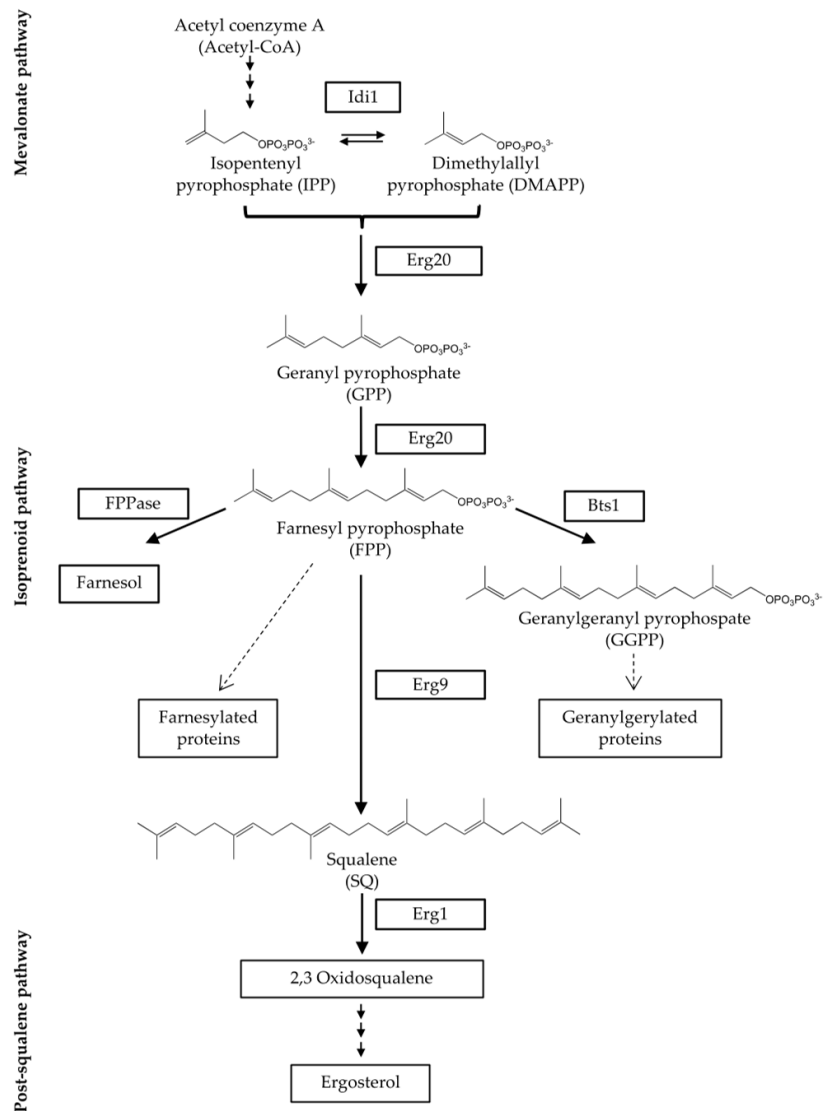


**Figure 1.** Scheme of ergosterol biosynthesis in fungi with the isoprenoid pathway in detail. Farnesyl pyrophosphatase (FPPase); farnesyl pyrophosphate synthase (Erg20); geranylgeranyl pyrophosphate synthase (Bts1); isopentenyl pyrophosphate isomerase (Idi1); squalene epoxidase (Erg1), squalene synthase (Erg9).

**Table 1.** Overview of methods described in the literature for the analysis of intermediates of the pre-squalene pathway: dimethylallyl pyrophosphate (DMAPP), farnesyl pyrophosphate (FPP), geranyl pyrophosphate (GPP), geranylgeranyl pyrophosphate (GGPP), isopentenyl pyrophosphate (IPP), mevalonate phosphate (MVP), mevalonate pyrophosphate (MVPP), mevalonic acid (MVA), squalene (SQ); n.d. not determined.

Reference	Analytical System	Analytes	Biological Matrix	Quantification Limit (ng/mL)
Bruenger, E. et al., 1988 [35]	TLC-scintillation	IPP, FPP	mice liver	n.d.
McTaggart, F. et al., 1996 [34]	HPLC-scintillation	IPP, GPP, FPP, GGPP, SQ	rat hepatic microsomes	n.d.
Song, L. 2003 [36]	GC-MS	FPP	cultured fungal cells	n.d.
Tong, H. et al., 2005 [37]	HPLC-fluorescence	FPP, GGPP	cultured human cell lines	n.d.
Hooff, G. et al., 2008 [38]	HPLC-MS/MS	FPP, GGPP	human brain cells	10 (FPP) 50 (GGPP)
Vallon, T. et al., 2008 [22]	GC-MS	FPP, GGPP	bacteria	77 (FPP) 90 (GGPP)
Henneman, L. et al., 2008 [39]	HPLC-MS/MS	MVA, MVP, MVPP, IPP/DMAPP, GPP, FPP, GGPP	cultured human cell lines	618 (MVA) 951 (MVP) 1285 (MVPP) 31 (IPP/DMAPP) 103 (GPP) 42 (FPP) 59 (GGPP)
Huang, B. et al., 2011 [33]	GC-MS	GPP, FPP, GGPP, SQ	cultured fungal cells	218 (GPP) 143 (FPP) 21 (GGPP) 6 (SQ)
Rodriguez, S. et al., 2014 [17]	GC-MS	MVA, FPP, SQ	cultured fungal cells	500 (MVA) 500 (FPP) 500 (SQ)
Chhonker, Y. et al., 2018 [40]	HPLC-MS/MS	GPP, FPP, GGPP	cultured human cell lines and human plasma	0.04 (GPP) 0.04 (FPP) 0.04 (GGPP)
Castaño-Cerezo, S. et al., 2019 [41]	HPLC-HRMS	MVA, MVP, MVPP, IPP/DMAPP, GPP, FPP, GGPP	cultured fungal cells	22 (MVA) 2 (MVP) 3 (MVPP) 5 (IPP) 3 (DMAPP) 16 (GPP) 8 (FPP) 36 (GGPP)

For the analysis of these radioactively labeled analytes, a scintillation counter was used. In the early 2000s, an increasing number of cellular models was established where radioactive labeling methods were replaced with mass spectrometry (MS) detection, a radioactivity-free detection method. This has led to the development of several efficient high-performance liquid chromatography (HPLC) and GC-MS methods that were limited to single analytes and did not cover the whole isoprenoid pathway. Henneman et al. [39] published an assay in 2008 that is based on human Hep2G cells, covering eight analytes of the pre-squalene pathway including mevalonate and its mono- and di-phosphate species, intermediates of the mevalonate pathway. Due to the use of an HPLC-MS/MS system, the analytes do not have to be dephosphorylated and can be analyzed directly. However, a

distinction between the isomers IPP and DMAPP was not possible with this approach [39]. An effective GC-MS method was applied by Huang et al. [33] in 2011. In their approach, they were able to quantify four intermediates of the isoprenoid pathway including geraniol (GOH), farnesol (FOH), geranylgeraniol (GGOH) and squalene (SQ). However, the method was not very efficient, considering incubation periods (105 min for the dephosphorylation step), the total run time of the GC method (37 min) and the necessity of large amounts of biomass (100 mL of an  $OD_{600} \sim 0.1$ ; incubation for 48 h at 30 °C). In addition, method validation was not performed in line with the appropriate analytical guideline, resulting in missing thresholds for the validation parameters [33]. Rodriguez et al. [17] were capable of analyzing mevalonate (MVA) in addition to FOH and SQ levels from fungal cells. Therefore, three different GC-MS methods had to be used to cover the whole scope of analytes: metabolite profiling of MVA, metabolic profiling of sesquiterpenes including FOH, and metabolic profiling of SQ and ergosterol. Chhonker et al. [40] analyzed isoprenoids from human cancer cell lines and plasma using HPLC–MS/MS. Even though they were able to quantify the intermediates GPP, FPP and GGPP at basal levels, their protocol did not cover the remaining isoprenoid biosynthesis pathway, missing IPP, DMAPP and SQ. In a more recent work, Castaño-Cerezo et al. [41] used an HPLC-high-resolution (HR)MS system to quantify the eight intermediates of the pre-squalene pathway in *S. cerevisiae*. Compared to Henneman et al. [39], they were able to implement several improvements; however, the limitations of the LC system remain. Therefore, the separation and distribution of IPP and DMAPP was not possible in their approach.

In this work, we present a novel, selective and reproducible assay to analyze the intermediates of the isoprenoid pathway, including the isomers IPP and DMAPP, in fungal cell matrices (*A. fumigatus*, *S. cerevisiae*), using a quick and simple approach. The developed methodology was validated according to European Medicines Agency (EMA) guideline on bioanalytical method validation [42]. As proof of concept, we analyzed lyophilized *A. fumigatus* cells and their associated growth medium as well as terbinafine-treated wild type (wt) cells to give detailed insights into isoprenoid and sterol trafficking in fungal cells for the first time.

## 2. Materials and Methods

### 2.1. Chemicals

**Solvents:** All solvents were purchased in HPLC grade or in *pro analysis* quality from Sigma Aldrich (Schnelldorf, Germany). Deionized water was prepared with an in-house ion-exchanger. Double-distilled water was purchased from Fresenius Kabi Deutschland GmbH (Bad Homburg, Deutschland).

**Standards:** Dimethylallyl pyrophosphate (DMAPP) (95%), farnesyl pyrophosphate (FPP) (95%) and geranylgeranyl pyrophosphate (GGPP) (95%) were from Cayman Chemicals (Michigan, MI, USA); prenol (POH) (97%) and farnesol (FOH) (97%) were purchased from Alfa Aesar (Karlsruhe, Germany). Isoprenol (IOH) (98%) was from Tokyo Chemical Industry Co. (Tokyo, Japan). Geraniol (GOH) (98%) and squalene (SQ) (98%) were purchased from Sigma Aldrich (Steinheim, Germany); geranylgeraniol (GGOH) (85%) and 1-heptadecanol (internal standard for isoprenoid analysis,  $IS_{Iso}$ ) (98%) were from Sigma Aldrich (Saint Louis, MO, USA). The second internal standard for sterol analysis, 5 $\alpha$ -cholestane (internal standard for sterol analysis,  $IS_{Sterol}$ ) (97%), was purchased from Sigma Aldrich (Steinheim, Germany). Doxycycline monohydrate (97%) was purchased from Sigma Aldrich (Steinheim, Germany) and terbinafine (98%) was obtained from BLDpharm (Kaiserslautern, Germany).

**Enzymatic deconjugation step:** Bovine alkaline phosphatase (P7640) was purchased from Sigma Aldrich (Steinheim, Germany). Diethanolamine (99%) was purchased from Tokyo Chemical Industry Co. (Tokyo, Japan). Magnesium chloride hexahydrate (99%) and glycine (98%) were purchased from Sigma Aldrich (Steinheim, Germany). Sodium chloride was purchased from Bernd Kraft GmbH (Duisburg, Germany).

**Derivatization step:** *tert*-Butyldiphenylchlorosilane (tBDPSCI) (98%) and imidazole (99%) from Sigma Aldrich (Steinheim, Germany) were used for derivatization of isoprenoids. For silylation of sterols, a mixture of *N*-methyl-*N*-trimethylsilyltrifluoroacetamide (MSTFA) and *N*-trimethylsilylimidazole (TSIM) from Macherey Nagel (Düren, Germany) was used (10/1; *v/v*).

## 2.2. Reagents

Analyte and internal standard (IS<sub>Iso</sub>, 1-heptadecanol; IS<sub>Sterol</sub>, 5 $\alpha$ -cholestane) stock solutions (each 1 mg/mL) were prepared in *n*-hexane. Working standard solutions were prepared (100  $\mu$ g/mL in *n*-hexane) and diluted as needed. From pyrophosphates (DMAPP, FPP, GGPP), equimolar working solutions corresponding to the analyte concentration in  $\mu$ g/mL were prepared in methanol/ammonium hydroxide (7/3; *v/v*). IS<sub>Iso</sub> and IS<sub>Sterol</sub> stock solutions were diluted and combined to achieve one internal standard working solution containing 50  $\mu$ g/mL (IS<sub>Iso</sub>) and 10  $\mu$ g/mL (IS<sub>Sterol</sub>). All stock solutions were stored at  $-20$  °C, tempered for 1 h and shaken before use. The aqueous 1 M diethanolamine buffer solution pH 8.6 was prepared in a stock of 100 mL containing magnesium chloride hexahydrate (0.5 mM) (DEA-buffer). Working solutions and buffers were stored at 4 °C, tempered for 15 min and shaken before use.

## 2.3. Fungal Strains Used in This Study

The non-homologous end-joining-deficient *A. fumigatus* strain AfS35, a derivative of D141, served as the wt strain in this study [43,44]. The conditional *erg1<sub>tetOn</sub>* and *erg9<sub>tetOn</sub>* strains were generated by replacing the promoters of the respective genes (*erg1*, AFUA\_5G07780; *erg9*, AFUA\_7G01220) with a doxycycline-inducible Tet-On promoter, essentially as described before [45,46]. *S. cerevisiae* was obtained from DSMZ (German Collection of Microorganisms and Cell Cultures; DSM-No. 1333, Braunschweig, Germany).

## 2.4. Fungal Growth and Culture Conditions

For sterol analysis, wt and tunable *A. fumigatus* strains were grown in *Aspergillus* minimal medium (AMM) containing 20 mM ammonium tartrate as the nitrogen source and 1% glucose as the carbon source [47]. Cultures were inoculated with a final concentration of  $1.0 \times 10^6$  spores/mL of each strain and incubated for 20 h at 37 °C, 200 rpm. Mycelia were harvested through filtration, shock-frozen and freeze-dried.

For *S. cerevisiae*, the DSMZ 186 universal medium for yeast was used for cultivation. The medium contained 3.0 g of yeast extract, 10.0 g of glucose and 15.0 g of agar from Sigma Aldrich (Steinheim, Germany); 3.0 g of malt extract from AppliChem GmbH (Darmstadt, Germany); and 5.0 g of peptone from soyabean from Oxoid (Basingstoke, Hampshire, UK). All components were dissolved in 1000 mL of deionized water and autoclaved for 10 min at 121 °C before use. Cell cultures were maintained at 28 °C and split once a week to keep the yeast in a log phase [28,48].

Cell matrix for method development and validation was obtained by incubating 2 mL of  $5.0 \times 10^5$  CFU/mL in DSMZ 186 medium in 24-well plates at 28 °C for  $48 \pm 2$  h.

## 2.5. Instruments and Equipment

### 2.5.1. Sample Preparation

For shaking, a Vortex-Genie 2 by Scientific Industries, Inc. (Bohemia, NY, USA) was used. Centrifugation of 2 mL microcentrifuge tubes was performed with an Eppendorf 5415 D centrifuge (Hamburg, Germany). Derivatization and enzymatic deconjugation were conducted in a Binder ED23 laboratory drying cabinet from VWR (Ismaning, Germany).

### 2.5.2. GC-MS Analysis of Isoprenoid tBDPS Ethers, Squalene and Sterol TMS Ethers

Gas chromatography was performed on an Agilent 7820A gas chromatograph coupled to a quadrupole 5977B MS from Agilent (Santa Clara, CA, USA). The 7693A automatic liquid sampler (ALS) from Agilent (Santa Clara, CA, USA) was used with the G4513A

split/splitless injector from Agilent (Santa Clara, CA, USA). Data analysis and instrument control were carried out with the Masshunter 8.0 software from Agilent (Santa Clara, CA, USA). The column was an Agilent DB5-*ms* capillary column (Santa Clara, CA, USA) of 30 m in length, 0.25 mm in inner diameter and 0.25  $\mu\text{m}$  in film thickness. Chromatography was performed with 99.9990% ALPHAGAZ™ 1 HELIUM/He from Air Liquide (Düsseldorf, Germany) as the carrier gas at a constant flow rate of 1.4 mL/min. The inlet temperature was kept at 270 °C and the injection volume was 1  $\mu\text{L}$ . Initial column temperature was 75 °C, which was held for 0.5 min. With a heating rate of 25 °C/min, temperature was increased to 180 °C until it was held for 1.0 min. Subsequently, temperature increased to 225 °C with a heat rate of 15 °C/min. After reaching 225 °C, the heating rate was increased to 50 °C/min to reach the final temperature of 320 °C, where the column was held for 5.9 min. The total run time was 16.5 min, followed by a 2.5 min post run with an increased flow rate of 2.0 mL/min. Transfer line temperature was 270 °C. The ion source temperature was 230 °C and the quadrupole temperature was 150 °C. The detection of the isoprenoid *t*BDPS ethers and squalene started after a solvent delay of 9.5 min in single-ion-monitoring (SIM) mode (see details in Table 2) at 70 eV. A selected ion chromatogram of the quantifier ions from different concentrations can be seen in Supplementary Material Figure S2. In addition, SIM and full-scan spectra (50–500 (*m/z*)) of the isoprenoid ethers,  $\text{IS}_{\text{Iso}}$  and squalene can be seen in Supplementary Material Figures S3 and S4, respectively.

**Table 2.** Analytical details of the analyzed isoprenoid *t*BDPS ethers and squalene. Absolute retention time (RT); relative retention time (RRT); in bold, quantifier ions.

Trivial Name	RT (min)	RRT	Qualifier and Quantifier Ions ( <i>m/z</i> )
isoprenol	9.90	0.707	69, <b>225</b> , 267
prenol	9.96	0.712	69, 189, <b>267</b>
geraniol	11.35	0.811	69, <b>335</b> , 392
squalene	12.03	0.860	<b>69</b> , 81, 410
farnesol	12.73	0.910	<b>69</b> , 203, 403
1-heptadecanol ( $\text{IS}_{\text{Iso}}$ )	14.00	1.000	71, 123, <b>437</b>
geranylgeraniol	15.26	1.090	<b>69</b> , 81, 471

Analysis of sterol TMS ethers was performed according to Müller et al. [9,28]. The sterol TMS ethers were analyzed in full scan mode by GC-MS (Table 3). The amount of each sterol is expressed as  $\mu\text{g}$  per mg dry weight. The results were obtained with a method that was not fully validated for the extraction solvent *n*-hexane.

**Table 3.** Analytical details of the analyzed sterol TMS ethers according to Müller et al. [9,28]. Absolute retention time (RT); relative retention time (RRT); in bold, quantifier ions.

Trivial Name	RT (min)	RRT	Qualifier and Quantifier Ions ( <i>m/z</i> )
cholestane ( $\text{IS}_{\text{Sterol}}$ )	11.75	1.000	203, <b>217</b> , 357
lanosterol	16.83	1.440	241, <b>393</b> , 498
eburicol	17.46	1.501	<b>407</b> , 498, 512
ergosterol	15.54	1.329	337, <b>363</b> , 378

### 2.5.3. Final Sample Preparation

For the analysis of *S. cerevisiae* samples, the cell suspension of each well was transferred into a 2.0 mL microcentrifuge safe-lock tube and centrifuged for 5 min at 9000  $\times$  g at room temperature (RT). After centrifugation, the supernatant was decanted from the cell pellet (Figure 2I). For the analysis of *A. fumigatus* samples, lyophilized mycelia were pulverized, and  $5 \pm 0.2$  mg was transferred into a 2.0 mL microcentrifuge safe-lock tube.

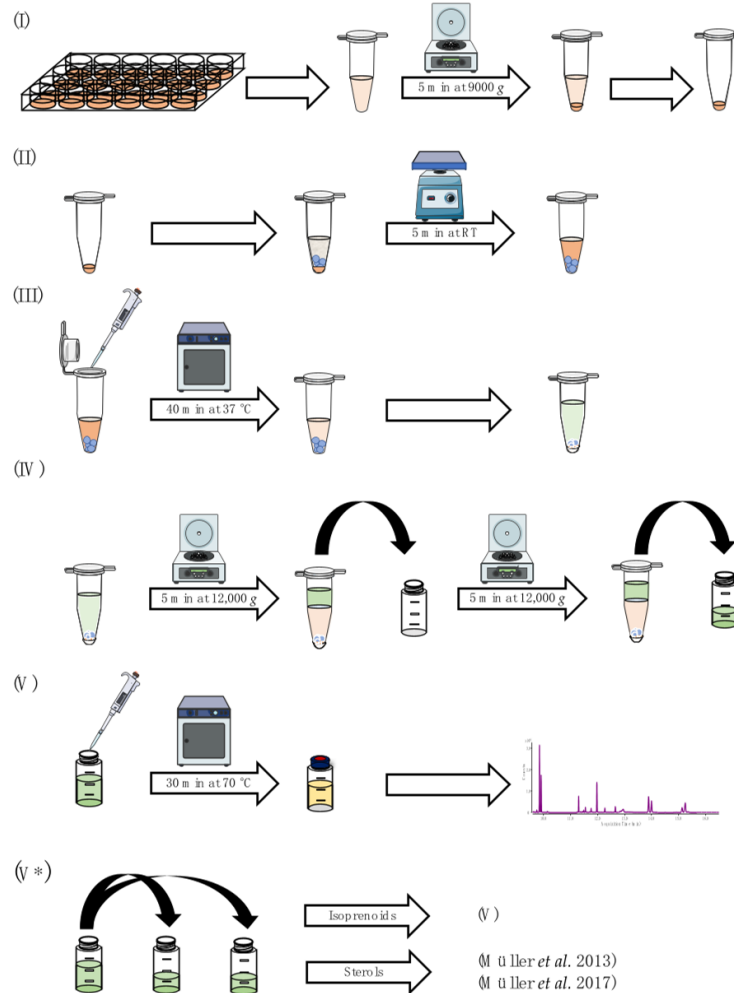


**Figure 2.** Schematic overview of the sample preparation, which can be divided into five individual steps: (I) preparation of cellular matrix; (II) mechanical lysis of cells/lyophilized mycelia in enzymatic buffer; (III) enzymatic deconjugation and preparation of liquid-liquid extraction; (IV) liquid-liquid extraction; (V) derivatization and GC-MS measurement; (V\*) alternative sample preparation for additional sterol pattern analysis [9,28]. Parts of this figure were created using Servier Medical Art templates, licensed under a Creative Commons Attribution 3.0 Unported License (<https://smart.servier.com> (accessed on 19 July 2023)).

For mechanical cell lysis, three 1.5 mm and three 3.0 mm glass beads were added to the remaining cell pellet/lyophilized cells and resuspended in 590  $\mu\text{L}$  of DEA-buffer, before the microcentrifuge safe-lock tube was vortexed for 5 min (Figure 2II). Then, 10  $\mu\text{L}$  of a bovine alkaline phosphatase suspension in DEA-buffer (0.4 mg/mL) was added and the mixture was incubated for 40 min at 37 °C. Afterward, the enzymatic reaction was stopped by adding  $300 \pm 6$  mg of NaCl, 300  $\mu\text{L}$  of acetonitrile/acetone (2/1; v/v), 350  $\mu\text{L}$  of *n*-hexane and 100  $\mu\text{L}$  of the internal standard mixture containing 1-heptadecanol ( $IS_{\text{Iso}}$ , 50  $\mu\text{g}/\text{mL}$  in *n*-hexane) and cholestane ( $IS_{\text{Sterol}}$ , 10  $\mu\text{g}/\text{mL}$  in *n*-hexane) (Figure 2III). After vigorously shaking for 1 min per hand, the sample was centrifuged for 5 min at  $12,000 \times g$  at RT. Then, 450  $\mu\text{L}$  of the upper *n*-hexane layer was transferred into a GC-vial (first extraction step). The mixture was extracted a second time in the same manner with another 750  $\mu\text{L}$  of

*n*-hexane (second extraction step). After centrifugation, 650  $\mu$ L of the organic upper layer was transferred to the GC-vial from the first extraction step (Figure 2IV). The combined organic extracts were derivatized by adding 30  $\mu$ L of *tert*-butyldiphenylchlorosilane and 30  $\mu$ L of imidazole solution (262 mg/mL in tetrahydrofuran). For complete derivatization, the sample was stored for 30 min at 70  $^{\circ}$ C before being subjected to GC-MS analysis (Figure 2V). Analysis of culture supernatant harvested after incubation was conducted using the residues from 1.0 mL of freeze-dried medium and resuspending it in 590  $\mu$ L of DEA-buffer (starting at Figure 2II). A chromatogram of spiked *A. fumigatus* sample is shown in Figure 3.

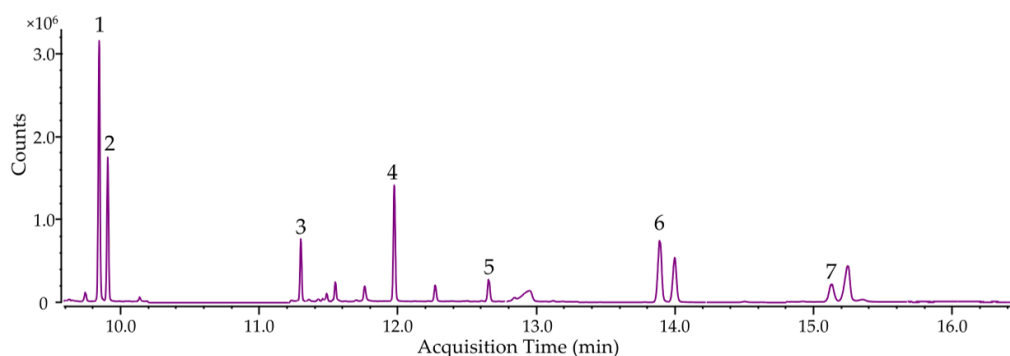


**Figure 3.** Selected ion chromatogram of spiked isoprenes (1000 ng/mL) detected as *t*BDPS ethers (squalene is not derivatized) in *A. fumigatus*. Isoprenol (1), prenol (2), geraniol (3), squalene (4), farnesol (5),  $IS_{Iso}$  (6), geranylgeraniol (7).

For additional sterol analysis, the combined organic extracts were split. Five hundred microliters was transferred into a new GC-vial and evaporated to dryness before the sample was analyzed according to Müller et al. [9,28]. For the analysis of the isoprenoids, the remaining 600  $\mu$ L of the organic extract was derivatized as described above (Figure 2V\*).

#### 2.6. Method Validation

Method validation was performed according to the EMEA guideline on bioanalytical method validation EMEA/CHMP/EWP/192217/2009 [42]. According to the guideline, the following criteria were determined: selectivity, linearity, lower limit of quantification (LLOQ), accuracy, precision, carry over, dilution integrity, matrix effects and stability. In addition, the parameters recovery and injection precision were determined (Supplementary Material, Method validation).

#### 2.7. Growth Tests of the Conditional *erg<sup>9</sup><sub>tetOn</sub>* and *erg<sup>1</sup><sub>tetOn</sub>* Strains

A total of 1500 conidia suspended in 3  $\mu$ L of double-distilled water were spotted on AMM plates and incubated at 37  $^{\circ}$ C for 48  $\pm$  2 h. The plates were then photographed and the diameter of each colony was determined using ImageJ [49]. The strains were tested in triplicates.

#### 2.8. Identification of Isoprenoid Patterns in *A. fumigatus*

The applicability of the previously validated method was tested on lyophilized cells and lyophilized growth medium from *A. fumigatus*. Cells from doxycycline inducible mutant strains were compared to doxycycline-treated wt cells. In addition, a distinction between intermediates originating from pyrophosphates that were generated by enzymatic deconjugation during sample preparation and their corresponding free alcohols was made. This was accomplished by splitting one lyophilized sample into two samples. The samples were analyzed with/without enzymatic deconjugation step (see Section 2.5.3, Figure 2III).

Besides mutant strains that contain inducible gene variants of *erg9* or *erg1*, terbinafine-treated wt cells were also analyzed and compared to untreated wt cells.

### 3. Results

#### 3.1. Sample Preparation

##### 3.1.1. Extraction Solvent

Several methods have been described for the extraction of lipids and sterols from biological matrices, mainly based on the well-known methods from Bligh and Dyer [50] or Folch et al. [51]. Both original methods use the cancerogenic organic solvent chloroform in combination with methanol, which were replaced by ethyl acetate and ethanol in more recent approaches [52]. For the extraction of sterols, more specific methods have been developed, performing liquid–liquid extraction using only one organic solvent, e.g., diethyl ether, *n*-hexane or methyl *tert*-butyl ether [9,53]. Due to the aim of simultaneous analysis of the intermediates of the isoprenoid pathway along with distal sterol biosynthesis intermediates, method development was based on an approach for sterol extraction [9]. Preliminary tests using water revealed that *n*-hexane is the best organic solvent for extraction of isoprenoids (Figure 4, green bars: *n*-hexane). Even though *iso*-hexane and *n*-heptane were as efficient as *n*-hexane in terms of recovery, their recovery values were accompanied by a higher standard deviation (SD). Because recovery should be further improved during method development, a low SD was preferred in the beginning of method development. Especially for the small terpenes isoprenol and prenol that were extracted most inefficiently, the SD was low when *n*-hexane was used. Diethyl ether, ethyl acetate and methyl *tert*-butyl ether were not capable of extracting the isoprenoids in an efficient way compared to *iso*-hexane, *n*-heptane or *n*-hexane.

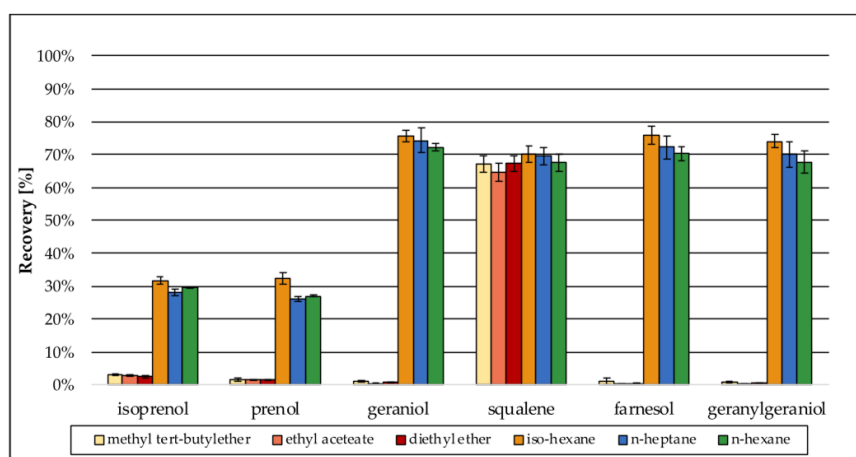


**Figure 4.** Preliminary recovery of the analytes during method development in different organic solvents that were tested for their capability to extract isoprenoids from water. Values were normalized using standards of the analytes (1000 ng/mL) in *n*-hexane. Error bars represent the standard deviation of five technical replicates.

The extraction procedure was improved by salting out the aqueous phase using sodium chloride in excess, to increase the recovery of the short-carbon-chain alcohols isoprenol and prenol (C<sub>5</sub>) that are better miscible with water than the C<sub>10</sub>–C<sub>20</sub> isoprenoids. In matrix-matched approaches, (*S. cerevisiae*) recovery for all analytes decreased due to interactions of the isoprenoids with the cellular matrix (Figure 5, purple bars: *n*-hexane). To increase recovery in matrix-matched approaches again, mixtures of *n*-hexane with acetonitrile or acetone in the first of two extraction steps were efficient. Especially, farnesol (FOH) and geranylgeraniol (GGOH) were extracted more successfully when only one of

those organic solvents was present, whereas the extractability for the smaller hemiterpenes (C<sub>5</sub>) decreased in the presence of acetonitrile (Figure 5).

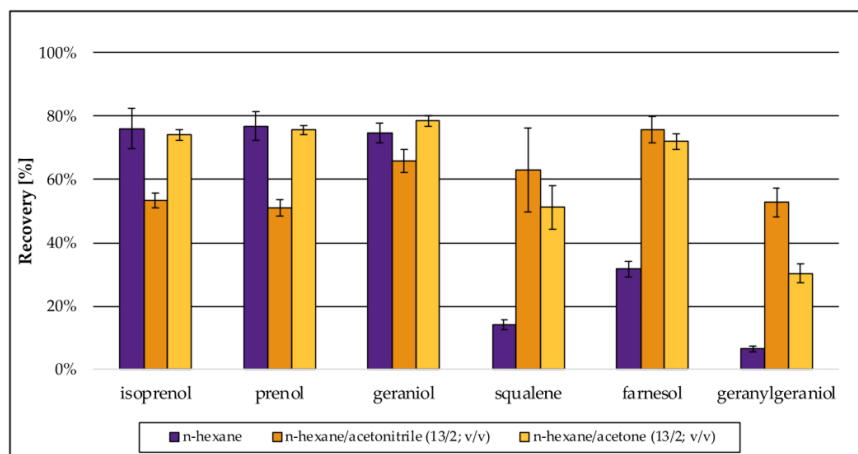


**Figure 5.** Preliminary recovery of isoprenoids extracted from *S. cerevisiae* matrix during method development: *n*-hexane was used as single extraction solvent or in combination with acetonitrile or acetone. Values were normalized using standards of the analytes (1000 ng/mL) in *n*-hexane. Error bars represent the standard deviation of five technical replicates.

The addition of acetonitrile (first extraction: *n*-hexane/acetonitrile (11/4; *v/v*)) was most beneficial for the extraction of larger terpenes (squalene, farnesol, geranylgeraniol), whereas the extraction for the smaller terpenes (isoprenol, prenol, geraniol) with acetonitrile (first extraction: *n*-hexane/acetonitrile (11/4; *v/v*)) was less effective. The use of *n*-hexane/acetone (first extraction: *n*-hexane/acetone (11/4; *v/v*)) gave similar results for the smaller terpenes (isoprenol, prenol, geraniol) as pure *n*-hexane, but lower recovery levels especially for geranylgeraniol (Figure 5). Therefore, the optimized extraction solvent was a mixture of *n*-hexane, acetone and acetonitrile (9/4/2; *v/v/v*) in the first extraction step. Without the addition of the solvent mixture in the first extraction step, recovery of geranylgeraniol was below 10% in matrix-matched samples, which could be improved to >40% (Table 4). Hence, the final solvent mixture for the salt-assisted liquid–liquid extraction (SALLE) was a mixture of *n*-hexane/acetone/acetonitrile (9/4/2; *v/v/v*) for the first extraction step followed by a second extraction with *n*-hexane (ratio after second extraction step: *n*-hexane/acetone/acetonitrile (12/2/1; *v/v/v*)) (see Supplementary Material, S2.7 Recovery).

**Table 4.** Recovery and SD values of spiked isoprenoids extracted from *S. cerevisiae*. Values were normalized using matrix-matched standards (1000 ng/mL). SD is the standard deviation from six technical replicates.

	Isoprenol	Prenol	Geraniol	Squalene	Farnesol	Geranyl-Geraniol
Recovery (%)	88	83	74	73	67	42
SD (%)	5	4	3	5	8	7

### 3.1.2. Enzymatic Deconjugation

For the analysis of isoprenoids as *t*BDPS ethers by GC-MS, the free alcohols of the pyrophosphorylated isoprenoids are mandatory. For this reason, an additional step for deconjugation is essential. According to literature, enzymatic deconjugation is a convenient

way to perform ester cleavage of phosphates and pyrophosphates. Therefore, the use of phosphatase is an established method [30–33]. The enzyme is most commonly obtained from bovine intestine [31,32] but can also be extracted from human placenta [30], bacteria or fungi [33]. Due to the different sources the enzyme can originate from, specific activity optima depending on the buffer system, pH, temperature and incubation time had to be considered. In contrast to Huang et al. [33], where two specific enzymes were needed (pyrophosphatase and phosphatase) to cleave the diphosphate esters, in this approach, only bovine alkaline phosphatase was used, which is capable of performing as a diphosphatase as well as an orthophosphatase. The use of a diethanolamine (DEA) buffer according to the manufacturer's protocol generates a higher enzyme activity for alkaline phosphatase from bovine kidney compared to tris or glycine buffers [54]. The buffer was supplemented with magnesium chloride, which is essential for the orthophosphatase activity but can also be rate-limiting for diphosphatase activity, if concentrations were not adjusted [31]. As a critical parameter, the pH was adjusted to 8.6, whereas higher pH values were accompanied by decreased recovery (Figure 6). Recovery for the analyte dimethylallyl pyrophosphate was best when the enzymatic reaction was stopped after 40 min compared to shorter and longer incubation times. Also, the amount of enzyme was considered, because the ability of enzymes to catalyze reactions is not limited to one direction. The optimized enzymatic deconjugation step consists of 40 min of incubation time at 37 °C using a 1 M diethanolamine buffer pH 8.6 containing magnesium chloride hexahydrate (0.5 mM). In a matrix-matched approach (Figure 7), the recovery of prenol (64%) was slightly decreased compared to the previous tests in buffer (75%) (Figure 6), whereas the extraction of farnesol was 114% and was therefore quantitative. The recovery of geranylgeraniol was 35%, which could already be expected due to the lower recovery from extraction (see Section 3.1.1; Table 4).

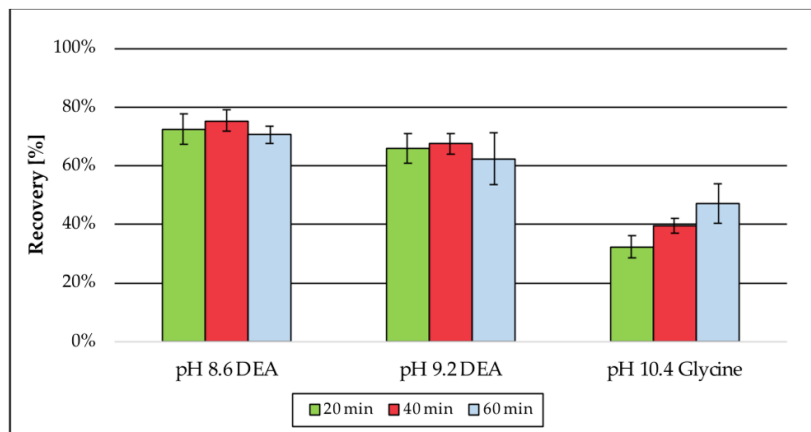


**Figure 6.** Recovery of prenol generated by enzymatic deconjugation from dimethylallyl pyrophosphate depending on pH and incubation time. The samples were dissolved in the corresponding buffers and normalized using standards of prenol in *n*-hexane (5 µM). Error bars represent the standard deviation of six technical replicates.

### 3.2. Validation of the Test System

An overview of tested parameters and the results is given in Table 5. For full validation data and more detailed explanation, see Supplementary Material: S1. Method validation and S2. Validation results.

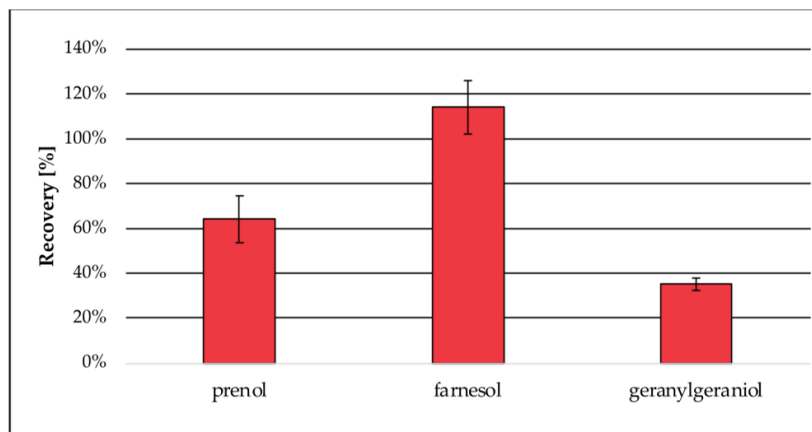


**Figure 7.** Recovery of prenol, farnesol and geranylgeraniol generated by enzymatic deconjugation from their corresponding pyrophosphates in matrix (*S. cerevisiae*). Peak areas were normalized using matrix-matched standards of the analytes (5  $\mu$ M). Error bars represent the standard deviation of six technical replicates.

**Table 5.** Overview of validation data; n.d., not determined.

Validation Parameter		Isoprenol	Prenol	Geraniol	Squalene	Farnesol	Geranyl-Geraniol
Linearity (ng/mL)	Calibration range	2.5–1000	2.5–1000	2.5–1000	2.5–1000	2.5–1000	2.5–1000
Average Accuracy (%)	Day 1	91	90	104	98	109	111
	Day 2	92	87	94	83	97	105
	Day 3	100	104	104	100	107	109
Precision (%)	Day 1	3	4	3	5	4	3
	Day 2	5	4	6	6	3	3
	Day 3	4	3	3	4	3	3
Matrix factor	Low QC	1.11	1.03	1.05	1.66	1.99	1.21
	High QC	1.01	1.02	0.99	1.16	1.03	1.05
Carry over (%)		35	33	29	90	61	49
Dilution Integrity		confirmed	confirmed	confirmed	confirmed	confirmed	confirmed
Stability		stability was tested after 5/30 days—storage should be performed in a freezer (−20 °C)					
Recovery (%)	<i>S. cerevisiae</i>	n.d.	107	n.d.	n.d.	133	44
	<i>A. fumigatus</i>	n.d.	85	n.d.	n.d.	109	37

### 3.3. Application on Biological Samples from *A. fumigatus*

#### 3.3.1. Analysis of the Conditional *erg9* Strain

Downregulation of *erg9* gene expression leads to the inability of *A. fumigatus* to grow (Supplementary Material Figure S1). In the presence of low doxycycline concentrations (1  $\mu$ g/mL and 2  $\mu$ g/mL), growth of the conditional *erg9* strain is still possible, although reduced when compared to the wt or the fully induced *erg9* mutant strain. As shown in Figure 8, this reduced growth is accompanied by an accumulation of the free alcohols isoprenol, farnesol and geranylgeraniol (Figure 8). This accumulation of free alcohols, corresponding to their isoprenoid pathway intermediates, is Dox-dependent and reaches from n.d. (2  $\mu$ g/mL Dox) to approx. 1 ng/mg (on dry weight basis (dw); 1  $\mu$ g/mL Dox) of isoprenol, 8 ng/mg (dw; 2  $\mu$ g/mL Dox) to 339 ng/mg (dw; 1  $\mu$ g/mL Dox) of farnesol, and 2 ng/mg (dw; 2  $\mu$ g/mL Dox) to 8 ng/mg (dw; 1  $\mu$ g/mL Dox) of geranylgeraniol. The use of alkaline phosphatase (compare Figure 2III) capturing pyrophosphorylated intermediates did not influence terpene levels.

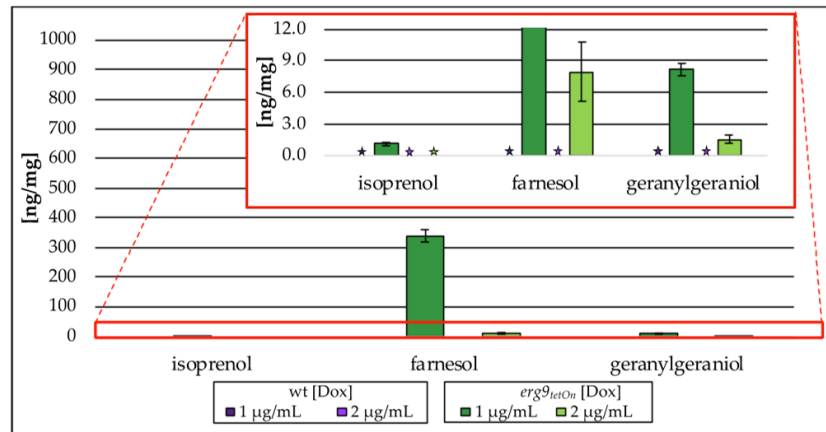


**Figure 8.** Amount of isoprenol, farnesol and geranylgeraniol in ng per mg biomass (dry weight) extracted from the conditional *erg9<sup>letOn</sup>* strain cultured with different concentrations of doxycycline (Dox; 1 µg/mL, 2 µg/mL). In the red box, the zoomed *y*-axis is depicted. Error bars represent the standard deviation from three biological replicates, each analyzed as technical duplicates. ★ not detected (n.d.).

Lanosterol and eburicol, representative sterols of the post-squalene pathway, were hardly affected, whereas ergosterol levels were decreased to 410 ng/mg (dw; 1 µg/mL Dox)-839 ng/mg (dw; 2 µg/mL Dox; Figure 9), which is a decrease of 67% (1 µg/mL Dox)-10% (2 µg/mL Dox) compared to their respective wt strain. In addition, the amount of squalene was reduced to 46 ng/mg (dw; 1 µg/mL Dox)/43 ng/mg (dw; 2 µg/mL Dox), a decrease of 14% (1 µg/mL Dox)/15% (2 µg/mL Dox) in relation to the wt. The associated *A. fumigatus* wt strain did not contain any isoprenoids of the isoprenoid pathway of ergosterol biosynthesis above the lower limit of quantification.

### 3.3.2. Analysis of the Conditional *erg1* Strain

The growth analysis of the conditional *erg1* mutant strain also revealed a growth defect under fully repressed conditions (Supplementary Material Figure S1). Low doxycycline concentrations enabled this mutant to grow, even though growth was reduced when compared to the wt or the mutant under fully induced conditions. The reduced growth is accompanied by a Dox-dependent accumulation of squalene and a decrease in eburicol (Figure 10). The squalene levels increased 3–50-fold (100 ng/mg (dw; 3 µg/mL Dox)-2236 ng/mg (dw; 0.5 µg/mL Dox)), compared to the wt strain 32 ng/mg (dw; 3 µg/mL Dox)-45 ng/mg (dw; 0.5 µg/mL Dox), whereas eburicol levels were between 6 ng/mg (dw; 3 µg/mL Dox) and 1 ng/mg (dw; 0.5 µg/mL Dox) compared to 9 ng/mg (dw; 3 µg/mL Dox) and 14 ng/mg (dw; 0.5 ng/mL Dox) in wt, a decrease of 32% (3 µg/mL Dox)-92% (0.5 µg/mL Dox). Lanosterol and ergosterol amounts, however, slightly increased when the mutant strain was exposed to high concentrations of Dox (3 µg/mL), whereas a low Dox concentration (0.5 µg/mL) resulted in a 76% decrease in lanosterol amount (3 ng/mg; dw) and 62% decrease in ergosterol amount (370 ng/mg; dw). None of the isoprenoid pathway intermediates were detected in samples from the *erg1* mutant strain as well as the associated wt strain.

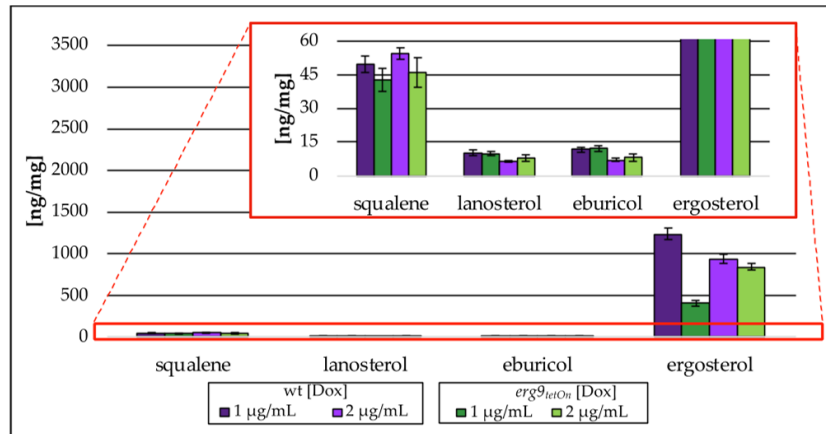


**Figure 9.** Amount of squalene and intermediates of the post-squalene pathway in ng per mg biomass (dry weight) extracted from the conditional *erg9<sup>tetOn</sup>* strain cultured with different concentrations of doxycycline (Dox; 1 µg/mL, 2 µg/mL). In the red box, the zoomed *y*-axis is depicted. Error bars represent the standard deviation from three biological replicates, each analyzed as technical duplicates.

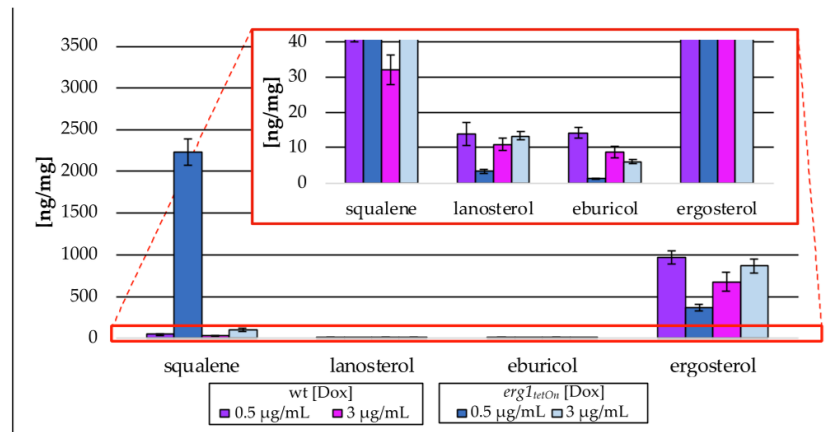


**Figure 10.** Amount of squalene and intermediates of the post-squalene pathway in ng per mg biomass (dry weight) extracted from the conditional *erg1<sup>tetOn</sup>* strain cultured with different concentrations of doxycycline (Dox; 0.5 µg/mL, 3 µg/mL). In the red box, the zoomed *y*-axis is depicted. Error bars represent the standard deviation from three biological replicates, each analyzed as technical duplicates.

### 3.3.3. Analysis of *erg9/erg1* Culture Supernatants

Analysis of lyophilized culture supernatants did not show any intermediates of the isoprenoid pathway in medium collected from the conditional *erg1* mutant strain when the corresponding gene was downregulated. The culture supernatant gained from the conditional *erg9* mutant strain during low induction (1 µg/mL/2 µg/mL Dox), however, showed high levels of farnesol (Figure 11). This farnesol was generated from farnesyl pyrophosphate by enzymatic deconjugation during sample preparation (compare Figure 2III). If the enzymatic deconjugation was conducted as a part of sample preparation, 135 ng/mL of medium farnesol was detected in the culture supernatant of the *erg9* mutant strain incubated with 1 µg/mL of Dox, whereas without the enzymatic step, only 9 ng/mL of medium were detected. Also, the culture supernatant harvested from the *erg9* mutant strain incubated with 2 µg/mL of

Dox contained farnesyl pyrophosphate, which was analyzed as farnesol. The amount was 2 ng/mL of medium without the use of alkaline phosphatase and 6 ng/mL of medium when the enzyme was used. Further isoprenoids could not be detected.

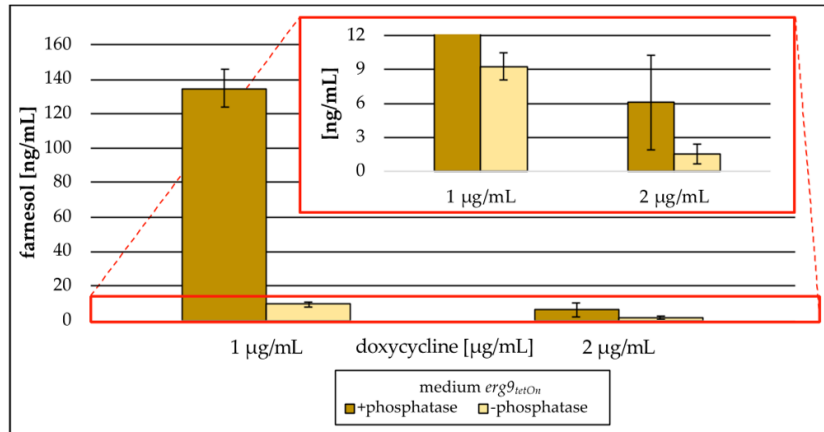


**Figure 11.** Amount of farnesol in ng per mL medium (freeze-dried) gained from the conditional *erg9<sup>tetOn</sup>* strain cultured with different concentrations of doxycycline (1 µg/mL, 2 µg/mL). In the red box, the zoomed y-axis is depicted. Error bars represent the standard deviation from three biological replicates.

### 3.3.4. Terbinafine Treatment of the Wild Type Strain

As proof of concept, the Erg1 inhibitor terbinafine was tested [11,29]. Terbinafine treatment resulted in a concentration-dependent accumulation of squalene (270–2793 ng/mg; dw) and a severe decrease in ergosterol (228 ng/mg; dw) at the highest (0.0500 µg/mL) terbinafine concentration tested (Figure 12). Exposure of wt to the two lower terbinafine concentrations (0.0250 and 0.0125 µg/mL) neither led to a decrease in ergosterol nor the reduction in its precursor sterol lanosterol and eburicol. Intermediates from the isoprenoid pathway could not be detected. Taken together, terbinafine treatment resulted in a similar sterol pattern as it was observed in the *erg1* repression model (see Figure 10).

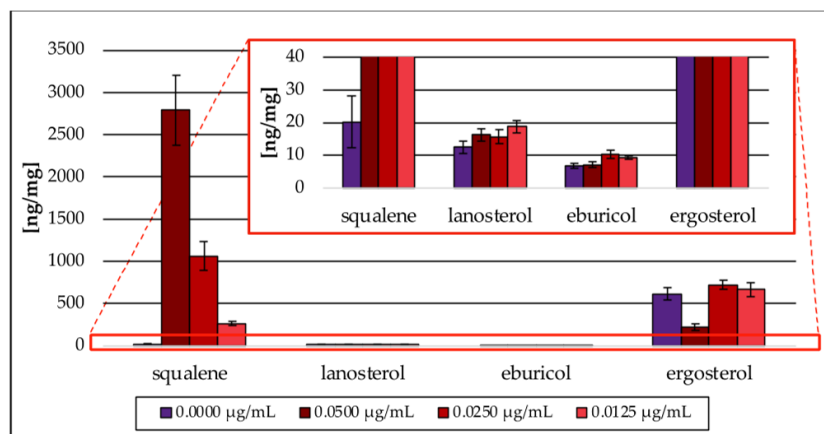


**Figure 12.** Amount of squalene and intermediates of the post-squalene pathway in ng per mg biomass (dry weight) extracted from *A. fumigatus* wt strain treated with different concentrations of terbinafine. In the red box, the zoomed y-axis is depicted. Error bars represent the standard deviation from three biological replicates, each analyzed as technical duplicates.

#### 4. Discussion

A novel gas chromatography–mass spectrometry (GC-MS) method for the analysis of intermediates of the isoprenoid pathway was developed. The method was optimized for the extraction of pyrophosphorylated terpenes from different fungal sources. Covering a calibration range from 2.5/25 to 1000 ng/mL (terpenes/squalene), the approach is sensitive to measuring small changes in levels of isoprenoid biosynthesis intermediates. In addition, signals are measured with a high accuracy (low, medium and high level: 93–112%; LLOQ: 82–115%) and selectivity (low, medium and high level: <6%; LLOQ: <14%). To our knowledge, this is the first GC-based approach covering the whole isoprenoid pathway including the isomers dimethylallyl pyrophosphate and isopentenyl pyrophosphate in one straightforward protocol. By combining this new isoprenoid assay (five involved enzymes including *Bts1*) with the established post-squalene ergosterol biosynthesis assay (Müller et al. [9,28]; ten involved enzymes), effects on 15 different enzymes can be covered from one sample. This will make it easier to identify mechanisms of action for new potential antifungals affecting ergosterol biosynthesis. Further advantages are the small amount of sample matrix that is required (dw;  $5 \pm 0.2$  mg), as well as the short time of analysis (23 min cycle time). The only disadvantage of the approach is its limitation to the intermediates of the isoprenoid pathway. A potential inhibition of mevalonate pathway enzymes can only be assumed as a change in the downstream sterol pattern but cannot be assigned to a specific enzyme. Up until now, only liquid chromatography (LC)-based approaches have been available for the analysis of mevalonate pathway intermediates (Table 1). In LC methods, mono- and di-phosphates can be distinguished, whereas the simultaneous analysis of the isomers isopentenyl pyrophosphate and dimethylallyl pyrophosphate is not possible [39].

The analysis of the *A. fumigatus* mutant strain revealed that the main part of the detected terpenes was already intracellularly available as free alcohols and enzymatic deconjugation could not increase the detected terpene levels (Section 3.3.1). Our approach confirmed that only negligible amounts of farnesyl pyrophosphate were available in cells from the *erg9* mutant, whereas the main part was already dephosphorylated (Section 3.3.1). Besides farnesol, small amounts of geranylgeraniol and isoprenol were also found. Those analytes could be detected because of a strong farnesyl pyrophosphate accumulation, which increased the production of geranylgeranyl pyrophosphate and induced an accumulation of the upstream substrate isopentenyl pyrophosphate (Figure 1). Even though the pyrophosphates were suspected to have accumulated, it must be assumed that intracellular dephosphorylation occurred.

The analysis of the post-squalene pathway showed a slight reduction in squalene levels as well as a Dox-dependent decrease in ergosterol in the mutant strain, which is the expected consequence of an *erg9* downregulation. The generated sterol pattern therefore is in accordance with the results from the growth test of the conditional *erg9* strain (Supplementary Material Figure S1).

In the *erg1* mutant, no isoprenoid pathway intermediate could be detected above the limit of detection, even though upstream intermediates were expected as a secondary effect of squalene accumulation in the same way geranylgeraniol and isoprenol were found in the *erg9* mutant. Post-squalene pathway analysis showed increased squalene levels and decreased ergosterol amounts, which could be expected due to *erg1* downregulation. This outcome is similar to that observed for terbinafine treatment of the (*A. fumigatus*) wt strain (Section 3.3.4). Squalene levels in terbinafine-treated cells were increased and are in line with reduced amounts of ergosterol.

Surprisingly, the analysis of lyophilized growth medium revealed high amounts of farnesyl pyrophosphate, which were quantified as farnesol-*t*BDPS ether (Section 3.3.3). In comparison to an approach where the enzymatic deconjugation step was skipped, farnesol levels in culture supernatant were 4–14-fold higher when alkaline phosphatase was used. This indicates that farnesyl pyrophosphate is the preferred form to be extruded when increased intracellular levels occur. In contrast, farnesol is the preferred substrate

accumulating intracellularly. Those results are contrary to the findings of Song [36], who identified increased farnesyl pyrophosphate levels in cells from *S. cerevisiae* *erg9* mutant strains and assumed higher farnesol levels extracellularly in the culture medium [18].

The intra- and extracellular appearance of farnesol is of great interest because of its diverse attributes. In its role as a quorum-sensing molecule, farnesol is used to signal extracellularly with the environment, including other fungi and bacteria, and therefore has effects on virulence and biofilm formation [55,56]. Several reports [55,57] suggest that due to its immunomodulatory properties, the molecule promotes disease and even increases mortality during systemic *C. albicans* infection. On the other hand, synergistic effects with several antifungal drugs were identified, which are caused by a farnesol-mediated inhibition of the ABC drug transporters [58].

Besides the vague role of farnesol in fungal cells that must be further investigated, the interest in the whole isoprenoid pathway should be increased. Based on the essential role of isoprenoid pathway genes, the associated enzymes are promising targets for drug development. Since the isoprenoid pathway is part of both human and fungal metabolism, one of the largest challenges will therefore be the selectivity of potential drug candidates in fungal cells, as well as the investigation of the effect of isoprenoids on the host biosystem. However, the success of the imidazoles/triazoles, which also target both the mammalian and fungal sterol C14-demethylase, is indisputable. Expanding the established test system on mammalian cells should be a promising option to confirm selectivity.

**Supplementary Materials:** The following supporting information can be downloaded at: <https://www.mdpi.com/article/10.3390/jof9070768/s1>, Figure S1: Doxycycline-dependent growth of the conditional *erg9* and *erg1* strains. Validation results included. Figure S2: Selected ion chromatogram of quantifier ions at different concentrations. Figure S3: Single-ion-monitoring spectra of the isoprenoid *t*BDPS ethers, the internal standard *t*BDPS ether and squalene. Figure S4: Full-scan spectra of the isoprenoid *t*BDPS ethers, the internal standard *t*BDPS ether and squalene. Figure S5: Investigation of matrix effects comparing signal areas of low- and high-QC samples in *n*-hexane and sample matrix. Figure S6: Sample stability over 30 days comparing stability on days 0, 5 and 30. Figure S7: Recovery of three representative pyrophosphates from *S. cerevisiae* and *A. fumigatus* matrix. Table S1: Evaluation of method accuracy measured on three subsequent days. Table S2: Evaluation of method precision measured on three subsequent days. Table S3: Matrix effects determined at two different concentrations and the associated standard deviation. Table S4: Carry over. Table S5: Standard deviation as additional criterion for recovery.

**Author Contributions:** Conceptualization, M.L., J.W., F.G. and C.M.; methodology, M.L., H.E., P.M. and C.M.; validation, M.L. and L.H.; formal analysis, M.L., L.H., P.M. and F.G.; investigation, M.L., L.H., H.E., J.W., P.M., F.G. and C.M.; resources, J.W., F.G. and C.M.; data curation, M.L., L.H., J.W., F.G. and C.M.; writing—original draft preparation, M.L. and C.M.; writing—review and editing, M.L., J.W., F.G. and C.M.; visualization, M.L. and H.E.; supervision, J.W., F.G. and C.M. All authors have read and agreed to the published version of the manuscript.

**Funding:** This work was supported by the Austrian Science Fund (F.G., P35951) and by the German Research Foundation (J.W., DFG-WA3016/4-1).

**Institutional Review Board Statement:** Not applicable.

**Informed Consent Statement:** Not applicable.

**Data Availability Statement:** Data available from the corresponding author.

**Acknowledgments:** M.L. and C.M. thank Franz Bracher for providing his laboratories, resources and discussions.

**Conflicts of Interest:** The authors declare that there are no conflict of interest.

## References

1. Houšť, J.; Spížek, J.; Havlíček, V. Antifungal drugs. *Metabolites* **2020**, *10*, 106. [CrossRef] [PubMed]
2. Denning, D.W.; Bromley, M.J. How to bolster the antifungal pipeline. *Science* **2015**, *347*, 1414–1416. [CrossRef] [PubMed]

3. Osset-Trénor, P.; Pascual-Ahuir, A.; Proft, M. Fungal drug response and antimicrobial resistance. *J. Fungi* **2023**, *9*, 565. [CrossRef] [PubMed]
4. WHO. Fungal Priority Pathogens List to Guide Research, Development and Public Health Action. Available online: <https://www.who.int/publications/i/item/9789240060241> (accessed on 24 March 2023).
5. Hoenigl, M. Invasive fungal disease complicating coronavirus disease 2019: When it rains, it spores. *Clin. Infect. Dis.* **2021**, *73*, e1645–e1648. [CrossRef]
6. Narayanan, S.; Chua, J.V.; Baddley, J.W. Coronavirus disease 2019–associated mucormycosis: Risk factors and mechanisms of disease. *Clin. Infect. Dis.* **2022**, *74*, 1279–1283. [CrossRef]
7. Song, G.; Liang, G.; Liu, W. Fungal co-infections associated with global COVID-19 pandemic: A clinical and diagnostic perspective from China. *Mycopathologia* **2020**, *185*, 599–606. [CrossRef]
8. Bhatt, K.; Agolli, A.; Patel, M.H.; Garimella, R.; Devi, M.; Garcia, E.; Amin, H.; Domingue, C.; Guerra Del Castillo, R.; Sanchez-Gonzalez, M. High mortality co-infections of COVID-19 patients: Mucormycosis and other fungal infections. *Discoveries* **2021**, *9*, e126. [CrossRef]
9. Müller, C.; Binder, U.; Bracher, F.; Giera, M. Antifungal drug testing by combining minimal inhibitory concentration testing with target identification by gas chromatography-mass spectrometry. *Nat. Protoc.* **2017**, *12*, 947–963. [CrossRef]
10. Grabinska, K.; Palamarczyk, G. Dolichol biosynthesis in the yeast *Saccharomyces cerevisiae*: An insight into the regulatory role of farnesyl diphosphate synthase. *FEMS Yeast Res.* **2002**, *2*, 259–265. [CrossRef]
11. Jordá, T.; Puig, S. Regulation of ergosterol biosynthesis in *Saccharomyces cerevisiae*. *Genes* **2020**, *11*, 795. [CrossRef]
12. Homann, V.; Mende, K.; Arntz, C.; Ilardi, V.; Macino, G.; Morelli, G.; Böse, G.; Tudzynski, B. The isoprenoid pathway: Cloning and characterization of fungal FPPS genes. *Curr. Genet.* **1996**, *30*, 232–239. [CrossRef] [PubMed]
13. Mayer, M.P.; Hahn, F.M.; Stillman, D.J.; Poulter, C.D. Disruption and mapping of IDI1, the gene for isopentenyl diphosphate isomerase in *Saccharomyces cerevisiae*. *Yeast* **1992**, *8*, 743–748. [CrossRef] [PubMed]
14. Chemler, J.A.; Yan, Y.; Koffas, M.A. Biosynthesis of isoprenoids, polyunsaturated fatty acids and flavonoids in *Saccharomyces cerevisiae*. *Microb. Cell Fact.* **2006**, *5*, 20. [CrossRef]
15. Paramasivan, K.; Mutturi, S. Progress in terpene synthesis strategies through engineering of *Saccharomyces cerevisiae*. *Crit. Rev. Biotechnol.* **2017**, *37*, 974–989. [CrossRef]
16. Hu, T.; Zhou, J.; Tong, Y.; Su, P.; Li, X.; Liu, Y.; Liu, N.; Wu, X.; Zhang, Y.; Wang, J.; et al. Engineering chimeric diterpene synthases and isoprenoid biosynthetic pathways enables high-level production of miltiradiene in yeast. *Metab. Eng.* **2020**, *60*, 87–96. [CrossRef] [PubMed]
17. Rodriguez, S.; Kirby, J.; Denby, C.M.; Keasling, J.D. Production and quantification of sesquiterpenes in *Saccharomyces cerevisiae*, including extraction, detection and quantification of terpene products and key related metabolites. *Nat. Protoc.* **2014**, *9*, 1980–1996. [CrossRef]
18. Song, L. A soluble form of phosphatase in *Saccharomyces cerevisiae* capable of converting farnesyl diphosphate into E,E-farnesol. *Appl. Biochem. Biotechnol.* **2006**, *128*, 149–158. [CrossRef]
19. Meganathan, R. Ubiquinone biosynthesis in microorganisms. *FEMS Microbiol. Lett.* **2001**, *203*, 131–139. [CrossRef]
20. Singkaravanit, S.; Kinoshita, H.; Ihara, F.; Nihira, T. Geranylgeranyl diphosphate synthase genes in entomopathogenic fungi. *Appl. Microbiol. Biotechnol.* **2010**, *85*, 1463–1472. [CrossRef]
21. Nes, W.D. Biosynthesis of cholesterol and other sterols. *Chem. Rev.* **2011**, *111*, 6423–6451. [CrossRef]
22. Vallon, T.; Ghanegaonkar, S.; Vielhauer, O.; Müller, A.; Albermann, C.; Sprenger, G.; Reuss, M.; Lemuth, K. Quantitative analysis of isoprenoid diphosphate intermediates in recombinant and wild-type *Escherichia coli* strains. *Appl. Microbiol. Biotechnol.* **2008**, *81*, 175–182. [CrossRef] [PubMed]
23. Heuston, S.; Begley, M.; Gahan, C.G.M.; Hill, C. Isoprenoid biosynthesis in bacterial pathogens. *Microbiology* **2012**, *158*, 1389–1401. [CrossRef] [PubMed]
24. Chambon, C.; Ladeveze, V.; Oulmouden, A.; Servouse, M.; Karst, F. Isolation and properties of yeast mutants affected in farnesyl diphosphate synthetase. *Curr. Genet.* **1990**, *18*, 41–46. [CrossRef] [PubMed]
25. Berthelot, K.; Estevez, Y.; Deffieux, A.; Peruch, F. Isopentenyl diphosphate isomerase: A checkpoint to isoprenoid biosynthesis. *Biochimie* **2012**, *94*, 1621–1634. [CrossRef]
26. Zhao, J.; Li, C.; Zhang, Y.; Shen, Y.; Hou, J.; Bao, X. Dynamic control of ERG20 expression combined with minimized endogenous downstream metabolism contributes to the improvement of geraniol production in *Saccharomyces cerevisiae*. *Microb. Cell Factories* **2017**, *16*, 17. [CrossRef]
27. Peng, B.; Nielsen, L.K.; Kampranis, S.C.; Vickers, C.E. Engineered protein degradation of farnesyl pyrophosphate synthase is an effective regulatory mechanism to increase monoterpene production in *Saccharomyces cerevisiae*. *Metab. Eng.* **2018**, *47*, 83–93. [CrossRef]
28. Müller, C.; Staudacher, V.; Krauss, J.; Giera, M.; Bracher, F. A convenient cellular assay for the identification of the molecular target of ergosterol biosynthesis inhibitors and quantification of their effects on total ergosterol biosynthesis. *Steroids* **2013**, *78*, 483–493. [CrossRef]
29. Alcazar-Fuoli, L.; Mellado, E. Ergosterol biosynthesis in *Aspergillus fumigatus*: Its relevance as an antifungal target and role in antifungal drug resistance. *Front. Microbiol.* **2012**, *3*, 439. [CrossRef]

30. Lorenz, B.; Schröder, H.C. Mammalian intestinal alkaline phosphatase acts as highly active exopolyphosphatase. *Biochim. Biophys. Acta* **2001**, *1547*, 254–261. [CrossRef]
31. Fernley, H.N.; Walker, P.G. Studies on alkaline phosphatase. Inhibition by phosphate derivatives and the substrate specificity. *Biochem. J.* **1967**, *104*, 1011–1018. [CrossRef]
32. Saisho, Y.; Morimoto, A.; Umeda, T. Determination of farnesyl pyrophosphate in dog and human plasma by high-performance liquid chromatography with fluorescence detection. *Anal. Biochem.* **1997**, *252*, 89–95. [CrossRef] [PubMed]
33. Huang, B.; Zeng, H.; Dong, L.; Li, Y.; Sun, L.; Zhu, Z.; Chai, Y.; Chen, W. Metabolite target analysis of isoprenoid pathway in *Saccharomyces cerevisiae* in response to genetic modification by GC-SIM-MS coupled with chemometrics. *Metabolomics* **2011**, *7*, 134–146. [CrossRef]
34. McTaggart, F.; Brown, G.R.; Davidson, R.G.; Freeman, S.; Holdgate, G.A.; Mallion, K.B.; Mirrlees, D.J.; Smith, G.J.; Ward, W.H. Inhibition of squalene synthase of rat liver by novel 3' substituted quinuclidines. *Biochem. Pharmacol.* **1996**, *51*, 1477–1487. [CrossRef] [PubMed]
35. Bruenger, E.; Rilling, H.C. Determination of isopentenyl diphosphate and farnesyl diphosphate in tissue samples with a comment on secondary regulation of polyisoprenoid biosynthesis. *Anal. Biochem.* **1988**, *173*, 321–327. [CrossRef]
36. Song, L. Detection of farnesyl diphosphate accumulation in yeast ERG9 mutants. *Anal. Biochem.* **2003**, *317*, 180–185. [CrossRef]
37. Tong, H.; Holstein, S.A.; Hohl, R.J. Simultaneous determination of farnesyl and geranylgeranyl pyrophosphate levels in cultured cells. *Anal. Biochem.* **2005**, *336*, 51–59. [CrossRef]
38. Hooff, G.P.; Volmer, D.A.; Wood, W.G.; Müller, W.E.; Eckert, G.P. Isoprenoid quantitation in human brain tissue: A validated HPLC-fluorescence detection method for endogenous farnesyl- (FPP) and geranylgeranylpyrophosphate (GGPP). *Anal. Bioanal. Chem.* **2008**, *392*, 673–680. [CrossRef]
39. Henneman, L.; van Cruchten, A.G.; Denis, S.W.; Amolins, M.W.; Placzek, A.T.; Gibbs, R.A.; Kulik, W.; Waterham, H.R. Detection of nonsterol isoprenoids by HPLC-MS/MS. *Anal. Biochem.* **2008**, *383*, 18–24. [CrossRef]
40. Chhonker, Y.S.; Haney, S.L.; Bala, V.; Holstein, S.A.; Murry, D.J. Simultaneous quantitation of isoprenoid pyrophosphates in plasma and cancer cells using LC-MS/MS. *Molecules* **2018**, *23*, 3275. [CrossRef]
41. Castaño-Cerezo, S.; Kulyk-Barbier, H.; Millard, P.; Portais, J.C.; Heux, S.; Truan, G.; Bellvert, F. Functional analysis of isoprenoid precursors biosynthesis by quantitative metabolomics and isotopologue profiling. *Metabolomics* **2019**, *15*, 115. [CrossRef]
42. Guideline on Bioanalytical Method Validation. Available online: [https://www.ema.europa.eu/en/documents/scientific-guideline/guideline-bioanalytical-method-validation\\_en.pdf](https://www.ema.europa.eu/en/documents/scientific-guideline/guideline-bioanalytical-method-validation_en.pdf) (accessed on 28 March 2023).
43. Krappmann, S.; Sasse, C.; Braus, G.H. Gene targeting in *Aspergillus fumigatus* by homologous recombination is facilitated in a nonhomologous end-joining-deficient genetic background. *Eukaryot. Cell* **2006**, *5*, 212–215. [CrossRef] [PubMed]
44. Wagener, J.; Echtenacher, B.; Rohde, M.; Kotz, A.; Krappmann, S.; Heesemann, J.; Ebel, F. The putative alpha-1,2-mannosyltransferase AfMnt1 of the opportunistic fungal pathogen *Aspergillus fumigatus* is required for cell wall stability and full virulence. *Eukaryot. Cell* **2008**, *7*, 1661–1673. [CrossRef] [PubMed]
45. Helmschrott, C.; Sasse, A.; Samantaray, S.; Krappmann, S.; Wagener, J. Upgrading fungal gene expression on demand: Improved systems for doxycycline-dependent silencing in *Aspergillus fumigatus*. *Appl. Environ. Microbiol.* **2013**, *79*, 1751–1754. [CrossRef] [PubMed]
46. Neubauer, M.; Zhu, Z.; Penka, M.; Helmschrott, C.; Wagener, N.; Wagener, J. Mitochondrial dynamics in the pathogenic mold *Aspergillus fumigatus*: Therapeutic and evolutionary implications. *Mol. Microbiol.* **2015**, *98*, 930–945. [CrossRef]
47. Pontecorvo, G.; Roper, J.A.; Hemmons, L.M.; Macdonald, K.D.; Bufton, A.W. The genetics of *Aspergillus nidulans*. *Adv. Genet.* **1953**, *5*, 141–238. [CrossRef]
48. Renard, D.; Perruchon, J.; Giera, M.; Müller, J.; Bracher, F. Side chain azasteroids and thiaasteroids as sterol methyltransferase inhibitors in ergosterol biosynthesis. *Bioorg. Med. Chem.* **2009**, *17*, 8123–8137. [CrossRef]
49. Schneider, C.A.; Rasband, W.S.; Eliceiri, K.W. NIH Image to ImageJ: 25 years of image analysis. *Nat. Methods* **2012**, *9*, 671–675. [CrossRef]
50. Bligh, E.G.; Dyer, W.J. A rapid method of total lipid extraction and purification. *Can. J. Biochem. Physiol.* **1959**, *37*, 911–917. [CrossRef]
51. Folch, J.; Lees, M.; Sloane Stanley, G.H. A simple method for the isolation and purification of total lipides from animal tissues. *J. Biol. Chem.* **1957**, *226*, 497–509. [CrossRef]
52. Breil, C.; Abert Vian, M.; Zemb, T.; Kunz, W.; Chemat, F. “Bligh and Dyer” and Folch methods for solid-liquid-liquid extraction of lipids from microorganisms. Comprehension of solvation mechanisms and towards substitution with alternative solvents. *Int. J. Mol. Sci.* **2017**, *18*, 708. [CrossRef]
53. Giera, M.; Müller, C.; Bracher, F. Analysis and experimental inhibition of distal cholesterol biosynthesis. *Chromatographia* **2015**, *78*, 343–358. [CrossRef]
54. Phosphatase, Alkaline from Bovine Kidney. Available online: <https://www.sigmaaldrich.com/DE/de/product/sigma/p4653> (accessed on 22 May 2023).
55. Polke, M.; Leonhardt, I.; Kurzai, O.; Jacobsen, I.D. Farnesol signalling in *Candida albicans*—More than just communication. *Crit. Rev. Microbiol.* **2018**, *44*, 230–243. [CrossRef] [PubMed]
56. Hornby, J.M.; Jensen, E.C.; Lisec, A.D.; Tasto, J.J.; Jahnke, B.; Shoemaker, R.; Dussault, P.; Nickerson, K.W. Quorum sensing in the dimorphic fungus *Candida albicans* is mediated by farnesol. *Appl. Environ. Microbiol.* **2001**, *67*, 2982–2992. [CrossRef]

57. Leonhardt, I.; Spielberg, S.; Weber, M.; Albrecht-Eckardt, D.; Bläss, M.; Claus, R.; Barz, D.; Scherlach, K.; Hertweck, C.; Löffler, J.; et al. The fungal quorum-sensing molecule farnesol activates innate immune cells but suppresses cellular adaptive immunity. *mBio* **2015**, *6*, e00143. [[CrossRef](#)] [[PubMed](#)]
58. Sharma, M.; Prasad, R. The quorum-sensing molecule farnesol is a modulator of drug efflux mediated by ABC multidrug transporters and synergizes with drugs in *Candida albicans*. *Antimicrob. Agents Chemother.* **2011**, *55*, 4834–4843. [[CrossRef](#)] [[PubMed](#)]

**Disclaimer/Publisher’s Note:** The statements, opinions and data contained in all publications are solely those of the individual author(s) and contributor(s) and not of MDPI and/or the editor(s). MDPI and/or the editor(s) disclaim responsibility for any injury to people or property resulting from any ideas, methods, instructions or products referred to in the content.

4.4 Supporting Information

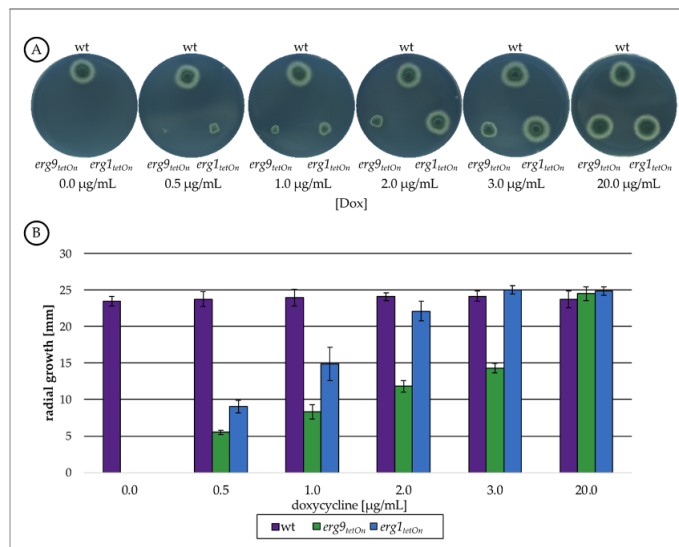


**Figure S1.** Doxycycline-dependent growth of the conditional *erg9* and *erg1* strains. 1,500 conidia of the indicated strains were spotted on AMM agar plates with the indicated concentration of doxycycline [Dox]. Plates were then incubated at 37 °C. A: Representative photos were taken after 48 h of incubation. B: The diameters of three colonies per strain and condition was measured after 48 h and plotted in the graph. The error bars indicate standard deviations.

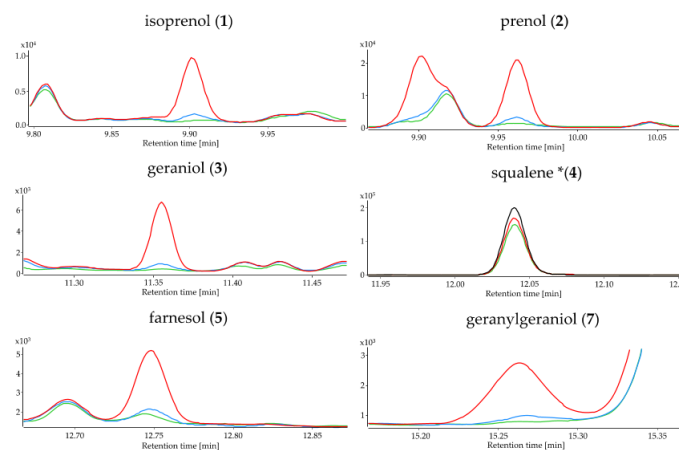


**Figure S2.** Selected ion chromatogram of quantifier ions at different concentrations analyzed from matrix matched samples (*S. cerevisiae*). Green: matrix blank; blue: lower limit of quantification (LLOQ) 2.5 ng/mL; red: 25 ng/mL; black: 100 ng/mL; \* Squalene is an endogenous analyte; no squalene free matrix was available.

# Quantifying Isoprenoids in the Ergosterol Biosynthesis by GC-MS

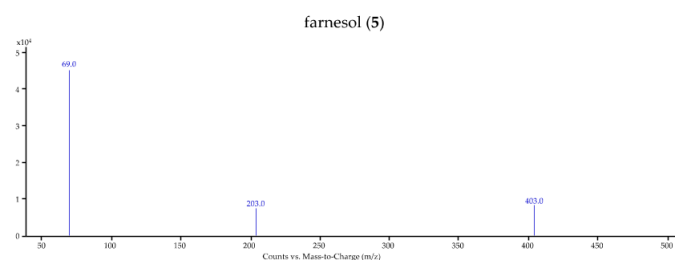
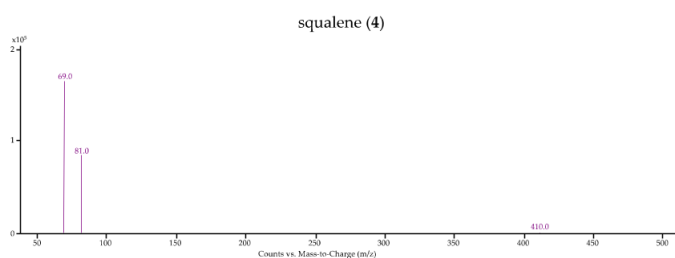
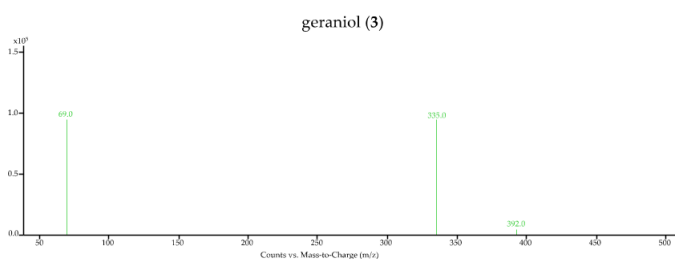
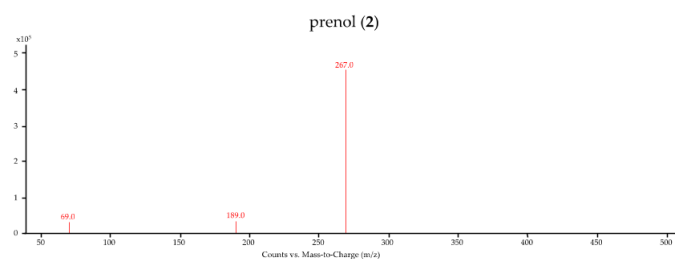
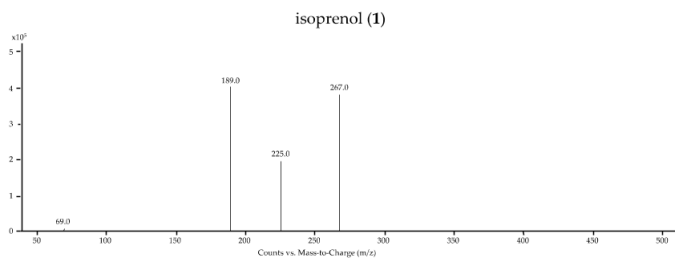
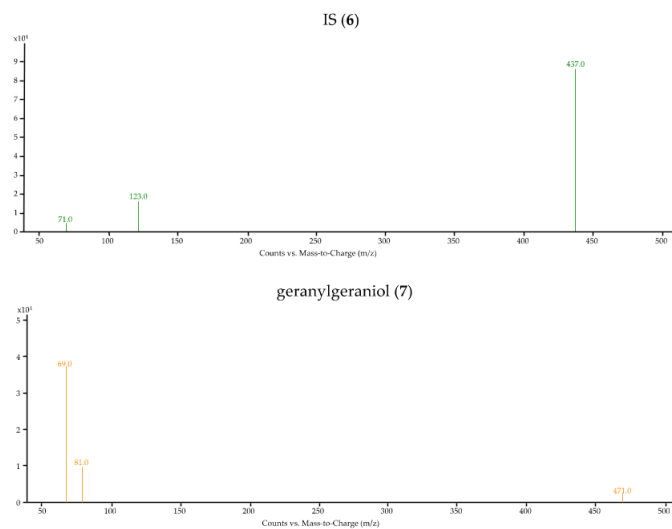
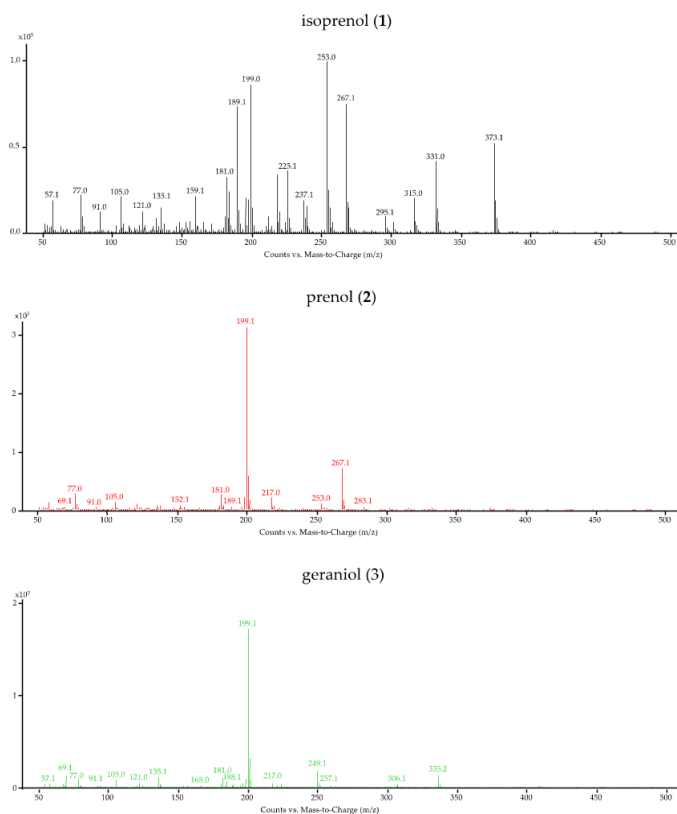


Figure S3. (continued)

# Quantifying Isoprenoids in the Ergosterol Biosynthesis by GC-MS



**Figure S3.** Single ion monitoring (SIM) spectra of the isoprenoid *t*BDPS ethers, the internal standard (1-heptadecanol; IS) *t*BDPS ether and squalene.



**Figure S4.** (continued)

# Quantifying Isoprenoids in the Ergosterol Biosynthesis by GC-MS

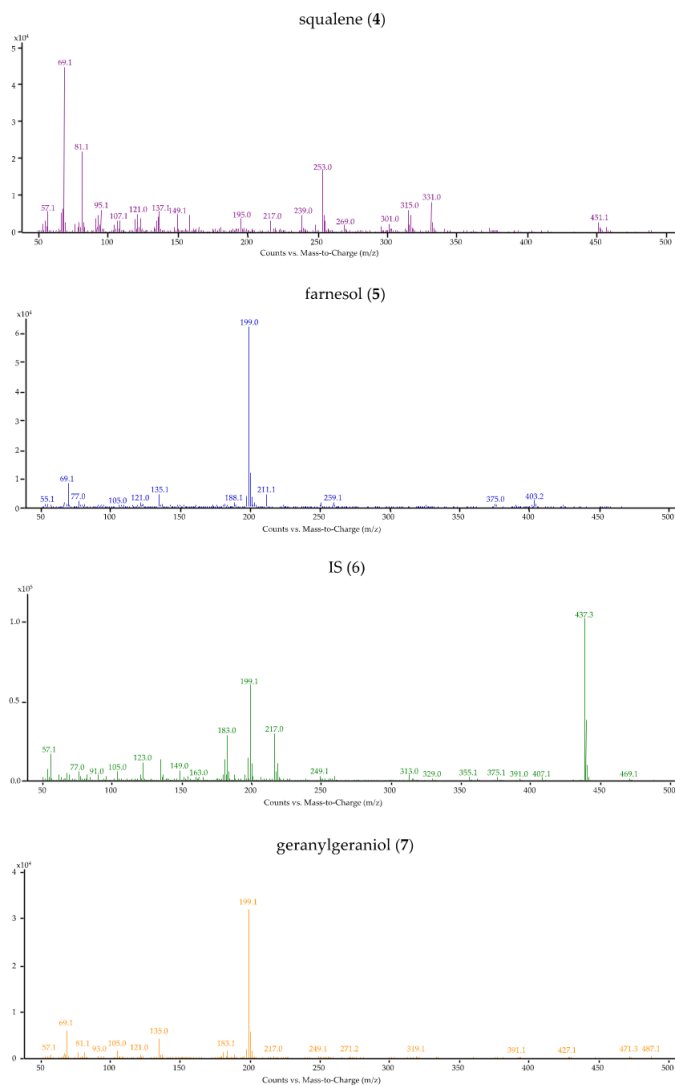


**Figure S4.** Full Scan spectra  $m/z$  50-500 of the isoprenoid *t*BDPS ethers, the internal standard (1-heptadecanol; IS) *t*BDPS ether and squalene.

## S1. Method validation

Method validation was performed based on the European Medicines Agency (EMA) guideline on bioanalytical method validation EMA/CHMP/EWP/192217/2009 [1].

### 1.1 Selectivity

Selectivity was confirmed by the relative retention time (RRT) of each analyte relating to the internal standard 1-heptadecanol (IS<sub>iso</sub>) and using three characteristic ions, two qualifiers and one quantifier ion (*Article: Table 2, Table 3*).

### S1.2 Linearity

Linearity of the calibration curves were determined by measuring spiked samples (matrix matched). Nine levels (2.5, 5.0, 10, 25, 50, 100, 250, 500 and 1,000 ng/mL) with a consistent concentration of IS<sub>iso</sub> (5 µg/mL) were analyzed in triplicates. Peak area ratios from quantifier ions of analytes and IS<sub>iso</sub> were plotted against the corresponding analyte concentration. The calibration curve was weighted (1/x) and used to back-calculate the individual concentration. The back-calculated concentration was further used to determine the standard deviation (SD), which should be within ±15% (lower limit of quantification (LLOQ) ±20%) of the nominal concentration. At least 75% of the calibration standards and 50% of the used replicates must fit those parameters.

### S1.3 Lower limit of quantification (LLOQ)

The lower limit of quantification (LLOQ) is defined as the lowest level of the calibration curve that can be quantified reliably. As additional criteria the parameters for accuracy and precision (*Supplementary material: Chapter 2.2*) were considered, whereas contrary to the guideline a peak area five-times higher than a blank sample (matrix blank) was not taken into account due to the endogeneity of squalene and interferences from consumables (*Supplementary material: Chapter 2.1*).

### S1.4 Accuracy and method precision

Accuracy and method precision were determined at LLOQs, low level (3×LLOQ), medium level (500 ng/mL) and high level (1,000 ng/mL) level. Therefore, sample matrix was prepared as described in *Article: Chapter 2.5.3* and pooled. The quality control (QC) samples were prepared by spiking matrix with 10 µL of an appropriate stock solution containing a mixture of all analytes before derivatization (n=6). To approve accuracy, the analyte signals were used to back-calculate the concentration of each level based on the calibration curve which was prepared independently from the QC samples with separately prepared stock solutions. The calculated concentration was divided by the nominal concentration. The SD of every level was calculated from the average relative response. Between-run accuracy and between-run precision were determined by repeating the analysis on three consecutive days.

# Quantifying Isoprenoids in the Ergosterol Biosynthesis by GC-MS

## S1.5 Instrument precision

The instrument precision was determined by calculating the SD for all analytes at different concentrations (LLOQ, low QC, medium QC, and high QC) after sixfold injection.

## S1.6 Investigation of matrix effects

Matrix effects were determined by comparing spiked samples prepared in matrix to samples prepared in *n*-hexane at two different concentrations (low and high; *n*=6). Matrix was prepared as described in *Article*: Chapter 2.5.3. For the evaluation of matrix effects the EMEA guideline recommends the use of blank matrix but due to high variations in endogenous squalene concentrations, pooled matrix was used [1]. The overall SD for the calculated concentration should not be greater than 15%.

## S1.7 Carry-over

Carry-over was determined by measuring matrix blanks (*n*=3), subsequently after analyzing standards at 1,000 ng/mL. The resulting signal areas were compared to the average areas of matrix blanks (*n*=6).

## S1.8 Dilution integrity

Dilution integrity was confirmed by preparing a stock solution containing 2,000 ng/mL of all analytes in matrix. This concentration was twofold higher than the upper limit of quantification which is the highest level of the calibration curve (1,000 ng/mL). From this stock solution 500, 250 or 25  $\mu$ L were diluted with freshly prepared sample extract (*Article*: Chapter 2.5.3) as a solvent (*n*=6) to generate dilution integrity samples of 1,000  $\mu$ L (corresponding to a dilution factor of 2, 4 and 40). Using a calibration curve, the actual dilution integrity sample concentration was back-calculated and compared to the nominal concentration.

## S1.9 Stability

Long time stability was determined using six matrix matched samples of low (3 $\times$ LLOQ) and high level that were stored under two different conditions. One batch of samples was stored at room temperature (RT) whereas the other batch was stored at -20 °C. Samples were analyzed on days 0, 5 and 30. The relative change of analyte concentration was determined by comparing the relative responses (area analyte/area IS<sub>iso</sub>) of each analyte with the values from day 0.

## S1.10 Recovery

Recovery was determined on equimolar concentrations to low, medium, and high QC samples, due to the use of pyrophosphates instead of the free alcohols. The analyses were carried out on three different representative analytes: dimethylallyl pyrophosphate (C<sub>3</sub>), farnesyl pyrophosphate (C<sub>15</sub>), and geranylgeranyl pyrophosphate (C<sub>20</sub>). The prepared samples were analyzed (*n*=6) and compared to spiked QC samples of the same concentration.

## S2. Validation results

### S2.1 Selectivity

No interfering peaks from endogenous compounds were detected in the range of the retention times of the analyzed isoprenoid *t*BDPS ethers and squalene, until the samples were spiked. Only squalene as an endogenous matrix component was present in all samples that contain matrix. For the derivatized isoprenol, prenol and farnesol *t*BDPS ethers interferences from consumables were detected (**Figure S2**). Those interferences could be avoided by switching from 2 mL plastic microcentrifuge safe-lock tubes to glass vials. Because plastic microcentrifuge safe-lock tubes were essential for further sample preparation, they cannot be exchanged and interferences from these consumables must be considered. A matrix matched standard preparation considering these interferences, is therefore mandatory.

### S2.1 Linearity and LLOQ

For all analytes a linear fit could be determined ( $R^2 \geq 0.994$ ). The linear range for isoprenol, prenol, geraniol, farnesol and geranylgeraniol was 2.5 to 1,000 ng/mL. The linear range for squalene was 25 to 1,000 ng/mL because endogenous squalene was detected in blank matrix. According to the EMEA guideline the lowest level of the calibration range which can be quantified with an acceptable accuracy ( $\pm 20\%$ ) and precision ( $\pm 20\%$ ) is defined as the lower limit of quantification (LLOQ) [1].

### S2.2 Accuracy, method precision and injection precision

For evaluation of accuracy six QC samples of four concentrations LLOQ (2.5/25 ng/mL), low (7.5/75 ng/mL), medium (500 ng/mL), and high (1,000 ng/mL) were analyzed (**Table S1**). The analyte peak area of each sample was used to calculate the sample concentration and was further compared to the nominal concentration (**Table S1, Day 1, Day 2, Day 3**), whereas the three days average was the mean value from three independent accuracy measurements (**Table S1, Average**). The average concentration should be within 85% to 115% at the low, medium, and high QC, whereas for the LLOQ 80% to 120% were accepted. All analyte levels fulfilled the criteria for accuracy (**Table S1, Day 1, Day 2, Day 3**). Only geranylgeraniol reached the limits slightly with accuracy values of 120% at the LLOQ on day 1 and 119% at the high concentration on day 3 (**Table S1 Day 1, Day 3**). To confirm between-day accuracy the test for accuracy was performed on three consecutive days. The average accuracy of three different batches was in between 93% (prenol) and 112% (geranylgeraniol) at concentrations above the LLOQ whereas at the LLOQ variations were between 82% (squalene), and 115% (geranylgeraniol) were detected (**Table S1, Average**).

Method precision was evaluated within the same batch of samples (**Table S1**). Method precision was calculated as the SD of the individual analyte responses on different days. The precision at the LLOQ did not exceed a SD of 14% (squalene) which was below the limit of 20% (**Table S2, Day 2**). Also, in low (6%; **Table S2, Day 3**; geraniol), medium (6%; **Table S2, Day 2**; geraniol), and high (4%; **Table S2, Day 3**; farnesol and geranylgeraniol) QCs met the criterion of  $SD < 15\%$ .

Injection precision was determined at four levels (LLOQ, low, medium, high). The highest SDs were calculated for the analytes

## Quantifying Isoprenoids in the Ergosterol Biosynthesis by GC-MS

isoprenol, prenol, and geranylgeraniol at LLOQ with values between 6 and 10% (sixfold injection). At low QC the maximum SD of 5% was calculated for geranylgeraniol, whereas in the medium and high QCs none of the analytes exceeded a SD > 4% (data not shown).

**Table S1.** Evaluation of method accuracy measured on three subsequent days (n=6) including the average accuracy.

Accuracy [%]						
	isoprenol	prenol	geraniol	squalene	farnesol	geranylgeraniol
<b>Day 1</b>						
LLOQ	87	81	114	99	115	120
low	90	88	105	112	104	106
medium	95	97	99	93	111	107
high	93	95	97	88	107	109
<b>Day 2</b>						
LLOQ	94	80	100	63	91	116
low	94	87	89	89	90	96
medium	89	90	92	90	102	101
high	89	91	94	90	104	108
<b>Day 3</b>						
LLOQ	90	100	99	85	103	109
low	102	103	104	104	105	99
medium	102	104	102	102	108	109
high	107	109	109	107	113	119
<b>Average</b>						
LLOQ	90	87	104	82	103	115
low	95	93	100	102	100	100
medium	95	97	98	95	107	106
high	97	98	100	95	108	112

**Table S2.** Evaluation of method precision measured on three subsequent days (n=6).

Precision [%]						
	isoprenol	prenol	geraniol	squalene	farnesol	geranylgeraniol
<b>Day 1</b>						
LLOQ	2	4	3	11	5	3
low QC	3	4	3	4	5	2
medium QC	4	4	3	3	2	3
high QC	3	3	4	4	3	3
<b>Day 2</b>						
LLOQ	8	4	10	14	2	3
low QC	4	2	4	5	4	5
medium QC	5	5	6	2	3	3
high QC	3	3	3	3	2	3

# Quantifying Isoprenoids in the Ergosterol Biosynthesis by GC-MS

Table S2. (continued)

	Precision [%]					
	isoprenol	prenol	geraniol	squalene	farnesol	geranylgeraniol
	Day 3					
LLOQ	6	2	2	9	4	3
low QC	4	3	6	3	2	5
medium QC	3	3	2	1	2	2
high QC	3	3	3	3	4	4

### S2.3 Matrix effects

The low QC and high QC samples were prepared in pooled sample matrix to generate a stable level of squalene because no squalene free matrix was available. The matrix effects were determined by comparing the peak areas of spiked samples in matrix to samples prepared in *n*-hexane (Table S3, Matrix factor). For the analytes farnesol, squalene, and geranylgeraniol concentration dependent matrix effects which were stronger in low QC samples, were determined. Peak areas were decreased in *n*-hexane (Figure S5). In contrast, the internal standard peak areas were increased when *n*-hexane was used. According to the guideline the SD of the peak area should be <15%, which is fulfilled for all analytes at both concentrations (Table 3 RSD). Only squalene (15%) was at the upper limit of the criterion at the low QC. Due to the detected matrix effects, calibration standards should be prepared in sample matrix, as already mentioned in *Supplementary material*: Chapter 2.1

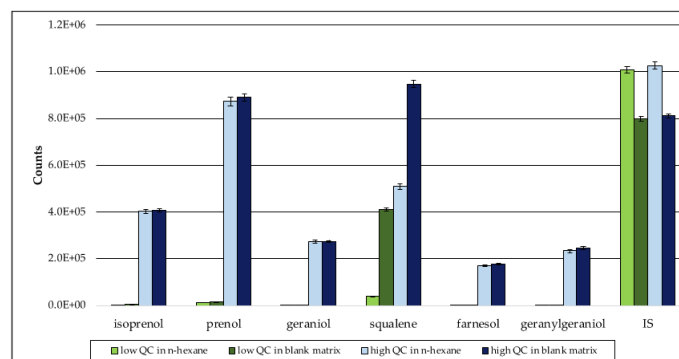


Figure S5. Peak areas of low and high QC samples in *n*-hexane and sample matrix. Error bars represent the standard deviation (n=6).

Table S3. Matrix effects determined at two different concentrations and the associated RSD (n=6).

	Matrix factor						
	isoprenol	prenol	geraniol	squalene	farnesol	geranylgeraniol	IS
	low QC	1.11	1.03	1.05	1.66	1.99	1.21
high QC	1.01	1.02	0.99	1.16	1.03	1.05	0.79
	RSD [%]						
low QC	5	3	5	15	8	9	1

## Quantifying Isoprenoids in the Ergosterol Biosynthesis by GC-MS

**Table S3.** (continued)

	RSD [%]						
	isoprenol	prenol	geraniol	squalene	farnesol	geranylgeraniol	IS
high QC	2	2	2	2	2	2	1

### S2.4 Carry-over

By analyzing blank matrix samples after high concentration samples, the influence of carry-over (CO) was investigated. According to the guideline, signals from blank samples injected right after high concentration samples (high QC; 1,000 ng/mL) should not exceed 20% of the signal area of LLOQ samples (5% for the IS<sub>iso</sub>). Due to the interferences induced by consumables for the signals of prenol, isoprenol and farnesol (*Supplementary material*: Chapter 2.1) as well as the matrix composition including high amounts of squalene, the parameter could not be fulfilled according to the guideline, even though there was no visible CO. For geraniol (29%) and geranylgeraniol (49%) that were not affected by any interfering signals CO could be seen, whereas the internal standard (IS<sub>iso</sub>) was not affected (2%) (**Table 4**). To test this parameter on the remaining analytes (isoprenol, prenol, squalene and farnesol), the approach was adapted (see *Supplementary material*: Chapter 1.7). The variation between matrix blanks measured after high QC samples and independent matrix blanks (matrix blanks measured prior to the first samples that can therefore not be affected by CO) was determined. The biggest differences were detected for isoprenol (13%), prenol (19%), and the IS<sub>iso</sub> (15%), whereas for geraniol, squalene, farnesol, and geranylgeraniol values below 10% were calculated (**Table S4; Carry over (adapted)**). This means that according to the adapted approach, the difference was below 20% and therefore samples analyzed subsequently after high concentration standards are not significantly affected by a previous high concentration sample.

**Table S4.** Carry over determined according the EMEA guideline, as well as an adapted approach (n=3).

	Carry-over (EMEA) [%]						
	isoprenol	prenol	geraniol	squalene	farnesol	geranylgeraniol	IS
	35	33	29	90	61	49	2
	Carry-over (adapted) [%]						
relative change	13	19	9	2	7	4	15

### S2.5 Dilution integrity

Usually, calibration ranges are selected to cover the expected concentration range. Nevertheless, biological samples can also contain analyte levels above the expected amounts. For this reason, dilution should be possible in a linear range to fit the sample concentration levels to the calibration range. The parameter of dilution integrity was determined diluting a stock solution of 2,000 ng/mL (all analytes), which was above the highest calibration level (1,000 ng/mL), to generate samples with 1,000 ng/mL (factor 2) 500 ng/mL (factor 4) and 50 ng/mL (factor 40). None of the prepared concentration levels (n=6) varied more

than 15% from the nominal concentration and therefore showed a linear correlation (data not shown).

## S2.6 Stability

The evaluation of sample stability was performed analyzing samples of low (3×LLOQ) and high (1,000 ng/mL) concentrations (n=6) repeatedly after storing under different storing conditions (RT, -20 °C; **Figure S6**). After five days mostly all samples showed SD values ±15%. Only replicates of squalene (3×LLOQ) stored at room temperature (day 5) exceeded the parameters with a relative response of 127% compared to their reference value (day 0). After a storage period of 30 days the samples stored at room temperature could not be quantified reliably anymore. For samples at 3×LLOQ only two out of six analytes showed the expected response (low QC (RT) day 30), whereas high concentrations could be analyzed more reliably. Samples stored in a freezer were more stable and showed lower SD values. Only two (isoprenol and farnesol) out of six low QC analytes did not meet the stability criteria. Therefore, the samples

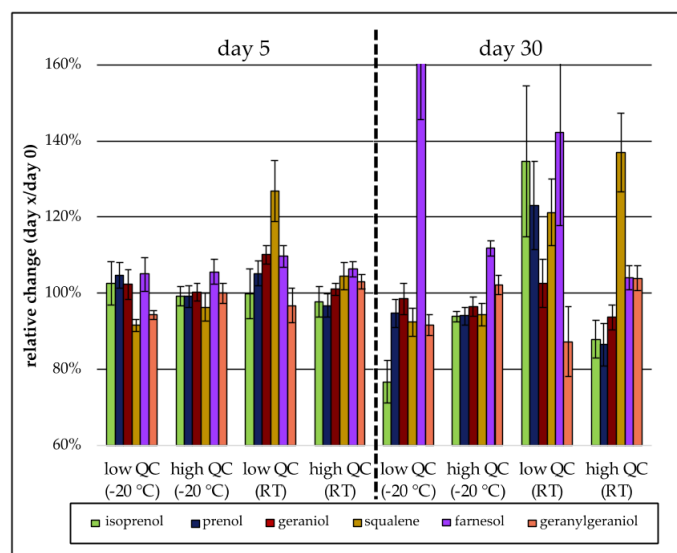


**Figure S6.** Analyte stability over 30 days. The relative response of every analyte was calculated as the ratio between analyte response on day 5 or 30 divided by analyte response on day 0. Left side: relative change after 5 days. Right side: relative change after 30 days. The error bars show the SD of the replicates (n=6).

## S2.7 Recovery

Recovery was investigated in addition to the validation process due to the use of different matrices, that have the potential to influence the extractability of analytes. Recovery was tested using three pyrophosphates (dimethylallyl pyrophosphate, farnesyl pyrophosphate and geranylgeranyl pyrophosphate) in equimolar concentrations to low QC, medium QC and high QC samples in two matrices (*S. cerevisiae*, *A. fumigatus*). The average recovery of prenol, the alcohol originating from dimethylallyl pyrophosphate, was 107% in *S. cerevisiae* and 85% in *A. fumigatus* (**Figure S7**). The mean recovery for farnesol was 133% (*S.*

*cerevisiae*) and 109% (*A. fumigatus*). For geranylgeraniol the mean recovery was 44% (*S. cerevisiae*) and 37% (*A. fumigatus*). Even though recovery differed from an expected 100% value, the values showed the same tendencies for both matrices and are therefore comparable and independent of the fungal cell matrix. In addition, the SD for the individual values in *S. cerevisiae* was below 10% for all replicates besides geranylgeranyl pyrophosphate at the low QC (Table S5, *S. cerevisiae*). In *A. fumigatus* SD was below 10% for all analytes besides farnesyl pyrophosphate at the low QC (Table S5, *A. fumigatus*).

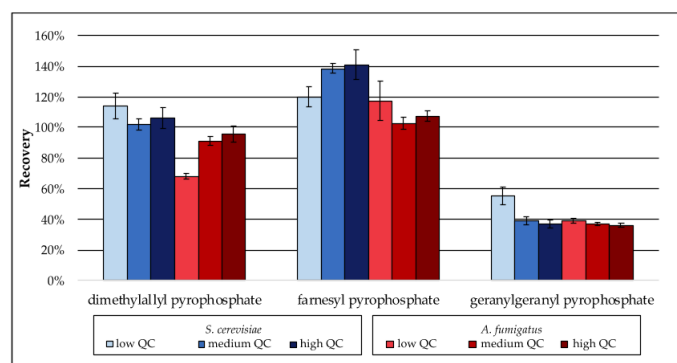


**Figure S7.** Recovery of three representative pyrophosphates from *S. cerevisiae* and *A. fumigatus* matrix. Error bars represent the standard deviation from six replicates.

**Table S5.** Relative standard deviation at three different concentrations (n=6).

	dimethylallyl pyrophosphate RSD [%]	farnesyl pyrophosphate RSD [%]	geranylgeranyl pyrophosphate RSD [%]
<i>S. cerevisiae</i>			
low QC	7	5	10
medium QC	4	2	6
high QC	6	7	7
<i>A. fumigatus</i>			
low QC	3	11	4
medium QC	3	4	3
high QC	6	3	4

### 3. References

1. Guideline on bioanalytical method validation. Available online: [https://www.ema.europa.eu/en/documents/scientific-guideline/guideline-bioanalytical-method-validation\\_en.pdf](https://www.ema.europa.eu/en/documents/scientific-guideline/guideline-bioanalytical-method-validation_en.pdf) (accessed on 28 March 2023).

## 5. Targeting the Isoprenoid Pathway in Cholesterol Biosynthesis: An Approach to Identify Isoprenoid Biosynthesis Inhibitors

**M. Liebl**, F. Olander, C. Müller; Targeting the isoprenoid pathway in cholesterol biosynthesis – An approach to identify isoprenoid biosynthesis inhibitors. *Archiv der Pharmazie*. 2025; Volume 359, Issue 2. Impact factor: 4.3 (2/2025)

### 5.1 Summary

Unlike polyenes (target: ergosterol, see Chapter 1.7) or echinocandins (target: beta 1,3- $\beta$ -glucan synthase) that target fungal specific structures with high affinity, the enzymatic targets of mammalian and fungal isoprenoid biosynthesis are identical (see Chapter 1.1.2). Therefore, selectivity of novel drug candidates towards one organism's enzymes is an essential feature that must be considered during drug development. For identification of enzymatic targets in the post-squalene pathway we already use two closely related self-developed approaches described by Müller *et al.* to test for ergosterol [22] and cholesterol [18] biosynthesis inhibition in the post-squalene pathway.

In this work we approved our isoprenoid biosynthesis assay (see Chapter 4) to be a useful tool for evaluating selectivity of compounds, as it is applicable to fungal and mammalian matrices. While initial qualitative screening (analysis of changes in the isoprenoid patterns after incubation with the test compounds) can reveal the affected enzyme, the degree of isoprenoid accumulation (quantitative screening) can be used as an indicator for the inhibitor's affinity towards the target enzyme.

Therefore, the assay was adapted and revalidated on a human HL60 cell line before subsequently predictive drugs and experimental inhibitors (16 in total) of the pre- and post-squalene pathway were tested. Half maximal inhibitory concentrations ( $IC_{50}$ ) were determined to estimate the substances' potential for lowering total cholesterol biosynthesis before we confirmed whether the actual target of the inhibitor was in the isoprenoid (assay described in Chapter 4) or the distal part of cholesterol biosynthesis [18]. As expected, inhibitors targeting a fungal enzyme showed lower activity on the mammalian biosynthesis than substances developed to inhibit the mammalian enzyme. In addition, not all literature described inhibitors showed activity in our test system.

Interestingly, we identified 6-fluoromevalonate as isopentenyl pyrophosphate isomerase inhibitor, a biological activity which was previously unknown. Furthermore, as the role of isoprenoid pathway intermediates is not limited to sterol biosynthesis (see Chapter 1.2), we determined isoprenoid patterns, which can be used to visualize differences in concentrations and phosphorylation state of isoprenoids and isoprenoid pyrophosphates in extracellular and intracellular matrices (**Figure 15**). The main form of isoprenoids, independent of the observed matrix, was a dephosphorylated state.

# Targeting the Isoprenoid Pathway in Cholesterol Biosynthesis: An Approach to Identify Isoprenoid Biosynthesis Inhibitors

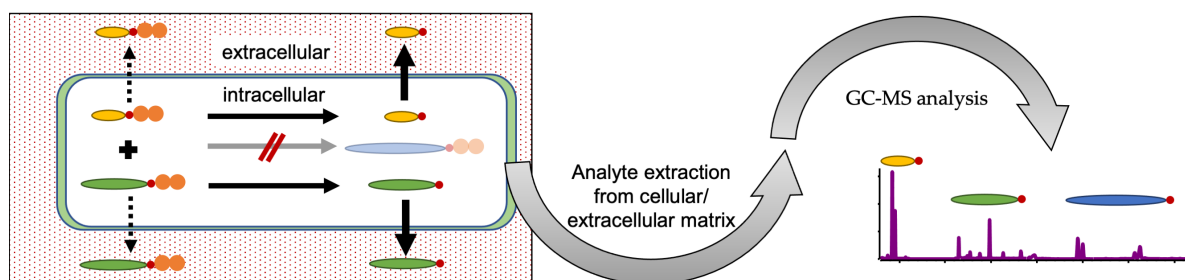


**Figure 15:** Workflow of isoprenoid distribution under isoprenoid pathway inhibition in HL60 cells and intra- and extracellular distribution of isoprenoids (left side). Schematic chromatogram (right side) of analyzed isoprenoid *t*BDPS-ethers (*t*BDPS group not shown). Orange dots: phosphate group, red dots: alcohol group, straight black arrows: main pathway, dotted black arrows: alternative pathway.

## 5.2 Personal Contribution

### Overview:

Conceptualization:	M.L., C.M.
Methodology:	M.L., C.M.
Data curation:	M.L.
Formal analysis:	M.L., F.O.
Writing – original draft:	M.L., C.M.
Writing – review and editing:	M.L., C.M.

### Note:

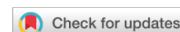
My contribution to this work was the conceptualization, method adaption and validation. All samples and matrices (intra and extracellular) used for validation, analysis of isoprenoid patterns and determination of IC<sub>50</sub> values were prepared by me. Method application on biological samples (isoprenoid patterns) was a further part of my contribution. This included the planning and execution of necessary experiments as well as the formal analysis and curation of the measurement data. In addition, the visualization of the obtained results as well as writing of the original draft, reviewing and editing were done by me.

Florian Olander was supervised by me, as he contributed to this work by performing the formal analysis of IC<sub>50</sub> samples according to Müller *et al.*[18].

Dr. Christoph Müller was involved in the conceptualization of the project as well as the experimental design of the whole investigation. He was involved in the development of the article structure, writing of the original draft as well as reviewing and editing. In addition, funding of the project was provided by Dr. Müller.

# Targeting the Isoprenoid Pathway in Cholesterol Biosynthesis: An Approach to Identify Isoprenoid Biosynthesis Inhibitors

## 5.3 Article



Received: 14 October 2024 | Revised: 18 December 2024 | Accepted: 14 January 2025

DOI: 10.1002/ardp.202400807

FULL PAPER

ARCH PHARM DPhG  
Archiv der Pharmazie

## Targeting the isoprenoid pathway in cholesterol biosynthesis: An approach to identify isoprenoid biosynthesis inhibitors

Maximilian Liebl | Florian Olander | Christoph Müller

Department of Pharmacy—Center for Drug Research, Ludwig-Maximilians-Universität München, Munich, Germany

### Correspondence

Christoph Müller, Department of Pharmacy—Center for Drug Research, Ludwig-Maximilians-Universität München, Butenandtstraße 5-13, 81377 Munich, Germany.  
Email: [christoph.mueller@cup.uni-muenchen.de](mailto:christoph.mueller@cup.uni-muenchen.de)

### Funding information

None

### Abstract

The development of novel cholesterol biosynthesis inhibitors is a task of major concern due to the diverse roles of cholesterol and its precursors in physiological processes. Therefore, appropriate screening assays are required, which can be used to identify and quantify specific inhibitors targeting the desired enzyme. Here, we developed a whole-cell screening assay based on a HL60 cell line, which can be used to characterize inhibitors interacting with enzymes of the isoprenoid part of cholesterol biosynthesis. Due to the change of the isoprenoid pattern under enzyme inhibition, an identification of the targeted enzyme is possible. With the described assay, we can distinguish between free and pyrophosphorylated isoprenoids after enzymatic cleavage in cellular and extracellular matrices. The approach was validated in line with the European Medicines Agency guideline on bioanalytical method validation. As proof of concept, literature-described inhibitors of the isoprenoid pathway were tested. We characterized the effect of 11 isoprenoid biosynthesis inhibitors, and we identified 6-fluoromevalonate as an isopentenyl pyrophosphate isomerase inhibitor, a biological activity that was previously unknown. Furthermore, isoprenoid patterns revealed that, independent of the analyzed matrix, the predominant form of the detected isoprenoids were dephosphorylated isoprenoids and only small amounts were present as pyrophosphates.

### KEYWORDS

6-fluoromevalonate, GC-MS, isoprenoid trafficking, pre-squalene pathway, pyrophosphate

## 1 | INTRODUCTION

Sterols are ubiquitous in eukaryotic cells and play an important role for membrane stability, flexibility, and rigidity.<sup>[1]</sup> They are precursors of bile acids, as well as secosteroids like Vitamin D3 and have an essential role in the endocrine system.<sup>[2]</sup> Their biosynthetic precursors, the isoprenoids, are not less important as they support several

physiological processes. Next to the formation of dolichols, ubiquinone, heme A, and fungal carotenoids, one of their key roles is their participation in multiple posttranslational modification reactions of small GTPases such as Ras, Rab, Rho, and Rac.<sup>[3–6]</sup> Isoprenoids can even modify specific transfer RNA (tRNA) sections.<sup>[7]</sup>

In general, sterol biosynthesis can be divided into two major parts, the pre- and the post-squalene pathway. While in mammalian

This is an open access article under the terms of the [Creative Commons Attribution](https://creativecommons.org/licenses/by/4.0/) License, which permits use, distribution and reproduction in any medium, provided the original work is properly cited.

© 2025 The Author(s). *Archiv der Pharmazie* published by Wiley-VCH GmbH on behalf of Deutsche Pharmazeutische Gesellschaft.

*Arch. Pharm.* 2025;358:e2400807.  
<https://doi.org/10.1002/ardp.202400807>

[wileyonlinelibrary.com/journal/ardp](https://wileyonlinelibrary.com/journal/ardp) | 1 of 16

# Targeting the Isoprenoid Pathway in Cholesterol Biosynthesis: An Approach to Identify Isoprenoid Biosynthesis Inhibitors

cells cholesterol is the main product of its sterol biosynthesis, the fungal equivalent is ergosterol (Figure 1). Plants produce several main sterols including sitosterol, stigmasterol, and campesterol.<sup>[8]</sup> The formation of the post-squalene pathway intermediates is catalyzed by organism-specific enzymes that often distinguish in their affinity for drug substances, thereby making them a selective target for treatment (Figure 1). One class of inhibitors targeting the enzymes of the post-squalene pathway are allylamines such as terbinafine and naftifine (Figure 2, L) which demonstrate a high affinity toward fungal squalene epoxidase (SE, Figure 1, L). In contrast, the mammalian SE (EC 1.14.14.17) is not affected by these compounds at concentrations that are therapeutically relevant.<sup>[9]</sup> Conversely, the experimental inhibitor NB-598 (Figure 2, L) is a selective and potent inhibitor of the mammalian SE, only displaying minimal effects on the corresponding yeast enzyme.<sup>[9]</sup> A comparable degree of selectivity is observed with the azole antimycotics clotrimazole<sup>[10]</sup> and voriconazole<sup>[11]</sup> (Figure 2, N) that only affect mammalian lanosterol 14 $\alpha$ -demethylase (N, EC 1.14.14.154) at concentrations exceeding their therapeutic application limit.

The up to now only poorly investigated presqualene pathway of sterol biosynthesis can be further divided into a mevalonate and an isoprenoid section that results in squalene, the branching point of sterol biosynthesis in diverse organisms (fungi, plants, mammals) (Figure 1). Statins, for example, simvastatin (Figure 2, D), inhibitors of the enzyme 3-hydroxy-3-methyl-glutaryl-coenzyme A (HMG-CoA) reductase (Figure 1 C, EC 2.3.3.10), are the most prominent drugs affecting the presqualene pathway. They are used as first-line therapy in hyperlipidemia. Besides statins no further drugs target enzymes of the mevalonate section of cholesterol biosynthesis. The most common disadvantage of statin treatment is the occurrence of adverse effects, which prevent up to 29% of the patients from using statins at the doses required for therapeutic efficacy.<sup>[12–14]</sup> Side effects, like the primary muscular complaints are attributable to the impact of statins on skeletal muscle, wherein downstream products of HMG-CoA are essential for the normal functioning of muscle cells.<sup>[12]</sup> Therefore, in 2020 bempedoic acid, (Figure 2, A) was approved by the Food and Drug Administration (FDA) as well as by the European Medicines Agency (EMA) for the treatment of hypercholesterolemia in statin-intolerant patients.<sup>[14]</sup> This prodrug is a first-in-class drug that is selectively activated in liver tissue, where it affects cholesterol biosynthesis by inhibiting ATP citrate lyase (Figure 1 A, EC 2.3.3.8), an enzyme providing acetyl-CoA, the precursor of the mevalonate pathway.<sup>[14,15]</sup> A less prominent substance targeting the isoprenoid pathway is 6-fluoromevalonate (Figure 2, G, H) which has originally been described as an inhibitor of mevalonate pyrophosphate decarboxylase (Figure 1 G, EC 4.1.1.33), the enzyme converting mevalonate-5-R-pyrophosphate (5-PP-R-MVA) into isopentenyl pyrophosphate (IPP).<sup>[16]</sup> In 2011, Henneman et al.<sup>[17]</sup> identified further accumulating intermediates in their assays after 6-fluoromevalonate treatment. Next to 5-PP-R-MVA, the upstream precursors mevalonate-5-R-phosphate (5-P-R-MVA) and R-mevalonate (R-MVA), as well as the downstream isoprenoid pyrophosphates, IPP, and/or dimethylallyl pyrophosphate (DMAPP)

were identified. The authors were unable to differentiate between IPP and DMAPP due to their analytical setup.

The group of nitrogen-containing bisphosphonates (NBP), for example, zoledronic acid and YM-175 (Figure 2, I)<sup>[18]</sup> affect the isoprenoid pathway by inhibiting farnesyl pyrophosphate synthase (FPPS; Figure 1 I, EC 2.5.1.1/EC 2.5.1.10), resulting in a lack of farnesyl pyrophosphate (FPP) and geranylgeranyl pyrophosphate (GGPP). Those two substrates are essential in posttranslational modification reactions of GTPases, small signaling proteins, regulating various cellular processes that are important for osteoclast function.<sup>[4]</sup> In addition, FPP and GGPP were proven to exhibit a pivotal role in cancer cell signaling and expansion.<sup>[19,20]</sup> Due to the inhibitory effect on FPPS, NBPs affect sterol biosynthesis and showed to have beneficial effects on total sterol levels in cases of hyperlipidemia.<sup>[21]</sup> The reason why NBPs cannot be used for the treatment of hyperlipidemia is their poor membrane permeability in combination with a high affinity toward bone minerals, which explains the interest in non-NBP inhibitors of FPPS.<sup>[4,22]</sup> One attempt to identify new classes of inhibitors was therefore made by Lindert et al.<sup>[22]</sup> using in silico screening, where several bisamidines, including BPH-1358 (Figure 2, I) as the most promising one, showed their potential as FPPS inhibitors. Carnosic acid, also a non-NBP compound (Figure 2, I), was identified by Han et al.<sup>[23]</sup> who investigated the molecular targets of rosemary and sage extract that are known for their antitumor, antimicrobial, and cholesterol-lowering effects.

The enzyme squalene synthase (SQS; Figure 1 J, EC 2.5.1.21) is a further promising target in the pre-squalene pathway. With chlorogenic acid (Figure 2, orange) a naturally occurring SQS inhibitor was extracted from the fruit of *Prunus mume* by Choi et al.<sup>[24]</sup> The authors determined an inhibitory effect of the substance on pig liver SQS in nanomolar concentrations. An additional hit was "carbazole 11" (Figure 2, J), which was the most potent compound out of several propylamine derivatives, to inhibit SQS in HepG2 cells resulting in lower total plasma cholesterol levels in rats after oral dosing.<sup>[25]</sup> However, the best described inhibitors of SQS are the three closely related zaragozic acids (ZA) A/B/C which were isolated from the fungal species *Sporominella intermedia* and *Leptodontium elatius* in the 1990s. The most potent of them, ZA A, was therefore named squalastatin.<sup>[26]</sup> Based on their structure, new SQS inhibitors were designed to treat hyperlipidemia and lapaquistat (TAK-475; Figure 2, J) was the most promising drug candidate that could have been the first SQS inhibitor on the market. However, late clinical studies and the further development were terminated in 2008 when a dose-dependent increased liver toxicity was observed for lapaquistat.<sup>[27,28]</sup> One explanation for the observed hepatotoxicity could be an increase of the metabolic precursor farnesol, which can affect the cell cycle and induce apoptosis.<sup>[20,29]</sup> The group of Nagashima et al.<sup>[29]</sup> therefore developed an SQS knockout mouse model in which they observed transient liver dysfunction which they correlated with increased farnesol concentrations. Nevertheless, the role of SQS inhibitors as sterol biosynthesis inhibitors as well as therapeutic targets for previously seemingly unrelated diseases (like Alzheimer's disease) is of major concern.<sup>[30]</sup>

# Targeting the Isoprenoid Pathway in Cholesterol Biosynthesis: An Approach to Identify Isoprenoid Biosynthesis Inhibitors

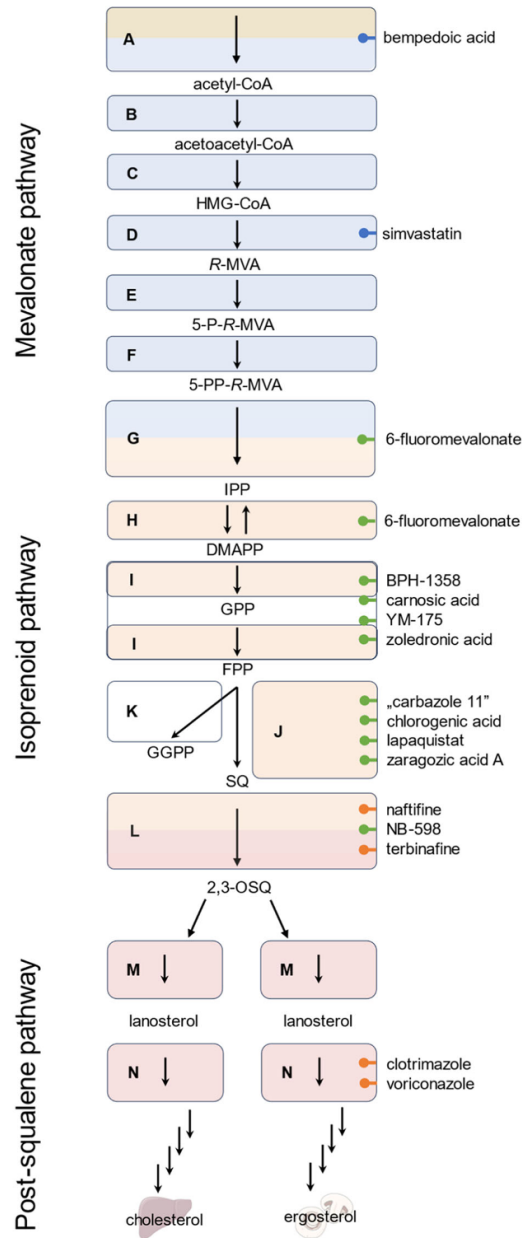


**FIGURE 1** The subpathways of sterol biosynthesis with a spotlight on the presqualene part. Drugs for treating hyperlipidemia are depicted in blue bullets, drugs for antifungal therapy (orange bullets), and postulated experimental isoprenoid biosynthesis inhibitors (green bullets). Blue boxes contain enzymes of the mevalonate pathway, orange boxes contain enzymes of the isoprenoid pathway, white boxes contain enzymes that are not involved in sterol biosynthesis, red boxes contain enzymes of the post-squalene pathway. Two-colored boxes contain enzymes that interconnect two subpathways. Intermediates: acetyl coenzyme A (acetyl-CoA); acetoacetyl coenzyme A (acetoacetyl-CoA); 3-hydroxy-3-methylglutaryl coenzyme A (HMG-CoA); R-mevalonate (R-MVA); mevalonate-5-R-phosphate (5-P-R-MVA); mevalonate-5-R-pyrophosphate (5-PP-R-MVA); isopentenyl pyrophosphate (IPP); dimethylallyl pyrophosphate (DMAPP); geranyl pyrophosphate (GPP); farnesyl pyrophosphate (FPP); geranylgeranyl pyrophosphate (GGPP); squalene (SQ); 2,3-oxidosqualene (2,3-OSQ). Enzymes: Adenosine triphosphate citrate synthase (ATP citrate synthase, (A); acetoacetyl-CoA thiolase (B); HMG-CoA synthase (C); HMG-CoA reductase (D); mevalonate-5-kinase (E); phosphomevalonate kinase (F); mevalonate pyrophosphate decarboxylase (G); IPP isomerase (H); FPP synthase (I); squalene synthase (J); GGPP synthase (K); squalene epoxidase (L); lanosterol pyrophosphate decarboxylase (M); lanosterol 14 $\alpha$ -demethylase (N). Parts of this figure were created using Servier Medical Art templates, licensed under a Creative Commons Attribution 3.0 Unported License (<https://smart.servier.com>, accessed October 2024).

# Targeting the Isoprenoid Pathway in Cholesterol Biosynthesis: An Approach to Identify Isoprenoid Biosynthesis Inhibitors

4 of 16

**DPhG ARCH PHARM**  
Archiv der Pharmazie

LIEBL ET AL.

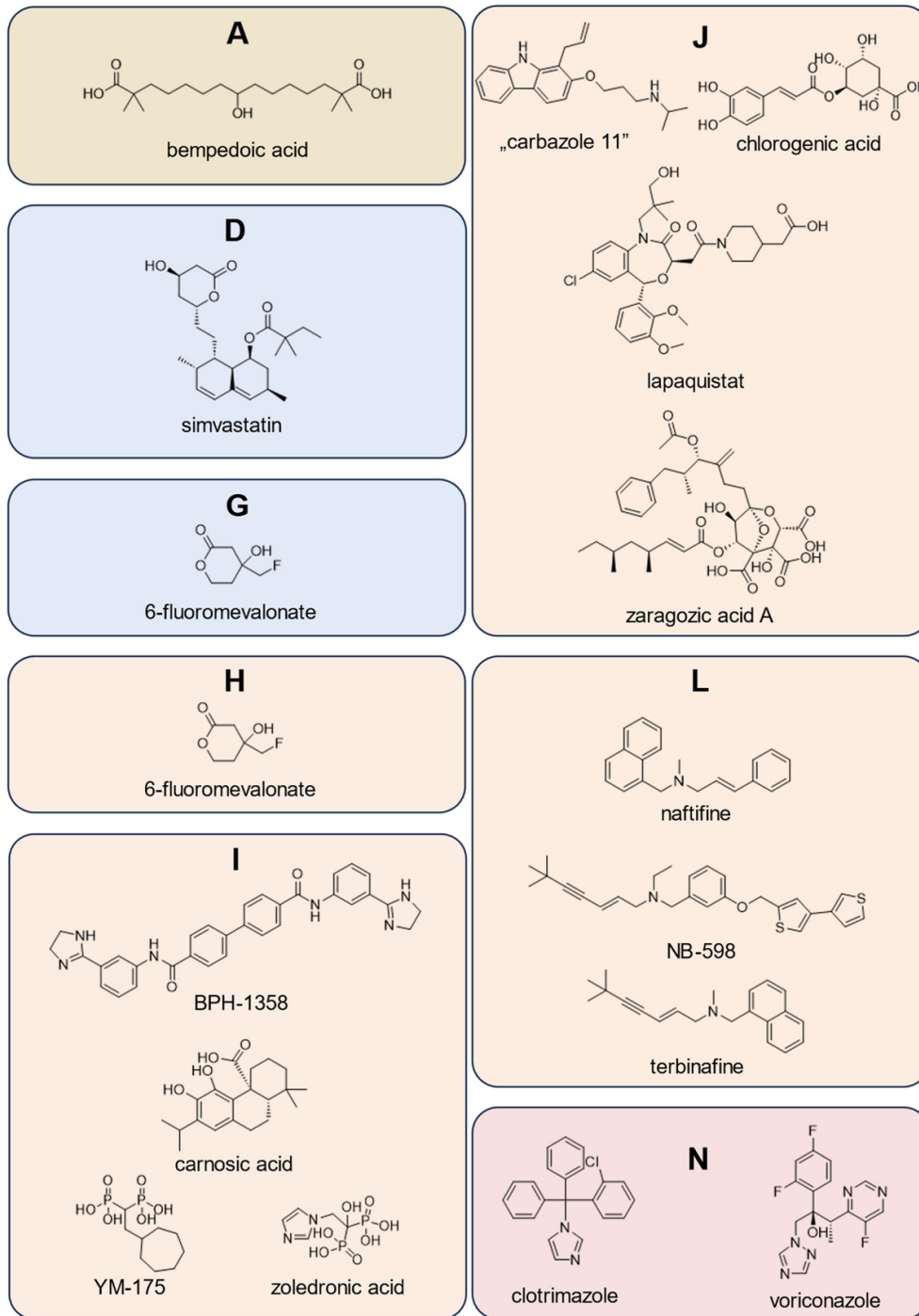


**FIGURE 2** Sterol biosynthesis inhibitors with a focus on the isoprenoid pathway. Colors show the subpathway where the putative inhibited enzyme belongs to: brown (before mevalonate pathway); blue (mevalonate pathway); orange (isoprenoid pathway); red (post-squalene pathway). Putative target enzymes: Adenosine triphosphate citrate synthase (ATP citrate synthase, **A**); HMG-CoA reductase (**D**); mevalonate pyrophosphate decarboxylase (**G**); isopentenyl pyrophosphate isomerase (**H**); farnesyl pyrophosphate synthase (**I**); squalene synthase (**J**); squalene epoxidase (**L**); lanosterol 14 $\alpha$ -demethylase (**N**). HMG-CoA, 3-hydroxy-3-methylglutaryl coenzyme A.

# Targeting the Isoprenoid Pathway in Cholesterol Biosynthesis: An Approach to Identify Isoprenoid Biosynthesis Inhibitors

**TABLE 1** Validation data for cellular matrix.

Validation parameter	Value	Concentration	Analytes						Average
			Isoprenol	Prenol	Geraniol	Squalene	Farnesol	Geranylgeraniol	
Linearity	Linear range (ng/mL)	-	2.5–1000	2.5–1000	2.5–1000	10–1000	2.5–1000	2.5–1000	-
	R <sup>2</sup>	-	≥0.993	≥0.996	≥0.996	≥0.995	≥0.998	≥0.997	-
Matrix effects	Matrix factor	Low*	0.75	1.13	1.03	3.99	1.08	1.56	1.59
		High	0.92	0.96	1.01	1.06	1.09	1.07	1.02
	RSD (%)	Low*	4	1	5	3	4	7	4
		High	3	3	3	6	5	5	4
Method accuracy	-	LLOQ*	1.00	0.82	1.19	1.20	0.92	0.86	1.00
		Low*	0.98	0.90	1.01	1.15	0.91	0.97	0.99
		Medium	1.00	1.05	1.05	1.01	1.00	0.98	1.02
		High	0.98	1.00	1.01	0.98	0.99	0.98	0.99
		Average	0.99	0.95	1.07	1.09	0.95	0.95	-
Method precision (%)	-	LLOQ*	4	3	5	3	10	10	6
		Low*	6	3	4	3	15	13	7
		Medium	1	2	4	2	4	4	3
		High	3	4	3	5	5	4	4
		Average	4	3	4	3	9	8	-
Recovery	Recovery (SD) (%)	LLOQ	-	91 (5)	-	-	150 (17)	50 (8)	97 (10)
		Low	-	77 (3)	-	-	133 (6)	35 (8)	82 (6)
		Medium	-	76 (4)	-	-	160 (7)	28 (2)	88 (4)
		High	-	73 (2)	-	-	166 (2)	34 (2)	91 (2)
		Average	-	79 (3)	-	-	152 (8)	37 (5)	-

Note: LLOQ, 2.5 ng/mL; low, 7.5 ng/mL; medium, 500 ng/mL; high, 1000 ng/mL. LLOQ\* (squalene), 10 ng/mL; low\* (squalene), 25 ng/mL. Abbreviations: -, not determined/applicable; RSD, relative standard deviation; SD, standard deviation; R<sup>2</sup>, linear fit.

One of the biggest challenges in developing potential drug candidates targeting sterol biosynthesis is to guarantee the selectivity of a new compound to a desired target. Therefore, cell-based in vitro assays are necessary where in a quick and easy setup, multiple compounds can be tested for their activity on numerous enzymes. For the screening of distal sterol biosynthesis, several potent approaches exist.<sup>[31–35]</sup> Nevertheless, the pre-squalene pathway was disregarded in these approaches so far. For this reason, we recently developed an assay that gives us an enlarged view on ergosterol biosynthesis capturing the isoprenoid pathway.<sup>[36]</sup> In this work, we extended our approach to mammalian isoprenoid biosynthesis by validating the assay on human leukemia cells (HL60) using the EMA guideline on bioanalytical method validation.<sup>[37]</sup> In combination with our HL60-based assay for the identification of distal cholesterol biosynthesis inhibitors,<sup>[31]</sup> we are expanding our analytical scope for the analysis of inhibitors in the pre-squalene pathway. We can evaluate "hits" on mammalian or fungal sterol biosynthesis and thereby provide information about organism specificity. In addition, our assay can be used to analyze isoprenoid and isoprenoid pyrophosphate trafficking between cellular and extracellular

matrices. As proof of concept, we characterized, to the best of our knowledge, the most important predictive drugs, and other well-known experimental inhibitors of the isoprenoid pathway of cholesterol biosynthesis on HL60 cells. We determined substance specific isoprenoid patterns by analyzing intracellular and extracellular isoprenoid and isoprenoid pyrophosphate levels. Furthermore, we determined IC<sub>50</sub> values, based on the total reduction of cholesterol biosynthesis, to characterize the cholesterol-lowering activity of the compounds of interest.

## 2 | RESULTS AND DISCUSSION

### 2.1 | Validation results cellular matrix

#### 2.1.1 | Linearity and quantification limits

For all analytes, a linear fit (R<sup>2</sup> ≥ 0.993) was determined for the matrix-matched calibration (Table 1, linearity). The linear range was from 2.5 to 1000 ng/mL. Therefore, the lower limit of quantification

# Targeting the Isoprenoid Pathway in Cholesterol Biosynthesis: An Approach to Identify Isoprenoid Biosynthesis Inhibitors

(LLOQ) was set at 2.5 ng/mL for all isoprenoids. Squalene was quantified reliably in concentrations from 10 to 1000 ng/mL.

## 2.1.2 | Matrix effects

Due to the absence of squalene free matrix, pooled sample matrix was used to generate a constant level of squalene in all samples. Especially in the low quality control (QC; 7.5/25 ng/mL) samples (Table 1, matrix effects), matrix induced signal changes were detected. The highest influence of cellular matrix on signal areas was determined for squalene where a high MF of 3.99 was detected, but the signal of geranylgeraniol was also increased in the presence of cellular matrix (matrix factor [MF] = 1.56). The opposite effect was detected for isoprenol in the low QC samples, where the signals were decreased (MF = 0.75). In the high QC (1000 ng/mL) samples, only the signals of isoprenol were decreased (MF = 0.92), whereas the remaining analytes were not influenced significantly (average MF = 1.02). In accordance with the EMA guideline, RSD was  $\leq 7\%$  in both concentrations and therefore fits the guideline's limits of  $< 15\%$ .

## 2.1.3 | Method accuracy and precision

Method accuracy was evaluated at four concentrations: LLOQ (2.5/10 ng/mL), low (7.5/25 ng/mL), medium (500 ng/mL), and high (1000 ng/mL). For each concentration, six QC samples were analyzed. The accuracy was determined by comparing the back-calculated concentration to the theoretical concentration of its respective level. The average accuracy was between 0.99 and 1.02 in the respective levels (Table 1, method accuracy). Considering the different analytes, average values reach from 0.95 (prenol, farnesol, geranylgeraniol) to 1.09 (squalene). In addition, none of the single values exceeded the recommended limits of  $1.00 \pm 0.20$  (LLOQ) and  $1.00 \pm 0.15$  (remaining levels). Only squalene reached 1.20 at LLOQ and 1.15 at the low concentration. Method precision was evaluated within the same batch of samples and should be within 20% (LLOQ) or 15% (remaining levels). Method precision was  $\leq 9\%$  (farnesol) considering the average precision of the different analytes. Single QC levels did not exceed an RSD of 15% (Table 1, method precision).

## 2.1.4 | Recovery of isoprenoids from isoprenoid pyrophosphates

Recovery was assessed as an additional validation parameter, due to the use of different matrices that could probably influence extraction efficiency. Solutions of three pyrophosphates (DMAPP, FPP, and GGPP) were spiked in equimolar concentrations to LLOQ, low QC, medium QC, and high QC samples and compared with respective QC standards. The mean recovery ranged from 82% to 97% for the different concentrations (Table 1, recovery). While the average recovery for prenol, the alcohol originating from DMAPP, was 79%, the mean recovery for farnesol (originating from FPP) was 152%. For geranylgeraniol

(originating from GGPP) the recovery was 37%. Even though recovery values differed from the expected 100%, they were comparable and constant to our previous results for *Saccharomyces cerevisiae* and *Aspergillus fumigatus* cell matrices (prenol 107% and 85%, farnesol 133% and 109%, geranylgeraniol 44% and 37%).<sup>[36]</sup> In addition, recovery values were precise with SDs  $\leq 8\%$ , except farnesol at the LLOQ (17%).

## 2.2 | Validation results extracellular matrix

### 2.2.1 | Linearity and quantification limits

The matrix-matched calibration of lyophilized extracellular matrix was linear in a range from 2.5 to 1000 ng/mL for all analytes including squalene (Table 2, linearity). Linear correlation was given with  $R^2 \geq 0.994$ . The LLOQs were determined at 2.5 ng/mL.

### 2.2.2 | Matrix effects

The influences of the extracellular matrix on signal intensities were also investigated using a pooled matrix. For low QC (7.5 ng/mL) samples, effects could be detected in all samples (average MF = 1.29; Table 2, matrix effects). The least affected analyte was prenol (MF = 1.03), whereas squalene showed the highest differences compared with the *n*-hexane standards (MF = 1.63). In the high QC (1000 ng/mL) samples, the influence of the matrix on signal areas was low with an average MF of 1.03. The highest influence of matrix was determined for geranylgeraniol (MF = 1.11). Although, concentration-dependent matrix effects were present, the observed RSD in both levels was  $\leq 10\%$  and below the required limit of 15%.

### 2.2.3 | Accuracy and precision

Accuracy was tested using six QC samples of four different concentrations LLOQ (2.5 ng/mL), low (7.5 ng/mL), medium (500 ng/mL), and high (1000 ng/mL). The average accuracy was between 1.00 and 1.08 in the separate levels (Table 2, method accuracy). Considering the different analytes, average values reached from 1.01 (squalene, farnesol) to 1.16 (geraniol). In the LLOQ QC samples, the recommended range ( $1.00 \pm 0.20$ ) was exceeded for geraniol (1.29). The analysis of all further QC samples gave accuracy values between 0.86 and 1.15 and therefore met the requirements. Method precision was  $\leq 4\%$  considering the average precision of the different analytes. All QC samples did not exceed an SD of 8% (Table 2, method precision).

### 2.2.4 | Recovery of isoprenoids from isoprenoid pyrophosphates

Recovery of the method was tested in an equivalent procedure to the cellular matrix. The mean recovery was between 80% and 93% (Table 2, recovery). Considering the individual analytes, the mean

# Targeting the Isoprenoid Pathway in Cholesterol Biosynthesis: An Approach to Identify Isoprenoid Biosynthesis Inhibitors

**TABLE 2** Validation data for extracellular matrix.

Validation parameter	Value	Concentration	Analytes						
			Isoprenol	Prenol	Geraniol	Squalene	Farnesol	Geranyl-geraniol	Average
Linearity	Linear range (ng/mL)	-	2.5–1000	2.5–1000	2.5–1000	2.5–1000	2.5–1000	2.5–1000	-
	R <sup>2</sup>	-	≥0.997	≥0.996	≥0.999	≥0.998	≥0.994	≥0.990	-
Matrix effects	Matrix factor	Low	1.22	1.03	1.26	1.63	1.20	1.37	1.29
		High	1.00	1.01	1.05	0.96	1.08	1.11	1.03
	RSD (%)	Low	7	7	9	10	9	9	9
		High	9	8	9	9	9	8	9
Method accuracy	-	LLOQ	1.13	1.11	1.29	0.86	1.04	1.05	1.08
		Low	1.01	1.09	1.09	0.98	0.88	0.94	1.00
		Medium	1.05	1.09	1.15	1.11	1.05	1.05	1.08
		High	1.00	1.04	1.09	1.11	1.07	1.10	1.07
		Average	1.05	1.08	1.16	1.01	1.01	1.04	-
Method precision	-	LLOQ	4	4	3	4	8	5	5
		Low	4	6	2	6	3	7	5
		Medium	1	1	1	0	1	1	1
		High	1	1	2	1	1	1	1
		Average	3	3	2	3	3	4	-
Recovery	Recovery (SD) (%)	LLOQ	-	86 (21)	-	-	140 (12)	51 (4)	93 (13)
		Low	-	82 (5)	-	-	136 (8)	41 (8)	86 (7)
		Medium	-	78 (2)	-	-	137 (5)	26 (1)	81 (3)
		High	-	72 (2)	-	-	141 (4)	27 (1)	80 (2)
		Average	-	80 (7)	-	-	139 (7)	37 (4)	-

Note: LLOQ, 2.5 ng/mL; low, 7.5 ng/mL; medium, 500 ng/mL; high, 1000 ng/mL.

Abbreviations: -, not determined/applicable; RSD, relative standard deviation; SD, standard deviation; R<sup>2</sup>, linear fit.

recovery for prenol from DMAPP was 80%. Farnesol was recovered by 139% from FPP in average and geranylgeraniol from GGPP by 37%. Overall samples, precision is given with SD values ≤12%, except for prenol at the LLOQ (21%). The results are consistent with the results obtained from the cellular matrix (see Section 2.1.4).

## 2.3 | Biological results

### 2.3.1 | Characterization of inhibitors

Inhibitory effects on the isoprenoid pathway were identified for eight of the 16 tested substances (Table 3, qualitative screening). In addition, effects on the post-squalene pathway were identified for two compounds according to Müller et al.<sup>[31]</sup> 6-Fluoromevalonate led to an accumulation of isoprenol in our screening. Given the absence of prenol, the second possible C<sub>5</sub> isoprenoid described by Henneman et al.,<sup>[17]</sup> we were able to confirm a selective inhibition of IPP isomerase (H) by this compound. The group of

Muehlbacher et al.<sup>[38]</sup> described a fluorinated IPP (3-(fluoromethyl)but-3-en-1-pyrophosphate) to be a selective inhibitor of IPP isomerase. However, 6-fluoromevalonate was not identified to be a pro-drug for 3-(fluoromethyl)but-3-en-1-pyrophosphate (data not shown). Both NBPs, zoledronic acid, and YM-175, led to an accumulation of isoprenol, prenol, and geraniol by inhibiting FPPS (I). The inhibitors ZA and lapaquistat led to an accumulation of farnesol and could be confirmed as inhibitors of SQS (J). For squalene epoxidase (L) we were able to confirm the three inhibitors NB-598, terbinafine, and naftifine, that led to an accumulation of squalene. The inhibitors of the mevalonate pathway, bempedoic acid, and simvastatin that target ATP citrate synthase (A) or HMG-CoA reductase (D) respectively, as well as the post-squalene pathway inhibitors clotrimazole and voriconazole, inhibiting lanosterol 14 $\alpha$ -demethylase (N) showed no changes on the isoprenoid pattern. Furthermore, the postulated effect of BPH-1358 and carnosic acid on FPPS (I, accumulation of DMAPP) as well as the effects of "carbazole 11" and chlorogenic acid on SQS (J, accumulation of FPP) could not be confirmed. In addition to the qualitative screening, IC<sub>50</sub> values were determined

# Targeting the Isoprenoid Pathway in Cholesterol Biosynthesis: An Approach to Identify Isoprenoid Biosynthesis Inhibitors

**TABLE 3** Characterization of cholesterol biosynthesis inhibitors.

Inhibitor	Qualitative screening		Quantitative screening		
	Postulated inhibited enzyme	Inhibited enzyme	IC <sub>50</sub> value [μM]	Confidence interval <sup>a</sup> [μM]	R <sup>2</sup>
Bempedaic acid	A	-	>1000	-	-
Simvastatin	D	-	0.580	0.361–0.930	0.948
6-Fluoromevalonate	G, H	H	>1000	-	-
BPH-1358	I	-	n.q.	-	-
Carnosic acid	I	-	4.2	3.1–5.7	0.973
Zoledronic acid	I	I	225	176–289	0.951
YM-175	I	I	337	264–432	0.965
“Carbazole 11”	J	-	0.001	0.001–0.002	0.990
Lapaquistat	J	J	2.8	2.0–3.8	0.975
Zaragozic acid	J	J	5.0	1.3–18.4	0.983
Chlorogenic acid	J	-	169	141–201	0.983
NB-598	L	L	0.006	0.003–0.013	0.986
Terbinafine	L	L	0.540	0.305–0.958	0.964
Naftifine	L	L	1.9	1.6–2.4	0.987
Clotrimazole	N	N	0.202	0.132–0.310	0.965
Voriconazole	N	N	45	33–61	0.937

Note: Target enzymes: A, ATP citrate synthase; D, HMG-CoA reductase; G, mevalonate pyrophosphate decarboxylase; H, isopentenyl pyrophosphate isomerase; I, farnesyl pyrophosphate synthase; J, squalene synthase; L, squalene epoxidase; N, lanosterol 14 $\alpha$ -demethylase.

Abbreviations: -, not determined/applicable; n.q., not quantified.

<sup>a</sup>Confidence interval for the IC<sub>50</sub> value was 95%; R<sup>2</sup> linear fit.

(Table 3, quantitative screening). Only BPH-1358 could not be fully characterized, which was due to the low solubility of the substance above concentrations of 50 μM. Bempedaic acid and 6-fluoromevalonate did not show any impact on total cholesterol levels, irrespective of the incubated concentration (Table 3, quantitative screening). Consequently, a specific IC<sub>50</sub> value could not be determined. For all three inhibitors of squalene epoxidase (L), IC<sub>50</sub> values were determined. The most potent one was NB-598, a described inhibitor of mammalian squalene epoxidase, with an IC<sub>50</sub> value of 0.006 μM, whereas the remaining two inhibitors, terbinafine and naftifine, inhibitors of fungal squalene epoxidase, were only effective in higher concentrations with IC<sub>50</sub> values between 0.540 and 1.9 μM. Also, two inhibitors of SQS (J), lapaquistat and ZA, were effective inhibitors of the cholesterol biosynthesis with IC<sub>50</sub> values ranging from 2 to 5 μM. The highest IC<sub>50</sub> values were determined for the two NBPs, YM-175 (337 μM) and zoledronic acid (225 μM). Even though no effect on the isoprenoid pathway or post-squalene pathway enzymes was detected, “carbazole 11” was identified as an effective inhibitor of total cholesterol biosynthesis with an IC<sub>50</sub> of 0.001 μM. A possible explanation could be an inhibition of enzymes upstream the isoprenoid pathway. Also, carnosic acid (IC<sub>50</sub> 4.2 μM) and chlorogenic acid (IC<sub>50</sub> 169 μM) showed an effect on cholesterol biosynthesis, without affecting the isoprenoid pathway. For the

inhibitor of HMG-CoA reductase (D), simvastatin, and the inhibitors of lanosterol 14 $\alpha$ -demethylase (N), clotrimazole, and voriconazole, IC<sub>50</sub> values between 0.2 and 45 μM were determined.

## 2.3.2 | Characterization of isoprenoids

In all samples where an accumulation of isoprenoid pyrophosphates was detected, also the corresponding isoprenoid was detected (see Section 2.3.3). The highest concentration of pyrophosphates was determined in the samples of 6-fluoromevalonate, with 88% of the measured isoprenol *tert*-butyldiphenylsilyl (tBDPS) ether derived from IPP. Considering pyrophosphate distribution of IPP, the major amount of IPP was measured intracellularly, with only 27% of the IPP detected in the extracellular matrix (Table 4, for quantification results [ng/sample] see Supporting Information S1: Table S1). In samples from both NBPs, zoledronic acid and YM-175 three different pyrophosphates were detected. Next to the two C<sub>5</sub> isomers IPP and DMAPP, also the C<sub>10</sub> intermediate geranyl pyrophosphate (GPP) was identified. Comparing the two NBPs, a higher concentration of pyrophosphorylated isoprenoids was determined in the samples of YM-175 where 68% of the measured isoprenol tBDPS ether and 40% of prenil tBDPS ether originated from IPP and DMAPP, respectively.

# Targeting the Isoprenoid Pathway in Cholesterol Biosynthesis: An Approach to Identify Isoprenoid Biosynthesis Inhibitors

**TABLE 4** Analyte ratio: Heatmap giving the relative amount of isoprenoid pyrophosphates in a ratio to the measured analytes per sample (free + deconjugated alcohols) of the whole sample (cellular + extracellular matrix).

Inhibitor	Concen-tration [µM]	Analyte ratio pyrophosphate/isoprenoid					Pyrophosphate distribution intra/extracellular							
		IPP	DMAPP	GPP	FPP	GGPP	IPP	DMAPP	GPP	FPP	GGPP			
Bempedoic acid	500	n.q.	n.q.	n.q.	n.q.	n.q.	n.q.	n.q.	n.q.	n.q.	n.q.	n.q.	isoprenoid 100%	intracellular 100%
Simvastatin	1	n.q.	n.q.	n.q.	n.q.	n.q.	n.q.	n.q.	n.q.	n.q.	n.q.	n.q.	n.q.	n.q.
6-Fluoromevalonate	500	n.q.	n.q.	n.q.	n.q.	n.q.	n.q.	n.q.	n.q.	n.q.	n.q.	n.q.	n.q.	n.q.
BPH-1358	50	n.q.	n.q.	n.q.	n.q.	n.q.	n.q.	n.q.	n.q.	n.q.	n.q.	n.q.	n.q.	n.q.
Carnosic acid	50	n.q.	n.q.	n.q.	n.q.	n.q.	n.q.	n.q.	n.q.	n.q.	n.q.	n.q.	n.q.	n.q.
YM-175	100	n.q.	n.q.	n.q.	n.q.	n.q.	n.q.	n.q.	n.q.	n.q.	n.q.	n.q.	n.q.	n.q.
Zoledronic acid	500	n.q.	n.q.	n.q.	n.q.	n.q.	n.q.	n.q.	n.q.	n.q.	n.q.	n.q.	n.q.	n.q.
"Carbazole 11"	1	n.q.	n.q.	n.q.	n.q.	n.q.	n.q.	n.q.	n.q.	n.q.	n.q.	n.q.	n.q.	n.q.
Chlorogenic acid	500	n.q.	n.q.	n.q.	n.q.	n.q.	n.q.	n.q.	n.q.	n.q.	n.q.	n.q.	n.q.	n.q.
Lapaquistat	50	n.q.	n.q.	n.q.	n.q.	n.q.	n.q.	n.q.	n.q.	n.q.	n.q.	n.q.	n.q.	n.q.
Zaragozic acid	10	n.q.	n.q.	n.q.	n.q.	n.q.	n.q.	n.q.	n.q.	n.q.	n.q.	n.q.	n.q.	n.q.
Naftifine	1	n.q.	n.q.	n.q.	n.q.	n.q.	n.q.	n.q.	n.q.	n.q.	n.q.	n.q.	n.q.	n.q.
NB-598	50	n.q.	n.q.	n.q.	n.q.	n.q.	n.q.	n.q.	n.q.	n.q.	n.q.	n.q.	n.q.	n.q.
Terbinafine	1	n.q.	n.q.	n.q.	n.q.	n.q.	n.q.	n.q.	n.q.	n.q.	n.q.	n.q.	n.q.	n.q.
Clotrimazole	1	n.q.	n.q.	n.q.	n.q.	n.q.	n.q.	n.q.	n.q.	n.q.	n.q.	n.q.	n.q.	n.q.
Voriconazole	500	n.q.	n.q.	n.q.	n.q.	n.q.	n.q.	n.q.	n.q.	n.q.	n.q.	n.q.	n.q.	n.q.

Note: Red color implements a high amount of isoprenoid pyrophosphates, while green color implements a high amount of the free isoprenoid. Blue color indicates an equal distribution between pyrophosphates and alcohols in the sample. Pyrophosphate distribution: Heatmap displaying the distribution of pyrophosphates between the matrices. Purple color indicates a high concentration of pyrophosphates in the extracellular matrix while orange color indicates a preferred intracellular distribution. The tested concentration is a maximum nontoxic concentration. Abbreviation: n.q., not quantified (<LLOQ).

# Targeting the Isoprenoid Pathway in Cholesterol Biosynthesis: An Approach to Identify Isoprenoid Biosynthesis Inhibitors

For the quantified geraniol tBDPS ether, 10% were attributed to GPP. Zoledronic acid samples only contained isoprenoid pyrophosphates in a range from 22% to 29%, of which 78%–100% were present in the cellular matrix. From YM-175 samples 60%–79% of the detected isoprenoid pyrophosphates were present intracellularly. Further compounds inducing an accumulation of pyrophosphorylated isoprenoids were the two SQS inhibitors ZA and lapaquistat. In samples from both inhibitors, FPP was detected. While in lapaquistat samples 23% of the measured farnesol tBDPS ether originated from FPP, in the ZA samples only 2% of the farnesol tBDPS ether originated from FPP. Samples from lapaquistat additionally contained the geranylgeraniol tBDPS ether, of which 33% originated from GGPP. In lapaquistat samples, the predominant fractions of FPP and GGPP, 65% and 68%, were present in cellular matrix. From ZA samples, FPP was only identified in the cellular matrix.

### 2.3.3 | Isoprenoid trafficking: Analyte distribution between the intra- and extracellular matrix

The analyte distribution of the isoprenoids (deconjugated + free isoprenoids) and squalene between the intra- and extracellular matrix are visualized in Table 5 (analyte distribution intra-/extracellular). In addition, the absolute amounts of analytes per sample (sum of extracellular + cellular matrix) are shown in Table 5. Results [ng/sample] can be found in Supporting Information S1: Table S1. Basal levels of all isoprenoids were below the LLOQ (2.5 ng/mL). Only squalene was quantified in untreated matrix samples with concentrations of approx. 76 ng/sample in cellular matrix samples and approx. A total of 15 ng/sample in extracellular matrix samples.

Isoprenol was detected in samples from six different inhibitors. The highest concentration of isoprenol was determined in samples from 6-fluoromevalonate, the direct inhibitor of IPP isomerase (H), followed by both FPPS (I) inhibitors, YM-175 and zoledronic acid (33–310 ng/sample). Furthermore, traces of isoprenol (10 ng/sample) were identified in samples from BPH-1358 (postulated inhibitor of I), "carbazole 11" (postulated inhibitor of J) and NB-598 (postulated inhibitor of L). While high concentrations were distributed equally between the two matrices showing only a slight tendency toward the intracellular matrix, low concentrations were only measured intracellular (BPH-1358, "carbazole 11") or extracellular (NB-598). Only three inhibitors (YM-175, zoledronic acid, and "carbazole 11") induced an accumulation of prenol. The maximum amount of prenol (480 ng/sample) was observed in samples from YM-175, followed by zoledronic acid (90 ng/sample) and "carbazole 11" (22 ng/sample). While in samples of the two NBPs (YM-175 and zoledronic acid) the extracellular prenol content was higher, in "carbazole 11," prenol was equally distributed. Additionally, geraniol was also detected in zoledronic acid (27 ng/sample) and in YM-175 (124 ng/sample) samples. It is noteworthy that a significant proportion of geraniol was identified in extracellular matrix, with only minimal amounts detected in the cellular matrix. Squalene was quantified in all

samples. The approximate concentration of squalene was between 30 and 50 ng in all samples, that were not affected by SQS (J) or squalene epoxidase (SE, L) inhibitors. Only samples from bempedoic acid (inhibitor of A) contained a lower amount of squalene (27 ng/sample) while samples from BPH-1358 contained a slightly higher amount (55 ng/sample). Both SQS inhibitors ZA and lapaquistat induced a reduction of squalene to approx. 25 ng/sample, whereas "carbazole 11" and chlorogenic acid did not decrease the squalene content. Samples from chlorogenic acid even contained an increased squalene content (56 ng/sample). All three SE inhibitors increased the squalene concentration >60 ng/sample. NB-598 was the most effective one, with more than 600 ng of squalene quantified in the respective samples. The effects of terbinafine and naftifine were almost 10-fold lower with amounts of 62 and 73 ng/sample, respectively. Squalene distribution between matrices depended on the used inhibitor. The effective SQS inhibitors ZA and lapaquistat decrease the intracellular squalene level so that a major part of the detected squalene was measured extracellularly. A very similar isoprenoid pattern was determined from bempedoic acid samples, where a major part of squalene was measured from extracellular matrix. The distribution of squalene due to SE inhibitors resulted in an intracellular accumulation of squalene. Similar observations were determined for the two NBPs (YM-175 and zoledronic acid) and simvastatin. Four inhibitors led to an accumulation of farnesol in quantifiable concentrations. Approximately 2000 ng farnesol per sample were detected in samples treated with ZA or lapaquistat. In addition, traces of farnesol were measured in samples treated with bempedoic acid and NB-598, with concentrations below 10 ng/sample. While farnesol was equally distributed between both matrices in samples from lapaquistat, the majority of farnesol was measured in the extracellular matrix of the remaining samples. Geranylgeraniol was only quantified in samples from the two SQS inhibitors, ZA (24 ng/sample) and lapaquistat (52 ng/sample). In contrast to the other isoprenoids, a substantial portion of geranylgeraniol was found in extracellular matrix.

## 3 | CONCLUSION

In this work, we present a fully validated gas chromatography-mass spectrometry (GC-MS) approach for the analysis of isoprenoids and isoprenoid pyrophosphates from cellular samples. Next to the cellular matrix, the corresponding extracellular matrix was analyzed. The high sensitivity (2.5 ng/mL for all isoprenoids, see Tables 1 and 2) of our method allows us to identify even minor alterations in the isoprenoid pattern. Furthermore, the broad calibration range (upper limit of 1000 ng/mL for all analytes, see Tables 1 and 2) allows us to quantify the extent of inhibitor-induced accumulations. Another advantage of the method is the high precision not exceeding a standard deviation of 15% over all samples and concentrations (see Tables 1 and 2). The recovery of the isoprenoid pyrophosphates underlines our findings from prior analyses<sup>[36]</sup> and gives constant results within the

# Targeting the Isoprenoid Pathway in Cholesterol Biosynthesis: An Approach to Identify Isoprenoid Biosynthesis Inhibitors

**TABLE 5** Analyte distribution: Heatmap depicting the ratio between intracellular and extracellular concentration of the detected isoprenoids.

Inhibitor	Concentration [µM]	Postulated target enzyme	Analyte distribution intra/extracellular										Absolute amount of analyte				
			Isoprenol	Prenol	Geraniol	Squalene	Farnesol	Geranylgeraniol	Isoprenol	Prenol	Geraniol	Squalene	Farnesol	Geranylgeraniol	intracellular 100%	ng/sample	
Bempedoic acid	500	A	n.q.	n.q.	n.q.	n.q.	n.q.	n.q.	n.q.	n.q.	n.q.	n.q.	n.q.	n.q.	n.q.	n.q.	1000
Simvastatin	1	D	n.q.	n.q.	n.q.	n.q.	n.q.	n.q.	n.q.	n.q.	n.q.	n.q.	n.q.	n.q.	n.q.	n.q.	1000
6-Fluoromevalonate	500	G, H	n.q.	n.q.	n.q.	n.q.	n.q.	n.q.	n.q.	n.q.	n.q.	n.q.	n.q.	n.q.	n.q.	n.q.	1000
BPH-1358	50	I	n.q.	n.q.	n.q.	n.q.	n.q.	n.q.	n.q.	n.q.	n.q.	n.q.	n.q.	n.q.	n.q.	n.q.	1000
Carnosic acid	50		n.q.	n.q.	n.q.	n.q.	n.q.	n.q.	n.q.	n.q.	n.q.	n.q.	n.q.	n.q.	n.q.	n.q.	1000
YM-175	100		n.q.	n.q.	n.q.	n.q.	n.q.	n.q.	n.q.	n.q.	n.q.	n.q.	n.q.	n.q.	n.q.	n.q.	1000
Zoledronic acid	500		n.q.	n.q.	n.q.	n.q.	n.q.	n.q.	n.q.	n.q.	n.q.	n.q.	n.q.	n.q.	n.q.	n.q.	1000
"Carbazole 11"	1	J	n.q.	n.q.	n.q.	n.q.	n.q.	n.q.	n.q.	n.q.	n.q.	n.q.	n.q.	n.q.	n.q.	n.q.	1000
Chlorogenic acid	500		n.q.	n.q.	n.q.	n.q.	n.q.	n.q.	n.q.	n.q.	n.q.	n.q.	n.q.	n.q.	n.q.	n.q.	1000
Lapaquistat	50		n.q.	n.q.	n.q.	n.q.	n.q.	n.q.	n.q.	n.q.	n.q.	n.q.	n.q.	n.q.	n.q.	n.q.	1000
Zaragozic acid	10		n.q.	n.q.	n.q.	n.q.	n.q.	n.q.	n.q.	n.q.	n.q.	n.q.	n.q.	n.q.	n.q.	n.q.	1000
Nafitfene	1	L	n.q.	n.q.	n.q.	n.q.	n.q.	n.q.	n.q.	n.q.	n.q.	n.q.	n.q.	n.q.	n.q.	n.q.	1000
NB-598	50		n.q.	n.q.	n.q.	n.q.	n.q.	n.q.	n.q.	n.q.	n.q.	n.q.	n.q.	n.q.	n.q.	n.q.	1000
Terbinafine	1		n.q.	n.q.	n.q.	n.q.	n.q.	n.q.	n.q.	n.q.	n.q.	n.q.	n.q.	n.q.	n.q.	n.q.	1000
Clotrimazole	1	N	n.q.	n.q.	n.q.	n.q.	n.q.	n.q.	n.q.	n.q.	n.q.	n.q.	n.q.	n.q.	n.q.	n.q.	1000
Voriconazole	500		n.q.	n.q.	n.q.	n.q.	n.q.	n.q.	n.q.	n.q.	n.q.	n.q.	n.q.	n.q.	n.q.	n.q.	1000

Note: Orange color indicates a high ratio of intracellular intermediates, while purple color indicates a high ratio of extracellular intermediates. Blue color indicates an equal distribution in both matrices. Absolute amount of analyte: Heatmap depicting the absolute amount of isoprenoid tBDPS ethers and squalene quantified in the whole samples (cellular + extracellular matrix). A, ATP citrate synthase; D, HMG-CoA reductase; G, mevalonate pyrophosphate decarboxylase; H, isopentenyl pyrophosphate isomerase; I, farnesyl pyrophosphate synthase; J, squalene synthase; L, lanosterol 14α-demethylase. Values are in ng/sample. The tested concentration is the maximum nontoxic concentration. Abbreviations: n.q., not quantified (<LLOQ); tBDPS, tert-butylidiphenylsilyl.

# Targeting the Isoprenoid Pathway in Cholesterol Biosynthesis: An Approach to Identify Isoprenoid Biosynthesis Inhibitors

measurements with SD values below 8% at all concentrations above the LLOQ.

As indicated by their  $IC_{50}$  values, the majority of inhibitors, with the exception of bempedoic acid, 6-fluoromevalonate (both  $IC_{50} > 1000 \mu M$ ), and BPH-1358 (no  $IC_{50}$  determined), had an impact on total cholesterol biosynthesis (Table 3). The lack of activity observed with bempedoic acid, an approved drug for the treatment of hyperlipidemia, can be attributed to the absence of the prodrug activation in our HL60 cell model. Given that the requisite enzyme, very long-chain acyl-CoA synthetase (EC 6.2.1.3), exhibits high tissue specificity, the drug is only activated in liver cells.<sup>[12]</sup>

The high separation efficiency of GC-MS systems enabled us to distinguish between the two  $C_5$  isomers prenol and isoprenol, which is normally not possible in liquid chromatography-mass spectrometry (LC-MS) approaches. Therefore, we revealed an effect of 6-fluoromevalonate on the enzyme IPP isomerase (H), which, to the best of our knowledge, has not been previously described in the literature. However, 6-fluoromevalonate seems to act as a multienzyme inhibitor, due to its additional effect on the upstream enzyme mevalonate pyrophosphate decarboxylase (G).<sup>[16]</sup> Henneman et al.<sup>[17]</sup> explained the accumulation of further mevalonate pathway intermediates by feedback mechanisms and reversible reactions. However, they could not explain whether the accumulation of  $C_5$  isoprenoids was due to direct inhibition of IPP isomerase (H)/FPPS (I) or a feedback mechanism. Our findings support the hypothesis of a direct inhibition of IPP isomerase (I) by the selective accumulation of isoprenol and IPP in our experiments involving 6-fluoromevalonate.

Further, we could not confirm the effects of some postulated pre-squalene pathway enzyme inhibitors, namely carnosic acid, which was expected to target FPPS (I), as well as "carbazole 11" and chlorogenic acid that were described as SQS (K) inhibitors even though an inhibitory effect on total sterol biosynthesis was observed for all of them (Table 3). However, neither the isoprenoid pathway, nor the post-squalene pathway were affected by them. Therefore, an inhibition of enzymes upstream the isoprenoid pathway must be considered.

The analysis of the pyrophosphate patterns (Table 4) revealed that most samples contained free isoprenoids next to pyrophosphorylated isoprenoids in similar concentrations after enzymatic inhibition. This was surprising because the pyrophosphorylated isoprenoids are the direct biosynthesis intermediates and were therefore expected to accumulate. Only samples treated with 6-fluoromevalonate and YM-175 (Table 4) contained IPP, the pyrophosphorylated form of isoprenol, in a higher amount than the free alcohol. The matrix distribution pattern of the pyrophosphorylated isoprenoids further revealed that all pyrophosphorylated analytes have a strong tendency to distribute into cellular matrix. Only low quantities of pyrophosphorylated analytes were identified in the corresponding extracellular matrix samples, which could be explained by a lower permeability of isoprenoid pyrophosphates through the cellular membrane.

The additional analysis of the total isoprenoid pattern, including the free alcohols next to the pyrophosphorylated

isoprenoids (Table 5), allowed us to analyze the isoprenoid trafficking in more detail. Overall, free isoprenoids seemed to be equally distributed between cellular and extracellular matrix, showing slight tendencies toward the intracellular matrix. A strong preference toward the intracellular matrix was observed for the free isoprenoid geranylgeraniol. The opposite trend, toward the extracellular matrix, was observed for geraniol and farnesol (Table 5). The matrix distribution pattern of the free isoprenoids, geraniol and farnesol, is contrary to their pyrophosphate distribution pattern (Table 4). Therefore, we concluded that the deconjugated forms of geraniol and farnesol were the preferred ones to be excreted from cells in our HL60 cell model. The presence of farnesol in the extracellular matrix is, however, in contrast to previous findings from *A. fumigatus* cells,<sup>[36]</sup> in which we identified FPP as the intermediate to be excreted when it comes to a downregulation of the essential *erg9* gene, which encodes for the fungal SQS enzyme (analog enzyme K). For this reason, analyzing the distribution patterns of isoprenoids and their corresponding pyrophosphates can help to understand potential effects, side effects, and mechanisms of action of substances targeting the isoprenoid pathway of sterol biosynthesis. In addition, the matrix distribution patterns as well as the pyrophosphate patterns can be used to point out differences between organisms using the identical isoprenoid biosynthesis pathway. The applicability of our assay toward fungal and mammalian cell matrices makes it a novel tool that can help to develop selective, organism-specific inhibitors of sterol biosynthesis. But also, beyond sterol biosynthesis, the investigation of pyrophosphate patterns is of high interest. Due to the significant role of farnesyl and GGPP in prenylation reactions, the interest in determining their concentration, and influencing their composition is of major importance.

## 4 | EXPERIMENTAL

### 4.1 | Chemicals and reagents

All solvents were purchased in *pro analysis* quality or high-performance liquid chromatography grade from Merck. Deionized water was prepared with an in-house ion-exchanger.

#### 4.1.1 | Standards

Prenol (97%) and farnesol (97%) were purchased from Alfa Aesar. Isoprenol (98%) was from Tokyo Chemical Industry Co. Geraniol (98%), squalene (98%) as well as 5 $\alpha$ -cholestane (97%) (Internal Standard for sterol analysis ( $IS_{Sterol}$ )) were from Merck, whereas geranylgeraniol (85%) and 1-heptadecanol (98%) (Internal Standard for isoprenoid analysis ( $IS_{Isoprenoid}$ )) were obtained from Merck. All three pyrophosphates (DMAPP (95%), FPP (95%), GGPP (95%)) were purchased from Cayman Chemicals. 2-<sup>13</sup>C-Acetate (99%) was purchased from Merck.

# Targeting the Isoprenoid Pathway in Cholesterol Biosynthesis: An Approach to Identify Isoprenoid Biosynthesis Inhibitors

## 4.1.2 | Inhibitors

6-Fluoromevalonate (90%), clotrimazole (98%), naftifine hydrochloride (99%), simvastatin (97%), terbinafine hydrochloride (98%), and voriconazole (98%) were purchased from Merck. Bempedoic acid (95%), BPH-1358 (95%), carnosic acid (95%), chlorogenic acid (95%), ZA A (95%), and zoledronic acid monohydrate (95%) were obtained from Cayman Chemicals. Lapaquistat (Tak-475; 99%) was purchased from BLD Pharmatech GmbH and NB-598 (99%) was purchased from MCE-MedChemExpress. "Carbazole 11" and YM-175 were synthesized in-house according to literature.<sup>[25,39]</sup>

## 4.1.3 | Sample preparation

Isoprenoid assay: An alkaline buffer pH 8.6 was used for enzymatic deconjugation containing diethanolamine (DEA; 99%) from Tokyo Chemical Industry Co. and magnesium chloride hexahydrate (99%) from Merck. Bovine alkaline phosphatase (P7640) was obtained from Merck. Sodium chloride was purchased from Bernd Kraft GmbH. For derivatization of isoprenoids, imidazole (99%) and *tert*-butyldiphenylchlorosilane (tBDPSCI) (98%) from Merck were used. Cholesterol assay: Phosphate-buffered saline (PBS) tablets from Merck were used to prepare PBS buffer pH 7.4 ± 0.2. Silylation of sterols was conducted with a mixture of *N*-methyl-*N*-trimethylsilyltrifluoroacetamide (MSTFA) and *N*-trimethylsilylimidazole (TSIM; 10/1; v/v) from Macherey Nagel.

## 4.1.4 | Cell culture

HL60 cells were obtained from the German Collection of Microorganisms and Cell Cultures GmbH (DSMZ) and cultivated at 37°C in a humidified atmosphere containing 5% CO<sub>2</sub> in RPMI 1640 medium with 10% fetal bovine serum (FBS) both from PAA Laboratories. Lipid-free HL60 medium was from PAN Biotech.

## 4.2 | Analytical instrument

All samples were analyzed with an Agilent 7820A gas chromatograph coupled to a quadrupole 5977B from Agilent. For sampling a 7693A automatic liquid sampler (ALS) combined with the G4513A split/splitless injector from Agilent was used. Chromatography was performed on an HP-5ms Ultra Inert (30 m × 0.25 mm × 0.25 μm) capillary column. The carrier gas was helium 5.0 from AIR Liquide used at a constant flow rate of 1.2 mL/min. For the analysis of isoprenoid tBDPS ethers, inlet temperature was kept at 270°C throughout the whole GC run and the injection volume was 1 μL. Initial oven temperature was set to 75°C, which was held for 0.5 min before it ramped to 180°C with a heat rate of 25°C/min. After a hold time of 1.0 min temperature was increased to 225°C with a heating rate of 15°C/min followed by a third ramp of 50°C/min up to 320°C, where the column was held for 5.9 min. For post-run, the flow rate was increased to

2.0 mL/min for 2.5 min, which makes a total run time of 19.0 min. Transfer line temperature was permanently set at 270°C. The 5977B single quadrupole was operated in single ion monitoring (SIM) mode at 70 eV after a solvent delay of 9.5 min (see details in Table 6). The ion source temperature was set at 230°C and the quadrupole temperature at 150°C. Instrument control and data analysis were performed with Agilent Masshunter 8.0 software from Agilent.

## 4.3 | Sample preparation

### 4.3.1 | General sample preparation of cellular and extracellular matrix

The incubation of HL60 cells with test substances was conducted in 24-well plates. In each well 1 × 10<sup>6</sup> cells per milliliters were seeded according to the protocol by Müller et al.<sup>[31]</sup> The inhibitor solutions were prepared by dissolving the respective substances in ethanol, dimethyl sulfoxide, or 0.1 M aqueous sodium hydroxide solution. Stock solutions of each substance were prepared and diluted in a lipid-free HL60 medium to the final test concentrations. For quantitative screening, an additional 2-<sup>13</sup>C-acetate solution (6.25 mg/mL) in purified water was added, followed by a 24 ± 2 h incubation period in a 37°C humidified atmosphere containing 5% CO<sub>2</sub>.

### 4.3.2 | Sample preparation procedure for the identification of target enzymes within the pre-squalene pathway

For initial qualitative screening of potential inhibitors, two distinct test concentrations were used (1 and 50 μM). For the analysis of HL60 cells, the suspended cells from each well were transferred

**TABLE 6** Analytical details of the analyzed isoprenoid tBDPS ethers and squalene.

Trivial name	RT [min]	RRT (IS <sub>isoprenoid</sub> )	Qualifier and quantifier ions [m/z]
Isoprenol	9.781	0.710	189, <b>225</b> , 267
Prenol	9.845	0.715	69, 189, <b>267</b>
Geraniol	11.243	0.816	69, <b>335</b> , 392
Squalene	11.918	0.865	<b>69</b> , 81, 410
Farnesol	12.578	0.913	<b>69</b> , 203, 403
1-Heptadecanol (IS <sub>isoprenoid</sub> )	13.775	1.000	71, 123, <b>437</b>
Geranylgeraniol	14.968	1.087	<b>69</b> , 81, 471

Note: Absolute retention time (RT); relative retention time (RRT); in bold quantifier ions.

Abbreviation: tBDPS, *tert*-butyldiphenylsilyl.

# Targeting the Isoprenoid Pathway in Cholesterol Biosynthesis: An Approach to Identify Isoprenoid Biosynthesis Inhibitors

into a 2.0 mL microcentrifuge safe-lock tube and centrifuged for 5 min at 600 g at room temperature (RT). After centrifugation, the supernatant (extracellular matrix) was decanted from the remaining cell pellet (cellular matrix). For further analysis of the extracellular matrix, the aqueous solution was lyophilized before being processed equivalent to cellular samples. The cell pellet/lyophilized medium was resuspended in 590  $\mu$ L DEA-buffer before it was mechanically lysed (only cellular samples) for 5 min on a vortex shaker using three 1.5 mm and three 3.0 mm glass beads. Subsequently, 10  $\mu$ L of bovine alkaline phosphatase suspension in DEA-buffer (40 mg/mL) were added and the samples were shaken vigorously for 1 min by hand before they were incubated for 40 min at 37°C. Enzymatic deconjugation was terminated by the addition of 300  $\pm$  6 mg NaCl, 300  $\mu$ L of acetonitrile/acetone (2/1; v/v), 350  $\mu$ L of *n*-hexane, and 100  $\mu$ L of an internal standard mixture containing 1-heptadecanol (50  $\mu$ g/mL, IS<sub>Isoprenoid</sub>) and cholestane (10  $\mu$ g/mL, IS<sub>Sterol</sub>) in *n*-hexane. The samples were shaken by hand for 1 min before they were centrifuged for 5 min at 12,000 g at RT. After centrifugation, 450  $\mu$ L of the upper, *n*-hexane layer were transferred into a GC-vial (first extraction step). For a second extraction, 750  $\mu$ L of *n*-hexane were added before samples were shaken by hand for 1 min before they were centrifuged for 5 min at 12,000 g at RT. After centrifugation, 650  $\mu$ L of the organic upper layer were combined with the extract from the first extraction. For complete derivatization, the combined organic extracts (1100  $\mu$ L) were stored for 30 min at 70°C after 30  $\mu$ L of *tert*-butyldiphenylchlorosilane (tBDPSCI) and 30  $\mu$ L of imidazole solution (262 mg/mL in tetrahydrofuran) were added. Derivatization was essential to increase the retention times of the volatile isoprenoids and to distinguish between the two C<sub>5</sub> isomers. The derivatized samples were subjected to GC-MS analysis.

### 4.3.3 | Determination of IC<sub>50</sub> values for inhibition of total cholesterol biosynthesis

IC<sub>50</sub> values were determined on total cholesterol biosynthesis, to generate comparable results unaffected by a possible multienzyme inhibition. To quantify *de novo* synthesized cholesterol, the protocol of Müller et al.<sup>[31]</sup> was used.

## 4.4 | Method validation

Method validation was performed in accordance with the EMA guideline on bioanalytical method validation EMEA/CHMP/EWP/192217/2009,<sup>[37]</sup> considering the parameters linearity and LLOQ, matrix effects, accuracy, precision, and recovery. Method validation was performed on HL60 cells and on the HL60 medium. The HL60 medium was lyophilized before use. In all validation tests (besides recovery), the free isoprenoids were analyzed.

### 4.4.1 | Linearity and LLOQ

For determination of linearity, sample matrix (cells or lyophilized medium) was spiked with analyte stock solutions of 11 different concentrations giving final concentrations of 1.0, 2.5, 5.0, 7.5, 10, 25, 50, 100, 250, 500, and 1000 ng/mL. All samples were prepared in triplicates and contained internal standard (IS<sub>Isoprenoid</sub>) in a consistent concentration (5  $\mu$ g/mL). In addition, nonspiked matrix blanks, only containing IS<sub>Isoprenoid</sub> were analyzed. Signal area ratios from the analyte and IS<sub>Isoprenoid</sub> quantifier ions were plotted against the corresponding analyte concentration. The calibration curve was weighted 1/x. The LLOQ was defined as the lowest concentration of the calibration curve which could be quantified reliably.

### 4.4.2 | Matrix effects

MF were investigated at low (3  $\times$  LLOQ) and high (1000 ng/mL) concentrations, by comparing spiked samples to samples of the same concentrations in *n*-hexane (*n* = 6). The EMA guideline recommends the use of blank matrix, which was not conductible in this case, due to the endogenous content of squalene in cellular samples, which could indicate false positive matrix effects for squalene. Therefore, the pooled matrix was used in both (cells and medium) approaches. As an indicator for matrix effects, the matrix factor was calculated as the quotient of the signal area in the matrix to signal area in *n*-hexane. In addition, the relative standard deviation (RSD) at both concentrations was calculated which should be  $\leq$ 15% according to the guideline.

### 4.4.3 | Method accuracy and precision

Method accuracy and method precision were determined at four different levels: the individual LLOQs, low ( $\leq$ 3  $\times$  LLOQ), medium (500 ng/mL), and high (1000 ng/mL) concentrations. Quality control (QC) samples of different concentrations were prepared by spiking previously prepared pooled sample matrix with an appropriate stock solution containing a mixture of all analytes before derivatization (*n* = 6). Signal areas of the QC samples were used to back-calculate their concentration using a calibration curve generated from calibration standards that were prepared independent of the QC standards. Finally, the back-calculated concentration was divided by the nominal concentration. Precision was expressed as the RSD of the QC samples at each of their four concentration levels (LLOQ, low, medium, high; *n* = 6).

### 4.4.4 | Recovery of isoprenoids from isoprenoid pyrophosphates

To determine the recovery of isoprenoids originating from their respective isoprenoid pyrophosphates, three representative pyrophosphates

# Targeting the Isoprenoid Pathway in Cholesterol Biosynthesis: An Approach to Identify Isoprenoid Biosynthesis Inhibitors

were used: DMAPP (C<sub>5</sub>), FPP (C<sub>15</sub>), and GGPP (C<sub>20</sub>). The pyrophosphates were used in equimolar concentrations to the LLOQ, low, medium, and high concentrations of the free isoprenoids. All samples were spiked with adequate pyrophosphate solutions previous to the resuspension step. Recovery was calculated as the quotient of normalized pyrophosphate sample areas and normalized matrix-matched QC standard areas ( $n = 6$ ).

## 4.5 | Biological tests

### 4.5.1 | Characterization of inhibitors

In a qualitative screening, all inhibitors were initially tested at two concentrations (1 and 50  $\mu$ M) to determine their capability to inhibit enzymes of the isoprenoid pathway. Next to the qualitative screening, every active compound, which showed an inhibition in the cholesterol biosynthesis, was subjected to a quantitative analysis. Therefore, an IC<sub>50</sub> value on total cholesterol biosynthesis was determined, by incubating HL60 cells in the presence of 2-<sup>13</sup>C-acetate. Thereby, newly synthesized cholesterol can be distinguished from existing cholesterol within the matrix. Every inhibitor was tested in triplicates at several concentrations to determine a sigmoidal dose-response curve. Furthermore, a Bradford assay<sup>[40]</sup> was conducted to quantify protein content which was used for normalization and identification of potentially toxic concentrations (for details see Müller et al.<sup>[31]</sup>).

### 4.5.2 | Isoprenoid trafficking—ratio between isoprenoid pyrophosphates and corresponding isoprenoids

To distinguish between isoprenoid pyrophosphates and their corresponding isoprenoids, the sample preparation was modified. Two samples from each of the six biological replicates were combined. The combined samples were then split equally to create two batches of samples with an equal composition (each batch  $n = 3$ ) that could be prepared with/without the enzymatic deconjugation step (see Section 4.3.2). After following the remaining sample preparation procedure (see Section 4.3.2), this adaption allows us to distinguish intermediates originating from pyrophosphates from the corresponding free isoprenoids. When the enzymatic step was conducted, the free alcohols and the deconjugated alcohols were measured as a sum. Whereas if the enzymatic step was not included, only the free alcohols were measured. The respective extracellular matrix of every sample was treated equivalent to the cellular sample.

According to this method, the free isoprenoid and isoprenoid pyrophosphate amounts were determined in the extracellular and cellular matrix. The whole sample analyte amount was defined as the sum of isoprenoid and isoprenoid pyrophosphate from one sample (sum of extracellular and cellular matrix). Therefore, the portion of isoprenoid pyrophosphate per sample was the quotient of isoprenoid pyrophosphate and the whole sample analyte amount of one sample. A value close to 1 was equivalent to a high isoprenoid pyrophosphate

(low isoprenoid) content, whereas a value close to 0 was equivalent to a low pyrophosphate (high isoprenoid) content. The pyrophosphate distribution was the quotient of cellular isoprenoid pyrophosphate and whole sample isoprenoid pyrophosphate (sum of extracellular and cellular matrix). A value close to 1 was equivalent to a high cellular (low extracellular) content, whereas a value close to 0 was equivalent to a low cellular (high extracellular) isoprenoid pyrophosphate distribution.

Inhibitor concentrations were considered as the maximum concentration which did not influence protein content (determined by Bradford assay). All isoprenoids were measured as their corresponding tBDPS ethers.

### 4.5.3 | Isoprenoid trafficking—distribution of the analytes between intracellular and extracellular compartments

To investigate the distribution of the analytes between the cellular and extracellular matrix, the total analyte amount (sum of isoprenoid pyrophosphate and isoprenoid) of the cellular samples was compared with the content of the whole sample amount (extracellular + cellular matrix). A value close to 1 was equivalent to a high cellular (low extracellular) content, whereas a value close to 0 was equivalent to a low cellular (high extracellular) analyte distribution. In addition, the whole sample amount was displayed.

## ACKNOWLEDGMENTS

The authors thank Dr. Florian Vetter for his preliminary work and the synthesis of "carbazole 11" and YM-175, and Prof. Dr. Franz Bracher for providing his laboratories, resources, and for fruitful discussions. Open Access funding enabled and organized by Projekt DEAL.

## CONFLICTS OF INTEREST STATEMENT

The authors declare no conflicts of interest.

## DATA AVAILABILITY STATEMENT

The data that support the findings of this study are available on request from the corresponding author. The data are not publicly available due to privacy or ethical restrictions.

## ORCID

Florian Olander  <http://orcid.org/0009-0000-2171-7455>

Christoph Müller  <http://orcid.org/0000-0002-1163-2527>

## REFERENCES

- [1] O. G. Mouritsen, M. J. Zuckermann, *Lipids* **2004**, *39*, 1101. <https://doi.org/10.1007/s11745-004-1336-x>
- [2] F. T. Doole, T. Kumarage, R. Ashkar, M. F. Brown, *J. Membr. Biol.* **2022**, *255*, 385. <https://doi.org/10.1007/s00232-022-00263-9>
- [3] G. Nürenberg, D. A. Volmer, *Anal. Bioanal. Chem.* **2012**, *402*, 671. <https://doi.org/10.1007/s00216-011-5262-2>
- [4] R. G. G. Russell, *Bone* **2011**, *49*, 2. <https://doi.org/10.1016/j.bone.2011.04.022>

# Targeting the Isoprenoid Pathway in Cholesterol Biosynthesis: An Approach to Identify Isoprenoid Biosynthesis Inhibitors

- [5] S. A. Holstein, R. J. Hohl, *Lipids* **2004**, *39*, 293. <https://doi.org/10.1007/s11745-004-1233-3>
- [6] G. Sandmann, *Molecules* **2022**, *27*, 1431. <https://doi.org/10.3390/molecules27041431>
- [7] U. Schweizer, S. Bohleber, N. Fradejas-Villar, *RNA Biol.* **2017**, *14*, 1197. <https://doi.org/10.1080/15476286.2017.1294309>
- [8] W. D. Nes, *Chem. Rev.* **2011**, *111*, 6423. <https://doi.org/10.1021/cr200021m>
- [9] Y. Iwasawa, M. Horie, *Drugs Future* **1993**, *18*, 911. <https://doi.org/10.1358/dof.1993.018.10.233081>
- [10] M. Giera, F. Plössl, F. Bracher, *Steroids* **2007**, *72*, 633. <https://doi.org/10.1016/j.steroids.2007.04.005>
- [11] A. G. S. Warrilow, J. E. Parker, C. L. Price, N. J. Rolley, W. D. Nes, D. E. Kelly, S. L. Kelly, *Int. J. Antimicrob. Agents* **2019**, *54*, 449. <https://doi.org/10.1016/j.ijantimicag.2019.07.011>
- [12] S. L. Pinkosky, R. S. Newton, E. A. Day, R. J. Ford, S. Lhotak, R. C. Austin, C. M. Birch, B. K. Smith, S. Filippov, P. H. E. Groot, G. R. Steinberg, N. D. Lalwani, *Nat. Commun.* **2016**, *7*, 13457. <https://doi.org/10.1038/ncomms13457>
- [13] L. Trapani, M. Segatto, P. Ascenzi, V. Pallottini, *IUBMB Life* **2011**, *63*, 964. <https://doi.org/10.1002/iub.522>
- [14] S. E. Nissen, A. M. Lincoff, D. Brennan, K. K. Ray, D. Mason, J. J. P. Kastelein, P. D. Thompson, P. Libby, L. Cho, J. Plutzky, H. E. Bays, P. M. Moriarty, V. Menon, D. E. Grobbee, M. J. Louie, C. F. Chen, N. Li, L. Bloedon, P. Robinson, M. Horner, W. J. Sasiela, J. McCluskey, D. Davey, P. Fajardo-Campos, P. Petrovic, J. Fedacko, W. Zmuda, Y. Lukyanov, S. J. Nicholls, *N. Engl. J. Med.* **2023**, *388*, 1353. <https://doi.org/10.1056/NEJMoa2215024>
- [15] A. C. Goldberg, L. A. Leiter, E. S. G. Stroes, S. J. Baum, J. C. Hanselman, L. T. Bloedon, N. D. Lalwani, P. M. Patel, X. Zhao, P. B. Duell, *JAMA* **2019**, *322*, 1780. <https://doi.org/10.1001/jama.2019.16585>
- [16] J. F. Nave, H. d'Orchymont, J. B. Ducep, F. Piriou, M. J. Jung, *Biochem. J.* **1985**, *227*, 247. <https://doi.org/10.1042/bj2270247>
- [17] L. Henneman, A. G. van Cruchten, W. Kulik, H. R. Waterham, *Biochim. Biophys. Acta Mol. Cell Biol. Lipids* **2011**, *1811*, 227. <https://doi.org/10.1016/j.bbalip.2011.01.002>
- [18] D. Amin, S. Cornell, S. Gustafson, S. Needle, J. Ullrich, G. Bilder, M. Perrone, *J. Lipid Res.* **1992**, *33*, 1657. [https://doi.org/10.1016/S0022-2275\(20\)41388-4](https://doi.org/10.1016/S0022-2275(20)41388-4)
- [19] S. Feltrin, F. Ravera, N. Traversone, L. Ferrando, D. Bedognetti, A. Ballestrero, G. Zoppoli, *Cancer Lett.* **2020**, *493*, 19. <https://doi.org/10.1016/j.canlet.2020.07.010>
- [20] J. H. Joo, A. M. Jetten, *Cancer Lett.* **2010**, *287*, 123. <https://doi.org/10.1016/j.canlet.2009.05.015>
- [21] E. Guney, G. Kisakol, A. G. Ozgen, C. Yilmaz, T. Kabalak, *Neuro. Endocrinol. Lett.* **2008**, *29*, 252.
- [22] S. Lindert, W. Zhu, Y. L. Liu, R. Pang, E. Oldfield, J. A. McCammon, *Chem. Biol. Drug Des.* **2013**, *81*, 742. <https://doi.org/10.1111/cbdd.12121>
- [23] S. Han, X. Li, Y. Xia, Z. Yu, N. Cai, S. R. Malwal, X. Han, E. Oldfield, Y. Zhang, *J. Med. Chem.* **2019**, *62*, 10867. <https://doi.org/10.1021/acs.jmedchem.9b01405>
- [24] S. W. Choi, N. Y. Hur, S. C. Ahn, D. S. Kim, J. K. Lee, D. O. Kim, S. K. Park, B. Y. Kim, M. Y. Baik, *J. Microbiol. Biotechnol.* **2007**, *17*, 1970.
- [25] T. Ishihara, H. Kakuta, H. Moritani, T. Ugawa, I. Yanagisawa, *Bioorg. Med. Chem.* **2004**, *12*, 5899. <https://doi.org/10.1016/j.bmc.2004.08.033>
- [26] J. D. Bergstrom, M. M. Kurtz, D. J. Rew, A. M. Amend, J. D. Karkas, R. G. Bostedor, V. S. Bansal, C. Dufresne, F. L. VanMiddlesworth, O. D. Hensens et al., *Proc. Natl Acad. Sci.* **1993**, *90*, 80. <https://doi.org/10.1073/pnas.90.1.80>
- [27] E. A. Stein, H. Bays, D. O'Brien, J. Pedicano, E. Piper, A. Spezzi, *Circulation* **2011**, *123*, 1974. <https://doi.org/10.1161/CIRCULATIONAHA.110.975284>
- [28] A. Marcuzzi, C. Loganes, C. Celeghini, G. Kleiner, *Curr. Med. Chem.* **2018**, *25*, 2783. <https://doi.org/10.2174/0929867324666170911161417>
- [29] S. Nagashima, H. Yagyu, R. Tozawa, F. Tazoe, M. Takahashi, T. Kitamine, D. Yamamuro, K. Sakai, M. Sekiya, H. Okazaki, J. Osuga, A. Honda, S. Ishibashi, *J. Lipid Res.* **2015**, *56*, 998. <https://doi.org/10.1194/jlr.M057406>
- [30] A. P. Kourounakis, E. Bavavea, *Arch. Pharm.* **2020**, *353*, e2000085. <https://doi.org/10.1002/ardp.202000085>
- [31] C. Müller, J. Junker, F. Bracher, M. Giera, *Nat. Protoc.* **2019**, *14*, 2546. <https://doi.org/10.1038/s41596-019-0193-z>
- [32] C. Müller, U. Binder, F. Bracher, M. Giera, *Nat. Protoc.* **2017**, *12*, 947. <https://doi.org/10.1038/nprot.2017.005>
- [33] L. Méjanelle, J. F. López, N. Gunde-Cimerman, J. O. Grimalt, *J. Lipid Res.* **2001**, *42*, 352.
- [34] S. Hammann, W. Vetter, *J. Agric. Food Chem.* **2016**, *64*, 3437. <https://doi.org/10.1021/acs.jafc.6b00383>
- [35] J. G. McDonald, D. D. Smith, A. R. Stiles, D. W. Russell, *J. Lipid Res.* **2012**, *53*, 1399. <https://doi.org/10.1194/jlr.D022285>
- [36] M. Liebl, L. Huber, H. Elsamani, P. Merschak, J. Wagener, F. Gsaller, C. Müller, *J. Fungi* **2023**, *9*, 768. <https://doi.org/10.3390/jof9070768>
- [37] European Medicines Agency, *Guideline on bioanalytical method validation*, <[https://www.ema.europa.eu/en/documents/scientific-guideline/guideline-bioanalytical-method-validation\\_en.pdf](https://www.ema.europa.eu/en/documents/scientific-guideline/guideline-bioanalytical-method-validation_en.pdf)> (2024).
- [38] M. Muehlbacher, C. D. Poulter, *Biochemistry* **1988**, *27*, 7315. <https://doi.org/10.1021/bi00419a021>
- [39] L. Widler, K. A. Jaeggi, M. Glatt, K. Müller, R. Bachmann, M. Bisping, A. R. Born, R. Cortesi, G. Guiglia, H. Jeker, R. Klein, U. Ramseier, J. Schmid, G. Schreiber, Y. Seltenmeyer, J. R. Green, *J. Med. Chem.* **2002**, *45*, 3721. <https://doi.org/10.1021/jm020819i>
- [40] M. M. Bradford, *Anal. Biochem.* **1976**, *72*, 248. <https://doi.org/10.1006/abio.1976.9999>

## SUPPORTING INFORMATION

Additional supporting information can be found online in the Supporting Information section at the end of this article.

**How to cite this article:** M. Liebl, F. Olander, C. Müller, *Arch. Pharm.* **2025**, *358*, e2400807. <https://doi.org/10.1002/ardp.202400807>

Targeting the Isoprenoid Pathway in Cholesterol Biosynthesis: An Approach to Identify  
Isoprenoid Biosynthesis Inhibitors

*5.4 Supporting Information*

**Targeting the isoprenoid pathway in cholesterol  
biosynthesis – An approach to identify isoprenoid  
biosynthesis inhibitors**

Maximilian Liebl<sup>1</sup>, Florian Olander<sup>1</sup> and Christoph Müller<sup>1\*</sup>

---

<sup>1</sup> Department of Pharmacy - Center for Drug Research, Ludwig-Maximilians-Universität München, Munich, Germany

\*Correspondence:

Christoph Müller, Department of Pharmacy - Center for Drug Research, Ludwig-Maximilians-Universität München, Butenandtstraße 5-13, 81377  
München, Germany

Email: [christoph.mueller@cup.uni-muenchen.de](mailto:christoph.mueller@cup.uni-muenchen.de)

# Targeting the Isoprenoid Pathway in Cholesterol Biosynthesis: An Approach to Identify Isoprenoid Biosynthesis Inhibitors

**Table S1.** Absolute concentration of analyte tBDPS ethers and squalene per sample. + enzyme covers free isoprenoids and deconjugated isoprenoids. – enzyme covers free isoprenoids. The tested concentration is a maximum non-toxic concentration. n.q. not quantified (<LLOQ).

inhibitor	concentration [μM]	ng/sample											
		cellular matrix						extracellular matrix					
		+ enzyme						- enzyme					
		isoprenol	prenol	geraniol	squalene	farnesol	geranylgeraniol	isoprenol	prenol	geraniol	squalene	farnesol	geranylgeraniol
bempedoic acid	500	n.q.	n.q.	n.q.	10	n.q.	n.q.	n.q.	n.q.	n.q.	14	n.q.	n.q.
simvastatin	1	n.q.	n.q.	n.q.	31	n.q.	n.q.	n.q.	n.q.	n.q.	24	n.q.	n.q.
6-fluoromevalonate	500	208	n.q.	n.q.	18	n.q.	n.q.	21	n.q.	n.q.	16	n.q.	n.q.
BPH-1358	50	3	n.q.	n.q.	33	n.q.	n.q.	3	n.q.	n.q.	29	n.q.	n.q.
carnosic acid	50	n.q.	n.q.	n.q.	23	n.q.	n.q.	n.q.	n.q.	n.q.	23	n.q.	n.q.
YM-175	100	103	199	17	28	n.q.	n.q.	18	47	9	25	n.q.	n.q.
zoledronic acid	500	18	38	6	36	n.q.	n.q.	9	20	n.q.	52	n.q.	n.q.
„carbazole 11“	1	6	12	n.q.	36	n.q.	n.q.	5	12	n.q.	35	n.q.	n.q.
chlorogenic acid	500	n.q.	n.q.	n.q.	38	n.q.	n.q.	n.q.	n.q.	n.q.	27	n.q.	n.q.
lapaquistat	50	n.q.	n.q.	n.q.	9	896	40	n.q.	n.q.	n.q.	15	607	29
zaragozic acid	10	n.q.	n.q.	n.q.	13	516	16	n.q.	n.q.	n.q.	13	471	17
naftifine	1	n.q.	n.q.	n.q.	56	n.q.	n.q.	n.q.	n.q.	n.q.	79	n.q.	n.q.
NB-598	50	n.q.	n.q.	n.q.	585	n.q.	n.q.	n.q.	n.q.	n.q.	549	n.q.	n.q.
terbinafine	1	n.q.	n.q.	n.q.	47	n.q.	n.q.	n.q.	n.q.	n.q.	53	n.q.	n.q.
clotrimazole	1	n.q.	n.q.	n.q.	26	n.q.	n.q.	n.q.	n.q.	n.q.	24	n.q.	n.q.
voriconazole	500	n.q.	n.q.	n.q.	13	n.q.	n.q.	n.q.	n.q.	n.q.	19	n.q.	n.q.
<b>extracellular matrix</b>													
bempedoic acid	500	n.q.	n.q.	n.q.	16	7	n.q.	n.q.	n.q.	n.q.	23	7	n.q.
simvastatin	1	n.q.	n.q.	n.q.	10	n.q.	n.q.	n.q.	n.q.	n.q.	7	n.q.	n.q.
6-fluoromevalonate	500	102	n.q.	n.q.	15	n.q.	n.q.	33	n.q.	n.q.	10	n.q.	n.q.
BPH-1358	50	n.q.	n.q.	n.q.	21	n.q.	n.q.	n.q.	n.q.	n.q.	11	n.q.	n.q.
carnosic acid	50	n.q.	n.q.	n.q.	16	n.q.	n.q.	n.q.	n.q.	n.q.	20	n.q.	n.q.
YM-175	100	105	281	107	11	n.q.	n.q.	48	240	103	14	n.q.	n.q.
zoledronic acid	500	15	52	21	10	n.q.	n.q.	15	50	20	18	n.q.	n.q.
„carbazole 11“	1	n.q.	10	n.q.	14	n.q.	n.q.	4	10	n.q.	7	n.q.	n.q.
chlorogenic acid	500	n.q.	n.q.	n.q.	19	n.q.	n.q.	n.q.	n.q.	n.q.	25	n.q.	n.q.
lapaquistat	50	n.q.	n.q.	n.q.	15	1026	12	n.q.	n.q.	n.q.	63	871	6
zaragozic acid	10	n.q.	n.q.	n.q.	13	1497	8	n.q.	n.q.	n.q.	18	1498	7
naftifine	1	n.q.	n.q.	n.q.	17	n.q.	n.q.	n.q.	n.q.	n.q.	25	n.q.	n.q.
NB-598	50	6	n.q.	n.q.	20	6	n.q.	10	n.q.	n.q.	21	4	n.q.
terbinafine	1	n.q.	n.q.	n.q.	15	n.q.	n.q.	n.q.	n.q.	n.q.	22	n.q.	n.q.
clotrimazole	1	n.q.	n.q.	n.q.	14	n.q.	n.q.	n.q.	n.q.	n.q.	21	n.q.	n.q.
voriconazole	500	n.q.	n.q.	n.q.	20	n.q.	n.q.	n.q.	n.q.	n.q.	17	n.q.	n.q.

## Targeting the Isoprenoid Pathway in Cholesterol Biosynthesis: An Approach to Identify Isoprenoid Biosynthesis Inhibitors

### 5.5 Is there an antifungal activity of mammalian isoprenoid biosynthesis inhibitors?

Designing selective inhibitors that target ergosterol biosynthesis without affecting the equivalent mammalian (host) enzyme is a key ambition in antimycotic drug development. While antifungal drugs are designed to kill the fungal germ, the same drug should not interact with the host's enzymes (when applied systemically). In a minimal inhibitory concentration (MIC) testing using *A. fumigatus*, the group of Assoc.-Prof. Gsaller screened eleven experimental compounds and approved drugs we previously had tested for their inhibition of enzymes in cholesterol biosynthesis on HL60 cells (see Chapter 5.3). In contrast to the IC<sub>50</sub> testing, where we tested the potential of compounds to reduce total cholesterol biosynthesis (see Chapter 5.3), the focus of MIC testing was on identifying an inhibitor concentration that was toxic to the fungal germ (**Table 2**). If one of the tested experimental compounds affected fungal growth and survival in MIC testing, an additional screening of the isoprenoid pathway according to Chapter 4 could be used to identify the potentially targeted fungal enzyme. An equivalent test (to MIC testing of fungal cells) to identify toxicity of experimental compounds on HL60 cells would be a MTT (3-(4,5-dimethylthiazol-2-yl)-2,5-diphenyltetrazoliumbromide) test, which is used to determine the metabolic activity (representing viability) of cells after exposure to different compound concentrations. Since the final therapeutic approaches are different in fungal (killing the germ) and mammalian (inhibiting cholesterol biosynthesis) cells, the determination of IC<sub>50</sub> values was preferred over MTT testing for HL60 cells.

Terbinafine, an approved inhibitor of fungal squalene monooxygenase was tested as proof of concept, showing growth reducing effects in MIC testing at low concentrations (MIC: 19 µM). However, due to the low specificity of terbinafine, the drug is only applied topically [68], as it also can inhibit total cholesterol biosynthesis (IC<sub>50</sub>: 0.54 µM). NB-598, a further inhibitor of squalene monooxygenase (see Chapter 5.3) interestingly showed no activity on fungal cell growth (MIC > 200 µM). This lacking effect of NB-598 however is in line with literature [69], as this experimental drug was specifically developed to target cholesterol biosynthesis. In HL60 cells NB-598 showed a very low IC<sub>50</sub> value (0.006 µM), which is in correlation with its high affinity to the mammalian enzyme (see Chapter 5.3).

From the tested mammalian squalene synthase inhibitors (see Chapter 5.3), only two showed effects on fungal growth. Lapaquistat showed low inhibitory effects (MIC: 155 µM) while zaragozic acid was already very effective in inhibiting fungal growth at a concentration of 0.6 µM (MIC). Since lapaquistat was developed from zaragozic acid with the aim to design a cholesterol lowering drug (see Chapter 5.3), the decreased activity towards the fungal cells could have been expected.

The remaining isoprenoid pathway inhibitors showed no effect on overall survival of *A. fumigatus* at the tested concentrations (**Table 2**). A detailed discussion of IC<sub>50</sub> values and inhibitory effects of all experimental drugs on HL60 cells is included in Chapter 5.3.

Targeting the Isoprenoid Pathway in Cholesterol Biosynthesis: An Approach to Identify  
Isoprenoid Biosynthesis Inhibitors

inhibitor	IC <sub>50</sub> value [μM]	MIC [μM]
	HL60	<i>A. fumigatus</i>
6-fluoromevalonate	>1000	>200
BPH1358	n.q.	>150
carnosic acid	4.2	>200
zoledronic acid	225	>350
YM175	337	>350
„carbazole 11”	0.001	>200
lapaquistat	2.8	155
zaragozic acid	5.0	0.6
chlorogenic acid	169	>200
NB-598	0.006	>200
terbinafine	0.540	19

**Table 2:** Characterization of eleven inhibitors for their affinity to target total cholesterol biosynthesis (IC<sub>50</sub> values) from HL60 cells (for details see Chapter 5.3) and MIC values from *A. fumigatus* cells indicating fungitoxic concentrations.

## 6. Is Dehydroepiandrosterone Excretion a Defense Mechanism of Plants Affecting Ergosterol Biosynthesis of *Alternaria brassicicola*?

C. Oktay, G. Shiko, **M. Liebl**, F. Feistel, S. Mußbach, K.L. Körber, E. Barth, L. Huber, A. Antony, R. Oelmüller, M. Reichelt, K. Ossetek, C. Müller, A.C.U. Furch, J. Klein; *Arabidopsis thaliana* accumulates dehydroepiandrosterone after infection with phytopathogenic fungi – effects on plants and fungi. *Plant Physiology and Biochemistry*. 2025; Volume 221, 109570. Impact factor: 6.1 (2/2025)

### 6.1 Summary

The potential threat by fungal germs is not exclusively based on the direct interaction between fungal pathogens and human hosts. As fungi can also infect fruits, agricultural products, and other plants they are capable to affect essential parts of the mammalian chain of nutrition. As a consequence, fungicides are next to insecticides and herbicides among the most frequently applied classes of pesticides in modern agriculture which are used to decrease the risks of harvest losses [70] (pesticides used 2022 in Germany: 4.06 kg/ha [71]). Besides the excessive amounts of pesticides that are used to protect agricultural products, several plants are capable to defend themselves against external threats by using molecular defense mechanisms. In this context endogenous plant steroids may play an important role as they are known to take part in plant development and stress resistance reactions [72]. Dehydroepiandrosterone (DHEA) is one of the widest spread plant steroids, whose exact function is however not fully understood [73]. Interestingly DHEA was identified to accumulate in shoots of *Arabidopsis thaliana* after they were infected with the pathogenic fungus *Alternaria brassicicola* (see Chapter 6.3).

In this work we wanted to enlighten the mechanism of action in which DHEA affects *A. brassicicola*. Therefore, different setups were generated to identify the effects of DHEA on the fungal pathogen (*A. brassicicola*), as well as the plant host (*Arabidopsis thaliana*). Due to a direct correlation between increasing DHEA concentrations and limited fungal growth and spore production, effects on sterol biosynthesis were considered. Whether DHEA affected an enzyme of the isoprenoid pathway or distal sterol biosynthesis pathway we have identified the target by analyzing the accumulating intermediate according to our sterol biosynthesis assays (see Chapter 4) [22]. Even though no changes in the isoprenoid or distal sterol biosynthesis patterns were observed after DHEA treatment, we increased insight into the previously undescribed ergosterol biosynthesis of *A. brassicicola*. By azole treatment we identified whether the preferred ergosterol biosynthesis pathway was *via* eburicol or lanosterol, as fungi usually prefer one of both pathways (see Chapter 1.1.3). As azoles inhibit fungal sterol C14-demethylase the treated fungus tends to accumulate the intermediate which is usually metabolized to ergosterol. In ketoconazole (sterol C14-demethylase inhibitor) treated samples we identified eburicol to be preferred over lanosterol, for ergosterol biosynthesis.

Since the observed effects of DHEA on fungal growth and spore formation were not correlated to changes in the sterol pattern, the antifungal effects were likely due to changes in fungal plasma membrane, which affects total fungal membrane integrity.

# Is Dehydroepiandrosterone Excretion a Defense Mechanism of Plants Affecting Ergosterol Biosynthesis of *Alternaria brassicicola*?

## 6.2 Personal contribution

### Overview:

Conceptualization:	J.K.
Methodology:	C.M., F.F., J.K.
Data curation:	C.O., G.S., <b>M.L.</b> , F.F., S.M., K.L.K., L.H., A.A., R.O., M.R., K.O., A.C.U.F., J.K.
Formal analysis:	E.B., J.K.
Writing – original draft:	C.O., G.S., <b>M.L.</b> , K.L.K., R.O., C.M., A.C.U.F., J.K.
Writing – review and editing:	C.O., G.S., <b>M.L.</b> , F.F., S.M., K.L.K., E.B., L.H., A.A., R.O., M.R., K.O., C.M., A.C.U.F., J.K.

### Note:

My contribution to this work was the performance of the experiments concerning the determination of the fungal isoprenoid and sterol patterns according to Liebl *et al.* (see Chapter 4) and Müller *et al.*[22]. The generated data were processed and formatted by me. Further I contributed to the original draft by preparing Tables S08 and S09. Figure 11C, and Figure 12 were prepared by me (Figure 12 A: only the used data and the figure conceptualization were prepared by me).

Dr. Christoph Müller was involved in this work as he and Dr. Jan Klein conceptualized the required sterol measurements in which Dr. Müller supervised Ludwig Huber (phytosterol measurements) and me.

Further analytical methodology and experimental design were prepared by Dr. Jan Klein and Dr. Felix Feistel.

Ceren Oktay, Glendis Shiko, Dr. Felix Feistel, Sarah Mußbach, Karl Ludwig Körber, Anna Anthony, Prof. Dr. Ralf Oelmüller, Dr. Michael Reichelt, Kilian Ossetek, Assoc.-Prof. Alexandra C. U. Furch and Dr. Jan Klein contributed to this article in the remaining experimental investigations and creation of data including data procession and formation.

Bioinformatic analysis and visualization of the generated data were performed by Dr. Emanuel Barth and Dr. Jan Klein.

The original draft was designed by Ceren Oktay, Glendis Shiko, Karl Ludwig Körber, Prof. Dr. Ralf Oelmüller, Dr. Christoph Müller, Assoc.-Prof. Alexandra C. U. Furch and Dr. Jan Klein.

Finally, all authors contributed to editing and reviewing of the manuscript.

# Is Dehydroepiandrosterone Excretion a Defense Mechanism of Plants Affecting Ergosterol Biosynthesis of *Alternaria brassicicola*?

## 6.3 Article

Plant Physiology and Biochemistry 221 (2025) 109570



Contents lists available at ScienceDirect

Plant Physiology and Biochemistry

journal homepage: [www.elsevier.com/locate/plaphy](http://www.elsevier.com/locate/plaphy)



## *Arabidopsis thaliana* accumulates dehydroepiandrosterone after infection with phytopathogenic fungi – Effects on plants and fungi

Ceren Oktay<sup>a</sup>, Glendis Shiko<sup>a</sup>, Maximilian Liebl<sup>b</sup>, Felix Feistel<sup>c</sup>, Sarah Mußbach<sup>a</sup>, Karl Ludwig Körber<sup>a</sup>, Emanuel Barth<sup>d</sup>, Ludwig Huber<sup>b</sup>, Anna Antony<sup>a</sup>, Ralf Oelmüller<sup>a</sup>, Michael Reichelt<sup>c</sup>, Kilian Ossetek<sup>e</sup>, Christoph Müller<sup>b</sup>, Alexandra C.U. Furch<sup>a</sup>, Jan Klein<sup>a,\*</sup>

<sup>a</sup> Plant Physiology, Matthias Schleiden Institute for Genetics, Bioinformatics and Molecular Botany, Friedrich Schiller University Jena, 07743, Jena, Germany

<sup>b</sup> Department of Pharmacy, Center for Drug Research, Ludwig-Maximilians-Universität München, 81377, Munich, Germany

<sup>c</sup> Department for Biochemistry, Max Planck Institute for Chemical Ecology, 07743, Jena, Germany

<sup>d</sup> Bioinformatics Core Facility, Friedrich Schiller University Jena, 07743, Jena, Germany

<sup>e</sup> Research Group Plant Defense Physiology, Max Planck Institute for Chemical Ecology, 07743, Jena, Germany

### ARTICLE INFO

#### Keywords:

*Arabidopsis thaliana*  
*Alternaria brassicicola*  
Dehydroepiandrosterone  
Mammalian steroids  
Fungal infection  
Ergosterol biosynthesis  
Cell membrane integrity

### ABSTRACT

Progesterones and androgens have been found in many plants, but little is known about their physiological function. We used a previously established UPLC-ESI-MS/MS method to analyze progesterone and androgen profiles in fungal infections. Here we show that dehydroepiandrosterone (DHEA), a C<sub>19</sub> steroid, specifically accumulates in shoots of *Arabidopsis thaliana* (L.) HEYNH. infected with *Alternaria brassicicola* (SCHWEIN.) WILTSHIRE. Elevated DHEA levels in plants seem not to be product of fungal sterol/steroid precursor activity, but an intrinsic plant response to the infection. DHEA was applied exogenously to analyze the effects of the androgen on development and gene expression in *A. thaliana*. Our findings reveal that DHEA treatment down-regulates membrane-associated, salicylic acid and abscisic acid-regulated, as well as stress-responsive genes. Notably, DHEA does not inhibit the isoprenoid or post-lanosterol pathway of the ergosterol biosynthesis. Moreover, *A. brassicicola* was also treated with DHEA to analyze the growth, sterol pattern and membrane-integrity. Our data suggest that DHEA enhances the permeability of plant and fungal biomembranes. We propose that DHEA accumulation is a plant defense response which reduces fungal growth in plant tissues.

### 1. Introduction

Plants are threatened by phytopathogenic fungi in natural environments and agricultural ecosystems (Stukenbrock and McDonald, 2008). Therefore, it is not surprising that fungal phytopathogens destroy 30% of all farm plant products through diseases and spoilage. Moreover, mycotoxin-producing fungi endanger the safety of plant products produced for human or animal consumption (Avery et al., 2019).

*Alternaria* species are globally spread, necrotic pathogens (Jindo et al., 2021). They cause various diseases on multiple crops (Rotem, 1998). Infection by these fungi, which cause early blight, led to yield losses of 35–78% in tomatoes and 5–40% in potatoes (Grigolli et al., 2011). In *brassica* species, *Alternaria* species cause the *Alternaria* blight. According to the Food and Agriculture Statistics of the United Nations

(FAOSTAT), edible brassicas are a major vegetable crop in 5th place in food production (Nowakowska et al., 2019). Moreover, brassicas are, except for soybean, the largest oil seed crop (Gupta, 2016). Therefore, 15–70% yield loss caused by *Alternaria* blight is economically harmful and endangers human nutrition (Nowakowska et al., 2019). *Alternaria* species sporulate best in an atmosphere with elevated CO<sub>2</sub> concentrations (Wolf et al., 2010). Therefore, the spread of fungal-caused plant diseases by climatic changes is to be feared (Al-Askar et al., 2014). *A. brassicicola* is an aggressive soil-borne pathogen. The first symptoms of infections are small brown to black spots often observed on older leaves of infected plants. Later, spots develop into irregularly shaped lesions, forming concentric rings. Yellow shadows often surround these rings (Nowicki et al., 2012). *Alternaria* produces mycotoxins, which can be split into three structural different groups: dibenzopyrone derivatives, the perylene derivative altretoxins, and tenuazonic acid. These

\* Corresponding author.

E-mail address: [jan.klein@uni-jena.de](mailto:jan.klein@uni-jena.de) (J. Klein).

<https://doi.org/10.1016/j.plaphy.2025.109570>

Received 5 July 2024; Received in revised form 6 January 2025; Accepted 25 January 2025

Available online 28 January 2025

0981-9428/© 2025 The Authors. Published by Elsevier Masson SAS. This is an open access article under the CC BY license (<http://creativecommons.org/licenses/by/4.0/>).

# Is Dehydroepiandrosterone Excretion a Defense Mechanism of Plants Affecting Ergosterol Biosynthesis of *Alternaria brassicicola*?

C. Oktay et al.

Plant Physiology and Biochemistry 221 (2025) 109570

Abbreviations:	
DHEA	dehydroepiandrosterone
SA	salicylic acid
ABA	abscisic acid
KC	ketoconazole

fungicides leads to accelerated developments of pathogen resistance and is a threat to natural environments (Fernández-Ortuño et al., 2008). Exemplarily: During the last 20 years the average use of pesticides per hectare in Germany increased from 2.98 kg in the year 2000 to 3.80 kg in 2019 (Schanzer et al., 2022). This results in the application of 30,000 tons of 285 different legally approved pesticides only in Germany in the year 2018 (Schanzer et al., 2021). Therefore, it is not surprising that *Alternaria* species developed resistance against widely used quinone outside inhibitors (e.g., pyraclostrobin) and succinate dehydrogenase

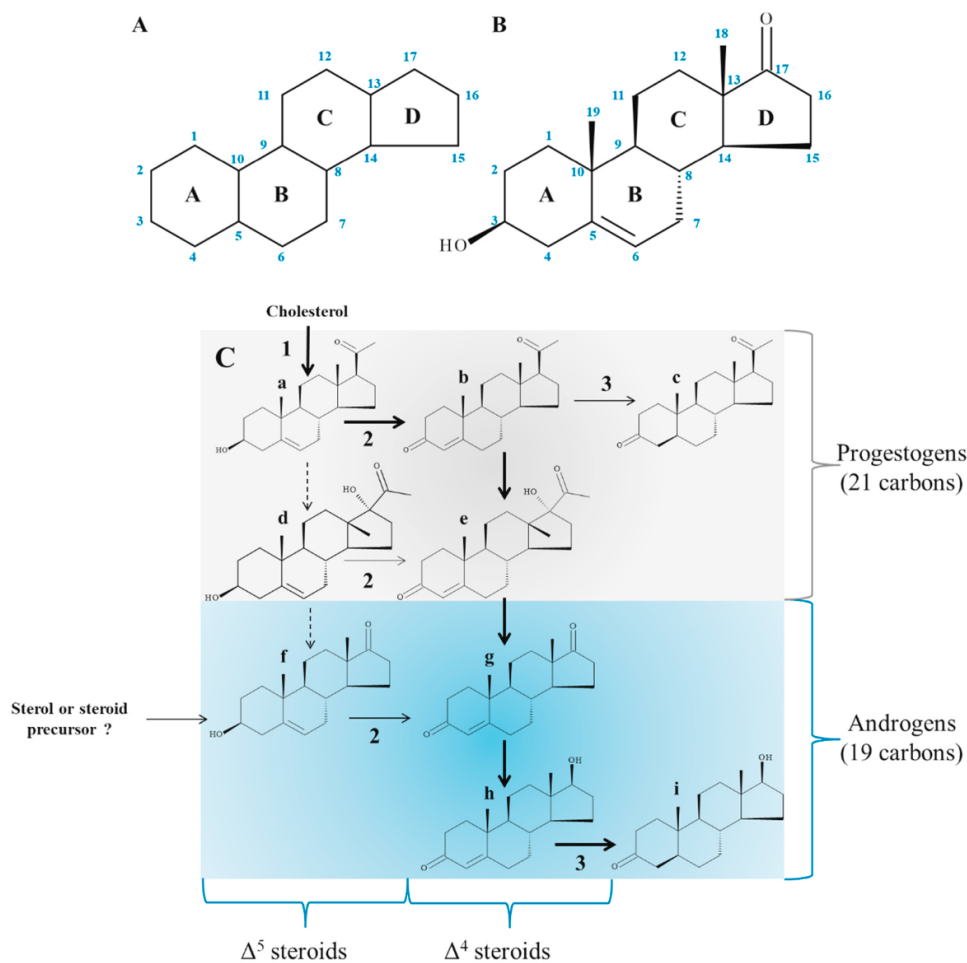


**Fig. 1. Structure of steroids and the conversion of steroids in plants – a theory of plant steroidogenesis** (Shiko et al., 2023). Steroids are tetracyclic tri-terpenoids with a sterane skeleton. This Figure depicts the sterane skeleton (A) of steroids. In dehydroepiandrosterone (B), the sterane skeleton is additionally substituted with a methyl group at C10 and C13, a hydroxyl group at C3, and an oxo moiety on C17, while a double bond connects C5 and C6. Carbon numbering and ring annotation follow IUPAC. (C) Findings of Shiko et al. (2023) show that reaction steps from mammal steroidogenesis are conserved in plants. Bold arrows depict the reaction steps of mammal steroidogenesis that could be found in all analyzed plants. It was suggested that androgen biosynthesis in plants favors a route using the  $\Delta^4$  pathway, which is described by an early conversion of  $\Delta^5$  into  $\Delta^4$  steroids (pregnenolone a into progesterone b). The analyzed steroids are abbreviated with the following letters (pregnenolone a; progesterone b; 5 $\alpha$ -dihydroprogesterone c; 17 $\alpha$ -hydroxypregnenolone d; 17 $\alpha$ -hydroxyprogesterone e; dehydroepiandrosterone f; androstenedione g; testosterone h; 5 $\alpha$ -dihydrotestosterone i). The identified enzymes of plant steroidogenesis are included as numbers (sterol side chain-cleavage enzyme 1;  $\beta$ -hydroxysteroid dehydrogenase and ketosteroid isomerase 2; steroid 5 $\alpha$ -reductases 3).

toxins can be detected in human food products such as tomatoes, apples, and cereals (Pinto and Patriarca, 2017).

Adding to the problem, the excessive use of giant amounts of

inhibitors (e.g., boscalid; Nottensteiner et al., 2019).

Therefore, a large unmet need exists to develop new pest management strategies. Steroids, produced by plants or pathogens, control

# Is Dehydroepiandrosterone Excretion a Defense Mechanism of Plants Affecting Ergosterol Biosynthesis of *Alternaria brassicicola*?

C. Oktay et al.

Plant Physiology and Biochemistry 221 (2025) 109570

many developmental, physiological, or growth processes, and especially the role of endogenous C<sub>21</sub>- (progestogens) and C<sub>19</sub>- (androgens) steroids in plants have not yet been sufficiently explored (Janeczko, 2021). It was shown that progestogens and androgens are widespread within the plant kingdom (Simons and Grinwich, 1989; Shiko et al., 2023). Shiko and colleagues (2023) identified dehydroepiandrosterone (DHEA; Fig. 1), a C<sub>19</sub> steroid, in 85 % of the analyzed plants, from green algae to angiosperms.

Moreover, plants have been shown to convert steroids in a conserved way. Plants can perform all enzymatic reactions of mammalian steroidogenesis, including 3 $\beta$ - and 17 $\beta$ -hydroxysteroid dehydrogenase activity, 5 $\alpha$ - and 5 $\beta$ -reduction of  $\Delta^4$  steroids, as well as 17 $\alpha$ -hydroxylation and 17,20-lyase reactions. These findings were used to build a hypothetical biosynthesis pathway similar to the canonical mammalian steroidogenesis (Shiko et al., 2023, Fig. 1).

It has been shown for several plant species that treatment with progesterone, a progestogen, enhances resistance against several (a)biotic stresses (Genisel et al., 2013; Janeczko et al., 2013; Hao et al., 2019; Sabzmejdani et al., 2020; reviewed in: Klein, 2024). Moreover, the expression of the bovine CYP11A1, an enzyme that converts cholesterol into pregnenolone, in tomato and tobacco results in enhanced values of pregnenolone and progesterone. Consequently, these plants show enhanced resistance against the fungal pathogen *Botrytis cinerea* (Shpakovski et al., 2017). This raises the question if endogenous steroids participate in pathogen response in *A. thaliana*. Within this study, we analyzed the profiles of endogenous C<sub>21</sub>- and C<sub>19</sub>-steroids in *A. thaliana* shoots after infection with *A. brassicicola*. We could detect that DHEA-levels are elevated in infected shoots, while other changes of the steroid levels were not detected. This indicates a role of DHEA in plant infections with fungal pathogens. Therefore, we analyzed the effects of DHEA on plants and the fungal pathogen *A. brassicicola*.

## 2. Material and methods

### 2.1. Plant material

10-day-old seedlings of *A. thaliana* (L.) HEYN. Col. 0 (*A. thaliana*) cultivated on MS-medium (Murashige and Skoog, 1962) were transferred to poor nutrient medium (PNM; Camehl et al., 2011) consisting of 5 mM KNO<sub>3</sub>, 2 mM MgSO<sub>4</sub>, 2 mM Ca(NO<sub>3</sub>)<sub>2</sub>, 0.01  $\mu$ M FeSO<sub>4</sub>, 70  $\mu$ M H<sub>3</sub>BO<sub>3</sub>, 14  $\mu$ M MnCl<sub>2</sub>, 0.5  $\mu$ M CuSO<sub>4</sub>, 1  $\mu$ M ZnSO<sub>4</sub>, 0.2  $\mu$ M Na<sub>2</sub>MoO<sub>4</sub>, 0.01  $\mu$ M CoCl<sub>2</sub>, 10.5 g L<sup>-1</sup> agar (pH 5.6). *Spirodela polyrhiza* clone 9509 was prepared from the stock collection of the Friedrich Schiller University Jena and cultivated on a sugar-free nutrient medium for *Lemnaceae* according to Appenroth et al. (1996, 2018). *Hordeum vulgare* cv. Avalon was obtained from Petra Sandjohann (Gut Obbach Schäfer GbR, Euerbach-Obbach, Germany) and cultivated as described before (Shiko et al., 2023).

### 2.2. Fungus cultivation

*Alternaria brassicicola* SCHWEIN. WILTSHIRE was cultivated in potato dextrose agar (PDA; pH = 6.5–6.8; Carl Roth GmbH, Germany) in the dark at 28 °C for 4 weeks. Plates were used for further experiments.

### 2.3. Infection of plants with *A. brassicicola*

10 mL of isolation solution (0.01% Tween-20 in sterile water) was added to well-grown fungal mycelium on the PDA plates. The suspended mycelium was carefully removed from the surface of the PDA agar surface. The fungal solution was filtered through 4 layers of nylon membrane (SEFAR NITEX 03–70; fibre material: PA 6.6, monofilament; mesh opening: 70  $\pm$  4  $\mu$ m; mesh count: 81 n cm<sup>-1</sup>; Sefar AG, Heiden, Switzerland). Spores were pelletized by centrifuging for 1 min at 12,000 g at 22 °C and resuspended in new isolation solution. This was repeated 4 times. The concentration of the spore solution was adjusted to 1  $\times$  10<sup>6</sup>

spores per mL using a hemocytometer. For infection of *A. thaliana* or *S. polyrhiza*, 2  $\mu$ L of spore solution was applied onto a single leaf.

### 2.4. Microscopy

Leaves of *S. polyrhiza* or Rhodamine stained hyphae of *A. brassicicola* were mounted on a glass slide with a cover slip for microscopic inspection using an Axio Imager.M2 (Zeiss Microscopy GmbH, Jena, Germany) equipped with a 10x objective (N-Achroplan 10 $\times$ /0.3). Bright-field images were recorded with a monochromatic camera: AxioCam 503 mono (Zeiss Microscopy GmbH). Fluorescence images (EX 545/25 and EM 605/70) were recorded with a color camera: AxioCam 503 color (Zeiss Microscopy GmbH, Jena) by use of DsRED filter (605/70 nm). Digital images were processed with the ZEN software (Zeiss Microscopy GmbH), treated with Adobe® Photoshop to optimize brightness, contrast and coloring.

### 2.5. Analysis of *A. brassicicola* growth and spore production influenced by DHEA

To analyze the effects of DHEA on fungal growth, a plug of well-grown *A. brassicicola* mycelium (d = 5 mm) was transferred to PDA plates supplemented with 3–30  $\mu$ M DHEA dissolved in DMSO, while pure DMSO was used for control treatment. The diameter of the grown colony was analyzed after 14 days.

To analyze spore production, 20  $\mu$ L of spore solution (see above) was spread onto a PDA plate supplemented with DHEA; after 14 days, spores were isolated as described above, and the spore concentration was analyzed using a hemocytometer.

### 2.6. Extraction and analyses of endogenous plant steroids

Steroid extraction was performed using 20 mg lyophilized plant material as described in Shiko et al. (2023). In brief: Flash-frozen plant material was lyophilized. The dried material was pulverized, and 20 mg aliquots of each sample were extracted with 1 mL of extraction mixture (80% MeOH in water containing 100 ng mL<sup>-1</sup> progesterone-*d*<sub>9</sub> as internal standard, Merck, Germany). Samples were vortexed for 60 s and sonicated (Sonorex Super RK 100 H, BANDELIN electronic, Germany) for 5 min at 22 °C. The crude extracts were centrifuged (HERMLE ZK233-M2, HERMLE Labortechnik GmbH, Germany) for 60 s at 16,000 g, and the supernatant used for the Steroid analysis. It was performed by LC-MS/MS on an Agilent 1260 series HPLC system (Agilent Technologies) with a tandem mass spectrometer QTRAP 6500 (SCIEX, Darmstadt, Germany). A detailed description of the method and the results are presented in the supplement (Suppl. Table S1, Suppl. Table S2, and Suppl. Table S3).

### 2.7. Phytosterol analysis

The analysis by gas chromatography single quadrupole MS (GC-MS) was performed on a 7820A Agilent gas chromatograph coupled to a MSD 5977B single quadrupole and 7693A autosampler with a split/splitless injector. Instrument control and data analysis were carried out with Agilent MassHunter Workstation Software package B.08.00 (Santa Clara, CA, USA). An Agilent HP-5MS UI capillary column of 30 m, 0.25mm inner diameter, 0.25  $\mu$ m film thickness was used at a constant flow rate of 1.4 mL min<sup>-1</sup>. Carrier gas was helium 99.999% from Linde AG (Munich, Germany). The single quadrupole (MS) was operated with electron ionization (EI) at 70 eV. The multiplier operated with a gain factor of 5. The samples were analyzed using a scan method (*m/z* 100–600). The total run time of the method was 20.0 min. The initial column temperature was 60 °C and was held for 1.0 min. Then the temperature was ramped up to 260 °C with 50 °C min<sup>-1</sup>. The steroids were eluted at a rate of 5 °C min<sup>-1</sup> until 310 °C. At the end, the temperature was increased to 320 °C at a rate of 50 °C min<sup>-1</sup> (hold time 2.4

# Is Dehydroepiandrosterone Excretion a Defense Mechanism of Plants Affecting Ergosterol Biosynthesis of *Alternaria brassicicola*?

C. Oktay et al.

Plant Physiology and Biochemistry 221 (2025) 109570

min). The solvent delay was 8.5 min. The injection volume was 3  $\mu\text{L}$ . The injection was performed in a splitless mode at an injector temperature of 250  $^{\circ}\text{C}$ . The temperature for the MS transfer line was set at 250  $^{\circ}\text{C}$ , for the MS source at 230  $^{\circ}\text{C}$ , and for the MS quadrupole at 150  $^{\circ}\text{C}$ . The sterols were identified by mass spectral analysis and by calculating the relative retention time in comparison with commercial references (a detailed description of the method can be found in the supplement (Suppl. Table S4).

The sample preparation procedure started with the comminution of the samples to ensure a homogeneous material. Approximately 5 mg of each sample was weighed and transferred into a 20 mL glass vial. The concentration was then adjusted to 1 mg mL<sup>-1</sup> by adding 2 M aqueous NaOH solution, followed by incubation at 80  $^{\circ}\text{C}$  for 2 h. After incubation, the sample was homogenized by vortexing to ensure uniformity. The sample preparation procedure is described in detail by Müller et al., (2017). Briefly, 1000  $\mu\text{L}$  aliquot was taken from the sample and 100  $\mu\text{L}$  of internal standard mix (1  $\mu\text{g mL}^{-1}$  desmosterol-*d*<sub>6</sub> and 1  $\mu\text{g mL}^{-1}$  cholesterol-*d*<sub>7</sub> in ethyl acetate) was added. 650  $\mu\text{L}$  of *tert*-butyl methyl ether (TBME) was added and the mixture was homogenized by hand for 1 min. Afterwards, the sample was centrifuged for 5 min at 11,000 g. The organic phase was transferred to a second microcentrifuge tube containing a mixture of 40 mg of anhydrous magnesium sulfate and PSA (7:1; dispersive solid-phase extraction (dSPE)). The extraction was repeated with an additional 750  $\mu\text{L}$  of TBME. The organic phases from both extractions were combined into the dSPE mixture, homogenized again and centrifuged for 5 min at 11,000 g. The supernatant was transferred to a GC-Vial and the solvent was evaporated under a gentle stream of nitrogen until the sample was dry. Finally, the sample underwent derivatization according to the method described by Junker et al., (2021) for the analysis of oxysterols. The detailed results are given in the supplement (Suppl. Table S5).

## 2.8. Phytohormone extraction and analyses

Plants were treated with 3 and 10  $\mu\text{M}$  DHEA. Therefore, 60  $\mu\text{L}$  of a 2.5 mM or an 8.34 mM DHEA stock solution (dissolved in DMSO) were added to 50 mL tap water, while 60  $\mu\text{L}$  DMSO in 50 mL tap water (=0.12% DMSO) was used as mock-treatment. *A. thaliana* or *H. vulgare* shoots, or *S. polyrhiza* plants were harvested 0.5, 1, and 3 h after the start of the treatment and immediately frozen in liquid nitrogen. 100–250 mg of the frozen plant material was homogenized using mortar and pestle in liquid nitrogen. Samples were extracted in 1 mL methanol containing 40 ng salicylic acid-*d*<sub>4</sub> (Santa Cruz Biotechnology, TX, USA), 40 ng jasmonate-*d*<sub>6</sub> (HPC Standards GmbH, Germany), 40 ng abscisic acid-*d*<sub>6</sub> (Toronto Research Chemicals, Toronto, Canada), and 8 ng jasmonate-isoleucin-*d*<sub>6</sub> (HPC Standards GmbH, Cunnorsdorf, Germany) as internal standards. Phytohormone analysis was performed by liquid chromatography (LC)-mass spectrometry (MS)/MS as described in Heyer et al. (2018) on an Agilent 1260 series HPLC system (Agilent Technologies, Santa Clara, CA, USA) with the modification that a tandem mass spectrometer QTRAP 6500 (SCIEX, Darmstadt, Germany) was used. A more detailed phytohormone analysis is presented in the supplement (Suppl. Table S6).

## 2.9. RNAseq analysis

7 days old *A. thaliana* plants were transferred to PNM medium. After 2 days of adaption to the new medium, plants were treated with 10  $\mu\text{M}$  DHEA (dissolved in 0.12% DMSO), while 0.12% DMSO was used as a mock-treatment. Shoots were harvested after 1 h and immediately frozen in liquid nitrogen. Additionally, *A. thaliana* plants were infected with *A. brassicicola* spore solution (in 0.12% DMSO) or spore solution supplemented with 10  $\mu\text{M}$  DHEA (in 0.12% DMSO). Shoots were harvested after 24 h and immediately frozen in liquid nitrogen. All samples were stored at  $-80^{\circ}\text{C}$ . RNA was isolated using TRIzol® Reagent (Invitrogen™ by Thermo Fisher Scientific, MA, USA), as described previously

(Chomczynski, 1993; Shiko et al., 2023). Integrity and concentration of plant RNA were analyzed using absorbance analysis with a NanoVue (GE Healthcare, Uppsala, Sweden).

Four biological replicates of all treatments and controls were analyzed by GENEWIZ Germany GmbH (Azenta Life Science, Leipzig, Germany) and processed as described in the following:

RNA samples were quantified using Qubit 2.0 Fluorometer (Life Technologies, Carlsbad, CA, USA) and RNA integrity was checked using Agilent Fragment Analyzer (Agilent Technologies, Palo Alto, CA, USA). RNA sequencing library preparation was prepared using NEBNext Ultra II RNA Library Prep Kit for Illumina following manufacturer's instructions (NEB, Ipswich, MA, USA). Briefly, mRNAs were first enriched with Oligo(dT) beads. Enriched mRNAs were fragmented. First strand and second strand cDNA were subsequently synthesized. The second strand of cDNA was marked by incorporating dUTP during the synthesis. cDNA fragments were adenylated at 3' ends, and indexed adapter was ligated to cDNA fragments. Limited cycle PCR was used for library amplification. The dUTP incorporated into the cDNA of the second strand enabled its specific degradation to maintain strand specificity. Sequencing libraries were validated using NGS Kit on the Agilent Fragment Analyzer (Agilent Technologies, Palo Alto, CA, USA), and quantified by using the Qubit 4.0 Fluorometer (Invitrogen, Carlsbad, CA, USA). The sequencing libraries were multiplexed and loaded on the flow cell on the Illumina NovaSeq 6000 instrument according to manufacturer's instructions. The samples were sequenced using a 2 × 150 Pair-End (PE) configuration v1.5. Image analysis and base calling were conducted by the NovaSeq Control Software v1.7 on the NovaSeq instrument. Raw sequence data (.bcl files) generated from Illumina NovaSeq was converted into fastq files and de-multiplexed using Illumina bcl2fastq program version 2.20. One mismatch was allowed for index sequence identification. Raw data are available on ncbi (Geo accession ID: GSE261582).

Raw sequencing reads were assessed for quality using FastQC (version 0.11.9; <https://www.bioinformatics.babraham.ac.uk/projects/fastqc>). Adaptor trimming, quality filtering, and read preprocessing were performed using fastp (version 0.23.2; Chen et al., 2018). In detail, 5' and 3' bases with a Phred quality score below 28 were cut, and reads were removed if they had more than one ambiguous base, an average quality score below 28, or a length of fewer than 15 bases. Processed reads were aligned to the current *A. thaliana* genome (tair10.1) using Hisat2 (version 2.2.1) with standard parameters (Kim et al., 2019). The aligned reads were sorted and indexed using SAMtools (version 1.11; Li et al., 2009). Read counting was performed using featureCounts (version 2.0.1; Liao et al., 2014) with the tair 10.1 annotation as reference. Differential gene expression analysis was performed using DESeq2 (version 1.38.3; Love et al., 2014), and comparisons having a false discovery rate (FDR; Benjamini and Hochberg, 1995) adjusted p value < 0.05 were deemed to be statistically significant.

Genes were categorized according to their function found on The Arabidopsis Information Resource (TAIR) database (February 2024) (Berardini et al., 2004). Keywords for each gene with locus identifier numbers were selected from GO-term classifications using an original code utilizing python and pandas library (McKinney, 2010). The code provided matches for the locus number with functions (GO-terms) recorded on TAIR, the number of genes that a function has matched with, as well as a bubble plot with desired variables from the RNAseq results.

## 2.10. Quantitative polymerase chain reaction

To verify the reliability of the RNAseq experiment, we quantified the expression PR1 by quantitative polymerase chain reaction (qPCR). qPCRs were executed as described previously (Klein et al., 2021a,b; Shiko et al., 2023). In brief: RNA was transcribed into cDNA by a RevertAid First Strand cDNA Synthesis Kit (ThermoFisher Scientific, Waltham, MA, USA). qPCRs were performed in a Bio-Rad CFX96

# Is Dehydroepiandrosterone Excretion a Defense Mechanism of Plants Affecting Ergosterol Biosynthesis of *Alternaria brassicicola*?

C. Oktay et al.

Plant Physiology and Biochemistry 221 (2025) 109570

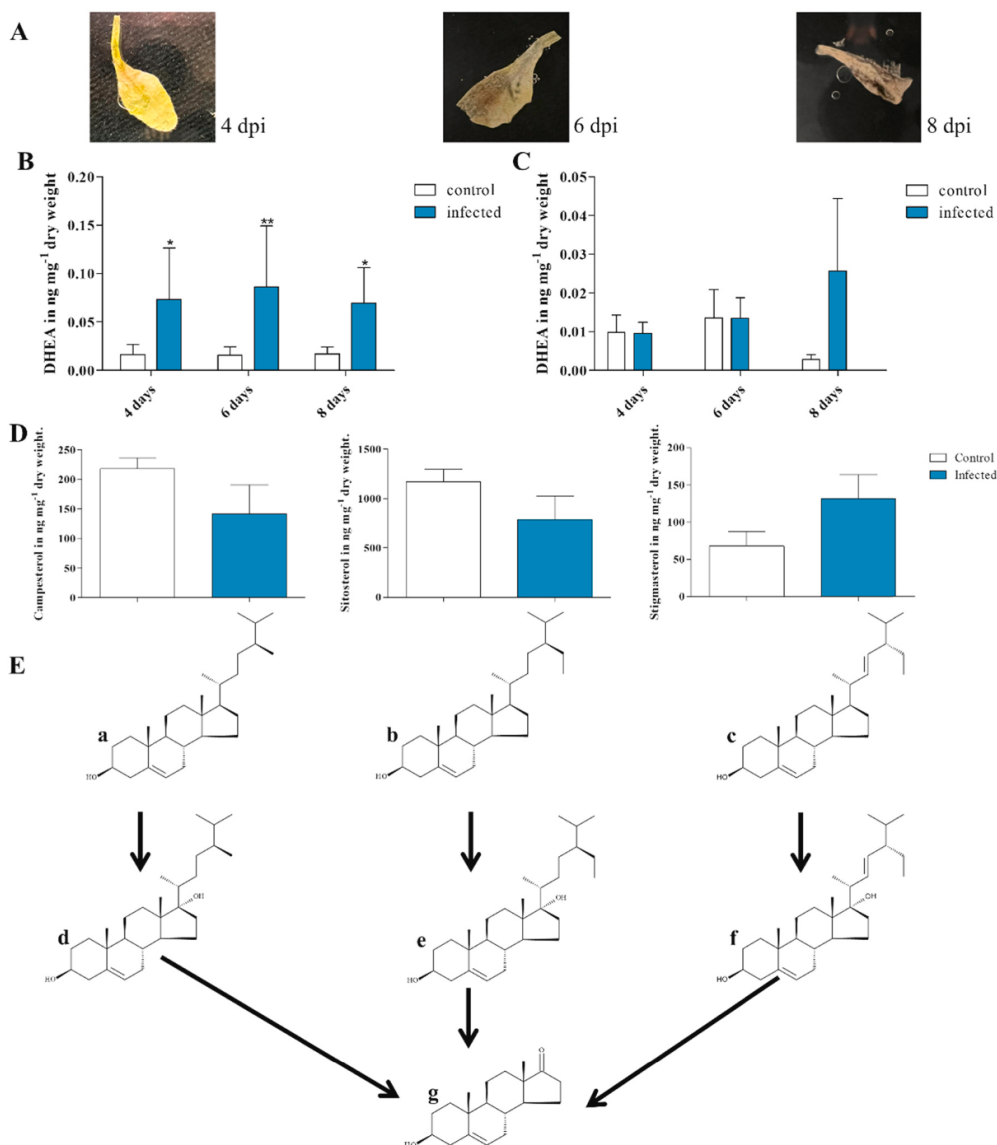


**Fig. 2.** Putative pathway leading to enhanced dehydroepiandrosterone (DHEA) accumulation in *A. brassicicola*-infected *A. thaliana* plants. (A) We here show leaves of *A. thaliana* 4, 6 and 8 days post infection (dpi) with *A. brassicicola*. (B) The graph shows DHEA values (blue) compared to the control (white) 4, 6, and 8 days post-infection (dpi). DHEA concentrations are given in  $\text{ng mg}^{-1}$  dry weight (means  $\pm$  SEM are shown;  $n > 3$ ;  $p < 0.05$ ). An asterisk indicates significant differences. (C) We give here additionally the DHEA values of *A. thaliana* roots of plants with *A. brassicicola*-infected shoots. The graph shows DHEA values (blue) compared to the control (white) 4, 6, and 8 days post-infection (dpi). DHEA concentrations are given in  $\text{ng mg}^{-1}$  dry weight (means  $\pm$  SEM are shown;  $n > 3$ ;  $p < 0.05$ ). No statistically significant differences could be detected. (D) Moreover, we show the contents of campesterol, sitosterol, and stigmasterol in *A. brassicicola*-infected *A. thaliana* shoots 4 dpi compared to uninfected controls. Sterol concentrations are given in  $\text{ng mg}^{-1}$  dry weight (means  $\pm$  SEM are shown;  $n > 3$ ;  $p < 0.05$ ). No statistically significant differences could be detected. (E) In mammals, DHEA is produced from pregnenolone with  $17\alpha$ -hydroxypregnenolone as intermediate. For plants, a direct conversion of sterols into DHEA was discussed (Shiko et al., 2023). In contrast to mammals, phytosterol precursors are more abundant compared to cholesterol. Therefore, a possible scenario for plants could be that the formation of DHEA starts from campesterol (a),  $\beta$ -sitosterol (b), or stigmasterol (c). A  $17\alpha$ -hydroxylation leads to the formation of the intermediates  $17\alpha$ -hydroxycampesterol (d),  $17\alpha$ -hydroxy- $\beta$ -sitosterol (e), or  $17\alpha$ -hydroxystigmasterol (f). DHEA (g) could be formed by  $17,20$ -lyase reactions of these  $17\alpha$ -hydroxysterols. (For interpretation of the references to color in this figure legend, the reader is referred to the Web version of this article.)

# Is Dehydroepiandrosterone Excretion a Defense Mechanism of Plants Affecting Ergosterol Biosynthesis of *Alternaria brassicicola*?

C. Oktay et al.

Plant Physiology and Biochemistry 221 (2025) 109570

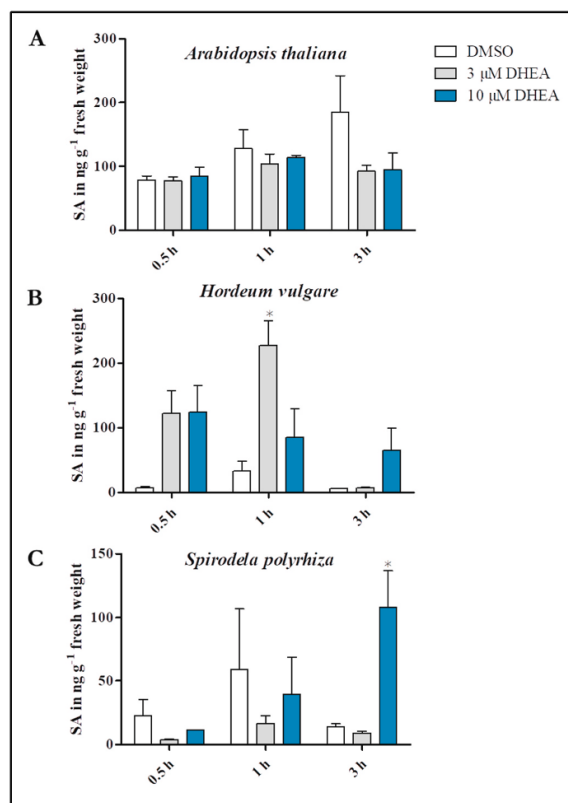


**Fig. 3.** Effects of exogenously applied DHEA on salicylic acid in plants. *A. thaliana* (A) and *H. vulgare* (B) were germinated and cultivated in long-day conditions for 7 days. *S. polyrrhiza* clones (C) were cultivated for 7 days in sugar-free medium according to Appenroth et al. (1996). Plants were treated with DHEA (3 or 10 μM) solutions. DMSO (0.12% in water) was used as a mock-treatment. Plant material (shoots of *A. thaliana* and *H. vulgare* and complete *S. polyrrhiza* plants) was harvested after 0.5, 1, and 3 h. Hormones were extracted from fresh shoot material. The graph depicts the salicylic acids (SA) concentrations in ng g<sup>-1</sup> fresh weight (Mean ± SEM are shown; 4 ≤ n ≤ 3). Differences were analyzed statistically by a one-way ANOVA with post hoc Bonferroni correction (p < 0.05).

Thermal Cycler (Bio-Rad Laboratories Inc., Göttingen, Germany). For each measurement a 20 μL reaction was prepared with 1.1 μL cDNA, 2 dNTPs (10 mM; ThermoFisher Scientific, Waltham, MA, USA), 1 μL EvaGreen® Plus Dye (Biotium, USA), 2 μL of each primer (100 μM), 0.2 μL DreamTaq DNA Polymerase, and 3.4 μL DreamTaq DNA Polymerase buffer (ThermoFisher Scientific, Waltham, MA, USA) were used. qPCRs were performed with a preincubation at 95 °C for 180 s, followed by 40 cycles at 95 °C for 10 s, 60 °C for 50 s, and 72 °C for 60 s. The following primers for qPCRs were used:

```
JK_RPS18_for: 5'GTCTCCAATGCCCTTGACAT'3
JK_RPS18_rev: 5'TCTTTCCTCTGCGACCAGTT'3
JK_AtPR1_for: 5'TCAGTGAGACTCGGATGTGC'3
JK_AtPR1_rev: 5'CGTTCACATAATTCCCACGAG'3
```

Four biological replicates were analyzed. We compared the normalized Count Reads of PR1 obtained by RNAseq and the CT values of PR1 obtained by qPCR, as well as the calculated Log<sub>2</sub> fold changes (RNAseq) and relative expression (qPCR). Relative expression was calculated by 2<sup>-ΔΔCT</sup> method (Livak and Schmittgen, 2001). RPS18 was used as reference gene for normalization as described before (Shiko et al., 2023).

## 2.11. Aequorin luminescence-based assay of intracellular calcium

The measurement of intracellular calcium follows the protocol described by Vadassery et al. (2009). *A. thaliana* lines expressing a cytosolic apoaequorin from *Aequorea victoria* (based on ecotype RLD) were used for Ca<sup>2+</sup> measurements (Polisensky and Braam, 1996). Plants were grown vertically in Hoagland's medium with 1% agar for 16 days. Roots were dissected from shoots and both reconstituted in 5 μM coelenterazine solution (P.J.K. GmbH, Kleinblittersdorf, Germany) containing 30 μM DHEA, DMSO (mock treatment) or water as control in the dark overnight at 21 °C. Bioluminescence counts (BIC) in *Arabidopsis* from roots were recorded as relative light units (RLU) sec<sup>-1</sup> in 5 s intervals for 20 min using a microplate luminometer (Luminoscan Ascent, version 2.4, Thermo Fisher Scientific, Waltham, USA). After a 1-min background reading, H<sub>2</sub>O<sub>2</sub> (Carl Roth GmbH, Karlsruhe, Germany) was added manually to the well (final concentration: 40 mM) and readings in RLU were taken for 20 min. Calibrations were performed by estimating the amount of aequorin remaining at the end of experiment by discharging all remaining aequorin in 0.1 M CaCl<sub>2</sub>, 10% ethanol, and the counts were recorded for 10 min. The luminescence counts obtained were calibrated using the equation by Rentel and Knight (2004) that takes a double logarithmic relationship between the concentration of free Ca<sup>2+</sup> present in the cell and the remaining aequorin discharged at any point of time into account. The calibration equation is: pCa = 0.332588(-log k) + 5.5593, where k is a rate constant equal to luminescence counts sec<sup>-1</sup> divided by total remaining counts. Results are given in the supplement (Suppl. Table S7).

## 2.12. Determination of the ergosterol biosynthesis pattern by GC-MS

To understand the ergosterol biosynthesis pathway in *A. brassicicola*, we analyzed the sterol pattern of azole-treated *A. brassicicola* hyphae. Therefore, we determined a non-lethal concentration of ketoconazole (KC; Merck, Darmstadt, Germany). We infected PDS plates supplemented with 0.5, 1, 2, 4, and 8 μg mL<sup>-1</sup> KC, using PDA supplemented with methanol (0.1%) as mock-treatment. Sterol pattern were analyzed in *A. brassicicola* hyphae grown for 7 days in potato dextrose broth (PDB; pH = 6.5–6.8; Carl Roth GmbH, Germany) supplemented with 2 μg mL<sup>-1</sup> KC, while methanol was used as mock-treatment. As a control, potato-dextrose agar supplemented with methanol (solvent for KC; 1) was used. Influence of DHEA on production of ergosterol in *A. brassicicola* was tested using PDB supplemented with 10 μM DHEA dissolved in DMSO, while pure DMSO was used as mock-treatment. Fungal tissue was harvested by centrifugation (10 min, 12,000 g, 22 °C) and lyophilized for 24 h.

Fungal tissue was harvested by centrifuging and lyophilized for 24 h. To determine the effect of DHEA treatment on the ergosterol biosynthesis pathway, the samples were analyzed by gas chromatography (GC) coupled to quadrupole MS. For analysis 2 × 5 mg lyophilized fungal biomass were used. The isoprenoid and the sterol pattern were determined by previously described protocols (Müller et al., 2017; Liebl et al., 2023). A detailed description of the analysis of isoprenoid and ergosterol patterns is found in the supplement (Suppl. Table S8). Content and composition of intermediates of the isoprenoid and post-lanosterol pathway of ergosterol biosynthesis of *A. brassicicola* samples confronted with 10 μM DHEA or ketoconazole compared to untreated controls can be found in the supplement (Suppl. Table S9).

## 2.13. Rhodamine-based membrane integrity assay

A plug of well-grown *A. brassicicola* mycelium (d = 5 mm) was cultivated in 3 mL PDB for 72 h. DHEA (30 μM; solved in DMSO) or DMSO (0.12 %; as mock-treatment) were added and the fungus was cultivated for additional 24 h. Rhodamine B (Merck, Darmstadt, Germany) dissolved in ethanol was added to a final concentration of 50 μM. After 30 min incubation the fungal tissues were washed in tap water.

# Is Dehydroepiandrosterone Excretion a Defense Mechanism of Plants Affecting Ergosterol Biosynthesis of *Alternaria brassicicola*?

C. Oktay et al.

Plant Physiology and Biochemistry 221 (2025) 109570

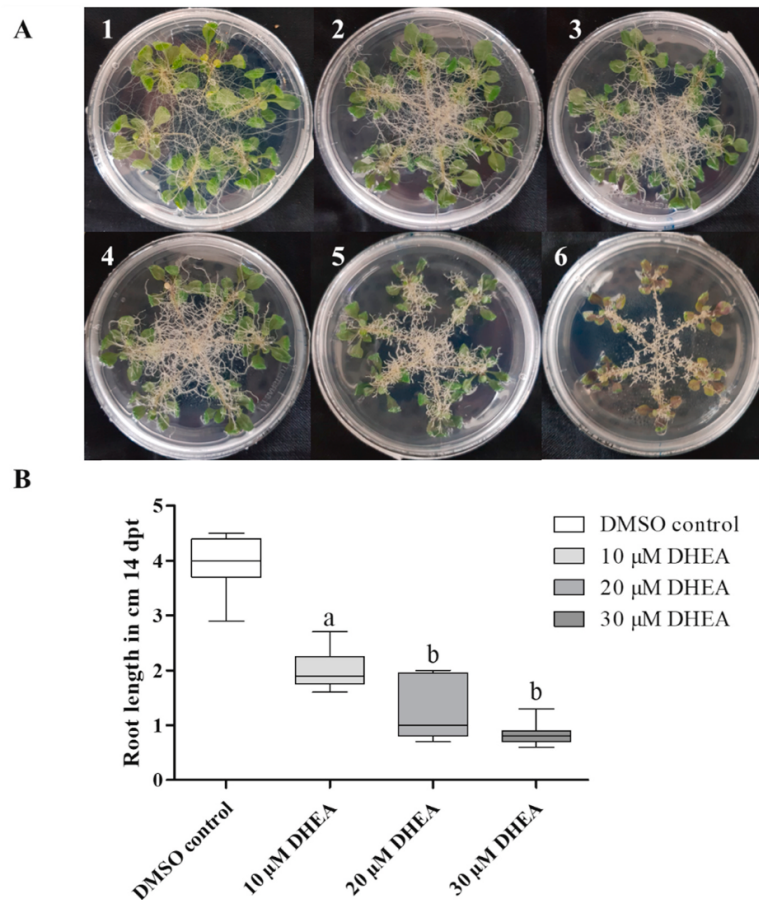


**Fig. 4. Effects of exogenous DHEA on root growth and morphology.** (A) *A. thaliana* plants were germinated on MS and cultivated in long-day conditions. 10-day old plants were transferred on MS-medium containing DHEA (3–30 μM dissolved in 0.12% DMSO). The graph shows pictures of plant roots 14 days after the treatment (days post-treatment dpt; DMSO (1), 3 μM DHEA (2); 5 μM DHEA (3); 10 μM DHEA (4); 20 μM DHEA (5); 30 μM DHEA (6). (B) Root length of 14 days old plants directly sown on DHEA-containing medium. Differences were analyzed statistically by a one-way ANOVA with post hoc Bonferroni correction (Mean ± SEM are shown;  $10 \leq n \leq 8$ ;  $p < 0.05$ ).

## 2.14. Statistical analysis

All data are expressed as the means ± SEM. Values of biological replicates are given as n within the **Figure** legends. Means between the various groups were compared by *t*-Test or one-way analysis of variance (ANOVA followed by Tukey's post hoc test). In case of multiple comparisons, a post hoc Bonferroni correction was applied. P values < 0.05 were considered statistically significant. Data were analyzed using GraphPad Prism 5 Software (GraphPad).

## 3. Results and discussion

### 3.1. DHEA levels and DHEA formation in *A. brassicicola* infected plants

It has been shown previously that exogenous treatment with progestogens helps plants cope with moderate (a)biotic stress (Genisel et al., 2013; Janeczko et al., 2013; Hao et al., 2019; Sabzmejdani et al., 2020; reviewed in: Klein, 2024). Therefore, we analyzed changes in *A. thaliana*'s endogenous progestogens and the chemically related androgens after infection with the economically critical pathogenic fungi *A. brassicicola*. We show that infection of *A. thaliana* leaves with

*A. brassicicola* enhances the amounts of DHEA in the shoot material by factor 5 (Fig. 2B). Pregnenolone and progesterone could be detected only in shoots of infected plants, while the 17α-hydroxypregnenolone, 17α-hydroxyprogesterone, androstenedione, testosterone, 5α-dihydroprogesterone were not detected at all (shoots: Suppl. Table S2; roots: Suppl. Table S3). Additionally, we detected changes in the 5α-pregnane-3,20-dione levels of roots (Suppl. Table S3), but data and changes were not consistent. That is why we focus on the detected elevated DHEA levels. Changes in the DHEA profiles could not be detected in the roots of these plants after 4, and 6 days of infection (Fig. 2C). Only 8 days post infection (dpi), we were able to detect enhanced DHEA values, but these changes were not statistically significant. We conclude that infection of *A. thaliana* shoots with the fungal pathogen *A. brassicicola* enhances the DHEA level in the infected tissue. We suggest that the enhanced values of DHEA after 8 dpi are caused by transport of DHEA or by growth of the phytopathogen into the roots.

Since we could not detect DHEA in *A. brassicicola* spores and hyphae when the fungus was cultivated on PDA medium, the elevated DHEA levels in infected *A. thaliana* shoots could be of plant origin or originating from a fungal precursor. We have shown previously that the aquatic monocot *Spirodela polyrrhiza* does not contain endogenous DHEA,

# Is Dehydroepiandrosterone Excretion a Defense Mechanism of Plants Affecting Ergosterol Biosynthesis of *Alternaria brassicicola*?

C. Oktay et al.

Plant Physiology and Biochemistry 221 (2025) 109570

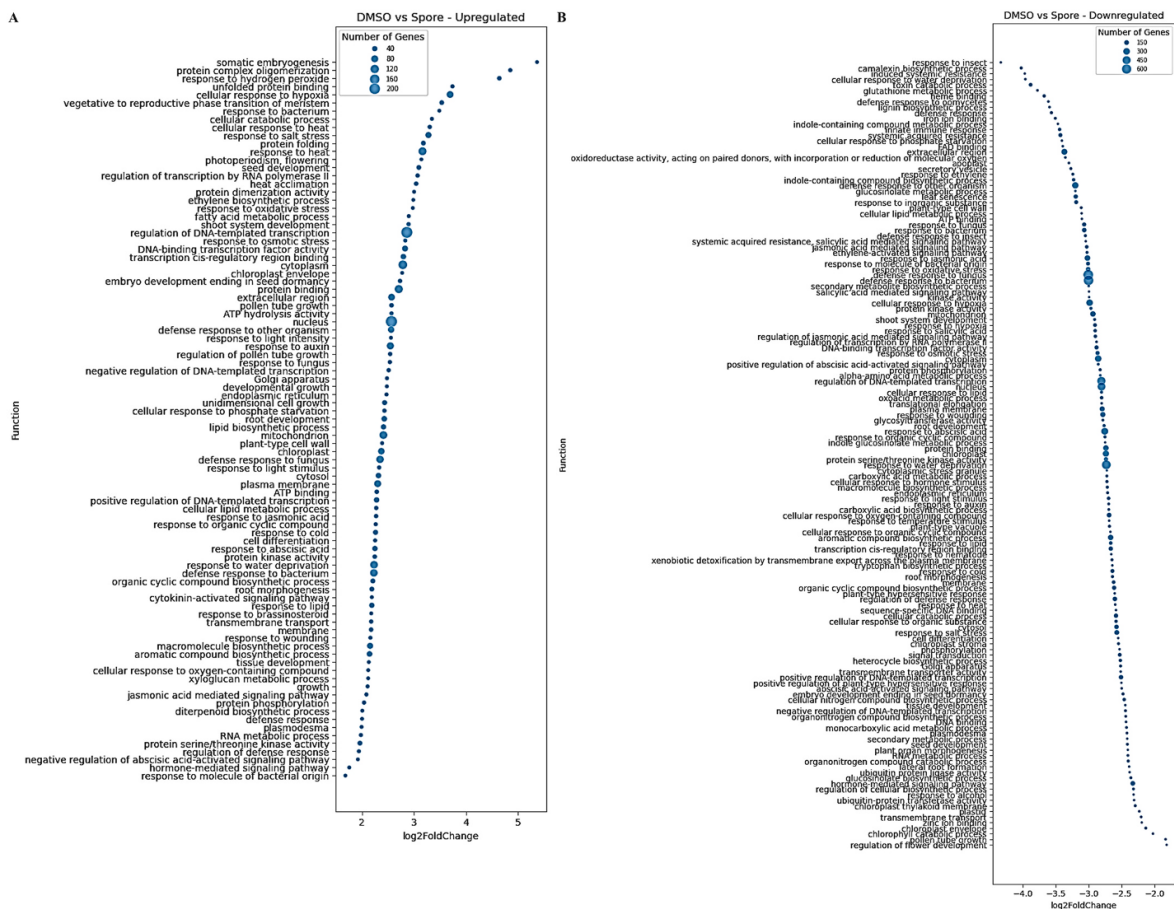


Fig. 5. Effects of *A. brassicicola* infection on gene expression of *A. thaliana*. The graph summarizes genes changed by DHEA treatment. The function-association of significantly changed transcripts ( $p < 0.05$ ) is based on TAIR database. The graph shows the number of changed transcripts associated with a particular function.

but converts steroid precursors quite efficiently into DHEA (Shiko et al., 2023). Since *A. brassicicola* can also infect *S. polyrhiza* leaves (Suppl. Fig. S1), we tested whether DHEA accumulates in *S. polyrhiza*, because the host plant converts a fungal precursor to DHEA. In previous studies we did not find DHEA in *S. polyrhiza*, but the plant was able to catalyze the conversion of progestogens into androgens (Shiko et al., 2023). Therefore, *S. polyrhiza* is able to convert the fungal precursor into DHEA (Shiko et al., 2023). We have to mention that we found small amounts of DHEA slightly above the detection limit in uninfected *S. polyrhiza* within these experiments. Nevertheless, DHEA values did not increase upon *A. brassicicola* infection.

We conclude that fungal precursors do not cause enhanced DHEA values in the infected *S. polyrhiza* host. If we assume that this is also true for *A. thaliana*, the elevated DHEA levels in the *A. brassicicola* – infected shoots could be caused by an altered steroid metabolism which leads to the observed enhanced DHEA levels in the infected plant organ. A possible scenario could be that the pathogen alters the phytosterol metabolism in *A. thaliana*. While the direct conversion of sterols into  $C_{19}$ -steroids is not known for mammals (pregnenolone is the precursor of all mammal steroids), a conversion of phytosterols and ergosterol was detected in Mycobacteria (Dovbnya et al., 2010). A comparable conversion of phytosterols could lead to the detected elevated DHEA levels in *Arabidopsis* shoots. In line with this theory, we could show that *A. brassicicola*-infected *A. thaliana* plants showed

changed sterol profiles compared to uninfected controls 4 days post infection (Suppl. Table S5). While the contents of squalene and cholesterol did not change in infected *A. thaliana* shoots, we found slightly reduced values of campesterol and sitosterol, while the values of stigmasterol were slightly increased. On a systematic level, it can be mentioned that no cholesterol was found in uninfected *A. thaliana* roots, while we were able to identify it in 2 of 3 experiments using infected root material. This indicates a changed sterol metabolism, which could lead to an enhanced DHEA production. This nicely fits to a metabolomics analysis of infected *A. thaliana* plants by Botanga and colleagues (Botanga et al., 2012), which could show that cholesterol levels of *A. thaliana* plants are significantly reduced 9 and 24 h after infection with *A. brassicicola*. A putative way from the three changed phytosterols in infected shoots (campesterol, sitosterol and stigmasterol) to DHEA is depicted in Fig. 2E. These possible pathways of DHEA formation have to be analyzed in further experiments.

### 3.2. Effects of DHEA treatment on plants

We could show that DHEA was enhanced in *A. thaliana* shoots infected with *A. brassicicola*, while this was not the case for *S. polyrhiza*. Therefore, we analyzed the effects of exogenously applied DHEA on these two plant species, while using DMSO as an organic solvent. Organic solvents are causing stress in plant cells. As a result SA

# Is Dehydroepiandrosterone Excretion a Defense Mechanism of Plants Affecting Ergosterol Biosynthesis of *Alternaria brassicicola*?

C. Oktay et al.

Plant Physiology and Biochemistry 221 (2025) 109570

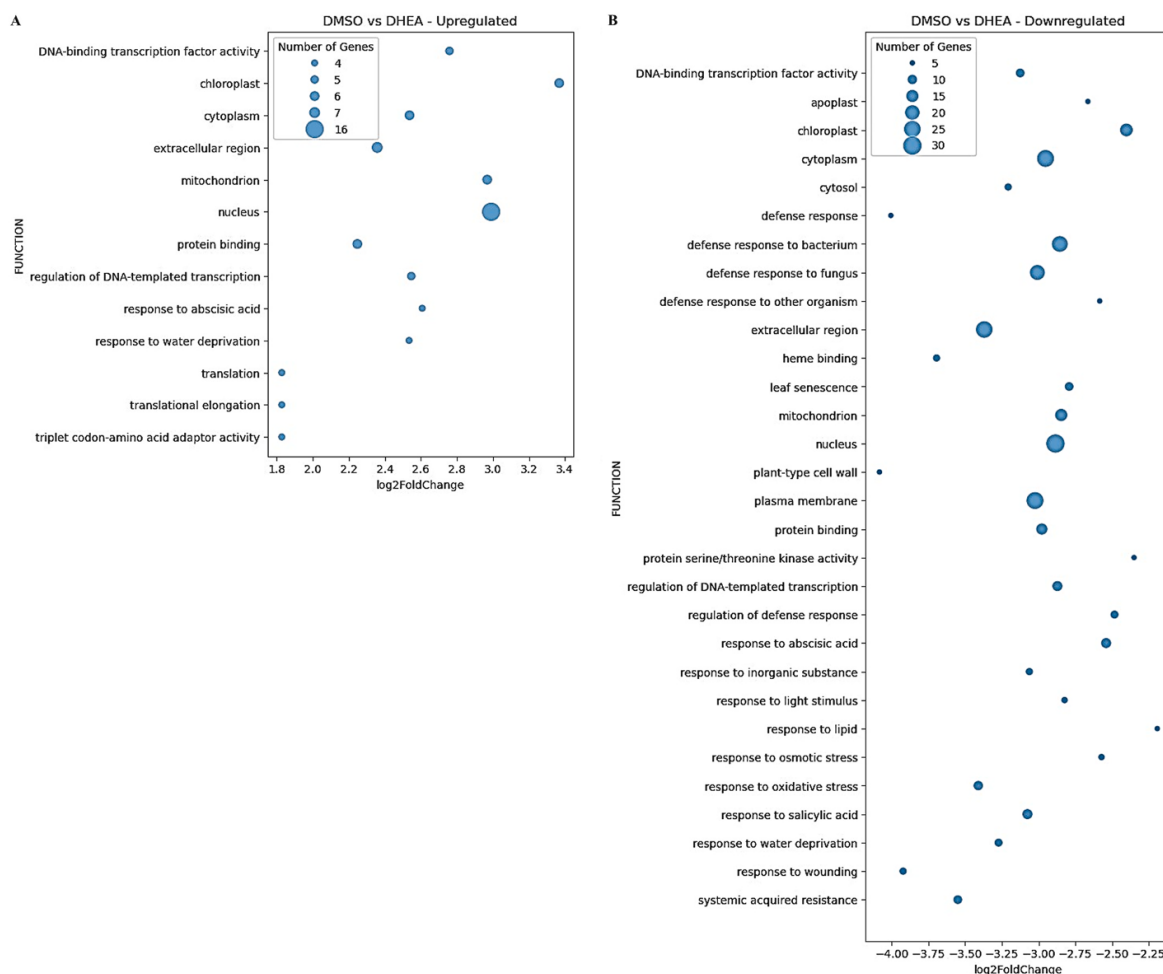


**Fig. 6.** Effects of DHEA on gene expression of *A. thaliana* 1 h after treatment. The graph summarizes genes changed by DHEA treatment. The function-association of significantly changed transcripts ( $p < 0.05$ ) is based on TAIR database. The graph shows the number of changed transcripts associated with a particular function.

accumulates in DMSO treated plants. While we have a peak in *S. polyrhiza* after 3 h, there is a constant, but not statistically significant increase in *A. thaliana*. An increase in SA could not be seen in DHEA treated *Arabidopsis* shoots, while DHEA-treated *S. polyrhiza* plants accumulated DHEA with a peak 3 h of treatment for *S. polyrhiza*. (Fig. 3).

To determine if SA accumulation as response to DHEA-treatment is *S. polyrhiza*-specific, we analyzed the effects of DHEA on another monocot species (*H. vulgare*), too. We were able to detect a SA accumulation in this species, too. In contrast to *S. polyrhiza* we found a SA peak for *H. vulgare* after 1 h. In summary, the reaction of both monocot species to DHEA is quite complicated and no direct dose-dependency can be detected. We conclude that DHEA activates SA-dependent pathogen response in both analyzed monocot species, but at least at the observed time points, not in *A. thaliana*. If there is a general difference in the effects of DHEA on monocots and dicots must be shown in further experiments.

We could detect effect even in other stress related phytohormones for the analyzed plant species. For *A. thaliana* 10  $\mu$ M DHEA lead to peaks of jasmonate and its conjugate jasmonoyl isoleucine (JA-Ile) (Suppl. Fig. S2), In *H. vulgare* 3  $\mu$ M DHEA lead to a peak of cis-OPDA levels (a

bioactive JA precursor). Treating this monocot species with 10  $\mu$ M DHEA results in reduced cis-OPDA levels, while a carboxylated JA (COOH-JA) peak was detected (Suppl. Fig. S3). In *S. polyrhiza* 10  $\mu$ M DHEA lead to elevated JA levels and a reduction of hydroxylated JA-Ile conjugates (OH-Ja-Ile; Suppl. Fig. S4). We conclude that DHEA leads to changes of stress hormone reaction for all analyzed plant species.

Moreover, we recognized a strong effect of DHEA-supplemented MS-medium on the root growth of *A. thaliana* (Fig. 4). Root growth was significantly reduced dose-dependently when 10  $\mu$ M DHEA or higher concentrations were found in MS-medium. For 20 and 30  $\mu$ M DHEA, reduced shoot growth and the formation of anthocyanins could be detected. It is unclear if this is caused by DHEA transport into the shoot material or starvation of the shoot material caused by limited root development. Additionally, 3  $\mu$ M DHEA lead to slightly thicker roots, but the effect was not statistically significant.

To get first insights into the mode of action of DHEA in plants, we realized an RNAseq experiment. 9-days-old *A. thaliana* plants on PNM were infected with *A. brassicicola* and harvest after 24 h (Fig. 5), or treated for 1 h with DHEA (in 0.12% DMSO), while 0.12% DMSO was used as a mock-treatment (Fig. 6). Moreover, 9-day-old *A. thaliana*

# Is Dehydroepiandrosterone Excretion a Defense Mechanism of Plants Affecting Ergosterol Biosynthesis of *Alternaria brassicicola*?

C. Oktay et al.

Plant Physiology and Biochemistry 221 (2025) 109570

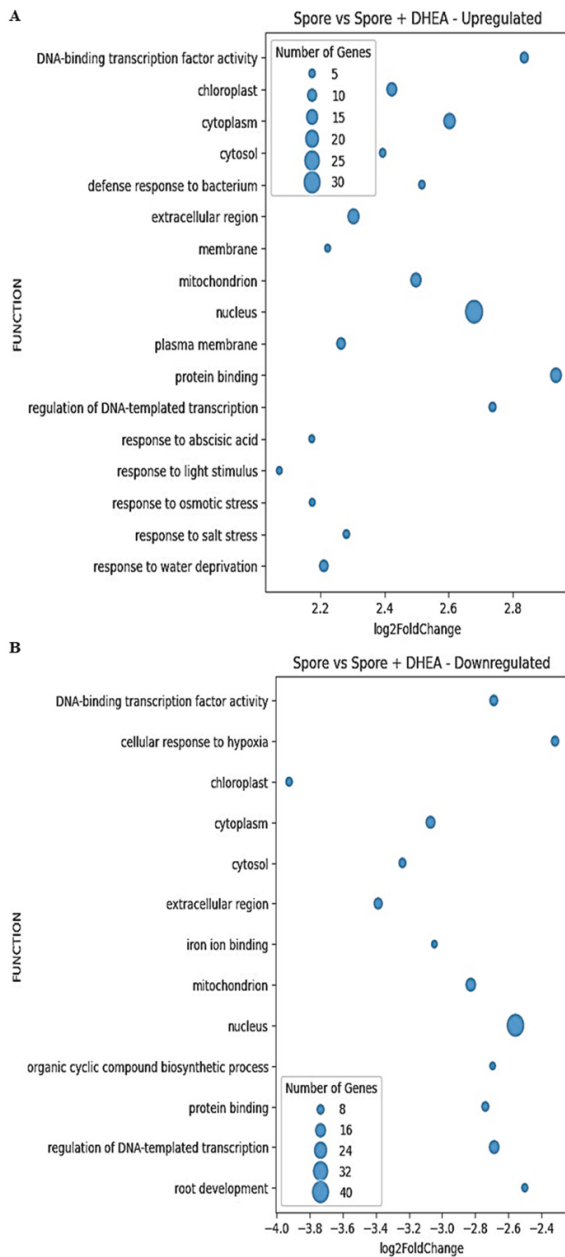


**Fig. 7. Effects of DHEA on gene expression of infected *A. thaliana* plants one day post infection.** The graph summarizes genes changed by infection with DHEA-supplemented *A. brassicicola* spores compared to a non-treated infection. The function-association of significantly changed transcripts ( $p < 0.05$ ) is based on TAIR database. The graph shows the number of changed transcripts associated with a particular function.

plants were infected with an *A. brassicicola* spore solution (spores in 0.12% DMSO) or a spore solution supplemented with 10  $\mu$ M DHEA. Shoots of infected plants were harvested 24 h after infection and immediately shock-frozen (Fig. 7).

To ensure the trustworthiness of our RNAseq data, we compared the normalized Count Reads of PR1 obtained by RNAseq and the CT values

of PR1 obtained by qPCR, as well as the calculated Log2 fold changes (RNAseq) and relative expression (qPCR). Results can be found in the supplement (Table S5).

As assumed, infected and non-infected plants showed the biggest difference (DEGs can be found in Suppl. Table 10). 24 h after infection led to significant ( $p < 0.05$ ) upregulation of 777 genes ( $\log_2$ FoldChange  $> 1.5$ ) and downregulation of 1677 genes ( $\log_2$ FoldChange  $< -1.5$ ; Fig. 5). (MA plots can be found in the supplement; Suppl. Fig. S5). This includes an upregulation of genes regulating abiotic stress responses. *A. brassicicola* is a necrotrophic fungus. It is not surprising that *A. brassicicola* infection induces primarily jasmonic acid induced responses (jasmonic acid mediated signaling pathway is not inducing programmed cell death), while elements of the SA mediated signaling are downregulated (SA-mediated systemic acquired resistance leads to programmed cell death). It was described previously, that JA drives defense response against *Alternaria* (exemplarily in apple leaves; Zhang et al., 2023). The suppression of certain parts of the stress response can be explained by the mutual exclusivity of the JA and SA signaling pathways (Caarls et al., 2015; Le Phuong et al., 2020), or by the restriction of specific defense responses (e.g., camalexin biosynthesis; Schuegger et al., 2007) to the site of infection. Additionally, the activity of *A. brassicicola* effectors may interfere with the expression of defense-related genes as it was shown for other phytopathogenic ascomycota (see here exemplarily for *Ustilagoidea viresns*-infections of rice; Fan et al., 2019).

Moreover, we could detect changes of transcripts of the plant metabolism. This includes many loci associated with oxidative stress, which is indicating the typical oxidative-burst of the fungal infection (Kámán-Tóth et al., 2019). Additionally, reprogramming of phenylpropanoid biosynthetic pathway involving lignin, hydroxycinnamic acids, scopoletin, anthocyanin genes was detected in *A. thaliana* after infection with *Alternaria brassicae* (Hamsa et al., 2024). Together with our data this indicates a strong change of the plant metabolism in response to infection.

Compared to *A. brassicicola*-infection DHEA-treatment results only in small differences within the *A. thaliana* transcriptome. Nevertheless, 1 h DHEA treatment led to significant ( $p < 0.05$ ) upregulation of 62 genes ( $\log_2$ FoldChange  $> 1.5$ ) and downregulation of 137 genes ( $\log_2$ FoldChange  $< -1.5$ ; Fig. 6). Infection of *A. thaliana* with a DHEA-containing spore solution led to the significant upregulation of 30 genes, while 35 genes were downregulated compared to mock infection (Fig. 7). Many of the downregulated genes are either directly or indirectly involved in defense and immune responses (58 of the 137 genes are described in TAIR to be involved in (a)biotic stress responses), code for channels or transporters (6 genes), enzymes required for cell wall synthesis or modifications (5 genes), control root (hair) growth (5 genes), repressors of growth and development (3 genes), auxin metabolism and GH3-mediated auxin conjugation (5 genes), enzymes involved in secondary defense metabolite biosynthesis (10 genes), redox regulation (8 genes),  $Ca^{2+}$  signaling and ubiquitination (2 genes each). This suggests that exogenously applied DHEA represses defense and stress responses as well as root (hair) growth. This could explain the detected changes of DHEA-treated *A. thaliana* roots. Genes which are upregulated by DHEA promote translation and amino acid metabolism (7 genes), transcription (5 genes), developmental processes including flower development (3 genes), lipid metabolism (2 genes), growth via auxin and gibberelin functions (2 genes), ubiquitination (3 genes), maintain cellular homeostasis and prevent cell death (1 gene). Therefore, up-regulated genes predominantly involved in processes promoting development and cellular functions. We therefore presume that exogenous DHEA shifts the balance between the antagonistic principles of stress response and growth towards growth. Moreover, we observed that a high percentage of DHEA-regulated genes were located in cell membranes (24% of the upregulated and 35% of the downregulated genes). A complete list of differential gene expression (DGE) between DHEA-treated and mock-treated *A. thaliana* shoots can be found in the supplement (Suppl.

# Is Dehydroepiandrosterone Excretion a Defense Mechanism of Plants Affecting Ergosterol Biosynthesis of *Alternaria brassicicola*?

C. Oktay et al.

Plant Physiology and Biochemistry 221 (2025) 109570

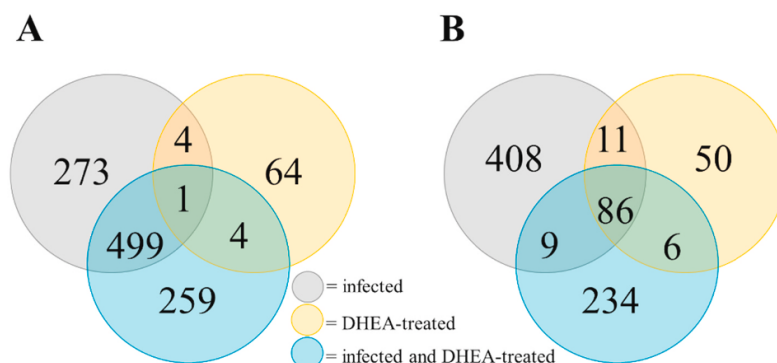


**Fig. 8. Transcriptome changes by infection, DHEA-treatment, and both.** We here show a Venn diagram that shows the numbers of genes differently expressed by infection, DHEA-treatment, and both infection and DHEA-treatment. We could show that all this conditions lead to a strong change of the transcriptomes. While the upregulated genes are comparable different (only one gene shared by all 3 conditions), a bigger set of shared genes is downregulated (78).

Table S11). Also infected plants treated with DHEA showed a strong change of membrane-associated genes (24% of the upregulated and 34% of the downregulated genes are localized in membranes). Interestingly, both treatments lead only to a minimal change of proteins annotated as cytosolic protein. A complete DGE list of transcripts differing between infected and infected and DHEA-treated *A. thaliana* shoots can be found in the supplement (Suppl. Table S12).

It was demonstrated previously that DHEA enhanced the permeability of mitochondria in human TM-3 cells (Shen et al., 2012; Liu et al., 2016). This could explain the changed mRNA values of membrane-localized proteins and the enhanced expression of genes associated with water deprivation detected in both plants treated with DHEA and infected + DHEA-treated (Fig. 6; Fig. 7).

Comparing the transcriptomes of plants infected with a DHEA-containing spore solution to uninfected control (MA plot can be found in Suppl. Fig. 5C) leads to the following results: 24 h infection led to significant ( $p < 0.05$ ) upregulation of 763 genes ( $\log_2\text{FoldChange} > 1.5$ ) and downregulation of 1498 genes ( $\log_2\text{FoldChange} < -1.5$ ; Fig. 5). If we compare genes infected plants and plants infected with DHEA-containing spore solution (MA plot can be found in Suppl. Fig. 5D), we can see that many genes which were transcribed in an enhanced manner (Fig. 7A) were somehow defense associated (defense response to bacteria, response to abscisic acid, response to osmotic stress, response to salt stress and response to water deprivation) and associated with changes in the membrane (membrane and plasma membrane). Portions are comparable to those found for DHEA-treated plants compared to the mock-treated control. Moreover, a lot of genes associated with cell organelles were changed (chloroplast, cytoplasm, cytosol, mitochondrion, nucleus). Considering that all organelles are cell compartments built by membranes, we see this as additional hint that DHEA changes membrane characteristics. It must be mentioned that even a lot of organelle-associated genes were downregulated (Fig. 7B).

All in all, we could detect that all 3 tested conditions (infected, DHEA-treated, and infected + DHEA-treated) lead to partially comparable changes of the *A. thaliana* transcriptome. It was analyzed which amount of the transcriptional changes was shared by all conditions. A Venn diagram can be found in Fig. 8. Nearly no common pattern could be identified in the upregulated genes. Only transcripts of locus At2g21910 were found at elevated levels in all conditions (Suppl. Table S13). At2g21910 encodes the P450-enzyme CYP96A5. P450 enzymes are monooxygenases many of them are involved in steroid metabolism (exemplarily: human CYP11A1; Schiffer et al., 2016; human CYP17A1; Neunzig et al., 2014; plant CYP87A4; Carroll et al., 2023). Considering that all conditions show higher DHEA concentrations, compared to the control, it can be discussed if CYP96A5 is involved in the steroid metabolism of *A. thaliana*. Unfortunately, the enzymatic

machinery of steroid metabolism in plants is poorly understood. Nevertheless, a protein blast against animalia ([https://blast.ncbi.nlm.nih.gov/Blast.cgi?PROGRAM=blastp&PAGE\\_TYPE=BlastSearch&LINK\\_LOC=blasthome](https://blast.ncbi.nlm.nih.gov/Blast.cgi?PROGRAM=blastp&PAGE_TYPE=BlastSearch&LINK_LOC=blasthome) [December 18, 2024]) shows the ultra-long-chain fatty acid omega-hydroxylase-like of *Ostrea edulis* and *Mercenaria*, as well as the cholesterol 24-hydroxylase-like of *Poecilia latipinna*, *Poecilia formosa*, *Scleropages formosus*, *Poecilopsis prolifica*, within the first results. Nevertheless, the hypothesis that CYP96A5 is involved in plant steroid metabolism has to be challenged in further experiments.

More common genes can be found that are downregulated (Fig. 8). From the 86 genes found downregulated (Suppl. Table S13) in all conditions around 10% are associated with the regulation of the defense response (At1g14880, At1g19250, At1g33960, At2g14560, At3g57260, At4g12500, At5g40990, At5g44420, At5g45090, At5g64810). Additionally, nearly 10% of the DEGs are involved in regulating oxygen-dependent reactions (At1g53620, At1g60740, At1g60750, At1g69880, At3g28580, At4g15330). We explain this with membrane disturbances caused by fungal infection or DHEA. In line with this hypothesis, around 10% of all genes downregulated in all conditions are membrane-/transport-associated (At1g12940, At1g21245, At1g74080, At2g29350, At3g28510, At5g41390).

Based on RNAseq experiments, we built the hypothesis that DHEA disturbs the integrity of plasma membranes in *A. thaliana* and *A. brassicicola*. This hypothesis is supported by the fact, that 12 plasma membrane-associated genes were downregulated in DHEA-treated *A. thaliana* shoots. It has to be mentioned, that we can't rule out that DHEA affects other membranes of plant cells, too. To analyze the effects of DHEA on membrane-integrity of *A. thaliana*, we treated roots of a transgenic *A. thaliana* line expressing the cytosolic apoaequorin from *A. victoria* (Polisensky and Braam, 1996) in 30  $\mu\text{M}$  DHEA using DMSO as mock treatment. After 24 h we used an aequorin-based assay to analyze the intracellular  $\text{Ca}^{2+}$  accumulation in response to hydrogen peroxide treatment. We expected that reduced membrane integrity will induce at least partial, membrane depolarization. This should lead to disturbed  $\text{Ca}^{2+}$  elevation into the cytosol. In line with this hypothesis we could detect significantly reduced  $\text{Ca}^{2+}$  peaks in *A. thaliana* roots pre-treated with DHEA compared to the mock-treatment (Fig. 9). A strong difference was also seen for DHEA-treated shoots compared to the water control, but this difference was also detected in DMSO controls. Nevertheless, we see these results as additional proof of reliability of RNAseq data.

Enhanced membrane-permeability could also explain the observed changes in ABA and SA regulated genes (Fig. 6), while no changes in SA and ABA concentrations were detectable in *A. thaliana* (Fig. 5). ABA and SA are transported in protonated form to their target, where they will be

# Is Dehydroepiandrosterone Excretion a Defense Mechanism of Plants Affecting Ergosterol Biosynthesis of *Alternaria brassicicola*?

C. Oktay et al.

Plant Physiology and Biochemistry 221 (2025) 109570

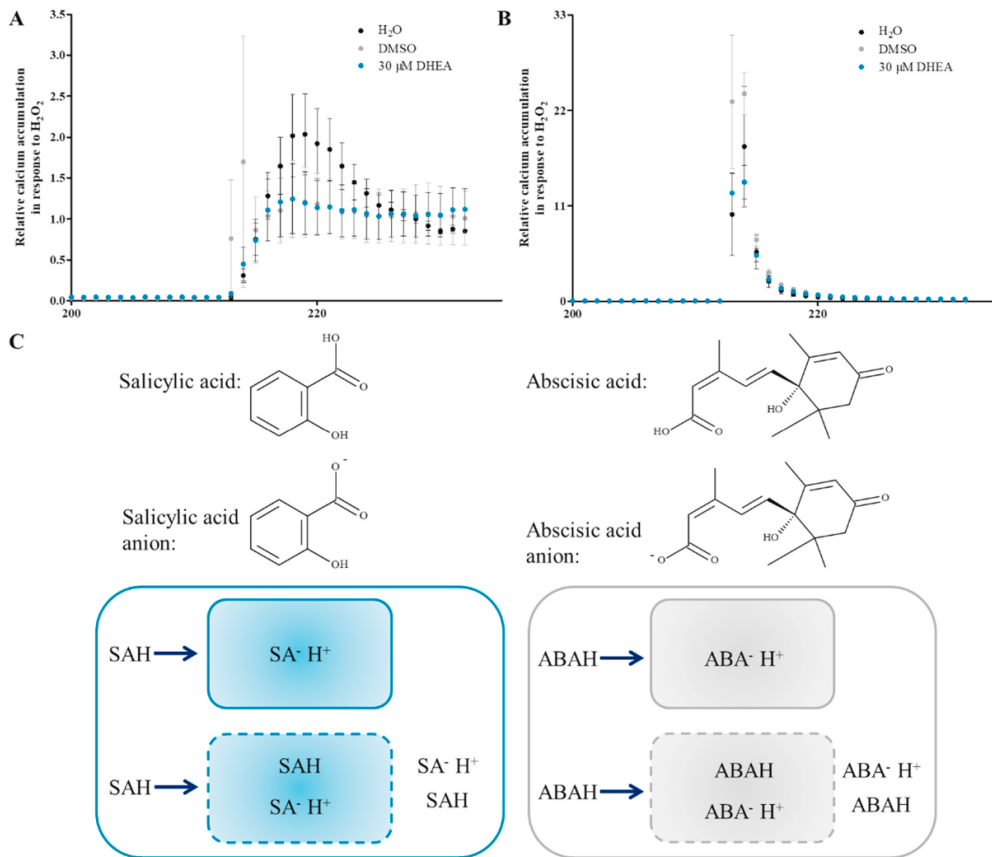


**Fig. 9. Calcium-accumulation in *A. thaliana* roots pretreated with DHEA in response to  $H_2O_2$ .** Shoots (A) and roots (B) of *A. thaliana* were pretreated with 30  $\mu M$  DHEA while  $H_2O$  and DMSO were used as mock-treatments. Bioluminescence counts (BIC) in *Arabidopsis* from roots were recorded as  $RLU\ sec^{-1}$  in 5 s intervals for 20 min using a microplate luminometer. After a 1-min background reading, 40 mM  $H_2O_2$  was added manually to the well and readings in RLU were taken for 20 min. The graph depicts the luminescence peak measured 16.83 min after the treatment. All data are given as mean  $\pm$  SEM (n control = 6; n DHEA = 8). The difference between the peak values was analyzed using a t-test; indicating a statistically significant difference for  $Ca^{2+}$  accumulation in the roots ( $p = 0.0057$ ), but no statistically difference between DMSO and DHEA in the shoot. (C) Abscisic and salicylic acid are transported in protonated forms to their targets. As weak acids, both hormones can diffuse bio-membranes passively. The pH values of the cytosol will lead to conversion into anionic forms of both phytohormones. Anionic forms of abscisic and salicylic acid cannot cross plasma membranes. This results in the expression of abscisic and salicylic acid-regulated genes. In cases of enhanced membrane permeability, deprotonated forms of salicylic and abscisic acid could leave the cytosol, which results in reduced expression of abscisic or salicylic acid-regulated genes.

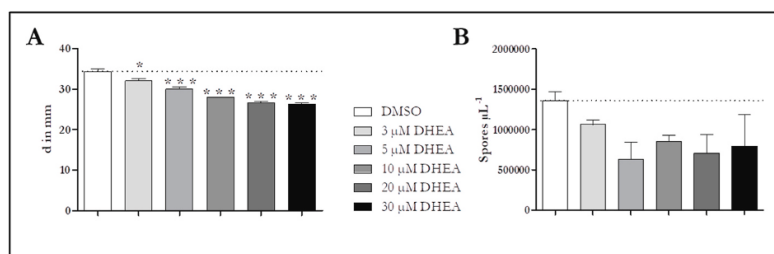


**Fig. 10. Effects of DHEA on *A. brassicicola*.** A plug of well-grown *A. brassicicola* tissue (diameter = 5 mm; a) or a solution of *A. brassicicola* spores was transferred to PDA medium containing different concentrations of DHEA or DMSO as control. The size of the *A. brassicicola* colony (A) or the number of spores produced by these colonies (B) were analyzed after 7 days. The graph depicts mean  $\pm$  SEM. Differences were analyzed statistically by a one-way ANOVA with post hoc Bonferroni correction (\* $p < 0.05$ ; \*\*\* $p < 0.001$ ; n = 3).

# Is Dehydroepiandrosterone Excretion a Defense Mechanism of Plants Affecting Ergosterol Biosynthesis of *Alternaria brassicicola*?

C. Oktay et al.

Plant Physiology and Biochemistry 221 (2025) 109570

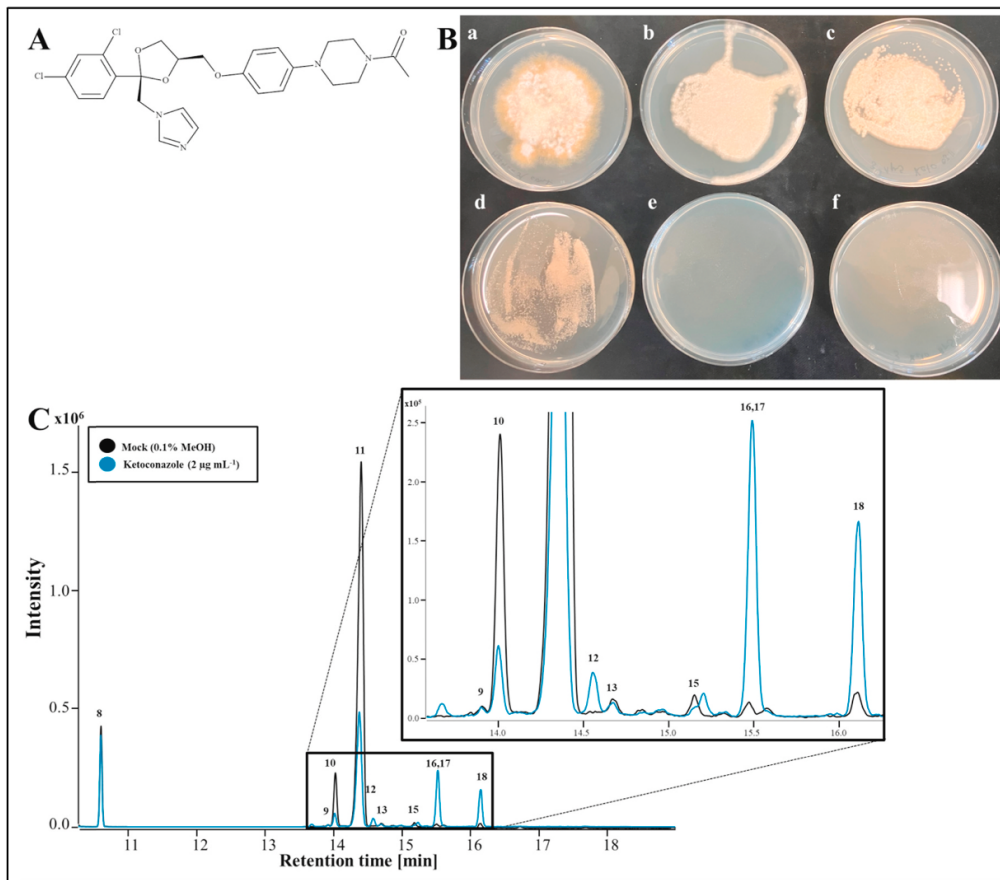


**Fig. 11. Ketoconazole treatment of *Alternaria brassicicola*.** To determine non-lethal concentrations of ketoconazole (KC; A) for *Alternaria brassicicola*, a spore solution was spread on potato-dextrose agar (B) supplemented with methanol (0.1%; solvent of KC; a) or 0.5 (b), 1 (c); 2 (d); 4 (e), and 8 (f)  $\mu\text{g mL}^{-1}$  KC dissolved in methanol. Plates were photographed 72 h after infection. The lethal concentration was found to be between 2 and 4  $\mu\text{g mL}^{-1}$  KC. (C) GC-MS was used to determine ergosterol biosynthesis pattern. The figure depicts the representative selected ion chromatograms ( $m/z$  217 + 251+343 + 363+393 + 407 + 466 + 467 + 469) of detected intermediates of untreated *A. brassicicola* sample (black) and sample confronted with 2  $\mu\text{g mL}^{-1}$  KC (turquoise) after 7 days; internal standard = cholestane (8), ergosta-5,8,22,24(28)-tetraen-3 $\beta$ -ol (9), lichesterol (ergosta-5,8,22-trien-3 $\beta$ -ol, 10), ergosterol (ergosta-5,7,22-trien-3 $\beta$ -ol, 11), 14-methylfecosterol (14-methylergosta-8,24(28)-dien-3 $\beta$ -ol, 12), ergosta-5,7,22,24(28)-tetraen-3 $\beta$ -ol (13), episterol (ergosta-7,24(28)-dien-3 $\beta$ -ol, 15), 14-methylergosta-8,24(28)-dien-3 $\beta$ ,6 $\alpha$ -diol (16), lanosterol (4,4,14-trimethylcholesta-8,24-dien-3 $\beta$ -ol, 17), eburicol (4,4,14-trimethylergosta-8,24(28)-dien-3 $\beta$ -ol, 18).

deprotonated. Anions of ABA and SA cannot cross plasma membranes. Consequently, ABA and SA accumulate in their target cells, where they induce the expression of SA- or ABA-related genes (Rocher et al., 2006; Rocher et al., 2009). In DHEA-treated plants, the intercellular transport mechanism of ABA and SA is strongly disturbed, and anions of SA and ABA can also leave the cytosol, which results in reduced expression of ABA or SA inducible genes. Moreover, enhanced bio-membrane permeability hampers the maintenance of the pH value needed for ABA and SA deprotonation. In summary, this leads to a dysfunctional intercellular transport of ABA and SA, resulting in decreased expression of SA or ABA related genes without reduced SA levels in the plant matrix. Moreover, this membrane disturbance can also explain why DHEA-treated *A. thaliana* shoots show lower SA levels after 3 h of treatment compared to the mock-treated control (Fig. 3A).

### 3.3. Effects of DHEA on *A. brassicicola*

Considering that elevated DHEA values were detected in response to fungal infections in infected *A. thaliana* shoots (Fig. 2B), we asked the

question: Has DHEA an effect on fungal pathogens?

We used the economically relevant *A. brassicicola* as our model system to analyze this question. Cvelbar and colleagues (Cvelbar et al., 2013) showed that DHEA has the most substantial growth-inhibiting effects of all tested progestogens and androgens on the analyzed ascomycetous fungi (*Hortaea werneckii*, *Saccharomyces cerevisiae*, and *Aspergillus oryzae*) followed by the androgens testosterone and androstenedione. Therefore, we analyzed if DHEA treatment can reduce the growth and spore production of *A. brassicicola* (Fig. 10).

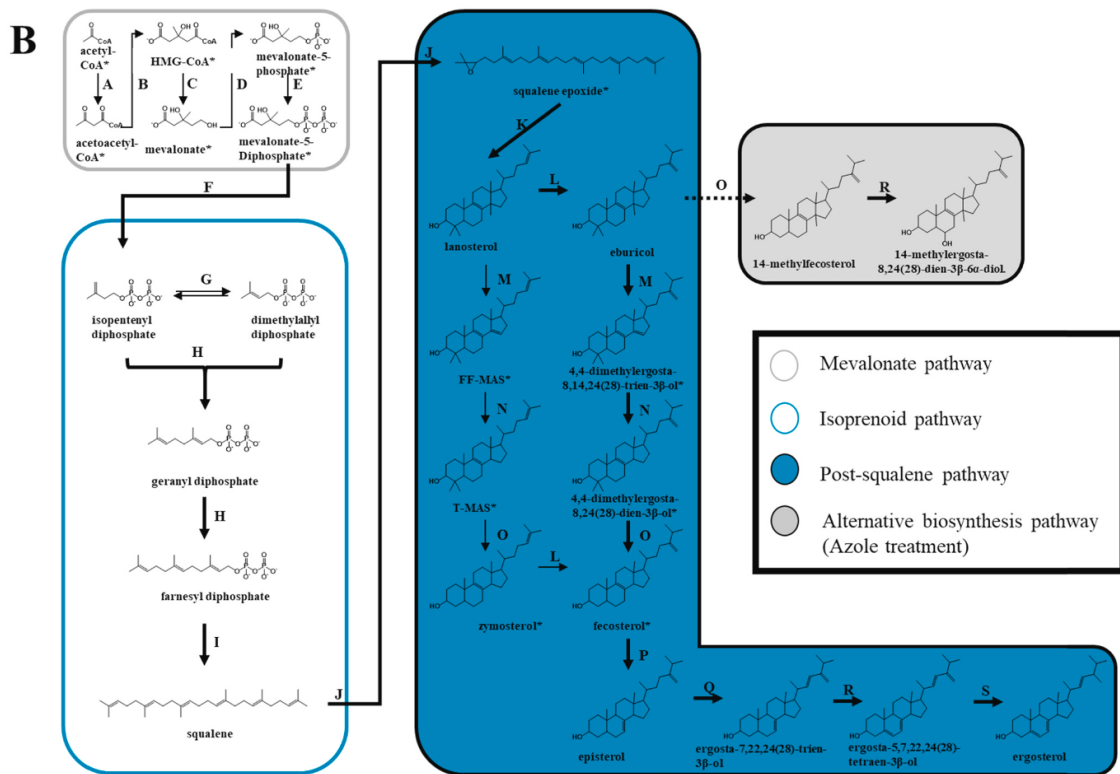
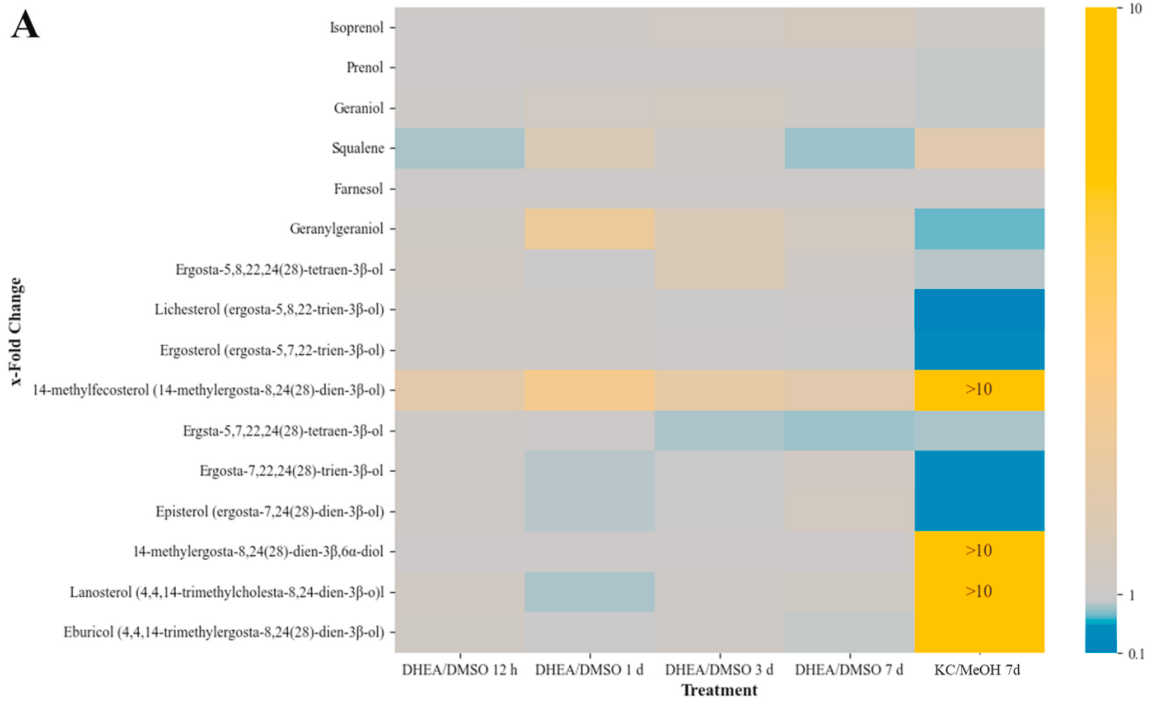
We could show that DHEA reduces the growth and spore production of *A. brassicicola* in a dose-dependent manner (Fig. 10). This could be seen already for 3  $\mu\text{M}$  DHEA. In contrast to changes in growth rates, changes in spore production are not statistically significant.

Cvelbar and colleagues (Cvelbar et al., 2013) assumed that reduced growth of ascomycetous fungi is caused by disturbed ergosterol biosynthesis. Ergosterol is the major sterol of fungal cell membranes (Zinser et al., 1993; Suchodolski et al., 2019) of nearly all fungi (Weete et al., 2010). Moreover, ergosterol is a transitory cell wall component, on its way to the extracellular environment, or it plays a role, for

# Is Dehydroepiandrosterone Excretion a Defense Mechanism of Plants Affecting Ergosterol Biosynthesis of *Alternaria brassicicola*?

C. Oktay et al.

Plant Physiology and Biochemistry 221 (2025) 109570



(caption on next page)

# Is Dehydroepiandrosterone Excretion a Defense Mechanism of Plants Affecting Ergosterol Biosynthesis of *Alternaria brassicicola*?

C. Oktay et al.

Plant Physiology and Biochemistry 221 (2025) 109570

**Fig. 12. Heatmap of intermediates of the isoprenoid and post-lanosterol pathway of ergosterol biosynthesis of *A. brassicicola* samples confronted with dehydroepiandrosterone (10  $\mu$ M; DHEA) or ketoconazole (2  $\mu$ g mL<sup>-1</sup>; KC) compared to mock-treated controls (DMSO or MeOH) and the identified favored ergosterol pathway of *A. brassicicola*.** (A) Isoprenoid pyrophosphates were analyzed by GC-MS as their corresponding isoprenoid *tert*-butyldiphenylsilyl ether by GC-MS after enzymatic pyrophosphate cleavage to the free isoprenoid and subsequent derivatization with *tert*-butyldiphenylchlorosilane. The relative amount has been normalized to untreated samples (Gsaller et al., 2016; Krauß et al., 2021). Boxes in yellow color >10-fold changes, in grey color no changes were observed (change = 1), and in blue color <0.1-fold changes. (B) Here we show the putative ergosterol biosynthesis pathway of *A. brassicicola*; this schematic ergosterol biosynthesis covers not all detected intermediates from the table in the supplement (Table S09); **Metabolites:** acetyl-coenzyme A, acetoacetyl-coenzyme A,  $\beta$ -hydroxy  $\beta$ -methylglutaryl-coenzyme A (HMG-CoA), mevalonate, mevalonate-5-phosphate, mevalonate-5-diphosphate, isopentenyl diphosphate, dimethylallyl diphosphate, geranyl diphosphate, farnesyl diphosphate, squalene, squalene epoxide, lanosterol (4,4,14-trimethylcholesta-8,24-dien-3 $\beta$ -ol), eburicol (4,4,14-trimethylergosta-8,24(28)-dien-3 $\beta$ -ol), FF-MAS (4,4-dimethylcholesta-8,14,24-trien-3 $\beta$ -ol), 4,4-dimethylergosta-8,14,24(28)-trien-3 $\beta$ -ol, T-MAS (4,4-dimethylcholesta-8,24-dien-3 $\beta$ -ol), 4,4-dimethylergosta-8,24(28)-dien-3 $\beta$ -ol, zymosterol (cholesta-8,24-dien-3 $\beta$ -ol), fecosterol (ergosta-8,24(28)-dien-3 $\beta$ -ol), episterol (ergosta-7,24(28)-dien-3 $\beta$ -ol), ergosta-7,22,24(28)-trien-3 $\beta$ -ol, ergosta-5,7,22,24(28)-tetraen-3 $\beta$ -ol, ergosterol (ergosta-5,7,22-trien-3 $\beta$ -ol), 14-methylfecosterol (14-methyl-ergosta-8,24(28)-dien-3 $\beta$ -ol), 14-methylergosta-8,24(28)-dien-3 $\beta$ ,6 $\alpha$ -diol; **Enzymes:** acetyl-coenzyme A-acetyltransferase (ACAT, A),  $\beta$ -hydroxy  $\beta$ -methylglutaryl-coenzyme A synthase (HMG-CoA synthase, B),  $\beta$ -hydroxy  $\beta$ -methylglutaryl-coenzyme A reductase (HMG-CoA reductase, C), mevalonate kinase (D), phosphomevalonate kinase (E), diphosphomevalonate decarboxylase (F), isopentenyl diphosphate isomerase (G), farnesyl diphosphate synthase (H), squalene synthase (I), squalene epoxidase (J), oxidosqualene cyclase (OSC, K), sterol C24-methyltransferase (24-SMT, L), sterol C14-demethylase (M), sterol C14-reductase (N), sterol C4-demethylase complex (O), sterol C8-isomerase (P), sterol C22-desaturase (Q), sterol C5-desaturase (R), sterol C24-reductase (S). \* not detected intermediates or not part of the analysis (mevalonate pathway). (For interpretation of the references to color in this figure legend, the reader is referred to the Web version of this article.)

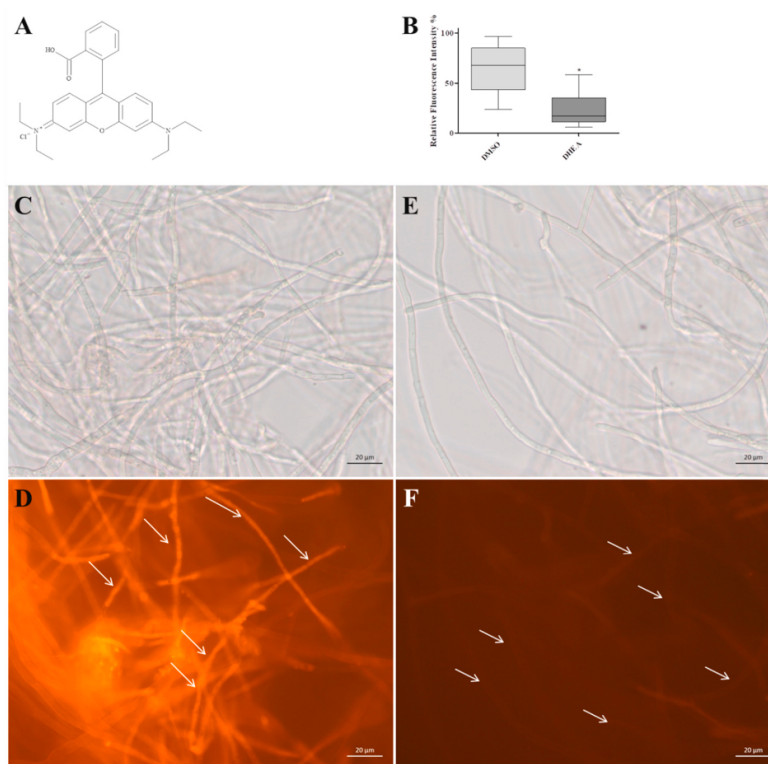


**Fig. 13. Rhodamine B-based assay for membrane integrity of *A. brassicicola*.** Rhodamine B (A) is a fluorescence dye was used to detect depolarization and de-energization of mitochondria pretreated with 30  $\mu$ M DHEA or mock-treated with DMSO for 24 h. Relative fluorescence intensity (RFI) was calculated using the highest fluorescence value of each experiment as reference (in all cases a value of the DMSO-treated control). The results are given as mean  $\pm$  SEM (n = 78; statistical analysis with *t*-Test;  $P < 0.001$ ). Microscopic inspections of mock-treated hyphae (C and D) and DHEA-treated hyphae (E and F) are depicted. For comparison bright-field images (C and E) are shown as well as fluorescence images by the use of DsRED filter (D and F). High fluorescence (D) or no fluorescent hyphae (F) are indicated by white arrows.

instance, in the formation of cell wall carbohydrate patches. Particularly, eburicol seems to play a prominent role in this latter process (Geißel et al., 2018; Elsamani et al., 2024). That is why the mode of action of many commercially available fungicides (e.g., KC used in the treatment of fungal infections of human cutis or mucus; Poojary, 2017; or fungicides used in agriculture e.g., chiral triazole fungicides like

prothioconazole; Zhang et al., 2019) is inhibition of ergosterol biosynthesis (Müller et al., 2013; reviewed in: Campoy and Adrio, 2017).

Ergosterol can be produced in an eburicol-dependent or an eburicol-independent pathway (Hosseini et al., 2024). These pathways differ in the preferred substrate of the involved sterol C14-demethylase (lanosterol or eburicol). Fungal sterol C14-demethylases can be inhibited by

# Is Dehydroepiandrosterone Excretion a Defense Mechanism of Plants Affecting Ergosterol Biosynthesis of *Alternaria brassicicola*?

C. Oktay et al.

Plant Physiology and Biochemistry 221 (2025) 109570

azole fungicides (e.g., KC; Venkateswarlu and Kelly, 1996). We analyzed which concentration of KC is lethal for *A. brassicicola* (Fig. 11B). We determined the preferred pathway of ergosterol biosynthesis in *A. brassicicola* to analyze the effects of DHEA on ergosterol biosynthesis. This was done by analyzing ergosterol pattern of *A. brassicicola* in presence of KC compared to mock-treated controls, as shown before (Müller et al., 2018).

Therefore, the highest non-lethal concentration of KC ( $2 \mu\text{g mL}^{-1}$  in our experiments) was used to treat *A. brassicicola* for 7 days. These tissues (hyphae and spores) of *A. brassicicola* were used to analyze sterol patterns.

We could show that eburicol accumulates after KC treatment by factor 9 ( $50 \text{ ng mg}^{-1}$  in the control and  $450 \text{ ng mg}^{-1}$  in KC treatment; Fig. 11), while lanosterol is enhanced by factor 10 ( $25 \text{ ng mg}^{-1}$  in the control and  $280 \text{ ng mg}^{-1}$  in KC treatment; Fig. 11). Therefore, we assume that the sterol C14-demethylase of *A. brassicicola* is not very substrate-specific but a substrate-promiscuous enzyme. Keeping in mind that lanosterol is a precursor of eburicol in eburicol-dependent ergosterol biosynthesis, we assume that the eburicol-dependent ergosterol pathway is preferred in *A. brassicicola*. A predicted pathway for ergosterol biosynthesis in *A. brassicicola* can be found in Fig. 12. The determined sterol pattern of *A. brassicicola* can be used to analyze next-level fungicides against the agricultural important *Alternaria* species.

*A. brassicicola* were cultivated in liquid PDA for 0.5 d (12 h), 1 d, 3 d, and 7 d confronted with  $10 \mu\text{M}$  DHEA, while 0.12% DMSO was used as mock-treatment. We analyzed patterns of the mevalonate pathway, the isoprenoid pathway, and the post-squalene pathway (Fig. 12). We were not able to detect a reduction of ergosterol in the DHEA-treated fungus compared to the control, but interestingly 14-methylfecosterol accumulated by factor 3 in the DHEA-treated fungus for all analyzed time point. In contrast KC treated *A. brassicicola* showed 90 times higher concentrations of 14-methylfecosterol. Additionally, we could detect an increase of squalene by factor 2, as well as the accumulation of 14-methylergosta-8,24(28)-dien-3 $\beta$ ,6 $\alpha$ -diol (from levels under detection limit to  $360 \text{ ng mg}^{-1}$  dry weight), lanosterol (factor 10), and eburicol (factor 9). In contrast lichesterol (factor 5), ergosterol (factor 5), ergosta-7,22,24(28)-trien-3 $\beta$ -ol (factor 2), and episterol (factor 2) were found reduced. The highest reduction total ( $4000 \text{ ng mg}^{-1}$ ) was detected for ergosterol in KC treated fungal cells. KC-treatment leads to eburicol accumulation in *A. brassicicola*. This indicates that ergosterol biosynthesis favors the eburicol-dependent pathway in this fungus. Nevertheless, based on these results we suggest that DHEA inhibits the growth of the ascomycetous fungus *A. brassicicola* in an ergosterol-independent way if this is the case for other ascomycetous plant-pathogens (e.g., *Verticillium dahliae*) has to be determined in future experiments.

Fungi and Mammalia are both part of the Opisthokonta group of the eukaryotes. Therefore, the biomembranes of fungi and mammalia are highly similar (Ntow-Boahene et al., 2023). Keeping in mind that DHEA causes enhanced membrane-permeability in human cells (Shen et al., 2012; Liu et al., 2016), we hypothesize that enhanced membrane-leakage can cause the reduced growth of *A. brassicicola* confronted with DHEA. We assume that this is an adaption of the plant metabolism to fungal attack that helps plants fight fungal pathogens.

To get first data ensuring this hypothesis, we performed Rhodamine B staining of *A. brassicicola* liquid cultures treated for 24 h with  $30 \mu\text{M}$  DHEA or control. We observed that Rhodamine B fluorescence of DHEA pretreated hyphae is just 35% of the mock-treated control (Fig. 13). This can be caused by depolarization and de-energization of mitochondria and impaired mitochondrial function, indicating a loss of mitochondrial membrane integrity (Brilhante et al., 2018). Therefore, we assume that membrane-changes are the working principle causing the reduced growth of DHEA-treated *A. brassicicola* hyphae.

Keeping in mind that fungi and animals are both Opisthokonta and comparable near relatives (compared to plants and fungi or animals and plants), we suggest that DHEA primarily interacts with the plasma membrane (Charalampopoulos et al., 2006; Lemcke et al., 2010).

All in all, our data indicate that DHEA is produced by infected plant tissues to fight fungal pathogens by attacking their membrane integrity. This can explain the high distribution of DHEA within the kingdom of plants. We could also show that this steroid enhances the leakage of plant cell membranes, too. Therefore, the accumulation of DHEA is a double-edged sword and its metabolism has to be strictly regulated.

## 4. Conclusion

This study demonstrates that during fungal infection, *Arabidopsis thaliana* accumulates the C<sub>19</sub>-steroid dehydroepiandrosterone (DHEA), a process localized to the infected plant organs. The effects of DHEA exhibit species-specific variations. In monocot species *Hordeum vulgare* and *Spirodela polyrhiza*, DHEA treatment led to increased salicylic acid levels, a response not observed in the dicot plant *A. thaliana*. Interestingly, while DHEA substantially affected root development in *A. thaliana*, this effect was absent in *H. vulgare*. At the transcriptome level, DHEA reduced the expression of membrane-associated genes in *A. thaliana*, indicating potential disruptions in cell and organelle membrane integrity. Moreover, DHEA inhibited the growth and spore production of the phytopathogenic fungus *Alternaria brassicicola*, although its ergosterol content remained unchanged, suggesting that the anti-fungal effect is likely due to disturbed fungal membranes.

## Informed consent statement

Not applicable.

## Institutional review board statement

Not applicable.

## Author contribution

Conceptualization: J.K.; Method development instrumental analytics: C.M., F.F., and J.K.; Investigation: C.O., G.S., M.L, F.F., S.M., K.L.K, H.L, A.A., R.O., M.R., K.O., A.C.U.F., and J.K.; Bioinformatic analysis: E. B., and J.K.; Writing—original draft preparation: C.O., G.S., M.L., K.L.K., R.O., C.M., A.C.U.F., and J.K.; All authors have read and agreed to the published version of the manuscript.

## Funding

This research was funded by IMPULSE<sup>project</sup> (IP2022-13) of Friedrich Schiller University Jena.

## Declaration of competing interest

The authors declare that they have no known competing financial interests or personal relationships that could have appeared to influence the work reported in this paper.

## Acknowledgements

We thank Franz Bracher (Department of Pharmacy, Center for Drug Research, Ludwig-Maximilians-Universität München), Jonathan Gershenzhon (Department for Biochemistry, Max Planck Institute for Chemical Ecology) for providing laboratories and equipment. We thank Klaus-Jürgen Appenroth for the preparation of *Spirodela polyrhiza* clones, Lilo Klein and Petra Sandjohann for the preparation of *Hordeum vulgare* seeds. Thanks are due to Svenja Tauber of research group of bioactive plant products for lyophilizing our plant material. Big thanks to Sandra Scholz for preparing plant cultures and infections. Moreover, we thank Hendrik Huthoff and Julie A. Z. Zedler for helpful advice regarding manuscript editing.

# Is Dehydroepiandrosterone Excretion a Defense Mechanism of Plants Affecting Ergosterol Biosynthesis of *Alternaria brassicicola*?

C. Oktay et al.

Plant Physiology and Biochemistry 221 (2025) 109570

## Appendix A. Supplementary data

Supplementary data to this article can be found online at <https://doi.org/10.1016/j.plaphy.2025.109570>.

## Data availability

Data is contained within the article or the supplement. Raw data of the RNAseq data are available on ncbi (Geo accession ID: GSE261582).

## References

- Al-Askar, A.A., Ghoneem, K.M., Rashad, Y.M., Abdulkhair, W.M., Hafez, E.E., Shabana, Y.M., Baka, Z.A., 2014. Occurrence and distribution of tomato seed-borne mycoflora in Saudi Arabia and its correlation with the climatic variables. *Microb. Biotechnol.* 7, 556–569.
- Appenroth, K.-J., Teller, S., Horn, M., 1996. Photophysiology of turion formation and germination in *Spirodela polyrrhiza*. *Biologia plant* 38.
- Appenroth, K.-J., Sree, K.S., Bog, M., Ecker, J., Seeliger, C., Böhm, V., Lorkowski, S., Sommer, K., Vetter, W., Tolzin-Banasch, K., Kirmse, R., Leiterer, M., Dawczynski, C., Liebisch, G., Jahreis, G., 2018. Nutritional value of the duckweed species of the genus *wolffia* (Lemnaceae) as human food. *Front. Chem.* 6, 483.
- Avery, S.V., Singleton, I., Magan, N., Goldman, G.H., 2019. The fungal threat to global food security. *Fungal Biol.* 123, 555–557.
- Benjamini, Y., Hochberg, Y., 1995. Controlling the false discovery rate: a practical and powerful approach to multiple testing. *J. Roy. Stat. Soc. B* 57, 289–300.
- Berardini, T.Z., Mundodi, S., Reiser, L., Huala, E., Garcia-Hernandez, M., Zhang, P., Mueller, L.A., Yoon, J., Doyle, A., Lander, G., Moseyko, N., Yoo, D., Xu, I., Zoeckler, B., Montoya, M., Miller, N., Weems, D., Rhee, S.Y., 2004. Functional annotation of the *Arabidopsis* genome using controlled vocabularies. *Plant Physiol.* 135, 745–755.
- Botanga, C.J., Bethke, G., Chen, Z., Gallie, D.R., Fiehn, O., Glazebrook, J., 2012. Metabolite profiling of *Arabidopsis* inoculated with *Alternaria brassicicola* reveals that ascorbate reduces disease severity. *Molecular plant-microbe interactions : MPMI (Mol. Plant-Microbe Interact.)* 25, 1628–1638.
- Brilhante, R.S.N., Oliveira, J.S. de, Jesus Evangelista, A.J. de, Pereira, V.S., Alencar, L.P., Castelo-Branco, D.d.S.C.M., Câmara, L.M.C., Lima-Neto, R.G. de, Cordeiro, R.d.A., Sidrim, J.J.C., Rocha, M.F.G., 2018. In vitro effects of promethazine on cell morphology and structure and mitochondrial activity of azole-resistant *Candida tropicalis*. *Med. Mycol.* 56, 1012–1022.
- Caarls, L., Pieterse, C.M.J., van Wees, S.C.M., 2015. How salicylic acid takes transcriptional control over jasmonic acid signaling. *Front. Plant Sci.* 6, 170.
- Camehl, I., Drzewiecki, C., Vadassery, J., Shahollari, B., Sherameti, I., Forzani, C., Munnik, T., Hirt, H., Oelmüller, R., 2011. The OXII kinase pathway mediates *Piriformospora indica*-induced growth promotion in *Arabidopsis*. *PLoS Pathog.* 7, e1002051.
- Campoy, S., Adrio, J.L., 2017. Antifungals. *Biochem. Pharmacol.* 133, 86–96.
- Carroll, E., Ravi Gopal, B., Raghavan, L., Mukherjee, M., Wang, Z.Q., 2023. A cytochrome P450 CYP87A4 imparts sterol side-chain cleavage in digoxin biosynthesis. *Nat. Commun.* 14, 4042.
- Charalampopoulos, I., Alexaki, V.-I., Lazaridis, I., Dermitzaki, E., Avlonitis, N., Tsatsanis, C., Calogeropoulou, T., Margioris, A.N., Castanas, E., Gravanis, A., 2006. G protein-associated, specific membrane binding sites mediate the neuroprotective effect of dehydroepiandrosterone. *FASEB journal : official publication of the Federation of American Societies for Experimental Biology* 20, 577–579.
- Chen, S., Zhou, Y., Chen, Y., Gu, J., 2018. fastp: an ultra-fast all-in-one FASTQ preprocessor. *Bioinformatics* 34, i884–i890.
- Chomczynski, P., 1993. A reagent for the single-step simultaneous isolation of RNA, DNA and proteins from cell and tissue samples. *Biotechniques* 15 (532–4), 536–537.
- Cvelbar, D., Zist, V., Kobal, K., Zigon, D., Zakelj-Mavric, M., 2013. Steroid toxicity and detoxification in ascomycetous fungi. *Chem. Biol. Interact.* 202, 243–258.
- Dobynya, D.V., Egorova, O.V., Donova, M.V., 2010. Microbial side-chain degradation of ergosterol and its 3-substituted derivatives: a new route for obtaining of deltaoids. *Steroids* 75, 653–658.
- Elsaman, H., Golubtsov, E., Brazil, S., Ng, N., Klugherz, L., Martin, R., Dichtl, K., Müller, C., Wagener, J., 2024. Toxic eburicol accumulation drives the antifungal activity of azoles against *Aspergillus fumigatus*. *Nat. Commun.* 15, 6312.
- Fan, J., Du, N., Li, L., Li, G.-B., Wang, Y.-Q., Zhou, Y.-F., Hu, X.-H., Liu, J., Zhao, J.-Q., Li, Y., Huang, F., Wang, W.-M., 2019. A core effector UV1261 promotes *Ustilagoidea vires* infection via spatiotemporally suppressing plant defense. *Phytopathology Research* 1.
- Fernández-Ortuño, D., Torés, J.A., Vicente, A. de, Pérez-García, A., 2008. Field resistance to QoI fungicides in *Podosphaera fusca* is not supported by typical mutations in the mitochondrial cytochrome b gene. *Pest Manag. Sci.* 64, 694–702.
- Geißel, B., Loiko, V., Klugherz, L., Zhu, Z., Wagener, N., Kurzai, O., van den Hondel, C.A. M.J.J., Wagener, J., 2018. Azole-induced cell wall carbohydrate patches kill *Aspergillus fumigatus*. *Nat. Commun.* 9, 3098.
- Genisel, M., Turk, H., Erdal, S., 2013. Exogenous progesterone application protects chickpea seedlings against chilling-induced oxidative stress. *Acta Physiol. Plant.* 35, 241–251.
- Grigolli, J.F.J., Kubota, M.M., Alves, D.P., Rodrigues, G.B., Cardoso, C.R., Da Silva, D.J. H., Mizubuti, E.S.G., 2011. Characterization of tomato accessions for resistance to early blight. *Crop Breed. Appl. Biotechnol.* 11, 174–180.
- Gsaller, F., Hortschansky, P., Furukawa, T., Carr, P.D., Rash, B., Capilla, J., Müller, C., Bracher, F., Bowyer, P., Haas, H., Brakhage, A.A., Bromley, M.J., 2016. Sterol biosynthesis and azole tolerance is governed by the opposing actions of SrbA and the CCAAT binding complex. *PLoS Pathog.* 12, e1005775.
- Gupta, S.K., 2016. Brassicas. In: *Breeding Oilseed Crops for Sustainable Production*. Elsevier, pp. 33–53.
- Hamsa, S., Rajarammohan, S., Aswal, M., Kumar, M., Kaur, J., 2024. Transcriptome responses of *Arabidopsis* to necrotrophic fungus *Alternaria brassicae* reveal pathways and candidate genes associated with resistance. *Plant Mol. Biol.* 114, 68.
- Hao, J., Li, X., Xu, G., Huo, Y., Yang, H., 2019. Exogenous progesterone treatment alleviates chilling injury in postharvest banana fruit associated with induction of alternative oxidase and antioxidant defense. *Food Chem.* 286, 329–337.
- Heyer, M., Reichelt, M., Mithöfer, A., 2018. A holistic approach to analyze systemic jasmonate accumulation in individual leaves of *Arabidopsis* rosettes upon wounding. *Front. Plant Sci.* 9, 1569.
- Hosseini, P., Keniya, M.V., Sagatova, A.A., Toepfer, S., Müller, C., Tyndall, J.D.A., Klinger, A., Fleischer, E., Monk, B.C., 2024. The molecular basis of the intrinsic and acquired resistance to azole antifungals in *Aspergillus fumigatus*. *Journal of Fungi* 10, 820.
- Janezko, A., Tóbiás, I., Skoczowski, A., Dubert, F., Gullner, G., Barna, B., 2013. Progesterone moderates damage in *Arabidopsis thaliana* caused by infection with *Pseudomonas syringae* or *P. fluorescens*. *Biologia plant.* 57, 169–173.
- Janezko, A., 2021. Estrogens and androgens in plants: the last 20 Years of studies. *Plants* 10, 10.
- Jindo, K., Evenhuis, A., Kempenaar, C., Pombo Sudré, C., Zhan, X., Goitom Teklu, M., Kessel, G., 2021. Review: holistic pest management against early blight disease towards sustainable agriculture. *Pest Manag. Sci.* 77, 3871–3880.
- Junker, J., Kamp, F., Winkler, E., Steiner, H., Bracher, F., Müller, C., 2021. Effective sample preparation procedure for the analysis of free neutral steroids, free steroid acids and sterol sulfates in different tissues by GC-MS. *J. Steroid Biochem. Mol. Biol.* 211, 105880.
- Kámán-Tóth, E., Dankó, T., Gullner, G., Bozsó, Z., Palkovics, L., Pogány, M., 2019. Contribution of cell wall peroxidase- and NADPH oxidase-derived reactive oxygen species to *Alternaria brassicicola*-induced oxidative burst in *Arabidopsis*. *Mol. Plant Pathol.* 20, 485–499.
- Kim, D., Paggi, J.M., Park, C., Bennett, C., Salzberg, S.L., 2019. Graph-based genome alignment and genotyping with HISAT2 and HISAT-genotype. *Nat. Biotechnol.* 37, 907–915.
- Klein, J., 2024. Progesterone metabolism in *Digitalis* and other Plants - 60 years research and recent results. *Plant Cell Physiol.* <https://doi.org/10.1093/pcp/pcae006>.
- Klein, J., Ernst, M., Christmann, A., Tropper, M., Leykauf, T., Kreis, W., Munkert, J., 2021a. Knockout of *Arabidopsis thaliana* VEP1, encoding a PRISE (progesterone 5 $\beta$ -reductase/iridoid synthase-like enzyme), leads to metabolic changes in response to exogenous methyl vinyl ketone (MVK). *Metabolites* 12.
- Klein, J., Horn, E., Ernst, M., Leykauf, T., Leupold, T., Dorfner, M., Wolf, L., Ignatova, A., Kreis, W., Munkert, J., 2021b. RNAi-mediated gene knockdown of progesterone 5 $\beta$ -reductases in *Digitalis lanata* reduces 5 $\beta$ -cardenolide content. *Plant Cell Rep.* 40, 1631–1646.
- Krauß, J., Müller, C., Klimt, M., Valero, L.J., Martínez, J.F., Müller, M., Bartel, K., Binder, U., Bracher, F., 2021. Synthesis, biological evaluation, and structure-activity relationships of 4-aminopiperidines as novel antifungal agents targeting ergosterol biosynthesis. *Molecules* 26.
- Le Phuong, T., Fitrianti, A.N., Luan, M.T., Matsui, H., Noutoshi, Y., Yamamoto, M., Ichinose, Y., Shiraishi, T., Toyoda, K., 2020. Antagonism between SA- and JA-signaling conditioned by saccharin in *Arabidopsis thaliana* renders resistance to a specific pathogen. *J. Gen. Plant Pathol.* 86, 86–99.
- Lemcke, S., Hönscheidt, C., Waschatko, G., Bopp, A., Lütjohann, D., Bertram, N., Gehrig-Burger, K., 2010. DHEA-Bodipy—a functional fluorescent DHEA analog for live cell imaging. *Mol. Cell. Endocrinol.* 314, 31–40.
- Li, H., Handsaker, B., Wysoker, A., Fennell, T., Ruan, J., Homer, N., Marth, G., Abecasis, G., Durbin, R., 2009. The sequence alignment/map format and SAMtools. *Bioinformatics* 25, 2078–2079. Oxford, England.
- Liao, Y., Smyth, G.K., Shi, W., 2014. featureCounts: an efficient general purpose program for assigning sequence reads to genomic features. *Bioinformatics* 30, 923–930.
- Liebl, M., Huber, L., Elsaman, H., Merschak, P., Wagener, J., Gsaller, F., Müller, C., 2023. Quantifying isoprenoids in the ergosterol biosynthesis by gas chromatography-mass spectrometry. *Journal of fungi (Basel, Switzerland)* 9.
- Liu, L., Wang, D., Li, L., Ding, X., Ma, H., 2016. Dehydroepiandrosterone inhibits cell proliferation and improves viability by regulating S phase and mitochondrial permeability in primary rat Leydig cells. *Mol. Med. Rep.* 14, 705–714.
- Livak, K.J., Schmittgen, T.D., 2001. Analysis of relative gene expression data using real-time quantitative PCR and the 2 $^{-\Delta\Delta Ct}$  Method. *Methods (San Diego, Calif.)* 25, 402–408.
- Love, M.I., Huber, W., Anders, S., 2014. Moderated estimation of fold change and dispersion for RNA-seq data with DESeq2. *Genome biology* 15, 550.
- McKinney, W., 2010. Data structures for statistical computing in Python. In: *Proceedings of the 9th Python in Science Conference*. Python in Science Conference. SciPy, pp. 56–61. Austin, Texas. June 28 - July 3 2010.
- Müller, C., Binder, U., Bracher, F., Giera, M., 2017. Antifungal drug testing by combining minimal inhibitory concentration testing with target identification by gas chromatography-mass spectrometry. *Nat. Protoc.* 12, 947–963.

# Is Dehydroepiandrosterone Excretion a Defense Mechanism of Plants Affecting Ergosterol Biosynthesis of *Alternaria brassicicola*?

C. Oktay et al.

Plant Physiology and Biochemistry 221 (2025) 109570

- Müller, C., Neugebauer, T., Zill, P., Lass-Flörl, C., Bracher, F., Binder, U., 2018. Sterol composition of clinically relevant mucorales and changes resulting from posaconazole treatment. *Molecules* 23.
- Müller, C., Staudacher, V., Krauss, J., Giera, M., Bracher, F., 2013. A convenient cellular assay for the identification of the molecular target of ergosterol biosynthesis inhibitors and quantification of their effects on total ergosterol biosynthesis. *Steroids* 78, 483–493.
- Murashige, T., Skoog, F., 1962. A revised medium for rapid growth and bio assays with tobacco tissue cultures. *Physiol. Plantarum* 15, 473–497.
- Neunzig, J., Sánchez-Guijo, A., Mosa, A., Hartmann, M.F., Geyer, J., Wudy, S.A., Bernhardt, R., 2014. A steroidogenic pathway for sulfonated steroids: the metabolism of pregnenolone sulfate. *The Journal of steroid biochemistry and molecular biology* 144 Pt B, 324–333.
- Nottensteiner, M., Absmeier, C., Zellner, M., 2019. QoI fungicide resistance mutations in *Alternaria solani* and *Alternaria alternata* are fully established in potato growing areas in bavaria and dual resistance against SDHI fungicides is upcoming. *Gesunde Pflanz.* 71, 155–164.
- Nowakowska, M., Wrzesińska, M., Kamiński, P., Szczechura, W., Lichocka, M., Tartanus, M., Kozik, E.U., Nowicki, M., 2019. *Alternaria brassicicola* – brassicaceae pathosystem: insights into the infection process and resistance mechanisms under optimized artificial bio-assay. *Eur. J. Plant Pathol.* 153, 131–151.
- Nowicki, M., Nowakowska, M., Niezgoda, A., Kozik, E., 2012. *Alternaria* black spot of crucifers: symptoms, importance of disease, and perspectives of resistance breeding. *J. Fruit Ornament. Plant Res.* 76, 5–19.
- Ntow-Boahene, W., Papandronicou, I., Miculob, J., Good, L., 2023. Fungal cell barriers and organelles are disrupted by polyhexamethylene biguanide (PHMB). *Sci. Rep.* 13, 2790.
- Pinto, V.E.F., Patriarca, A., 2017. *Alternaria* species and their associated mycotoxins. *Methods Mol. Biol.* 1542, 13–32.
- Polisenky, D.H., Braam, J., 1996. Cold-shock regulation of the *Arabidopsis* TCH genes and the effects of modulating intracellular calcium levels. *Plant Physiol.* 111, 1271–1279.
- Poojary, S., 2017. Topical antifungals: a review and their role in current management of dermatophytoses. *Clin Dermatol Rev* 1, 24.
- Rentel, M.C., Knight, M.R., 2004. Oxidative stress-induced calcium signaling in *Arabidopsis*. *Plant Physiol.* 135, 1471–1479.
- Rocher, F., Chollet, J.-F., Jousse, C., Bonnemain, J.-L., 2006. Salicylic acid, an ambimobile molecule exhibiting a high ability to accumulate in the phloem. *Plant Physiol.* 141, 1684–1693.
- Rocher, F., Chollet, J.-F., Legros, S., Jousse, C., Lemoine, R., Faucher, M., Bush, D.R., Bonnemain, J.-L., 2009. Salicylic acid transport in *Ricinus communis* involves a pH-dependent carrier system in addition to diffusion. *Plant Physiol.* 150, 2081–2091.
- Rotem, J., 1998. *The Genus Alternaria: Biology, Epidemiology, and Pathogenicity*. APS Press, St. Paul, Minn, p. 326.
- Sabzmeydani, E., Sedaghatooor, S., Hashemabadi, D., 2020. Progesterone and salicylic acid elevate tolerance of *poa pratensis* to salinity stress. *Russ. J. Plant Physiol.* 67, 285–293.
- Schanzer, S., Koch, M., Kiefer, A., Jentke, T., Veith, M., Bracher, F., Bracher, J., Müller, C., 2022. Analysis of pesticide and persistent organic pollutant residues in German bats. *Chemosphere* 305, 135342.
- Schanzer, S., Kröner, E., Wibbelt, G., Koch, M., Kiefer, A., Bracher, F., Müller, C., 2021. Miniaturized multiresidue method for the analysis of pesticides and persistent organic pollutants in non-target wildlife animal liver tissues using GC-MS/MS. *Chemosphere* 279, 130434.
- Schiffer, L., Brixius-Anderko, S., Hannemann, F., Zapp, J., Neunzig, J., Thevis, M., Bernhardt, R., 2016. Metabolism of oral turinabol by human steroid hormone-synthesizing cytochrome P450 enzymes. *Drug Metabol. Dispos.: the biological fate of chemicals* 44, 227–237.
- Schuhegger, R., Rauhut, T., Glawischnig, E., 2007. Regulatory variability of camalexin biosynthesis. *J. Plant Physiol.* 164, 636–644.
- Shen, X., Liu, L., Yin, F., Ma, H., Zou, S., 2012. Effect of dehydroepiandrosterone on cell growth and mitochondrial function in TM-3 cells. *Gen. Comp. Endocrinol.* 177, 177–186.
- Shiko, G., Paulmann, M.-J., Feistel, F., Ntefidou, M., Hermann-Ene, V., Vetter, W., Kost, B., Kunert, G., Zedler, J.A.Z., Reichelt, M., Oelmüller, R., Klein, J., 2023. Occurrence and conversion of progestogens and androgens are conserved in land plants. *New Phytol.* 240, 318–337.
- Shpakovski, G.V., Spivak, S.G., Berdichevets, I.N., Babak, O.G., Kubrak, S.V., Kilchevsky, A.V., Aralov, A.V., Slovokhotov, I.Y., Shpakovski, D.G., Baranova, E.N., Khaliluev, M.R., Shematorova, E.K., 2017. A key enzyme of animal steroidogenesis can function in plants enhancing their immunity and accelerating the processes of growth and development. *BMC Plant Biol.* 17, 189.
- Simons, R.G., Grinwich, D.L., 1989. Immunoreactive detection of four mammalian steroids in plants. *Can. J. Bot.* 67, 288–296.
- Stukenbrock, E.H., McDonald, B.A., 2008. The origins of plant pathogens in agro-ecosystems. *Annu. Rev. Phytopathol.* 46, 75–100.
- Suchodolski, J., Muraszko, J., Bernat, P., Krasowska, A., 2019. A crucial role for ergosterol in plasma membrane composition, localisation, and activity of Cdr1p and H<sup>+</sup>-ATPase in *Candida albicans*. *Microorganisms* 7.
- Vadassery, J., Ranf, S., Drzewiecki, C., Mithöfer, A., Mazars, C., Scheel, D., Lee, J., Oelmüller, R., 2009. A cell wall extract from the endophytic fungus *Piriformospora indica* promotes growth of *Arabidopsis* seedlings and induces intracellular calcium elevation in roots. *Plant J. : for cell and molecular biology* 59, 193–206.
- Venkateswarlu, K., Kelly, S.L., 1996. Biochemical characterisation of ketoconazole inhibitory action on *Aspergillus fumigatus*. *FEMS Immunol. Med. Microbiol.* 16, 11–20.
- Weete, J.D., Abril, M., Blackwell, M., 2010. Phylogenetic distribution of fungal sterols. *PLoS One* 5, e10899.
- Wolf, J., O'Neill, N.R., Rogers, C.A., Muilenberg, M.L., Ziska, L.H., 2010. Elevated atmospheric carbon dioxide concentrations amplify *Alternaria alternata* sporulation and total antigen production. *Environ. Health Perspect.* 118, 1223–1228.
- Zhang, S., Miao, W., Liu, Y., Jiang, J., Chen, S., Chen, F., Guan, Z., 2023. Jasmonate signaling drives defense responses against *Alternaria alternata* in chrysanthemum. *BMC Genom.* 24, 553.
- Zhang, Z., Gao, B., He, Z., Li, L., Zhang, Q., Kaziem, A.E., Wang, M., 2019. Stereoselective bioactivity of the chiral triazole fungicide prothioconazole and its metabolite. *Pestic. Biochem. Physiol.* 160, 112–118.
- Zinser, E., Paltauf, F., Daum, G., 1993. Sterol composition of yeast organelle membranes and subcellular distribution of enzymes involved in sterol metabolism. *J. Bacteriol.* 175, 2853–2858.

Biosynthesis of *Alternaria brassicicola*?

6.4 Supporting Information

**Supplement**

Article title: ***Arabidopsis thaliana* accumulates DHEA after infection with phytopathogenic fungi – effects on plants and fungi.**

Ceren Oktay, Glendis Shiko, Karl Ludwig Körber, Emanuel Barth, Kilian Osseteke, Felix Feistel, Maximilian Liebl, Lars Kaiser, Sandra Scholz, Michael Reichelt, Walter Vetter, Christoph Müller, Ralf Oelmüller, Julie A. Z. Zedler, Alexandra C. U. Furch, Jan Klein

The following Supporting Information is available for this article:



**Figure S1: Germination of *Alternaria brassicicola* spores on *Spirodela polyrhiza*.** To ensure that *A. brassicicola* is able to infect leaves of the Alismatales species *S. polyrhiza*, we treated leaves of *S. polyrhiza* with a spore solution of *A. brassicicola*. Plants were cultivated as described previously (Appenroth et al., 1996; Appenroth et al., 2018). 24 hours after infection leaves were analyzed using the bright-field of Axio Imager.M2 (Zeiss Microscopy GmbH, Jena, Germany). We could see the germination of *A. brassicicola* spores (black arrows shows hyphae material grown after spore germination) as well as the growth of hyphae through the stomata of *S. polyrhiza*.

Is Dehydroepiandrosterone Excretion a Defense Mechanism of Plants Affecting Ergosterol  
Biosynthesis of *Alternaria brassicicola*?

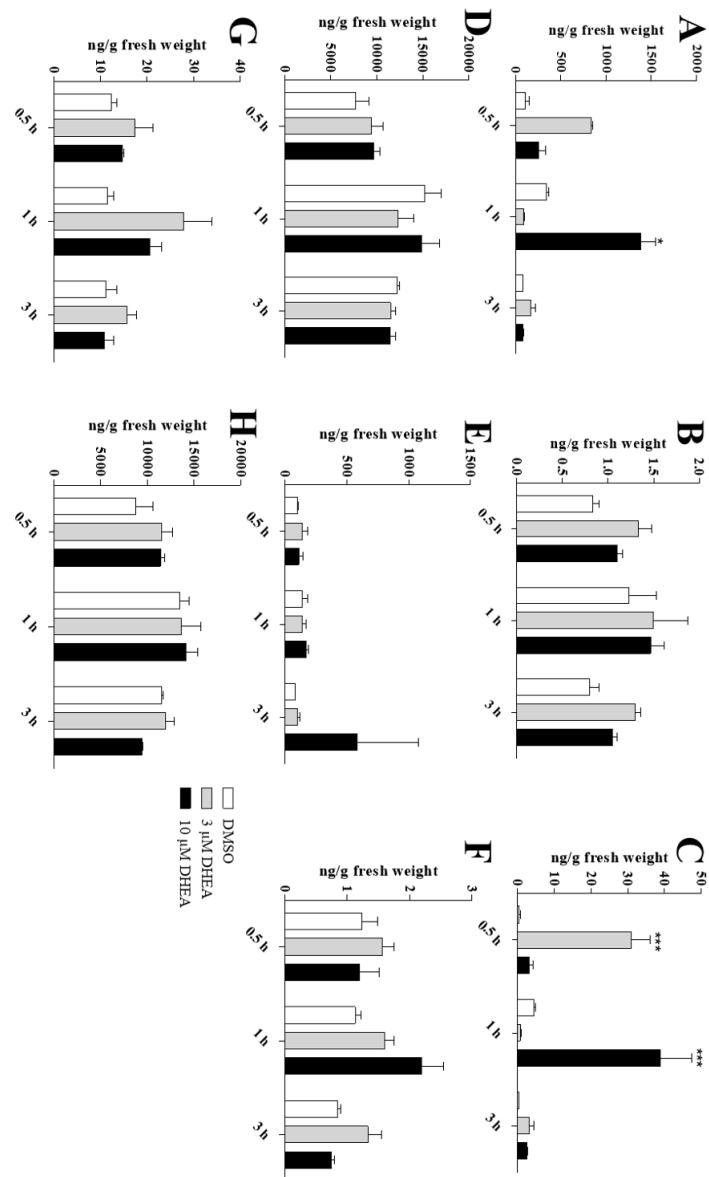


**Figure S2: Phytohormone values in *A. thaliana* after DHEA-treatment.** The graph depicts the phytohormone values in *A. thaliana* shoots after treatment with 3 (grey) or 10 μM (black) DHEA after 0.5, 1 and 3 h compared to the mock-treatment (DMSO; white). We analyzed the values of jasmonate (A), abscisic acid (B), jasmonate-isooleucin conjugates (C), *cis*-OPDA (D), hydroxyjasmonate (E), hydroxyjasmonate-isooleucin (F), carboxy-jasmonate-isooleucin conjugates (G) and dinor-OPDA (H). The graph shows mean ± SEM (n = 3).

Is Dehydroepiandrosterone Excretion a Defense Mechanism of Plants Affecting Ergosterol  
Biosynthesis of *Alternaria brassicicola*?

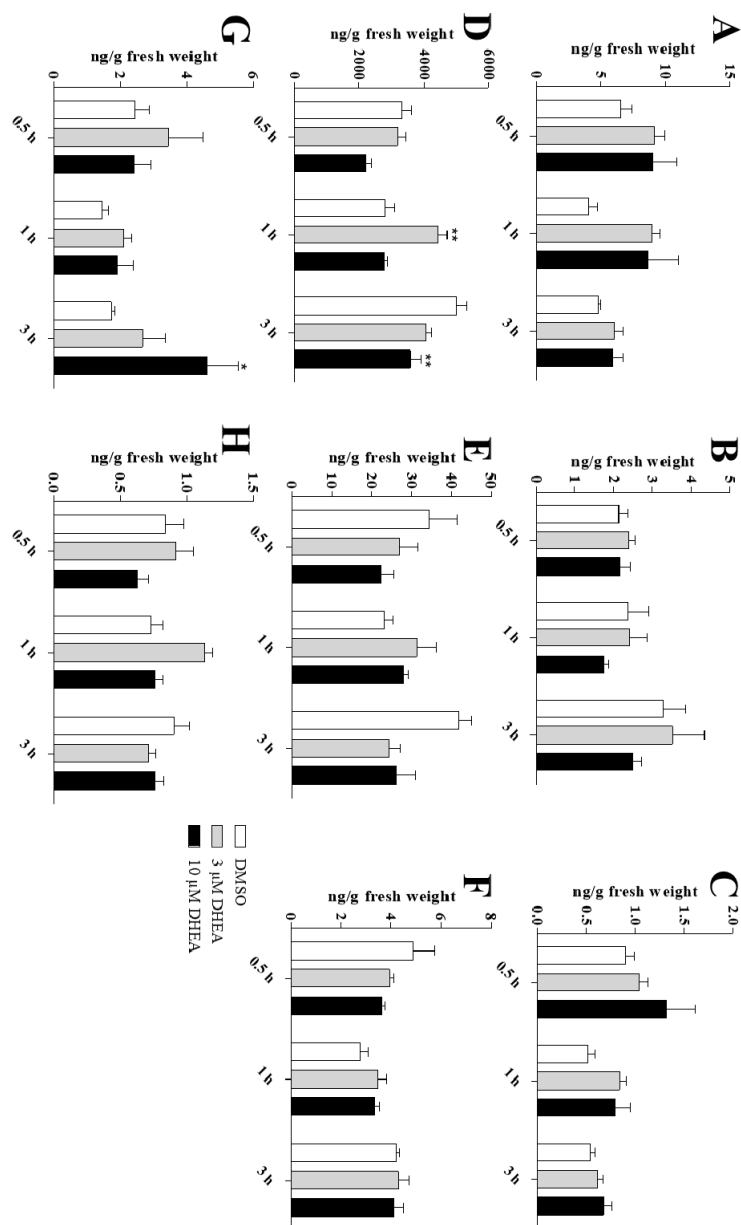


**Figure S3: Phytohormone values in *H. vulgare* after DHEA-treatment.** The graph depicts the phytohormone values in *H. vulgare* shoots after treatment with 3 (grey) or 10 μM (black) DHEA after 0.5, 1 and 3 h compared to the mock-treatment (DMSO; white). We analyzed the values of jasmonate (A), abscisic acid (B), jasmonate-isoleucin conjugates (C), *cis*-OPDA (D), hydroxyjasmonate (E), hydroxyjasmonate-isoleucin (F) and carboxy-jasmonate-isoleucin conjugates (G). The graph shows mean ± SEM (n = 5).

Is Dehydroepiandrosterone Excretion a Defense Mechanism of Plants Affecting Ergosterol  
Biosynthesis of *Alternaria brassicicola*?

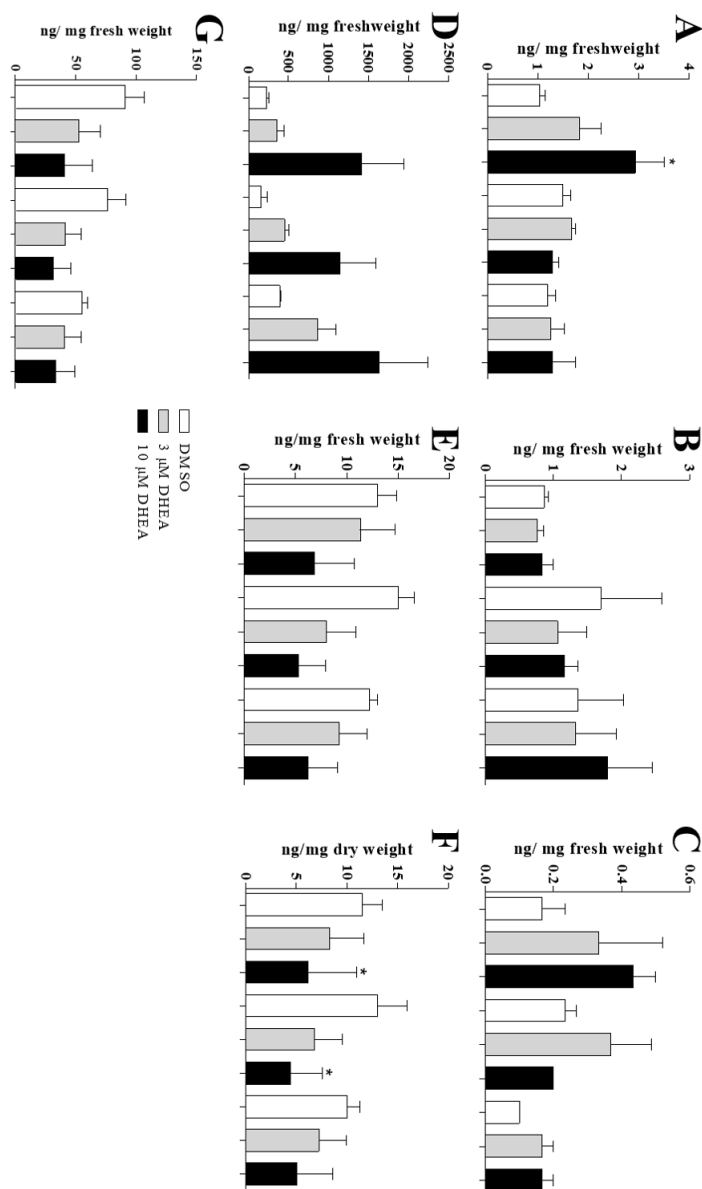


**Figure S4: Phytohormone values in *S. polyrhiza* after DHEA-treatment.** The graph depicts the phytohormone values in *S. polyrhiza* shoots after treatment with 3 (grey) or 10 μM (black) DHEA after 0.5, 1 and 3 h compared to the mock-treatment (DMSO; white). We analyzed the values of jasmonate (A), abscisic acid (B), jasmonate-isoleucin conjugates (C), *cis*-OPDA (D), hydroxyjasmonate (E), hydroxyjasmonate-isoleucin (F) and carboxy-jasmonate-isoleucin conjugates (G). The graph shows mean ± SEM (n = 5).

Is Dehydroepiandrosterone Excretion a Defense Mechanism of Plants Affecting Ergosterol  
Biosynthesis of *Alternaria brassicicola*?

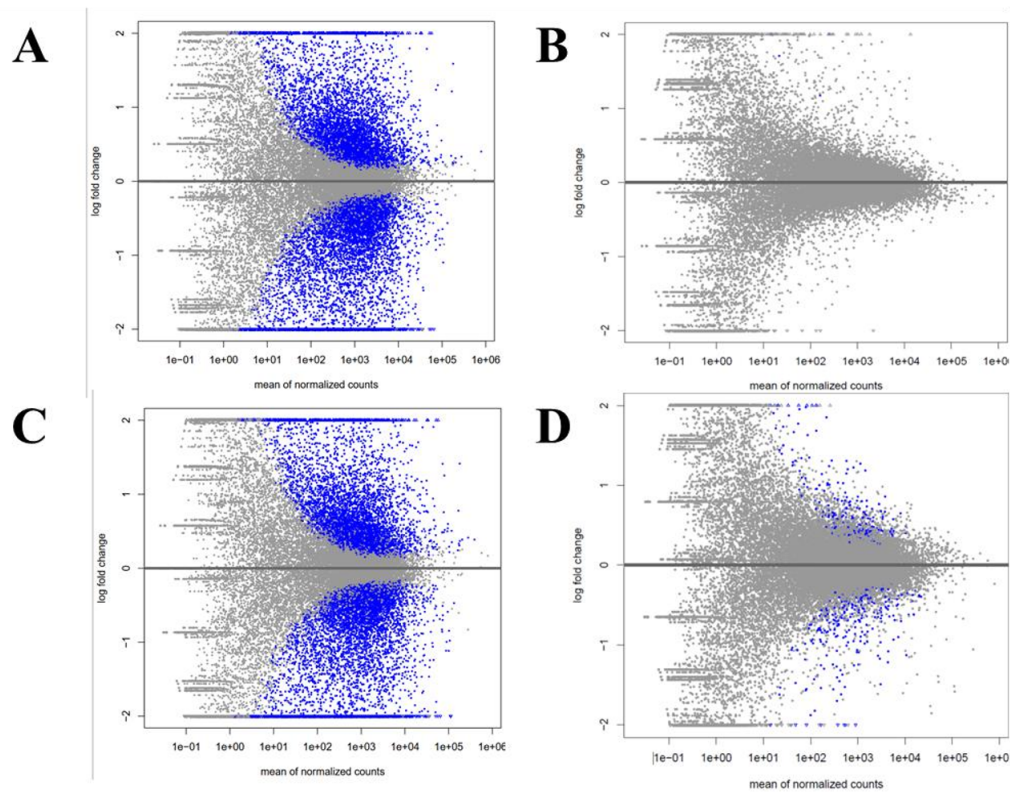


**Figure S5: MA plots of RNAseq experiments.** The graph depicts the MA plots for the RNAseq experiments within this study. The highest difference of transcripts can be found for infected plants compared to DMSO mock-treatment 24 h after infection (A), while DHEA-treatment compared to DMSO mock-treatment showed the smallest differences (B). Unsurprisingly, plants infected with DHEA-containing spore solution show a big difference compared to uninfected controls (C). Interestingly, infection vs. infection+DHEA-treatment showed stronger differences (D), than DHEA-treatment compared to the mock-treated control (D). The figure depicts MA plots for all conditions.

Biosynthesis of *Alternaria brassicicola*?

**Table S01: Details of analysis of steroids by LC-MS/MS.** A volume of 2  $\mu$ L was injected into an Agilent 1260 infinity II LC system, consisting of a binary pump G7112B, an autosampler G7167A and a column thermostat G7116A (Agilent Technologies, Santa Clara, CA, USA) without preconcentration or filtering. Chromatographic separation was carried out on a ZORBAX Eclipse XDB-C18 column (50  $\times$  4.6 mm, 1.8  $\mu$ m) from Agilent Technologies (Santa Clara, CA, USA). A binary solvent system was used as mobile phase consisting of A) 0.05% formic acid in water and B) acetonitrile with a constant flow rate of 1.1 mL/min at 20 °C column temperature. The following gradient was applied: 0.00-0.50 min, 60% A; 0.50-5.00 min, 60-10% A; 5.00-5.05 min, 10-0% A; 5.05-6.50 min, 0% A; 6.50-6.55 min, 0-60% A; 6.55-9.00 min, 60% A. The column outlet was connected to a QTRAP 6500+ triple quadrupole mass spectrometer (AB Sciex LLC, Framingham, MA, USA). The Turbo Spray IonDrive ion source was running in positive ionization mode with 5500 V ion spray voltage and 650 °C turbo gas temperature. The curtain gas was set to 40 psi; the collision gas to 'medium' and both ion source gases 1 & 2 were set to 70 psi. Scheduled multiple reaction monitoring (scheduled MRM) was used to monitor analyte parent ion  $\rightarrow$  product ion fragmentations. Q1 and Q3 quadrupoles were maintained at unit resolution. Analyst 1.6 software (Applied Biosystems) was used for data acquisition and processing. Nona-deuterated progesterone (PO- $d_9$ ) was used as internal standard (IS) for quantification. The response factors (analyte  $\times$  standard<sup>-1</sup>) of individual steroids relative to the internal standard have been experimentally determined. The table shows mass to charge ratio ( $m/z$ ), retention time (RT), collision energy (CE) and the response factor to the used internal standard ( $f$ ).

Compound	Usage:	$m/z$ :	RT [min]	CE [V]	$f$
PR	Quantifier	299 $\rightarrow$ 281	4.29	15	0.49
	Qualifier	317 $\rightarrow$ 299		13	
PO	Quantifier	315 $\rightarrow$ 97	4.43	25	1.23
	Qualifier	315 $\rightarrow$ 109		30	
DHP	Quantifier	317 $\rightarrow$ 299	5.31	17	0.23
	Qualifier	317 $\rightarrow$ 281		19	
17 $\alpha$ -OHPR-	Quantifier	315 $\rightarrow$ 297	2.80	13	0.11
	Qualifier	333 $\rightarrow$ 297		13	
DHEA	Quantifier	289 $\rightarrow$ 271	3.01	9	0.08
	Qualifier	289 $\rightarrow$ 253		15	
17 $\alpha$ -OHPO	Quantifier	331 $\rightarrow$ 97	3.15	27	0.57
	Qualifier	331 $\rightarrow$ 109		30	
AD	Quantifier	287 $\rightarrow$ 211	3.07	27	0.09
	Qualifier	287 $\rightarrow$ 173		29	
TO	Quantifier	289 $\rightarrow$ 97	2.58	25	1.34
	Qualifier	289 $\rightarrow$ 109		30	
DHT	Quantifier	291 $\rightarrow$ 255	3.45	21	0.84
	Qualifier	291 $\rightarrow$ 273		19	
PO- $D_9$	Quantifier	324 $\rightarrow$ 100	4.43	29	-
	Qualifier	324 $\rightarrow$ 113		33	

# Is Dehydroepiandrosterone Excretion a Defense Mechanism of Plants Affecting Ergosterol

## Biosynthesis of *Alternaria brassicicola*?

**Table S02: Steroid contents of *Alternaria brassicicola* infected *Arabidopsis thaliana* shoot material plants 4, 6 and 8 days post infection.**

We here show the results of steroid measurement of *A. thaliana* plants infected with *A. brassicicola* compared to uninfected controls (control). We here show three independent experiments' mean and standard deviation (SD). All results are given in ng mg<sup>-1</sup> dry weight.

	Day 4			
	Control		Infected	
	Mean	SD	Mean	SD
DHEA	6,02E-03	2,49E-03	2,03E-02	5,11E-03
Pregnenolone	0,00E+00	0,00E+00	5,05E-02	1,13E-02
Progesterone	0,00E+00	0,00E+00	0,00E+00	0,00E+00
5 $\alpha$ -pregnan-3,20-dione	0,00E+00	0,00E+00	0,00E+00	0,00E+00
Dihydrotestosterone	0,00E+00	0,00E+00	0,00E+00	0,00E+00
Testosterone	0,00E+00	0,00E+00	0,00E+00	0,00E+00
17 $\alpha$ -OH-progesterone	0,00E+00	0,00E+00	0,00E+00	0,00E+00
17 $\alpha$ -OH-pregnenolone	0,00E+00	0,00E+00	0,00E+00	0,00E+00
Androstenedione	0,00E+00	0,00E+00	0,00E+00	0,00E+00

	Day 6			
	Control		Infected	
	Mean	SD	Mean	SD
DHEA	7,10E-03	8,53E-04	2,36E-02	7,45E-03
Pregnenolone	0,00E+00	0,00E+00	1,70E-02	2,94E-02
Progesterone	0,00E+00	0,00E+00	0,00E+00	0,00E+00
5 $\alpha$ -pregnan-3,20-dione	0,00E+00	0,00E+00	0,00E+00	0,00E+00
diOH-testosterone	0,00E+00	0,00E+00	0,00E+00	0,00E+00
Testosterone	0,00E+00	0,00E+00	0,00E+00	0,00E+00
17 $\alpha$ -OH-progesterone	0,00E+00	0,00E+00	0,00E+00	0,00E+00
17 $\alpha$ -OH-pregnenolone	0,00E+00	0,00E+00	0,00E+00	0,00E+00
Androstenedione	0,00E+00	0,00E+00	0,00E+00	0,00E+00

	Day 8			
	Control		Infected	
	Mean	SD	Mean	SD
DHEA	1,13E-02	1,08E-02	3,36E-02	1,98E-02
Pregnenolone	0,00E+00	0,00E+00	5,51E-02	4,77E-02
Progesterone	0,00E+00	0,00E+00	1,12E-02	1,95E-02
5 $\alpha$ -pregnan-3,20-dione	0,00E+00	0,00E+00	0,00E+00	0,00E+00
Dihydrotestosterone	0,00E+00	0,00E+00	0,00E+00	0,00E+00
Testosterone	0,00E+00	0,00E+00	0,00E+00	0,00E+00
17 $\alpha$ -OH-progesterone	0,00E+00	0,00E+00	0,00E+00	0,00E+00
17 $\alpha$ -OH-pregnenolone	0,00E+00	0,00E+00	0,00E+00	0,00E+00
Androstenedione	0,00E+00	0,00E+00	0,00E+00	0,00E+00

Biosynthesis of *Alternaria brassicicola*?

**Table S03: Steroid contents of *Alternaria brassicicola* infected *Arabidopsis thaliana* root material plants 4, 6 and 8 days post infection.**

We here show the results of steroid measurement of *A. thaliana* plants infected with *A. brassicicola* compared to uninfected controls (control). We here show three independent experiments' mean and standard deviation (SD). All results are given in ng mg<sup>-1</sup> dry weight.

	Day 4			
	Control		Infected	
	Mean	SD	Mean	SD
DHEA	9,75E-03	4,47E-03	9,50E-03	2,91E-03
Pregnenolone	0,00E+00	0,00E+00	0,00E+00	0,00E+00
Progesterone	6,93E-03	6,04E-03	3,55E-03	3,12E-03
5α-pregnan-3,20-dione	4,52E-03	7,83E-03	1,05E-02	9,63E-03
Dihydrotestosterone	0,00E+00	0,00E+00	0,00E+00	0,00E+00
Testosterone	0,00E+00	0,00E+00	0,00E+00	0,00E+00
17α-OH-progesterone	0,00E+00	0,00E+00	0,00E+00	0,00E+00
17α-OH-pregnenolone	0,00E+00	0,00E+00	0,00E+00	0,00E+00
Androstenedione	0,00E+00	0,00E+00	0,00E+00	0,00E+00

	Day 6			
	Control		Infected	
	Mean	SD	Mean	SD
DHEA	1,35E-02	7,30E-03	1,34E-02	5,35E-03
Pregnenolone	0,00E+00	0,00E+00	0,00E+00	0,00E+00
Progesterone	0,00E+00	0,00E+00	1,89E-03	3,27E-03
5α-pregnan-3,20-dione	1,52E-02	3,48E-03	8,89E-03	8,39E-03
Dihydrotestosterone	0,00E+00	0,00E+00	0,00E+00	0,00E+00
Testosterone	0,00E+00	0,00E+00	0,00E+00	0,00E+00
17α-OH-progesterone	0,00E+00	0,00E+00	0,00E+00	0,00E+00
17α-OH-pregnenolone	0,00E+00	0,00E+00	0,00E+00	0,00E+00
Androstenedione	0,00E+00	0,00E+00	0,00E+00	0,00E+00

	Day 8			
	Control		Infected	
	Mean	SD	Mean	SD
DHEA	2,87E-03	1,12E-03	2,57E-02	1,87E-02
Pregnenolone	0,00E+00	0,00E+00	0,00E+00	0,00E+00
Progesterone	0,00E+00	0,00E+00	0,00E+00	0,00E+00
5α-pregnan-3,20-dione	0,00E+00	0,00E+00	2,01E-02	2,62E-02
Dihydrotestosterone	0,00E+00	0,00E+00	0,00E+00	0,00E+00
Testosterone	0,00E+00	0,00E+00	0,00E+00	0,00E+00
17α-OH-progesterone	0,00E+00	0,00E+00	0,00E+00	0,00E+00
17α-OH-pregnenolone	0,00E+00	0,00E+00	0,00E+00	0,00E+00
Androstenedione	0,00E+00	0,00E+00	0,00E+00	0,00E+00

# Is Dehydroepiandrosterone Excretion a Defense Mechanism of Plants Affecting Ergosterol

## Biosynthesis of *Alternaria brassicicola*?

**Table S04: Details of analysis of phytosterol pattern in *A. thaliana* by GC-MS.** Phytosterols were quantified by GC-MS using 5 mg lyophilized plant material. Extraction process and quantifications follows our previous protocols (Müller et al., 2017). The quantification was managed with six-point calibration curves ranged from 0-250 ng mL<sup>-1</sup> for each analyte. The results were normalized to the dried fungal biomass and expressed as ng per mg dried biomass (Liebl et al., 2023).

The table shows retention time (RT), mass to charge ratio (Quantifier [m/z]) and relative retention time (RRT).

Compound	RT [min]	Quantifier [m/z]	RRT
<b>Sterols</b>			
5 $\alpha$ -Cholestane	10.464	217.2	1.000
Squalene	10.003	137.1	0.956
Desmosterol-d6	13.603	447.4	1.300
Cholesterol	13.235	329.3	1.265
Cholesterol-d7	13.161	336.4	1.258
Cholestanol	13.338	215.1	1.275
Campesterol	14.498	459.5	1.374
Campestanol	14.378	382.3	1.386
Pregnenolone	10.185	386.2	0.990
Pregnenolone-2-C13-2d	10.168	390.3	0.989
Progesterone	11.024	372.3	1.072
Dehydroepiandrosterone	8.729	268.2	0.849
Allopregnanolone	9.551	388.3	0.929
5 $\alpha$ -Cholestan-3-one	13.722	415.3	1.334
5 $\beta$ -Cholestan-3-one	13.115	384.3	1.275
Cholest-4-en-3-on	14.167	413.3	1.378
7 $\alpha$ -Hydroxycholest-4-en-3-on	13.863	380.4	1.348
Sitosterol	15.353	357.4	1.467
Stigmasterol	14.699	394.4	1.405
Ergosterol	14.186	363.3	1.356

# Is Dehydroepiandrosterone Excretion a Defense Mechanism of Plants Affecting Ergosterol

## Biosynthesis of *Alternaria brassicicola*?

**Table S05: Phytosterol contents of *Alternaria brassicicola* infected *Arabidopsis thaliana* plants 4 days post infection.**

We here show the results of phytosterol measurement of *A. thaliana* plants infected with *A. brassicicola* compared to uninfected controls (control). We here show the individual results of three independent experiments. All results are given as mean  $\pm$  SEM in ng mg<sup>-1</sup> dry weight. n.q. = under limit of quantification.

Species	Condition	Tissue	Squalene	Cholesterol	Campesterol	Sitosterol	Stigmasterol
<i>A. thaliana</i>	Control	Shoot	77 $\pm$ 4	30 $\pm$ 6	218 $\pm$ 26	1171 $\pm$ 176	68 $\pm$ 28
<i>A. thaliana</i>	Infected	Shoot	69 $\pm$ 4	30 $\pm$ 4	141 $\pm$ 70	787 $\pm$ 333	132 $\pm$ 45
<i>A. thaliana</i>	Control	Root	173 $\pm$ 153	n.q. (<10 ng mL <sup>-1</sup> )	132 $\pm$ 15	548 $\pm$ 238	442 $\pm$ 150
<i>A. thaliana</i>	Infected	Root	78 $\pm$ 4	12 $\pm$ 2	139 $\pm$ 48	436 $\pm$ 57	382 $\pm$ 132

Biosynthesis of *Alternaria brassicicola*?

**Table S06: Details of analysis of phytohormone.** Phytohormone analysis was performed by LC-MS/MS as described by Heyer et al. (2018) on an Agilent 1260 series HPLC system (Agilent Technologies, Santa Clara, CA, USA) with the modification that a tandem mass spectrometer QTRAP 6500 (SCIEX, Darmstadt, Germany) was used. Chromatographic separation was achieved on a Zorbax Eclipse XDB-C18 column (50 × 4.6 mm, 1.8 μm, Agilent Technologies, Santa Clara, CA, USA). Water containing 0.05% formic acid and acetonitrile were employed as mobile phases A and B, respectively. The elution profile was: 0.00–0.50 min, 10% B; 0.50–4.00 min, 10–90% B; 4.00–4.02 min, 90–100% B; 4.02–4.50 min, 100% B and 4.51–7.00, min 10% B. Flow rate was kept at 1.1 mL min<sup>-1</sup> and column temperature was maintained at 25 °C. The mass spectrometer was equipped with a Turbo spray ion source operated in negative ionization mode. The ion spray voltage was maintained at -4,500 eV. The turbo gas temperature was set at 650 °C. Nebulizing gas was set at 60 psi, curtain gas at 40 psi, heating gas at 60 psi, and collision gas was set to “medium”. The mass spectrometer was operated in multiple reaction monitoring (MRM) mode. Since we observed that both, the *d*<sub>6</sub>-labeled JA and *d*<sub>6</sub>-labeled JA-Ile standards (HPC Standards GmbH, Cunnorsdorf, Germany) contained 40% of the corresponding *d*<sub>5</sub>-labeled compounds, the sum of the peak areas of *d*<sub>5</sub>- and *d*<sub>6</sub>-compound was used for quantification. The table shows mass transition (Q1 and Q3), retention time (RT) the used internal standard, response factor to the used internal standard (*f*) and the collision energy (CE).

Compound	Q1	Q3	RT [min]	Internal std	<i>f</i>	CE [V]
SA	136.93	93.00	3.3	D4-SA	1.0	-24
ABA	263.00	153.20	3.4	D6-ABA	1.0	-22
JA	209.07	59.00	3.6	D5-JA+D6-JA	1.0	-24
JA-Ile	322.19	130.10	3.9	D5+D6-JA-Ile	1.0	-30
OPDA	290.90	165.10	4.6	D5-JA+D6-JA	1.0	-24
OH-JA-Ile	338.10	130.10	3	D5+D6-JA-Ile	1.0	-30
OH-JA	225.10	59.00	2.6	D5-JA+D6-JA	1.0	-24
COOH-JA-Ile	352.10	130.10	3	D5+D6-JA-Ile	1.0	-30
dinor-OPDA	263.00	165.10	4.2	D5-JA+D6-JA	0.7	-20
D4-SA	140.93	97.00	3.3			-24
D6-ABA	269.00	159.20	3.4			-22
D6-JA	215.00	59.00	3.6			-24
D5-JA	214.00	59.00	3.6			-24
D6-JA-Ile	328.19	130.10	3.9			-30
D5-JA-Ile	327.19	130.10	3.9			-30

# Is Dehydroepiandrosterone Excretion a Defense Mechanism of Plants Affecting Ergosterol

## Biosynthesis of *Alternaria brassicicola*?

**Table S07: Comparison of RNAseq and qPCR results.** The table lists the normalized Count Reads of PR1 obtained by RNAseq and the CT values of PR1 and RPS18B (reference gene) obtained by qPCR, as well as the calculated Log2 fold changes (RNAseq) and relative expression (qPCR). We can clearly see, that both methods show the strong expression changes within the DHEA treated samples, while expression differences in DMSO control were underestimated by qPCR. All in all our data ensure the reliability of the RNAseq experiment, which is even more sensitive and accurate compared to qPCR.

RNAseq				qPCR		
No	Treatment	Normalized Count Reads PR1	Log2 Fold change	CT values PR1	CT values RPS18B	Relative Expression
1	DMSO	3.35	-7.12	30.14	22.95	1.25
2	DMSO	0.00		30.70	23.64	
3	DMSO	2.10		30.92	22.5	
4	DMSO	45.21		30.28	23.17	
1	DHEA	3705.57		23.16	22.63	62.3
2	DHEA	7.26		30.36	22.44	
3	DHEA	3365.53		22.93	22.46	
4	DHEA	1.78		29.18	22.33	
1	Spores	27.55	0.65	29.30	22.66	1.70
2	Spores	71.74		28.20	23.29	
3	Spores	91.93		24.96	22.27	
4	Spores	23.48		28.17	22.59	
1	Spores+DHEA	25.22		28.04	22.16	0.67
2	Spores+DHEA	37.08		29.20	22.69	
3	Spores+DHEA	39.82		26.33	21.89	
4	Spores+DHEA	35.02		28.57	22.35	

# Is Dehydroepiandrosterone Excretion a Defense Mechanism of Plants Affecting Ergosterol

## Biosynthesis of *Alternaria brassicicola*?

**Table S08: Details of analysis of sterol pattern in *A. brassicicola* by GC-MS.** To determine the effect of DHEA treatment on the ergosterol biosynthesis pathway, the samples were analyzed by gas chromatography (GC) coupled to quadrupole mass spectrometry (MS). For analysis  $2 \times 5$  mg lyophilized fungal biomass were used. The isoprenoid and the sterol pattern were determined by our previously described protocols (Müller et al., 2017; Liebl et al., 2023). Isoprenoid pyrophosphates were analyzed by GC-MS as their corresponding isoprenoid *tert*-butyldiphenylsilyl ether by GC-MS after enzymatic pyrophosphate cleavage to the free isoprenoid and subsequent derivatization with *tert*-butyldiphenylchlorosilane. As a positive control the azole antifungal ketoconazole was used in the post-lanosterol pathway of ergosterol biosynthesis. For The isoprenoid *t*BDPS ethers and squalene were identified by single ion monitoring (SIM) and their relative retention times (RRT) according to Liebl et al., 2023. The quantification was managed with six-point calibration curves ranged from 0-250 ng mL<sup>-1</sup> for each analyte. The results were normalized to the dried fungal biomass and expressed as ng per mg dried biomass (Liebl et al., 2023). Additionally, the sum of all detected peak areas of each sample was set as 100% and the percentage of each analyte of the isoprenoid pathway of ergosterol biosynthesis was calculated. For the post-lanosterol pathway of ergosterol biosynthesis, the sterols were identified as their corresponding trimethylsilyl (TMS) ethers by mass spectra and RRT according to Müller et al., 2017 The quantification, managed with an external calibration with ergosterol, consists of six levels (0-10,000 ng mL<sup>-1</sup>). The sum of all detected peak areas of each sample was set as 100% and the percentage of each sterol was calculated (Müller et al., 2018; Kühbacher et al., 2023). The table shows retention time (RT), mass to charge ratio (Quantifier [m/z]) and relative retention time (RRT).

Compound	RT [min]	Quantifier [m/z]	RRT
<b>Isoprenoids</b>			
Isoprenol	9.787	225	0.71
Prenol	9.851	267	0.71
Geraniol	11.239	335	0.82
Squalen	11.912	69	0.86
Farnesol	12.580	69	0.91
Heptadecanol (I.S.- Isoprenoid)	13.779	437	1.00
Geranylgeraniol	14.980	69	1.09

Is Dehydroepiandrosterone Excretion a Defense Mechanism of Plants Affecting Ergosterol  
Biosynthesis of *Alternaria brassicicola*?

Sterols			
Cholestan (I.S.-Sterol)	10.635	217	1.00
Ergosta-5,8,22,24-tetraen-ol	13.902	251	1.31
Lichesterol	14.033	363	1.32
Ergosterol	14.362	363	1.35
14-Methylfecosterol	14.556	469	1.37
Ergosta-5,7,22,24-tetraen-ol	14.685	466	1.38
Ergosta-7,22,24-trien-ol	15.155	343	1.43
Episterol	15.171	343	1.43
14-Methylergosta-8,24-dien-3,6-diol	15.490	467	1.46
Lanosterol	15.498	393	1.46
Eburicol	16.120	407	1.52

# Is Dehydroepiandrosterone Excretion a Defense Mechanism of Plants Affecting Ergosterol Biosynthesis of *Alternaria brassicicola*?

## References:

- Appenroth K-J, Teller S, Horn M. 1996.** Photophysiology of turion formation and germination in *Spirodela polyrhiza*. *Biologia plantarum* **38**.
- Appenroth K-J, Sree KS, Bog M, Ecker J, Seeliger C, Böhm V, Lorkowski S, Sommer K, Vetter W, Tolzin-Banasch K et al. 2018.** Nutritional Value of the Duckweed Species of the Genus *Wolffia* (Lemnaceae) as Human Food. *Frontiers in chemistry* **6**: 483.
- Heyer, M., Reichelt, M., Mithöfer, A. 2018.** A holistic approach to analyze systemic jasmonate accumulation in individual leaves of *Arabidopsis* rosettes upon wounding. *Frontiers in Plant Science*, **9**: 1569.
- Kühbacher, A., Merschak, P., Haas, H., Liebl, M., Müller, C., Gsaller, F., 2023.** The cytochrome P450 reductase CprA is a rate-limiting factor for Cyp51A-mediated azole resistance in *Aspergillus fumigatus*. *Antimicrobial agents and chemotherapy* **67**, e0091823.
- Liebl M, Huber L, Elsaman H, Merschak P, Wagener J, Gsaller F, Müller C. 2023.** Quantifying Isoprenoids in the Ergosterol Biosynthesis by Gas Chromatography-Mass Spectrometry. *Journal of fungi (Basel, Switzerland)* **9**.
- Müller C, Binder U, Bracher F, Giera M. 2017.** Antifungal drug testing by combining minimal inhibitory concentration testing with target identification by gas chromatography-mass spectrometry. *Nature protocols* **12**: 947–963.
- Müller, C., Neugebauer, T., Zill, P., Lass-Flörl, C., Bracher, F., Binder, U., 2018.** Sterol Composition of Clinically Relevant Mucorales and Changes Resulting from Posaconazole Treatment. *Molecules (Basel, Switzerland)* **23**.

## 7. Summary

Analysis of the isoprenoid pattern in sterol biosynthesis could lead to a better understanding of the effects isoprenoids have on fungal and mammalian organisms. Targeting isoprenoid pathway enzymes by specific inhibitors could further lead to the development of novel classes of drugs (antimycotic/antihypercholesterolemic drugs). The aim of this work was the implementation of an analytical assay that could be used to identify and quantify isoprenoids and their corresponding isoprenoid pyrophosphates in fungal and mammalian cells. Further the approach should be applied in the scope of several collaborative projects (see Chapters 4-6).

The general need for new approaches to treat invasive fungal infections was highlighted in Chapter 3, where we identified mutations in the electron support chain of CYP51A as a putative explanation for a previously not described mechanism of fungal resistance. Identification of those novel targets is essential to develop effective tools against an emerging number of resistance mechanisms against established drugs.

Enzymes of the isoprenoid pathway play an important role in fungal survival and therefore could be an interesting target for a new class of antimycotics (see Chapter 4). In this context, a GC-MS based assay for the analysis of intermediates of the isoprenoid pathway was introduced, which was optimized for the use in fungal matrices. Besides adaptations in sample handling, liquid-liquid extraction, enzymatic pyrophosphate deconjugation and derivatization, a novel analytical method was described, which was validated in line with the EMA guideline on analytical method validation on *S. cerevisiae* matrix. After validation, inducible *A. fumigatus* strains carrying mutations in isoprenoid pathway genes (*erg1/erg9*) were analyzed to describe their isoprenoid composition. Finally, we identified the essential role of *erg9* and its corresponding enzyme (fungal squalene synthase) for fungal survival and therefore as a potential new target for antifungal treatment.

Since one of the most important tasks in antifungal drug development is avoiding interactions with the mammalian host, the isoprenoid assay was adapted a second time to analyze mammalian isoprenoid biosynthesis and get better insights into structure-activity relationships of published enzyme inhibitors (see Chapter 5). By optimizations in sample preparation the approach was adopted to HL60 cells and extracellular matrix was included as an additional dimension for analysis. The analysis of 16 experimental isoprenoid and distal ergosterol pathway inhibitors revealed 6-fluoromevalonate as an inhibitor of isopentenyl pyrophosphate isomerase, a function which was previously not described in literature. Additionally, the subsequent analysis of isoprenoids and isoprenoid pyrophosphates from intra- and extracellular matrices was used to traffic isoprenoid patterns. Those patterns revealed the preferred deconjugated form of isoprenoids in the cellular matrix over the expected pyrophosphorylated condition, which is the known pathway intermediate.

With the implementation of the isoprenoid assay on fungal and mammalian matrices (cellular and extracellular), a potent tool for experimental drug screening and investigation of isoprenoid trafficking was developed. Selectivity of a compound towards one specific enzyme in fungal or mammalian cells can be confirmed which is of pivotal interest in all stages of drug development (also see Chapter 5.5).

In combination with the established assays of Müller *et al.* for distal cholesterol [18] and ergosterol [22] biosynthesis pathway analysis, the isoprenoid assays for fungal (see Chapter 4) and mammalian (see Chapter 5) isoprenoid biosynthesis are a powerful expansion to the original approaches. An application of the assays

## Summary

(isoprenoid + distal ergosterol biosynthesis) was performed, as described in Chapter 6, where the role of the putative plant sterol biosynthesis inhibitor dehydroepiandrosterone (DHEA) could not be confirmed.

## 8. Abbreviations

ACVD	atherosclerotic CVD
ADP	adenosine diphosphate
AmB	amphotericin B
AMPK	activated protein kinase
Arf	ADP ribosylation factor
ATP	adenosine triphosphate
CHILD	congenital hemidysplasia with ichthyosiform erythroderma and limb defects
CoA	coenzyme A
COPII	coat protein II
CoQ	coenzyme Q
CVD	cardiovascular disease
Cybe	cytochrome b <sub>5</sub> -reductase
CYP	cytochrome P
DHCR24	C24-dehydrocholesterol reductase
DHEA	dehydroepiandrosterone
DMAPP	dimethylallyl pyrophosphate
Dox	doxycycline
EMA	European Medicines Agency
ER	endoplasmic reticulum
FDA	Food and Drug Administration
FPP	farnesyl pyrophosphate
FSX	fosmanogepix
FT	farnesyl transferase
GAP	GTPase-activating protein
GC	gas chromatography
GC-MS	gas chromatography-mass spectrometry
GDP	guanosine diphosphate
GEF	guanine-nucleotide-exchange factor
GGPP	geranylgeranyl pyrophosphate
GGT	geranylgeranyl transferase
GPI	glycosylphosphatidylinositol
GPP	geranyl pyrophosphate
GTP	guanosine triphosphate
GTPase	guanosine triphosphatase
Gwt1	glycosylphosphatidylinositol-anchored wall protein transfer 1
HEM	hydrops ectopic calcification-moth-eaten
HIDS	hyperimmunoglobulinemia D and periodic fever syndrome
HL60	human leukemia 60
HMG	3-hydroxy-3-methylglutaryl
HMGR	HMG-CoA reductase

## Abbreviations

IC <sub>50</sub>	half maximal inhibitory concentration
IL	interleukin
INSIG	insulin-induced gene
IPP	isopentenyl pyrophosphate
LDL	low-density lipoprotein
MAA	mevalonic aciduria
MIC	minimal inhibitory concentration
MTT	3-(4,5-dimethylthiazol-2-yl)-2,5-diphenyltetrazoliumbromide
MVK	mevalonate kinase
NADP	nicotinamide adenine dinucleotide phosphate
OLF	olorofim
P	phosphate
PDSS1	decaprenyl diphosphate synthase subunit 1
PolyP-P	polyprenyl phosphate
PolyP-PP	polyprenyl pyrophosphate
PP	pyrophosphate
PSPP	pre-squalene pyrophosphate
QS	quorum sensing
QSM	quorum sensing molecule
Rab	Ras-related in brain
Ran	Ras-related nuclear
Ras	rat sarcoma virus
Rho	Ras homologue
S1P	site 1 protease
S2P	site 2 protease
SCAP	SREBP-cleavage-activating protein
SLOS	Smith-Lemli-Opitz syndrome
SREBP	sterol regulatory element binding protein
<i>t</i> BDPSCl	<i>tert</i> -butyldiphenylchlorosilane
TR	tandem repeat
UBIAD1	UbiA prenyltransferase domain-containing protein 1
WHO	World Health Organization

## 9. Literature

- [1] M.S. Brown; J.L. Goldstein. A receptor-mediated pathway for cholesterol homeostasis. Available online: <https://www.nobelprize.org/uploads/2018/06/brown-goldstein-lecture.pdf> (accessed on 08.11.2024).
- [2] T. Jordá; S. Puig. Regulation of ergosterol biosynthesis in *Saccharomyces cerevisiae*. *Genes (Basel)* **2020**, *11*, 7, doi:10.3390/genes11070795.
- [3] E.J. Dufourc. Sterols and membrane dynamics. *J Chem Biol* **2008**, *1*, 63-77, doi:10.1007/s12154-008-0010-6.
- [4] W.D. Nes. Biosynthesis of cholesterol and other sterols. *Chem Rev* **2011**, *111*, 6423-6451, doi:10.1021/cr200021m.
- [5] J.M. Berg; J.L. Tymoczko; G.J. Gatto jr.; L. Stryer. Biosynthese der Membranlipide und Steroide. In *Stryer Biochemie*; Springer Spektrum: Berlin, 2018; Volume 8. Auflage, pp. 905- 945.
- [6] S.L. Pinkosky; R.S. Newton; E.A. Day; R.J. Ford; S. Lhotak; R.C. Austin; C.M. Birch; B.K. Smith; S. Filippov; P.H.E. Groot; G.R. Steinberg; N.D. Lalwani. Liver-specific ATP-citrate lyase inhibition by bempedoic acid decreases LDL-C and attenuates atherosclerosis. *Nat Commun* **2016**, *7*, 13457, doi:10.1038/ncomms13457.
- [7] H.M. Mizioro. Enzymes of the mevalonate pathway of isoprenoid biosynthesis. *Arch Biochem Biophys* **2011**, *505*, 131-143, doi:10.1016/j.abb.2010.09.028.
- [8] P.C.M. Heinrich, M.; Graeve,L. Stoffwechsel von Cholesterin. In *Löffler/Petrides Biochemie und Pathobiochemie*; Springer-Verlag: Berlin, Heidelberg, 2014; Volume 9. Auflage, pp. 292-299.
- [9] W.J. Kovacs; K.N. Tape; J.E. Shackelford; X. Duan; T. Kasumov; J.K. Kelleher; H. Brunengraber; S.K. Krisans. Localization of the pre-squalene segment of the isoprenoid biosynthetic pathway in mammalian peroxisomes. *Histochem Cell Biol* **2007**, *127*, 273-290, doi:10.1007/s00418-006-0254-6.
- [10] N. Berndt; A.D. Hamilton; S.M. Sebt. Targeting protein prenylation for cancer therapy. *Nat Rev Cancer* **2011**, *11*, 775-791, doi:10.1038/nrc3151.
- [11] G. Nürenberg; D.A. Volmer. The analytical determination of isoprenoid intermediates from the mevalonate pathway. *Anal Bioanal Chem* **2012**, *402*, 671-685, doi:10.1007/s00216-011-5262-2.
- [12] K. Grabińska; G. Palamarczyk. Dolichol biosynthesis in the yeast *Saccharomyces cerevisiae*: an insight into the regulatory role of farnesyl diphosphate synthase. *FEMS Yeast Res* **2002**, *2*, 259-265, doi:10.1016/S1567-1356(02)00110-1.
- [13] J.A. Stefely; D.J. Pagliarini. Biochemistry of mitochondrial coenzyme Q biosynthesis. *TIBS* **2017**, *42*, 824-843, doi:10.1016/j.tibs.2017.06.008.
- [14] M. Bentinger; M. Tekle; G. Dallner. Coenzyme Q - biosynthesis and functions. *BBRC* **2010**, *396*, 74-79, doi:10.1016/j.bbrc.2010.02.147.
- [15] S.A. Holstein; R.J. Hohl. Isoprenoids: remarkable diversity of form and function. *Lipids* **2004**, *39*, 293-309, doi:10.1007/s11745-004-1233-3.
- [16] K. Rosam; B.C. Monk; M. Lackner. Sterol 14 $\alpha$ -demethylase ligand-binding pocket-mediated acquired and intrinsic azole resistance in fungal pathogens. *J Fungi (Basel)* **2020**, *7*, 1, doi:10.3390/jof7010001.
- [17] M. Giera; C. Müller; F. Bracher. Analysis and experimental inhibition of distal cholesterol biosynthesis. *Chromatographia* **2015**, *78*, 343-358, doi:10.1007/s10337-014-2796-4.
- [18] C. Müller; J. Junker; F. Bracher; M. Giera. A gas chromatography-mass spectrometry-based whole-cell screening assay for target identification in distal cholesterol biosynthesis. *Nat Protoc* **2019**, *14*, 2546-2570, doi:10.1038/s41596-019-0193-z.
- [19] L. Alcazar-Fuoli; E. Mellado; G. Garcia-Effron; J.F. Lopez; J.O. Grimalt; J.M. Cuenca-Estrella; J.L. Rodriguez-Tudela. Ergosterol biosynthesis pathway in *Aspergillus fumigatus*. *Steroids* **2008**, *73*, 339-347, doi:10.1016/j.steroids.2007.11.005.
- [20] C. Müller; T. Neugebauer; P. Zill; C. Lass-Flörl; F. Bracher; U. Binder. Sterol composition of clinically relevant mucorales and changes resulting from posaconazole treatment. *Molecules* **2018**, *23*, 1218, doi:10.3390/molecules23051218.
- [21] S. Dhingra; R.A. Cramer. Regulation of sterol biosynthesis in the human fungal pathogen *Aspergillus fumigatus*: opportunities for therapeutic development. *Front Microbiol* **2017**, *8*, 92, doi:10.3389/fmicb.2017.00092.
- [22] C. Müller; U. Binder; F. Bracher; M. Giera. Antifungal drug testing by combining minimal inhibitory concentration testing with target identification by gas chromatography-mass spectrometry. *Nat Protoc* **2017**, *12*, 947-963, doi:10.1038/nprot.2017.005.
- [23] U. Schweizer; S. Bohleber; N. Fradejas-Villar. The modified base isopentenyladenosine and its derivatives in tRNA. *RNA Biol* **2017**, *14*, 1197-1208, doi:10.1080/15476286.2017.1294309.
- [24] K. Wennerberg; K.L. Rossman; C.J. Der. The Ras superfamily at a glance. *J Cell Sci* **2005**, *118*, 843-846, doi:10.1242/jcs.01660.

## Literature

- [25] C.J. Marshall. Protein prenylation: a mediator of protein-protein interactions. *Science* **1993**, *259*, 1865-1866, doi:10.1126/science.8456312.
- [26] L. Hederstedt. Heme A biosynthesis. *BBA* **2012**, *1817*, 920-927, doi:10.1016/j.bbabi.2012.03.025.
- [27] B. Schenk; F. Fernandez; C.J. Waechter. The ins(ide) and out(side) of dolichyl phosphate biosynthesis and recycling in the endoplasmic reticulum. *Glycobiology* **2001**, *11*, 61R-70R, doi:10.1093/glycob/11.5.61r.
- [28] J. Avalos; M. Carmen Limón. Biological roles of fungal carotenoids. *Curr Genet* **2015**, *61*, 309-324, doi:10.1007/s00294-014-0454-x.
- [29] G. Sandmann. Carotenoids and their biosynthesis in fungi. *Molecules* **2022**, *27*, 1431, doi:10.3390/molecules27041431.
- [30] J.M. Hornby; E.C. Jensen; A.D. Lisec; J.J. Tasto; B. Jahnke; R. Shoemaker; P. Dussault; K.W. Nickerson. Quorum sensing in the dimorphic fungus *Candida albicans* is mediated by farnesol. *Appl Environ Microbiol* **2001**, *67*, 2982-2992, doi:10.1128/AEM.67.7.2982-2992.2001.
- [31] C. Braunsdorf; D. Mailänder-Sánchez; M. Schaller. Fungal sensing of host environment. *Cell Microbiol* **2016**, *18*, 1188-1200, doi:10.1111/cmi.12610.
- [32] P. Albuquerque; A. Casadevall. Quorum sensing in fungi – a review. *Med Mycol* **2012**, *50*, 337-345, doi:10.3109/13693786.2011.652201.
- [33] R. Kovács; L. Majoros. Fungal quorum-sensing molecules: a review of their antifungal effect against *Candida* biofilms. *J Fungi (Basel)* **2020**, *6*, 99, doi:10.3390/jof6030099.
- [34] D.H. Navarathna; J.M. Hornby; N. Hoerrmann; A.M. Parkhurst; G.E. Duhamel; K.W. Nickerson. Enhanced pathogenicity of *Candida albicans* pre-treated with subinhibitory concentrations of fluconazole in a mouse model of disseminated candidiasis. *J Antimicrob Chemother* **2005**, *56*, 1156-1159, doi:10.1093/jac/dki383.
- [35] M. Tashiro; S. Kimura; K. Tateda; T. Saga; A. Ohno; Y. Ishii; K. Izumikawa; T. Tashiro; S. Kohno; K. Yamaguchi. Pravastatin inhibits farnesol production in *Candida albicans* and improves survival in a mouse model of systemic candidiasis. *Med Mycol* **2012**, *50*, 353-360, doi:10.3109/13693786.2011.610037.
- [36] I. Leonhardt; S. Spielberg; M. Weber; D. Albrecht-Eckardt; M. Bläss; R. Claus; D. Barz; K. Scherlach; C. Hertweck; J. Löffler; K. Hünninger; O. Kurzai. The fungal quorum-sensing molecule farnesol activates innate immune cells but suppresses cellular adaptive immunity. *mBio* **2015**, *6*, e00143-15, doi:10.1128/mBio.00143-15.
- [37] J. Corliss. How it's made: cholesterol production in your body. Available online: <https://www.health.harvard.edu/heart-health/how-its-made-cholesterol-production-in-your-body> (accessed on 03.02.2025).
- [38] L. Trapani; M. Segatto; P. Ascenzi; V. Pallottini. Potential role of nonstatin cholesterol lowering agents. *IUBMB Life* **2011**, *63*, 964-971, doi:10.1002/iub.522.
- [39] C. Müller; E. Hank; M. Giera; F. Bracher. Dehydrocholesterol reductase 24 (DHCR24): medicinal chemistry, pharmacology and novel therapeutic options. *Curr Med Chem* **2022**, *29*, 4005-4025, doi:10.2174/092986732866621115121832.
- [40] J.J. Li. Genesis of statins. In *Triumph of the heart: the story of statins*; Oxford University Press, Inc.: New York, 2009; Volume 1st edition, pp. 33-36.
- [41] H. Elsaman; E. Golubtsov; S. Brazil; N. Ng; I. Klugherz; R. Martin; K. Dichtl; C. Müller; J. Wagener. Toxic eburicol accumulation drives the antifungal activity of azoles against *Aspergillus fumigatus*. *Nat Commun* **2024**, *15*, 6312, doi:10.1038/s41467-024-50609-1.
- [42] J. Luo; H. Yang; B.L. Song. Mechanisms and regulation of cholesterol homeostasis. *Nat Rev Mol Cell Biol* **2020**, *21*, 225-245, doi:10.1038/s41580-019-0190-7.
- [43] H.R. Waterham. Defects of cholesterol biosynthesis. *FEBS Lett* **2006**, *580*, 5442-5449, doi:10.1016/j.febslet.2006.07.027.
- [44] M. Nakanishi; J.L. Goldstein; M.S. Brown. Multivalent control of 3-hydroxy-3-methylglutaryl coenzyme A reductase. Mevalonate-derived product inhibits translation of mRNA and accelerates degradation of enzyme. *J Biol Chem* **1988**, *263*, 8929-8937, doi:10.1016/s0021-9258(18)68397-8.
- [45] World Health Organization (WHO). Cardiovascular diseases (CVDs). Available online: [https://www.who.int/news-room/fact-sheets/detail/cardiovascular-diseases-\(cvds\)](https://www.who.int/news-room/fact-sheets/detail/cardiovascular-diseases-(cvds)) (accessed on 09.12.2024).
- [46] S.E. Nissen; A.M. Lincoff; D. Brennan; K.K. Ray; D. Mason; J.J.P. Kastelein; P.D. Thompson; P. Libby; L. Cho; J. Plutzky; H.E. Bays; P.M. Moriarty; V. Menon; D.E. Grobbee; M.J. Louie; C.F. Chen; N. Li; L. Bloedon; P. Robinson; M. Horner; et al. Bempedoic acid and cardiovascular outcomes in statin-intolerant patients. *N Engl J Med* **2023**, *388*, 1353-1364, doi:10.1056/NEJMoa2215024.
- [47] A.C. Goldberg; L.A. Leiter; E.S.G. Stroes; S.J. Baum; J.C. Hanselman; L.T. Bloedon; N.D. Lalwani; P.M. Patel; X. Zhao; P.B. Duell. Effect of bempedoic acid vs placebo added to maximally tolerated statins on

## Literature

- low-density lipoprotein cholesterol in patients at high risk for cardiovascular disease: the CLEAR wisdom randomized clinical trial. *JAMA* **2019**, *322*, 1780-1788, doi:10.1001/jama.2019.16585.
- [48] C.M. Mulders-Manders; A. Simon. Hyper-IgD syndrome/mevalonate kinase deficiency: what is new? *Semin Immunopathol* **2015**, *37*, 371-376, doi:10.1007/s00281-015-0492-6.
- [49] L.A. Favier; G.S. Schulert. Mevalonate kinase deficiency: current perspectives. *Appl Clin Genet* **2016**, *9*, 101-110, doi:10.2147/TACG.S93933.
- [50] C.E. Flück; T. Tajima; A.V. Pandey; W. Arlt; K. Okuhara; C.F. Verge; E.W. Jabs; B.B. Mendonça; K. Fujieda; W.L. Miller. Mutant P450 oxidoreductase causes disordered steroidogenesis with and without Antley-Bixler syndrome. *Nat Genet* **2004**, *36*, 228-230, doi:10.1038/ng1300.
- [51] D.W. Denning. Global incidence and mortality of severe fungal disease. *Lancet Infect Dis* **2024**, *24*, e428-e438, doi:10.1016/S1473-3099(23)00692-8.
- [52] K.C. Gray; D.S. Palacios; I. Dailey; M.M. Endo; B.E. Uno; B.C. Wilcock; M.D. Burke. Amphotericin primarily kills yeast by simply binding ergosterol. *PNAS* **2012**, *109*, 2234-2239, doi:10.1073/pnas.1117280109.
- [53] A.C. Mesa-Arango; N. Trevijano-Contador; E. Román; R. Sánchez-Fresneda; C. Casas; E. Herrero; J.C. Argüelles; J. Pla; M. Cuenca-Estrella; O. Zaragoza. The production of reactive oxygen species is a universal action mechanism of amphotericin B against pathogenic yeasts and contributes to the fungicidal effect of this drug. *AAC* **2014**, *58*, 6627-6638, doi:10.1128/AAC.03570-14.
- [54] T.M. Anderson; M.C. Clay; A.G. Cioffi; K.A. Diaz; G.S. Hisao; M.D. Tuttle; A.J. Nieuwkoop; G. Comellas; N. Maryum; S. Wang; B.E. Uno; E.L. Wildeman; T. Gonen; C.M. Rienstra; M.D. Burke. Amphotericin forms an extramembranous and fungicidal sterol sponge. *Nat Chem Biol* **2014**, *10*, 400-406, doi:10.1038/nchembio.1496.
- [55] E.L. Berkow; S.R. Lockhart. Fluconazole resistance in *Candida* species: a current perspective. *Infect Drug Resist* **2017**, *10*, 237-245, doi:10.2147/IDR.S118892.
- [56] J. Houšť; J. Spížek; V. Havlíček. Antifungal drugs. *Metabolites* **2020**, *10*, 106, doi:10.3390/metabo10030106.
- [57] F. Bracher. Wirkstoffe und Wirkprinzipien: Angriffspunkt Ergosterolbiosynthese. *PharmuZ* **2003**, *32*, 118-123, doi:10.1002/pauz.200390028.
- [58] World Health Organization (WHO). WHO fungal priority pathogens list to guide research, development and public health action. Available online: <https://iris.who.int/bitstream/handle/10665/363682/9789240060241-eng.pdf?sequence=1> (accessed on 12.02.2025).
- [59] M. Hoenigl; R. Sprute; M. Egger; A. Arastehfar; O.A. Cornely; R. Krause; C. Lass-Flörl; J. Prattes; A. Spec; G.R. Thompson, 3rd; N. Wiederhold; J.D. Jenks. The antifungal pipeline: fosmanogepix, ibrexafungerp, olorofim, opelconazole, and rezafungin. *Drugs* **2021**, *81*, 1703-1729, doi:10.1007/s40265-021-01611-0.
- [60] A. Almajid; A. Bazroon; H.M. Al-Awami; H. Albarbari; I. Alqahtani; R. Almutairi; A. Alsuwajj; F. Alahmadi; J. Aljawad; R. Alnimer; N. Asiri; S. Alajlani; R. Alshelali; Y. Aljishi. Fosmanogepix: the novel antifungal agent's comprehensive review of in vitro, in vivo, and current insights from advancing clinical trials. *Cureus* **2024**, *16*, e59210, doi:10.7759/cureus.59210.
- [61] F. Vetter. Entwicklung eines Assays zur Identifizierung von Inhibitoren im Präsqalen-Abschnitt der Cholesterolsynthese. Dissertation, Ludwig-Maximilians-Universität München, Munich: Verlag Dr. Hut., 2018.
- [62] M. Liebl. Bestimmung von Terpenen im Präsqalen-Abschnitt der Cholesterolsynthese und Ergosterol-Biosynthese mittels GC-MS. Masterarbeit, Ludwig-Maximilians-Universität München, 2020.
- [63] European Medicines Agency (EMA). Guideline on bioanalytical method validation. Available online: [https://www.ema.europa.eu/en/documents/scientific-guideline/guideline-bioanalytical-method-validation\\_en.pdf](https://www.ema.europa.eu/en/documents/scientific-guideline/guideline-bioanalytical-method-validation_en.pdf) (accessed on 21.03.2024).
- [64] G.I. Lepesheva; M.R. Waterman. Structural basis for conservation in the CYP51 family. *BBA* **2011**, *1814*, 88-93, doi:10.1016/j.bbapap.2010.06.006.
- [65] P. Osset-Trénor; A. Pascual-Ahuir; M. Proft. Fungal drug response and antimicrobial resistance. *J Fungi (Basel)* **2023**, *9*, 565, doi:10.3390/jof9050565.
- [66] D.C. Lamb; D.E. Kelly; N.J. Manning; M.A. Kaderbhai; S.L. Kelly. Biodiversity of the P450 catalytic cycle: yeast cytochrome b5/NADH cytochrome b5 reductase complex efficiently drives the entire sterol 14-demethylation (CYP51) reaction. *FEBS Lett* **1999**, *462*, 283-288, doi:10.1016/S0014-5793(99)01548-3.
- [67] E. Puumala; S. Fallah; N. Robbins; L.E. Cowen. Advancements and challenges in antifungal therapeutic development. *Clin Microbiol Rev* **2024**, *37*, e0014223, doi:10.1128/cmr.00142-23.
- [68] J. Seiffert. Gelbe Liste - Terbinafin. Available online: [https://www.gelbe-liste.de/wirkstoffe/Terbinafin\\_16933](https://www.gelbe-liste.de/wirkstoffe/Terbinafin_16933) (accessed on 11.02.2025).
- [69] Y. Iwasawa; M. Horie. Mammalian squalene epoxidase inhibitors and structure-activity relationships. *Drugs Future* **1993**, *18*, 911-918, doi:10.1358/dof.1993.018.10.233081.

## Literature

- [70] S. Schanzer; M. Koch; A. Kiefer; T. Jentke; M. Veith; F. Bracher; J. Bracher; C. Müller. Analysis of pesticide and persistent organic pollutant residues in German bats. *Chemosphere* **2022**, *305*, 135342, doi:10.1016/j.chemosphere.2022.135342.
- [71] Food and Agriculture Organization of the United Nations (FAO). FAOSTAT Pesticides indicators. Available online: (accessed on 26.01.2025).
- [72] J. Klein. Progesterone metabolism in digitalis and other plants-60 years of research and recent results. *PCP* **2024**, *65*, 1500-1514, doi:10.1093/pcp/pcae006.
- [73] G. Shiko; M.J. Paulmann; F. Feistel; M. Ntefidou; V. Hermann-Ene; W. Vetter; B. Kost; G. Kunert; J.A.Z. Zedler; M. Reichelt; R. Oelmüller; J. Klein. Occurrence and conversion of progestogens and androgens are conserved in land plants. *New Phytol* **2023**, *240*, 318-337, doi:10.1111/nph.19163.